
# Synthesis and potential application of $Fe^{3+}/Mn^{2+}$ bimetal and hexadecyltrimethylammonium bromide (HDTMA-Br) modified clayey soils for arsenic removal in groundwater

A PhD thesis submitted to the University of Venda, School of Environmental Sciences, Department of Ecology and Resource Management in fulfilment of degree of Philosophy in Environmental Sciences

**By**

**Mudzielwana Rabelani (11600806)**

**Promoter: Prof W. M Gitari (University of Venda)**

**Co-promoter: Prof P. Ndungu (University of Johannesburg)**

# Declaration

I, Rabelani Mudzielwana, hereby declare that "Synthesis and potential application of $Fe^{3+}/Mn^{2+}$ bimetal and hexadecyltrimethylammonium bromide (HDTMA-Br) modified smectite rich clay soils for arsenic removal in groundwater" is my own work in design and execution and that it has never been submitted for any degree or examination in any other University, and that all the sources I have used or quoted have been indicated and duly acknowledged by complete references.

Full Names: Rabelani Mudzielwana

Signature: ……  Date: ……..

# Acknowledgement

I would like to thank the Lord Almighty for giving me wisdom, good health and making everything possible for me. I thank Him for His abundant love and His grace that has always been sufficient to me.

I would like to express my sincere and profound gratitude to my promoter **Professor Wilson Mugera Gitari** for his dedicated assistance, invaluable comments, suggestion and constructive criticisms throughout this project. His contribution made what looked almost impossible at the beginning to be possible at the end.

My co-promoter, **Professor Patrick Ndungu** of University of Johannesburg, is also appreciated for his support.

I would like to express my heartfelt gratitude to my mother, **Ms. Leah Tshisevhe**, my uncle, **Mr. Thomas Ndanduleni Tshisevhe** and all my siblings **(Ndivhuwo, Shumani, Rofhiwa, Pollet, Rotondwa and Murendeni)** for their moral support and encouragement.

My Mentor**, Dr. Steven Ndou** from Sasol Research and Technology, together with his team are extremely appreciated for their assistance with BET analysis.

I am grateful to **Dr. Segun** for his technical and conceptual contributions to this work.

To all my fellow postgraduate students and Environmental Remediation and Nanoscience Research Group members (**Glynn, Obijole, Tunde, Oses, Rhanzhu, Murendeni, Lloyd, Humbe, Nsovo, Rendani**) and my best friends, **Phathutshedzo Nemaguvhuni, Vhahangwele Munyai, Tshifhiwa Agnus Tjapudi, Mashaka Molepo, Comfort Phasha and Dipontso Mamabolo** for their support and funny moments we shared together thank you.

I would also like to thank the financial support from Sasol Inzalo Foundation, NRF, University of Venda RPC and Prof Gitari's research Incentives.

Lastly, I would like to thank Miranda Waldron of University of Cape Town, Remy Bucher of ithemba Lab and Riana Rossou of Stellenbosch University for their assistance with sample analysis. Dr Stam (HoD of Ecology and Resource Management, University of Venda) is also appreciated for allowing me to use the departmental funds to maintain the equipment's.

# Dedication

This work is dedicated to my late father, Mr. James Ratshibvimo Mudzielwana and to my late grandmother, Mrs. Ntavhanyeni Selinah Tshisevhe. May their souls continue to rest in peace.

# Abstract

The presence of arsenic in groundwater has drawn worldwide attention from researchers and public health officials due to its effects on human health such as, cancer, skin thickening, neurological disorders, muscular weakness, loss of appetite and nausea. World Health Organisation (WHO) has set the limit of 10 µg/L for arsenic in drinking water in trying to reduce the effects of arsenic. This was further adopted by South African National Standard (SANS). The present study aims at evaluating arsenic concentration in selected groundwater sources around Greater Giyani Municipality in Limpopo Province and further synthesize clay based adsorbents for arsenic removal using $Fe^{3+}$ and $Mn^{2+}$ oxides and hexadecylammonium bromide (HDTMA-Br) cationic surfactant as modifying agents.

The first section of the work presented the hydrogeochemical characteristics of groundwater in the Greater Giyani Municipality. The results showed that the pH of the samples ranges from neutral to weakly alkaline. The dominance of major anionic and cationic species was found to be in the order: $HCO_3^->Cl^->SO_4^{2-}>NO_3^-$ and $Na^+>Mg^{2+}>Ca^{2+}>K^+>Si^{4+}$, respectively. Hydrogeochemical facies identified in the study area include $CaHCO_3$ (90%) and mixed $CaNaHCO_3$ (10%) which shows the dominance of water-rock interaction. About 60% of the tested samples contains arsenic concentration above 10 µg/L as recommended by SANS and WHO. Concentration of arsenic was found to be ranging between 0.1 to 172.53 µg/L with the average of 32.21 µg/L.

In the second part of this work, arsenic removal efficiency of locally available smectite rich and kaolin clay was evaluated. Results showed that the percentage As(V) removal by kaolin clay was optimum at pH 2 while the percentage As(III) removal was greater than 60% at pH 2 to 12. For smectite rich clay soils, the percentage of As(III) and As(V) removal was found to be optimum at pH between 6 and 8. The adsorption isotherm data for As(III) and As(V) removal by both clays fitted better to Freundlich isotherm. Adsorption of both species of arsenic onto the clay mineral occurred via electrostatic attraction and ion exchange mechanisms. Both clay soils could be regenerated twice using $Na_2CO_3$ as a regenerant. Kaolin clay showed a better performance and was selected for further modification.

In the third section of this work, Fe-Mn bimetal oxide modified kaolin clay was successfully synthesized by precipitating $Fe^{3+}$ and $Mn^{2+}$ metal oxides to the interlayer surface of kaolin clay. Modification of kaolin clay increased the surface area from 19.2 $m^2/g$ to 29.8 $m^2/g$ and further

decreased the pore diameter from 9.54 to 8.5 nm. The adsorption data fitted to the pseudo second order of reaction kinetics indicating that adsorption of As(III) and As(V) occurred via chemisorption. The adsorption isotherm data was described by Langmuir isotherm models showing a maximum As(III) and As(V) adsorption capacities of 2.16 and 1.56 mg/g, respectively at a temperature of 289 K. Synthesized adsorbent was successfully reused for 6 adsorption-desorption cycles using $K_2SO_4$ as a regenerant. Column experiments showed that maximum breakthrough volume of ≈2 L could be treated after 6 hours using 5 g adsorbent dosage. Furthermore, the concentration of Fe and Mn were within the WHO permissible limit.

In the fourth part of the work kaolin clay was functionalized with hexadecyltrimethylamonium bromide (HDTMA-Br) cationic surfactant and its application in arsenic removal from groundwater was investigated. The results revealed that adsorption of As(III) and As(V) is optimum at pH range 4-8. The maximum As(III) and As(V) adsorption capacities were found 2.33 and 2.88 mg/g, respectively after 60 min contact time. Pseudo first order model of reaction kinetics described the adsorption data for As(V) better while pseudo second order model described As(III) adsorption data. The adsorption isotherm data for As(III) and As(V) fitted well to Langmuir model indicating that adsorption of both species occurred on a mono-layered surface. Adsorption thermodynamics model revealed that adsorption of As(III) and As(V) was spontaneous and exothermic. The As(III)/As(V) adsorption mechanism was ascribed to electrostatic attraction and ion exchange. The regeneration study showed that synthesized adsorbent can be used for up to 5 times.

In the firth part of the work inorgano-organo modified kaolin clay was successfully synthesized through intercalation of $Fe^{3+}$ and $Mn^{2+}$ metal oxides and HDTMA-Br surfactant onto the interlayers of the clay mineral. The batch experiments showed that As(III) removal was optimum at pH range of 4-6, while the As(V) removal was optimum at pH range 4-8. The adsorption data for both species of arsenic showed a better fit to pseudo second order of reaction kinetics which suggest that the dominant mechanism of adsorption was chemisorption. The isotherm studies showed better fit to Langmuir isotherm model as compared to Freundlich model. The maximum adsorption capacity As(III) and As(V) at room temperature as determined by Langmuir model were found to be 7.99 mg/g and 7.32 mg/g, respectively. The thermodynamic studies for sorption of As(III) and As(V) showed negative value of $\Delta G^O$ and $\Delta H^O$ indicating that adsorption process occurred spontaneously and is exothermic in nature. The regeneration study showed that the

inorgano-organo modified kaolin clay can be reused for up 7 adsorption-regeneration cycles using 0.01 M HCl as a regenerant. Thomas kinetic model and Yoon-Nelson model showed that the rate of adsorption increases with increasing flow rate and initial concentration and decreases with increasing of the bed mass.

In conclusions, adsorbents synthesized from this work showed a better performance as compared to other adsorbents available in the literature. Among the synthesized adsorbents, inorgano-organo modified clay showed highest adsorption capacity as compared to surfactant functionalized and Fe-Mn bimetal oxides modified kaolin clay. However, all adsorbents were recommended for use in arsenic remediation from groundwater. The following recommendations were made following the findings from this study: 1) routine monitoring of arsenic in groundwater of Greater Giyani Municipality, 2) evaluating the possible link between arsenic exposure and arsenic related diseases within Giyani in order to find the extent of the problem in order to establish the population at risk, 3) The toxicity assessment for HDTMA-Br modified kaolin clay should be carried out, 4) Materials developed in the present study should be modeled and tested at the point of use for arsenic removal, and lastly, 5) this study further encourage the development of other arsenic removal materials that can be used at household level.

Keywords: Arsenic; adsorption; hydrogeochemistry; kaolin clay; smectite rich clay soils; Fe-Mn bimetal oxides; HDTMA-Br surfactant.

# Academic output

**Published Book Chapter and Proceedings**

- Mugera W. Gitari and **Rabelani Mudzielwana**. (2018). Mineralogical and Chemical Characteristics of Raw and Modified Clays and Their Application in Arsenic and Fluoride Removal: Review, Current Topics in the Utilization of Clay in Industrial and Medical Applications, Mansoor Zoveidavianpoor, IntechOpen, DOI: 10.5772/intechopen.74474.
- **Mudzielwana R.,** Gitari W. M., Ndungu P., **2018**. **Performance evaluation of Fe-Mn bimetal modified kaolin clay mineral in As(III) removal from groundwater.** In Proceedings of the International Conference in Protection and Restoration of the Environment XIV. Editors: N. Theodossiou, C. Chirstodoulatos, A Koutsospyros, D Karpouzos and Z, Mallios. Page: 1172-1183. ISBN: 978-960-99922-4-4.

**Published and Accepted Manuscripts**

- **Mudzielwana R.,** Gitari W. M., Ndungu P., 2018. **Evaluation of the adsorptive properties of locally available alumino-silicate clay in As(III) and As(V) remediation from groundwater.** Journal of Physics and Chemistry of the Earth. https://doi.org/10.1016/j.pce.2018.11.008.
- **Mudzielwana R.,** Gitari W. M., Ndungu P., 2019. **Uptake of As(V) from Groundwater Using Fe-Mn Oxides Modified Kaolin Clay: Physicochemical Characterization and Adsorption Data Modeling.** Water Journal. **Accepted.**

**Submitted Review:**

- **Mudzielwana R.,** Gitari W. M., Ndungu P., Segun, S. A., Talabi O. A., 2019. **Hydrogeochemical characteristics assessment of arsenic rich groundwater samples in Greater Giyani Municipality, Limpopo Province, South Africa.** Groundwater for Sustainable Development. Under Revision.
- **Mudzielwana R.,** Gitari W. M., Ndungu P., 2019. **Removal of As(III) from synthetic groundwater using Fe-Mn bimetal modified kaolin clay: Adsorption kinetics, isotherm and thermodynamics studies.** Environmental Processes. Status: **Under Review.**

- **Mudzielwana R.,** Gitari W. M., Ndungu P., 2019. **Performance evaluation of surfactant modified kaolin clay in As(III) and As(V) adsorption from groundwater: Adsorption kinetics, isotherms and thermodynamics.** Heliyon Journal. **Under Review.**
- **Mudzielwana R.,** Gitari W. M., Ndungu P., 2019. **Synthesis of a clay based hybrid sorbent for As(III) and As(V) removal from groundwater: Adsorption kinetics, isotherms and thermodynamics.** Journal of Hazardous Materials. **Under Review**.

**Conferences Presentations**

- **R Mudzielwana,** M.W Gitari & P Ndungu**, Removal of As(III) and As(V) from groundwater using Fe-Mn bimetal oxide modified kaolin clay mineral: Adsorption modelling and mechanistic aspect.** First international conference on sustainable management of natural resources. 15th-17th October 2018, Bolivia Lodge, Polokwane, South Africa.

- **R Mudzielwana,** M.W Gitari & P Ndungu, Performance evaluation of Fe-Mn bimetal modified kaolin clay mineral in As(III) removal from groundwater. **International Conference in Protection and Restoration of the Environment XIV**. 03-06 July 2018, Thessaloniki, Greece.

- **R Mudzielwana,** M.W Gitari & P Ndungu. Evaluation of the adsorptive properties of locally available alumino-silicate clay in As(III) and As(V) remediation from groundwater. **18th waternet/WARFSA/GWP-SA symposium on integrated water resource development and management: Innovative Technological Advances for Water Security in Eastern and Southern Africa**. 25th -27th October 2017. Swakopmund, Namibia.

- **R Mudzielwana,** M.W Gitari & P. Ndungu, Removal of arsenic from water using smectite rich clay soil: insight from adsorption kinetics and adsorption isotherms. **15th International Conference on Environmental Sciences and Technology**. 31st August-2nd September 2017, Rhodes Island, Greece.

# Table of Contents

# Chapter 1: Introduction

## 1.1 Background

Arsenic is one of the ubiquitous elements in nature that is ranked 20$^{th}$ most common trace element available in the earth's crust (Rahman et al., 2018). It is a metalloid and it can easily be solubilized and mobilized in groundwater depending on pH, redox speciation, temperature and solution composition (Smedley and Kinnburgh, 2013; Bardach et al., 2015; Ding et al., 2015). In natural water, arsenic primarily occur in inorganic form as arsenite [As(III)] and arsenate [As(V)], depending on the redox conditions (Smedley and Kinnburgh, 2002). The pentavalent species of arsenic (As(V)) is widely found in oxidizing conditions while the trivalent species (As(III)) is found under reducing conditions (Duker et al., 2005). The contamination of water by arsenic may be due to its mobilization under natural conditions and anthropogenic activities such as mining, agricultural wastes and domestic wastes (Ungureanu et al., 2015; Bentahar et al., 2016).

The prolonged exposure to arsenic may give rise to health hazards like cancer, hyperpigmentation and gangrene to human (Duker et al., 2005; Bentahar et al., 2016). Due to its considerable health hazards, arsenic has attained worldwide attention. In trying to reduce the effects of arsenic on human health, the permissible limit of 10 µg/L of arsenic in drinking water was set by the World Health Organization (WHO, 2017). The South African government also set a limit of 10 µg/L of arsenic in groundwater (SANS-241, 2015). Therefore, areas that have arsenic concentration above the recommended levels will require arsenic removal.

Arsenic removal from water has received extensive attention from researchers and various techniques have been reviewed by Litter et al., (2012) and Mohan and Pittman, (2007) as well as by Jadhav et al., (2015). These techniques include adsorption, oxidation, coagulation and precipitation, as well as membrane process. Among the reviewed techniques, adsorption appears to be the most common because it is easy to operate, has high removal efficiency and its low cost. Various adsorbents have been evaluated for the adsorption of arsenic, including laterite soil (Maji et al., 2008), raw clays (Dousova et al., 2011), ferric-based layered double hydroxide (Hong et al., 2014), iron oxide and manganese oxide-pillared clays (Mishra and Mahato, 2016), Moroccan clays (Bentahar et al., 2016) and hydrous iron oxide-impregnated alginate beads (Sigdel et al., 2016). In many cases the tested adsorbents showed higher removal efficiency to As(V) as compared to As(III) removal efficiency. This is attributed to the fact that at the pH range of 4-10, As(III) species

are neutrally charged, while the As(V) species are negatively charged in the same pH range (Maji et al., 2008). Recently researches are being directed towards finding the adsorbent that will be cost effective and that will have higher binding efficiency for both species of arsenic simultaneously.

Naturally-occurring clay minerals have been widely applied in the removal of organic and inorganic pollutants from water due to their physicochemical properties such as high specific surface area, chemical and mechanical stability, high cation and anion exchange capacity and negative/positive character of surface (Bhattacharyya and Gupta, 2008). Moreover, the adsorption capacity of clay can be improved by modification with polycation (such as, $Fe^{3+}$ $Al^{3+}$, $Mn^{2+}$) and cationic surfactant (Gitari et al., 2013). Modification involves the replacement of exchangeable cations such as $Na^{+}$, $Ca^{2+}$, $K^{+}$ and $Mg^{2+}$ from the clay interlayers. Recently studies are focusing on the modification of clay soils using both inorganic polycations metal species and organic cations, also referred to as inorgano-organo modified clays for water treatment, because they possess two different sorption sites making them capable of removing different types of pollutants from the aqueous solutions simultaneously with an enhanced sorption capacity (Lee and Tiweri, 2012). Lee et al., (2015) reported an improved sorption capacity for both species of arsenic on hexadecyltrimethylammonium-aluminium (HDTMA-Al) bentonite, compared to hexadecyltrimetylammonium (HDTMA) bentonite. This was attributed to increased sorption sites of adsorbent. It was also said that modification of clay with HDTMA and Al give rise to strong chemical bonding between active aluminol group in the clay and that favours adsorption of arsenic species.

In the present study, arsenic adsorbent will be developed from smectite rich clay soil and kaolin clay that are naturally found in Mukondeni Village and Dzamba Village, respectively in Limpopo Province. The clay will be modified using $Fe^{3+}$/$Mn^{2+}$ polycation species and HDTMA-Br to further enhance its sorption capacity.

### 1.2 Problem statement

Rural communities around the world depend on groundwater as the main source of drinking water. However, the presence of elements such as arsenic in groundwater poses a threat to human health and has drawn worldwide attention. Prolonged exposure to arsenic may result in arsenicosis, which is a chronic illness caused by drinking water with a high concentration of arsenic (Naujokas et al., 2013). The disease is manifested by, cancer, skin thickening, neurological disorders, muscular

weakness, loss of appetite, and nausea (Ungureanu et al., 2015). Several epidemiological studies established a link between arsenic exposure and different types of cancer. In 2015, Bulka et al. evaluated the correlation between arsenic in drinking water and prostate cancer in Illinois counties and reported that there is a positive correlation between arsenic concentration in water and prostate cancer. In trying to reduce the effects of arsenic in human health, WHO has set a limit of 0.01 mg/L in drinking water. The guideline value is designated on the basis of the risk related to human exposure, treatment performance and analytical achievability (WHO, 2017).

Little is known about the distribution and availability of arsenic in South African groundwater and hence the population that is exposed to high arsenic levels are not known. High concentrations of arsenic have been recorded in Alldays, Sisheng, Vingerfontein, Vryheid (Sami and Druzynski, 2003). The other data on arsenic concentration is supplied by Department of Water and Sanitation. However, the data is quite patchy. As such there is a need to determine the arsenic concentration in groundwater, particularly in rural areas where groundwater is the main source of drinking water.

For areas having high arsenic concentration, developing a sustainable and flexible treatment system for arsenic removal appears to be the safe option for providing safest clean water. Adsorption of arsenic using natural clays appears to be the most common method the arsenic removal applied in rural areas because of the clays easy availability and comparatively low cost. However, the sorption capacity of these materials has been found to be insignificant. Additionally, these materials possess low settling properties; hence, limiting its practical implication in such purposes (Tiwari and Lee, 2012). Therefore, besides determining As concentration in groundwater there is a need to develop an adsorbent that will possess both good settling properties and that will offer higher sorption capacity for both species of arsenic from this groundwater. Clays modified with inorganic polymeric metal species and organic cationic species have drawn the attention of researchers for their application in water treatment. Inorgano-organo modified clay soils also offers enhanced applicability in water treatment as they are capable of removing both inorganic and organic impurities simultaneously from aqueous solution and they also possess improved settling properties (Hua, 2015). This is because the organic modifiers could change the surface property of the clays from hydrophilic to hydrophobic, while the polymeric metal modifier improves the adsorption affinity for inorganic contaminants, such as arsenic.

## 1.3 Objectives

### 1.3.1 Main objective

The main objective of the study is to synthesize $Fe^{3+}/Mn^{2+}$ bimetallic and hexadecyltrimetylammonium bromide (HDTMA-Br) modified clayey soils and to evaluate its applicability to arsenic removal in groundwater.

### 1.3.2 Specific objectives

- To determine the arsenic concentration in selected boreholes in Greater Giyani Municipality, Limpopo Province.
- To examine the physicochemical properties of the locally available smectite rich clay soils and kaolin clay mineral and compare their effectiveness towards arsenic removal from groundwater
- To evaluate the optimum conditions for synthesizing $Fe^{3+}/Mn^{2+}$ bimetal oxide and hexadecyltrimethylammonium bromide (HDTMA-Br) modified clay mineral for As(III) and As(V) removal from groundwater.
- To evaluate the applicability of synthesised adsorbent in As(III) and As(V) removal from groundwater using batch and column experiments.
- To determine the regeneration potential of the synthesized adsorbent.

## 1.4 Hypothesis

- There are some boreholes in Greater Giyani Municipality that have higher concentration of arsenic.
- Synthesized $Fe^{3+}/Mn^{2+}$ bimetallic and hexadecyltrimetylammonium bromide (HDTMA-Br) modified smectite-rich clay soils composite adsorbent can effectively remove As(III) and As(V) from drinking water simultaneously.

## 1.5 Assumption

- It is assumed that $Fe^{3+}/Mn^{2+}$ bimetallic and hexadecyltrimetylammonium bromide (HDTMA-Br) modified smectite rich clay soils composite adsorbent will effectively remove As(III) and As(V) from drinking water simultaneously from groundwater.
- The synthesized adsorbents will not result in secondary contaminants in the treated water.

## 1.6 Significance of the study

Groundwater is the main source of water for many of the rural communities in Greater Giyani Municipality of Limpopo Province. However, little is known about the chemical composition of this groundwater which may have detrimental effects on the health of the community that rely on groundwater. Therefore, this study will highlight the chemical composition of groundwater selected boreholes in Greater Giyani Municipality with the main focus on arsenic concentration. Furthermore, the study will propose possible low-cost composite adsorbents made of $Fe^{3+}/Mn^{2+}$ bimetallic and hexadecyltrimethylammonium (HDTMA-Br) modified local available smectite rich clay soils that can be used for arsenic removal at household level.

The findings of this study will shed light the concentration of arsenic in Greater Giyani Municipality, Limpopo Province. Furthermore, the findings will give possible solutions to remove arsenic from groundwater. This information will be essential to water suppliers. This findings will also be of essential towards achieving the United Nations Sustainable Development Goal 6 which focuses on provision of clean water for all. The improvement in water quality will also have positive contribution towards Goal 3 which aims at improving the health and well-being for all since lack of clean water has huge impact on human health.

## 1.7 Thesis layout

This section present the layout of the chapters:

Chapter 1: Introduction

Chapter 2: Literature review

Chapter 3: Hydrogeochemical characteristics of arsenic contaminated water in Greater Giyani Municipality, Limpopo Province, South Africa.

Chapter 4: Physicochemical characterization of smectite rich and kaolin clay mineral: potential application in As(III) and As(V) removal from groundwater.

Chapter 5: Removal of arsenic from groundwater using Fe-Mn bimetal oxide modified kaolin clay mineral: Adsorption modelling and mechanistic aspect.

Chapter 6: Preparation of surfactant modified kaolin clay mineral for As(III) and As(V) removal: Adsorption kinetics, isotherms and thermodynamics.

Chapter 7: Adsorption of As(III) and As(V) using inorgano-organo modified kaolin clay mineral: Batch and column studies.

Chapter 8: Conclusions and Recommendations.

## References

Bardach, A. E., Ciapponi, A., Soto, N., Chaparro, M. R, Calderon, M., Briatore, A., Cadoppi N., Tassara, R. & Litter, M. I., 2015. Epidemiology of chronic disease related to arsenic in Argentina: A systematic review. *Science of the Total Environment,* 538, pp. 802–816.

Bentahar, Y., Hurel, C., Draoui, K., Khairoun, S. & Marmier, N., 2016. Adsorptive properties of Moroccan clays for the removal of arsenic(V) from aqueous solution. *Applied Clay Science* 119, pp. 385–392.

Bhattachryya, K. G. & Gupta, S. S., 2008. Adsorption of few heavy metals on natural and modified kaolinite and montmorillonite: A review. *Advances in Colloid and Interface science*. 140, pp.114-131.

Ding, W. Wang, Y. Yu, Y. Zhang, X. Li, Y. & Wu, F., 2015. Photooxidation of arsenic(III) to arsenic(V) on the surface of kaolinite clay. *Journal of Environmental Sciences,* 36, pp. 29-37.

Doušová, B., Lhotka, M, Grygar, T., Machovič, V. & Herzogová, L., 2011. In situ co-adsorption of arsenic and iron/manganese ions on raw clays. *Applied Clay Science*, 54, pp.166–171.

Duker, A. A, Carranza, E. J. M. & Hale, M. 2005. Arsenic geochemistry and health. *Environment International*, 31, pp. 631– 641.

Gitari W. M., Ngulube T, Masindi V. & Gumbo J. R. 2013 Defluoridation of groundwater using $Fe^{3+}$- modified bentonite clay: Optimization of adsorption condition. *Desalination & Water Treatment*, pp. 1-13.

Hong, J., Zhu, Z., Lu, H. & Qiu Y. 2014. Synthesis and arsenic adsorption performances of ferric-based layered double hydroxide with alanine intercalation. *Chemical Engineering Journal*, 252, pp. 267–274.

Hua, J., 2015. Synthesis and characterization of bentonite based inorgano–organo-composites and their performances for removing arsenic from water. *Applied Clay Science*, 114, pp. 239-246.

Jadhav, S. V., Bringas E., Yadav, G. D, Rathod, V. K., Ortiz K. & Marathe, K. V., 2015. Arsenic and fluoride contaminated groundwaters: A review of current technologies for contaminants removal. *Journal of Environmental Management,* 162, pp. 306-325.

Lee, S. M. & Tiwari, D., 2012. Organo and inorgano-organo-modified clays in the remediation of aqueous solutions: An overview. *Applied Clay Science*, 59(60), pp.84-102.

Lee, S. M., Lalhmunsiama, Thanhmingliana, &Tiwari, D., 2015. Porous hybrid materials in the remediation of water contaminated with As(III) and As(V). *Chemical Engineering Journal*, 270, pp.496-507.

Litter, M. I., Alarcón-Herrera, M. T., Arenas, M. J., Armienta, M. A. & Avilés, M., et al., 2012. Small-scale and household methods to remove arsenic from water for drinking purposes in Latin America. *Science of the Total Environment*, 429, pp. 107–122.

Maji, S. K., Pal A. & Pal, T., 2008 Arsenic removal from real-life groundwater by adsorption on laterite soil. *Journal of Hazardous Materials,* 151, pp. 811–820.

Mishra, T. & Mahato, D. K., 2016. A comparative study on enhanced arsenic(V) and arsenic(III) removal by iron oxide and manganese oxide pillared clays from ground water. *Journal of Environmental Chemical Engineering*, 4, pp. 1224–1230.

Mohana, D. & Pittman, C. U, 2007 Arsenic removal from water/wastewater using adsorbents: A critical review. *Journal of Hazardous Materials,* 142, pp. 1–53.

Naujokas, M.F. Anderson, B. Ahsan, H. Aposhian H.V. Graziano, J.H. Thompson, C. Suk, W.A., 2013. The Broad Scope of Health Effects from Chronic Arsenic Exposure: Update on a Worldwide Public Health Problem. *Environmental Health Perspectives,* 121(3), pp. 295-302.

Rahman, M.A. Rahman, A. Khan, M.Z.K. Renzaho, A.M.N., 2018. Human health risks and socio-economic perspectives of arsenic exposure in Bangladesh: A scoping review. *Ecotoxicology and Environmental Safety*, 150, pp. 335–343.

Sami, K. & Druzynski A. L., 2003. Predicted Spatial Distribution of Naturally Occurring Arsenic, Selenium and Uranium in Groundwater in South Africa-Reconnaissance Survey. WRC Report No. 1236/1/03.

SANS-241-1. 2015. South African National Standards for drinking water-Part 1. 2nd ed.

Sigdel, A., Park, J., Kwak, H. & Park, P., 2016. Arsenic removal from aqueous solutions by adsorption onto hydrous iron oxide-impregnated alginate beads. *Journal of Industrial and Engineering Chemistry*, 35, pp. 277–286.

Smedley P. L & Kinniburgh, D. G., 2013. Arsenic in Groundwater and the Environment. British Geological Survey, Oxfordshire, UK.

Smedley, P. L, & Kinniburgh, D. G., 2002. A review of the source, behavior and distribution of arsenic in natural waters. *Applied Geochemistry*, 17, pp.517-568.

Tiwari, D. & Lee, S. M., 2012. Novel hybrid materials in the remediation of ground waters contaminated with As(III) and As(V). *Chemical Engineering Journal,* 204-206, pp. 23-31.

Ungureanu, G., Santos, S., Boaventura, R. & Botelho, C., 2015. Arsenic and antimony in water and wastewater: Overview of removal techniques with special reference to latest advances in adsorption. *Journal of Environmental Management*, 151, pp. 326-342.

World Health Organization (WHO) 2017 Guidelines for drinking-water quality: fourth edition incorporating the first addendum. Geneva: Switzerland. Licence: CC BY-NC-SA 3.0 IGO.

# Chapter 2: Literature Review

## 2.1 Introduction

Arsenic is the 20th most commonly-available trace element in the earth's crust. It is widely distributed in the natural environment and is also present in living organisms, human bones and soft tissues at trace levels (Kang et al., 2011; Navoni et al., 2014). Its products are mainly used in medicine and during the manufacture of products such as lasers and semiconductors, as well as in the processing of glass, pigments, textiles, paper, metal adhesives, wood preservatives and ammunition (Mandal and Suzuki, 2002). The presence of arsenic at elevated concentration in groundwater has drawn nationwide attention due to its far-reaching health implications and it is now considered as one of the most serious global threats to human health (Hong et al., 2014, Ayotte et al., 2015). This section presents a review of literature related to arsenic, its occurrence, distribution and factors affecting its distribution, effects on human health, history and development of its guideline standards for human consumption, status of arsenic in South Africa and present methods used for arsenic removal.

## 2.2 Arsenic in Groundwater

### 2.2.1 Occurrence of Arsenic in Groundwater

The contamination of groundwater by arsenic may occur via natural and anthropogenic process. Naturally arsenic may be leached into groundwater when water passes through rocks containing arsenic bearing minerals such as, pyrite ($FeS_2$), arsenopyrite ($AsFeS_2$), realgar (AsS) and orpiment ($As_2S_2$) and alluvial sediments, resulting in high arsenic concentrations in groundwater (Shankar et al., 2014). Anthropogenic activity that leads to elevated concentration of arsenic in groundwater includes, disposal of industrial chemicals, mining and smelting of iron ores and agricultural wastes (Singh et al., 2015; Cheng et al., 2016).

In groundwater, arsenic predominantly occurs in $As^{5+}$ and $As^{3+}$ oxidation states depending upon the redox potential and pH (Smedley and Kinniburgh, 2002; Pi et al., 2016). Under oxidizing conditions where Eh is greater than 600 mV, the pentavalent form of arsenic predominates and it exist $H_2AsO_4^-$ at pH below 6.9 and as $HAsO_4^{2-}$ at alkaline pH conditions (Zhang et al., 2017). Furthermore, at strong acidic and alkaline condition As(V) exist as $H_3AsO_4^0$ and $AsO_4^{2-}$, respectively (Sarkar and Paul, 2016). The trivalent species of arsenic (As(III) is commonly found in reducing environments as $H_3AsO_3^0$ at a pH less than 9 and as $H_2AsO_3^-$ $HAsO_3^{2-}$ and $AsO_3^{3-}$ at

higher pH conditions (Smedley and Kinniburgh, 2002). Figure 2.1 depicts pH-Eh diagram for aqueous As species.

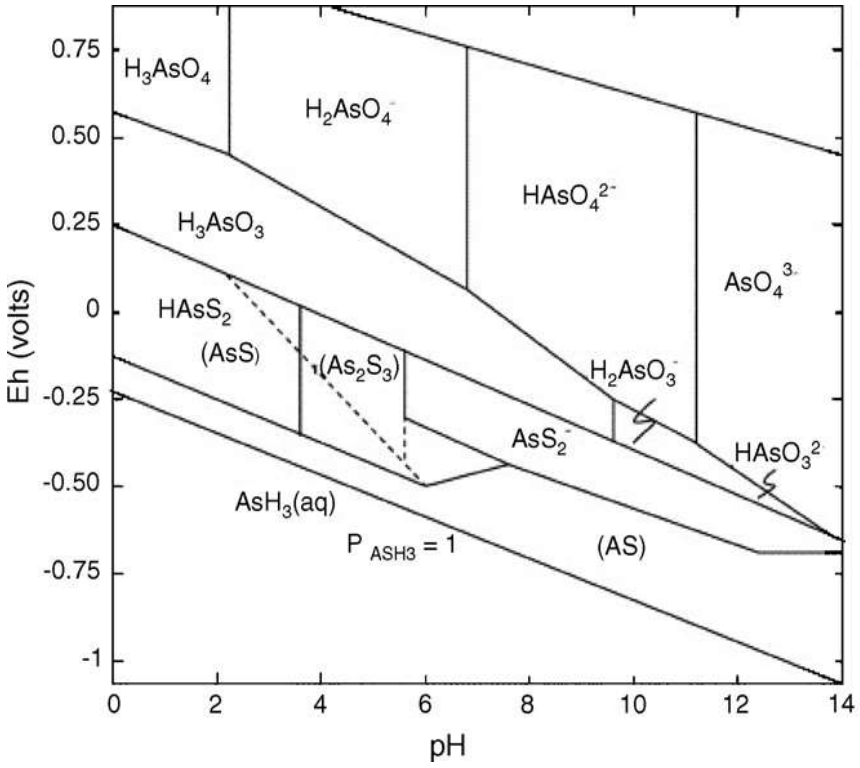


Figure 2.1: The Eh–pH diagram for arsenic (Mohan and Pittman, 2007).

### 2.2.2 Mobilisation of Arsenic in Groundwater

The mobility of arsenic in groundwater is influenced by various factors including the groundwater pH, presence of organic matter, water table, water saturation of sediments, limited supply of sulphur and microbial activities, groundwater flow direction, age of groundwater and topography (Sridharan and Nathan, 2018). Despite this factors, several studies have established three major mechanisms which triggers desorption of arsenic into the groundwater. These mechanisms includes oxidation and dissolution of As and Fe bearing minerals, weathering and reductive dissolution of As bearing and 3) competitive exchange of As by other compatible ions (Bhattacharya et al., 1997; Smedley and Kinniburgh, 2002; Sami and Druzynski, 2003).

#### 2.2.2.1 Oxidation and Dissolution of As and Fe bearing mineral

Under oxidizing conditions, iron is released during pyrite oxidation typically precipitate to iron (III) oxides which has stronger affinity toward binding arsenic (Smedley and Kinniburgh, 2002).

This process result in higher concentration of dissolved arsenic in groundwater. Sami and Druzynski (2003) summarized this process using equation 2.1 below:

$$FeAsS + \frac{7}{2}O_2 + 4H_2O = Fe(OH)_3 + H_3AsO_4 + H_2SO_4 \quad (2.1)$$

Depending on the solution pH $H_3AsO_4$ will dissociate to form $H_2SO_4^-$ at low pH and $HAsO_4^{2-}$ at higher pH. In the absence of free oxygen, inorganic oxidation of pyrite is still possible leading to dissolution of arsenic. This occurs in anoxic conditions via two step bacterially meditated process involving nitrates (Sami and Druzynski, 2003).

### 2.2.2.2 Weathering and Reductive Dissolution of As bearing

Under strong reducing conditions, weathering of iron oxyhydrates from base metal sulphide sediments could facilitate the release of arsenic into groundwater (Battacharya et al., 1997). The common cause of this is the rapid accumulation and burial of sediments which create a conducive environment for the reduction to occur (Smedley and Kinniburgh, 2002). The rate at which the reducing conditions are formed depend on the amount of organic contents. The reduction of organic matter could involve the reduction of iron oxyhdrixides and ferric oxides to release $As^{3+}$ and $Fe^{2+}$ to groundwater based on equation 2.2 (McArther, 1999).

$$4Fe(As)OOH + CH_2O + 7H_2CO_3 \rightarrow 4Fe^{2+}As^{3+} + 8HCO_3^- + 6H_2O \quad (2.2)$$

### 2.2.2.3 Competitive exchange between As and other major ions

The major ions such as $HCO_3^-$, $H_2PO_4^-$, $NO_3^-$, $Cl^-$, $Mg^{2+}$, $Na^+$ and $Ca^{2+}$ may inhibit or promote the mobilization of arsenic (Zhang et al., 2017). Under higher strong alkaline conditions, the weathering of rock mineral which release phosphate, silicate and bicarbonates and ion exchange combined with evaporation in arid and semi-arid regions favours the desorption of arsenic into the groundwater (Smedley and Kinniburgh, 2002). The ion exchange process between As and $HCO_3^-$, $PO_4^{2-}$ and $NO_3^-$ was also supported as the mechanism resulting in elevated arsenic concentration by Sridharan and Nathan (2018) who also indicated that arsenic mobilization is also facilitated by the weathering of $K^+$ containing minerals.

The presence of cations such as $Mg^{2+}$, $Na^+$ and $Ca^{2+}$ facilitates the adsorption of arsenic species onto the surface and this facilitation strengthen as the concentration of these cations increases. This is attributed to the fact that cations are able to attach to the surface of the adsorbent thereby

increasing its electropositivity and strengthening the electrostatic force with arsenic (Zhang et al., 2017). This has the effect of attracting a larger number of arsenic anions to attach onto the surface of the adsorbent; thus any increase in the cations concentrations would strengthen this process. Higher concentrations of arsenic are likely going to be found in water containing higher concentration of cations. The probability of higher arsenic concentration is high in groundwater with hydrochemical facies of Ca-Mg-$HCO_3$ and Na-Cl-$HCO_3$ (Smedley et al., 2002; Zhang et al., 2017; Taheri et al., 2017).

### 2.3 Arsenic Distribution around the World

Elevated concentration of arsenic in groundwater above the WHO guideline of 10 µg/L has been reported in many countries worldwide. The most affected countries are Argentina, Bangladesh, West Bangal, India, Mexico, Mongolia, Thailand, and Taiwan. Amongst these countries Bangladesh, West Bangal and India are the worst affected countries, with more than 130 million people affected (Smedley and Kinniburgh, 2013; Fatoki et al., 2013). In Bangladesh alone, over 10 million people are reported to be at risk due to consumption of arsenic from groundwater with high arsenic concentration of about 0.5-5 mg/L (Chakaraborti, 2015). High concentrations of arsenic in Bangladesh is attributed to both natural and anthropogenic activities (Ahmad and Khan, 2015). Figure 2.2 shows the distribution of arsenic in groundwater.

Based on the information that is currently available, Africa is the least affected continent. Although this may be due to the limited research that has been conducted on arsenic availability within the continent. However, there have been some cases of arsenic contamination of groundwater in Ghana, Burkina Faso, Zimbabwe and South Africa (Sami and Druzynski, 2003; Fakoti et al., 2013). In South Africa, higher arsenic concentrations have been reported in some parts of Northern Cape and Limpopo Province, where the concentration is said to be as high as 1000 µg/L and 114 µg/L, respectively (Sami and Druzynski, 2003).

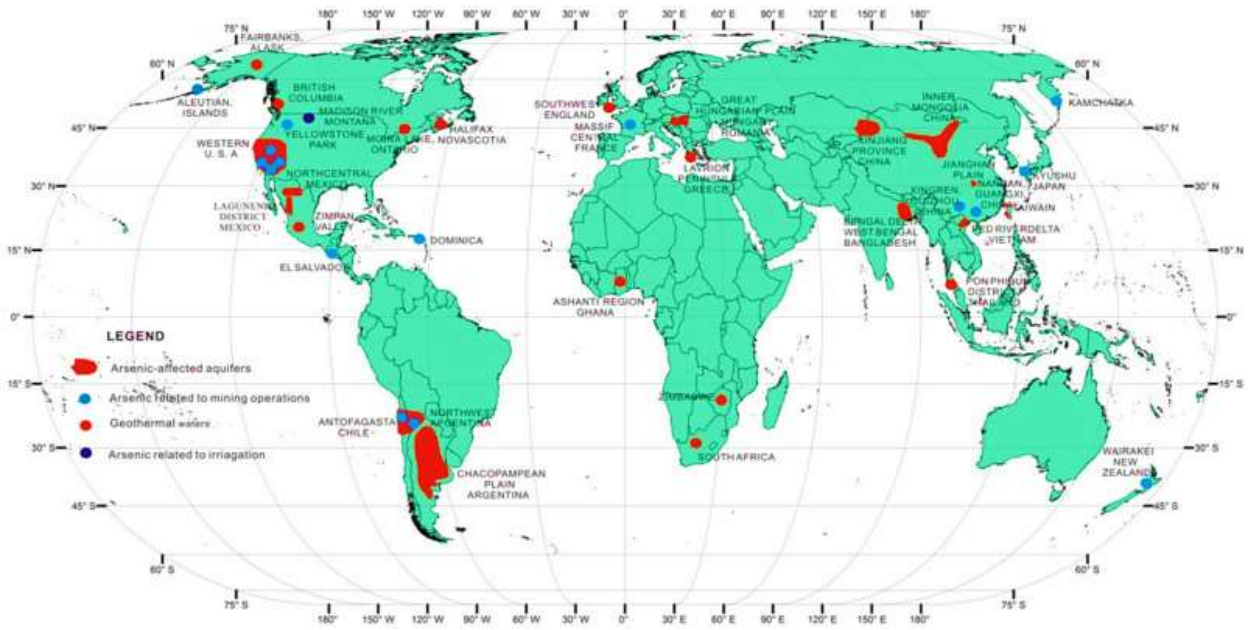


Figure 2.2: Distribution of well-known arsenic pollution incidences of aquifers and environmental caused by mining and geothermal waters (Zhang et al., 2017).

## 2.4 Health Effects of Arsenic

Arsenic is considered to be one of the most toxic trace elements in the environment and its presence in water is now a serious problem in several parts of the world (Shankar et al., 2014). Prolonged exposure to low or moderate arsenic concentrations through drinking water may have adverse effects, such as skin lesions, circulatory disorders, neurological complications, diabetes, respiratory complications, hepatic and renal dysfunction (Barringer and Reilly, 2013; Abdul et al., 2015). Exposure to arsenic may be acute or chronic. The symptoms of acute exposure to higher doses of arsenic develop much quicker and includes vomiting, abdominal pain and diarrhoea. These are followed by numbness and tingling of the extremities, muscle cramping and death, in extreme cases. Whereas clinical symptoms of chronic arsenic exposure develop over a prolonged period of exposure, this may lead to the development of malignant tumours (Fatoki et al., 2013; Sigdel et al., 2016). Table 2.1 summarises the health effects on major organ system of chronic exposure to arsenic.

Table 2.1: Effect of chronic exposure to arsenic on major organ system (Barringer and Reilly, 2013).

| **Major organ system** | **Health effects** |
|---|---|
| Dermal | Skin thickening, Hyperpigmentation |
| Liver | Enlargement, Jaundice, cirrhosis, non-cirrhotic portal hypertension |
| Nervous System | Peripheral neuropathy, hearing loss |
| Cardiovascular System | Blackfoot disease |
| Respiratory System | Lung Cancer |
| Endocrine System | Diabetes mellitus |

## 2.5 Arsenic Guidelines for Drinking Water

Due to the increasing number of population at risk of arsenic exposure, the World Health Organization (WHO) has set a guideline value for arsenic in drinking water at 0.01 mg/L (WHO, 2017). Historically, WHO had set a limit of 0.2 mg/L in 1958, which was reduced to 0.05 mg/L in 1963 and further reduced to 0.01 mg/L in 1993. This was due to ongoing concerns regarding its carcinogenicity in human. The WHO guideline value was therefore adopted by many nations, including South Africa, the United States and Canada. Other countries like China, India, Bangladesh, Argentina and Ghana are still using the old WHO limit of 0.05 mg/L. These countries are failing to enforce lower standards due to lack of sampling programmes, analytical equipment, and funding (Smith and Smith, 2004).

## 2.6 Arsenic Remediation

The chronic effects of arsenic on human beings are irreversible and therefore efforts should be directed towards prevention. Prevention can be done by either provision of arsenic-free water and in cases where there is no arsenic-free water available, the viable option is arsenic removal. Various technologies for arsenic removal have been improvised and reported in the literature. These technologies include oxidation, precipitation and coagulation, adsorption, ion exchange and membrane techniques (Langsch et al., 2012; Litter, 2012).

### 2.6.1 Oxidation

The removal of arsenite [As(III)] using adsorption, precipitation and coagulation requires oxidation to convert it to arsenate [As(V)]. It has been reported that As(III) weakly adsorbs to coagulants and adsorbents (O'Farrell et al., 2016). The oxidation stage is considered the initial stage of treatment to enable efficient production of arsenate that is easier to remove. Commonly used arsenic oxidation agent include oxygen, ozone, microorganisms, chlorine, hydrogen peroxide, manganese oxide and ferrous oxides (Shankar et al., 2014; Ungureanu et al., 2015; Xie et al., 2016). Arsenic oxidation followed by precipitation and coagulation or adsorption is effective for the removal of arsenic from the aqueous solution. This is because arsenate produced after oxidation is in ionized form at a wide range of pH. This increases the affinity for the adsorbent. Ocinski et al., (2016) evaluated the use of Fe/Mn coated adsorbent for the adsorption of arsenic from groundwater and maximum adsorption capacity for As(III) and As(V) of 132 mg/g and 77 mg/g, respectively were reported. Higher adsorption capacity for arsenite was attributed to its oxidation by iron oxides prior to adsorption, which was accompanied by the release of $Mn^{2+}$ cations followed by their adsorption on the sorbent surface.

Cheng et al. (2016) reported the adsorption, oxidation and reduction behaviour of Fe/Al bimetallic particles on the adsorption of As from water and concluded that Fe/Al bimetallic particles has enhanced As adsorption. This was attributed to oxidation and reduction of As(III) by Fe oxide prior to adsorption.

**Advantages of oxidation:**

- It oxidizes other impurities and kills microbes;
- It is relatively simple and rapid process;
- It does not generate residues that require disposal.

**Disadvantages of oxidation:**

- It mainly removes As(V) and accelerates the oxidation process for As(III) for adsorption and precipitation processes.

### 2.6.2 Adsorption

Adsorption is considered as the most cost competitive and effective method for arsenic removal (Lata and Sammader, 2016). It involves the passage of arsenic-rich water through an adsorbent bed, and arsenic is removed through physical ion-exchange or surface chemical reaction with an adsorbent. Physical adsorption occurs via van der Waals forces of attraction only, whereas chemical adsorption involves chemical interactions of the solute molecules with the solid surface of the adsorbent. Different adsorbents have been evaluated for use in arsenic removal. These include coal fly ash (Wang et al., 2008), red mud (Li et al., 2010), activated alumina (Camacho, 2015), activated carbon (Hassan et al., 2014) clay soils (Bentahar, 2016) and metal hydroxide (Kumar et al., 2016).

Sorption of arsenic onto iron(III) oxides and manganese oxide has been extensively studied and has shown greater potential for adsorption of arsenic as possess high binding affinity towards both arsenate and arsenite (Mishra and Mahato, 2016). Their higher sorption affinity may be attributed to their ability to oxidize As(III) to As(V), which can be easily adsorbed. The use of iron oxides modified sand, clay soils, activated carbon and activated alumina in adsorption of arsenic have been well documented and it was found that Fe-coated adsorbents exhibit higher arsenic adsorption capacity.

Recently, inorgano-organo modified clays have been successfully developed for use in arsenic adsorption. They exhibit high efficiency for both As(V) and As(III) species due to their important feature of having multiple sorption sites which are capable of removing different types of pollutants namely, organic and inorganic pollutants from the aqueous solutions simultaneously (Tiwari and Lee, 2016). Hua (2015) synthesized the complex modified bentonite with manganese oxides and polydimethyldiallylammonium chloride (PDMDAAC). The adsorbent showed the best adsorption properties for arsenic, which could be due to a synergistic effect between PDMDAAC and manganese oxides during modification process.

**Advantages of Adsorption:**

- It is relatively well-known and commercially available;
- It uses materials that are widely available in nature;
- It is cost effective.

**Disadvantages of Adsorption:**

- Needs replacement after four to five regeneration cycles;
- Not standardized and sometimes produces toxic solid waste.

### 2.6.3 Precipitation and Coagulation

Coagulation/ precipitation is the common and effective process for arsenic removal from water. The process involves three main steps namely, electrolytic coagulation, precipitation and filtration (Kowalski, 2014, Shaoxian & Marisol, 2014). Electrolytic coagulation is the first step, whereby arsenic colloidal solid particles suspended in water aggregates into coagulates in the process of $Al^{3+}$ and $Fe^{3+}$ electrolytic ions. This is followed by the precipitation step, whereby arsenate ions in the water would form ferric arsenate ($FeAsO_4$) or aluminum arsenate ($AlAsO_4$) precipitates, and lastly filtration, where in arsenic bearing precipitates are separated from the solution. Coagulation and precipitation is however found to be more effective to arsenate than to arsenite. As such for efficient removal of arsenic from water where both forms of arsenic are present or where only As(III) is present, it is necessary to oxidize As(III) in to As(V).

**Advantages Precipitation and Coagulation:**

- Major advantage of precipitation is that it permits large-scale treatment at relatively low cost;
- Good for community water supply scheme as it also removes other suspended solids in case of surface water source.

**Disadvantages Precipitation and Coagulation:**

- Low removal efficiency for As(III) and pre-oxidation may be required;
- Produces toxic sludge that require disposal.

### 2.6.3 Membrane Techniques

The membrane processes used in arsenic removal from contaminated water includes reverse osmosis, filtration and electro-dialysis. The removal of arsenic through membranes depends on two major principles; namely, size exclusion and Donnan exclusion (Uddin et al., 2007, Sarkar and Paul, 2016). Size exclusion is based on the sieving mechanism that separates arsenic from a solution based on relative particles sizes and the pore size of the membrane. The Donnan exclusion principle, on the other hand, concerns the type and magnitude of the electrostatic charge on the

surface of the membrane and the components of interest. Basically it is the charge repulsion phenomenon that causes the desired separation.

### 2.6.3.1 Filtration Technique

Arsenic can be present in water in a particulate and colloidal which can be removed through the filtration processes. It uses micro-filters with a pore diameter of 0.08-2 µm of ultra-filters with the pore diameter of 0.005 to 0.02 µm (Sarkar and Paul, 2016). The mechanism for removal of arsenic is based on the size exclusion principle. Filtration technique cannot remove arsenic concentration to < 0.01 mg/L since arsenic is mostly found in dissolved state and this limits the removal via filtration process (Wimalawansa, 2013). To enhance arsenic removal via filtration processes, oxidation followed by coagulation processes are required for pre-treatment of water before filtration.

### 2.6.3.2 Reverse Osmosis

The reverse osmosis technique is an effective arsenic removal technology that is commonly used for both small scale and pilot scale. In reverse osmosis systems, contaminated water is pumped under high pressure through synthetic membranes with extremely small pores (Alarcón-Herrera et al., 2013). Diffusion and sieving mechanisms are the two basic mass transport mechanisms involved in reverse osmosis. In diffusion mechanism, the movement of solute and solvent is controlled by the molecular diffusion in the polymer and it is driven by concentration gradients set up within the membrane by the applied pressure difference. In sieve type mechanism, the solvent and solute move through the micro-pores in essentially viscous flow. Reverse osmosis systems can remove up to 100% of arsenate but can be significantly less efficient in removing arsenite. Chlorination of feed water improves the arsenite removal efficiency through reverse osmosis up to 91% from groundwater by oxidizing the $As^{3+}$ to $As^{5+}$ (Walker et al., 2008). Oxidation of arsenite is not recommended in reverse osmosis because the use of an oxidizing agent may damage the membrane (Abejon et al., 2015).

**Advantages of Membrane Technique:**

- Membrane technologies can effectively remove portions of dissolved solids, including arsenic from feed water and even removes microorganisms;
- Membrane does not accumulate arsenic, so its disposal is easy;

- It does not require routine maintenance operation requirements.

**Disadvantage of Membrane Technique:**

- It has low volumetric flux;
- High capital and running costs.

### 2.6.4 Ion Exchange

In ion exchange technique, well-designed synthetic resins are used as sorption media where arsenic is removed by exchanging with ions attached to the resins. Resins are made from organic, inorganic or natural polymeric materials that contain ionic functional groups to which exchangeable ions are attached (Sarkar and Paul, 2016). Chloride based resins are commonly used for arsenic removal by ion exchange through the exchange with $Cl^-$ anions in the resin. At neutral pH As(V) is found in anionic form and can be held electrostatically on the resin sites. As(III) is neutrally charged species and cannot be removed easily, an oxidation step is required prior to treatment of arsenite solution (Ungureanu et al., 2015). The arsenic removal by chloride resins can be represented by equation 2.3, where **R** represents ion exchange resins and $Cl^-$ is an ion attached to the resin.

$$2\mathbf{R}\text{-Cl} + HAsO_4^{2-} \leftrightarrow \mathbf{R}_2HAsO_4 + 2Cl^- \quad (2.3)$$

The ion exchange resin may be periodically regenerated to remove the adsorbed contaminants and reload the exchanged ions. Regeneration of the resin using NaCl as regeneration agent is represented by equation 2.4 below.

$$\mathbf{R}_2HAsO_4 + 2Na^+ + 2Cl^- \leftrightarrow 2\mathbf{R}\text{-Cl} + HAsO_4^{2-} + 2Na^+ \quad (2.4)$$

**Advantage of Ion Exchange:**

- With ion exchange it is possible attain an outlet arsenic concentration equal or below 1 mg/L.

**Disadvantage of Ion Exchange:**

- The main disadvantage is the influence of competing anions that limit the application ion exchange resins in arsenic removal;
- High cost medium; high-tech operation and maintenance.

## 2.7 Arsenic Removal at Small-scale and Household level

Arsenic removal technologies rely on basic chemical and physical processes that can either be applied alone, simultaneously or in sequence. These processes include oxidation, adsorption, co-precipitation and filtration, ion exchange and membrane techniques (Litter et al., 2012). For small scale and household water treatment, technology should be economically feasible, have a high removal efficiency and be easy to operate (Delowar et al., 2006; Shafiquzzaman et al., 2011). Furthermore, it should make use of material that can be regenerated and does not generate waste that will require disposal. Different small-scale and household technologies for arsenic removal have been developed and are currently in use. These include Steven Institute Technology and two bucket treatment (Ahmed, 2001), three-pitcher and natural iron-sand filter (Delowar et al., 2006).

### 2.7.1 Bucket treatment unit

This method of removing arsenic is based on the principles of oxidation, coagulation, co-precipitation and adsorption (Ahmed, 2001). Two buckets of 20 litres each are placed above one another. Arsenic rich water is then poured in the top bucket. This is followed by the addition of coagulants or oxidants in powder form. The mixture is then stirred vigorously using a stick for two minutes. Thereafter the mixture is stirred gently to allow flocculation for another two or three minutes. The mixture is then allowed to settle for two hours. After settling the supernatant water from the top bucket is then gently poured into the bottom bucket which is filled with filter and adsorbent sand and which removes the remaining micro-flocculants. A schematic diagram of the two-bucket treatment unit is shown in Figure 2.3. The use of this unit is discouraged in areas having arsenic concentrations above 500 ppb as it may not remove it up to the desired levels. This device was easily adopted among rural masses in Bangladesh and India by keeping the chemicals involved and raw material for buckets locally available to keep its cost low enough for the poor (Luqman et al., 2013).

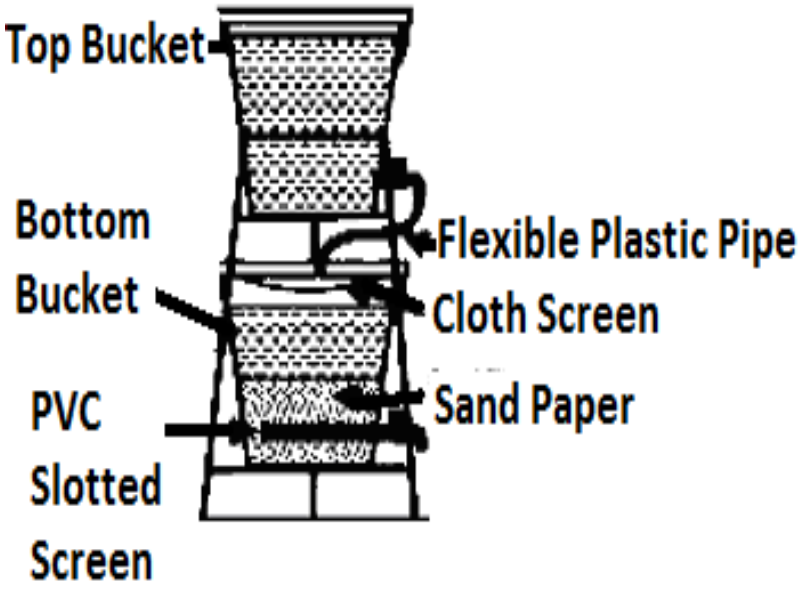


Figure 2.3: A schematic diagram of the two bucket treatment (Luqman et al., 2013).

### 2.7.2 Steven Institute Technology

This technology involves the use of two buckets and it uses the coagulation and co-precipitation principle, followed by filtration to remove arsenic from water. The other bucket is for mixing water with the coagulants either iron sulfate and calcium hypochloride and the other bucket removes flocs through sedimentation and filtration. After the addition of chemicals, large visible coagulates are formed with continuous stirring using stick. This technology has shown a reduced arsenic concentration by up to a concentration below 50 µg/L in 80-95% of the samples tested. The sand bed used for filtration requires washing at least twice a week to remove flocs (Ahmed, 2001). Figure 2.4 shows the schematic diagram of Steven Institute Technology.

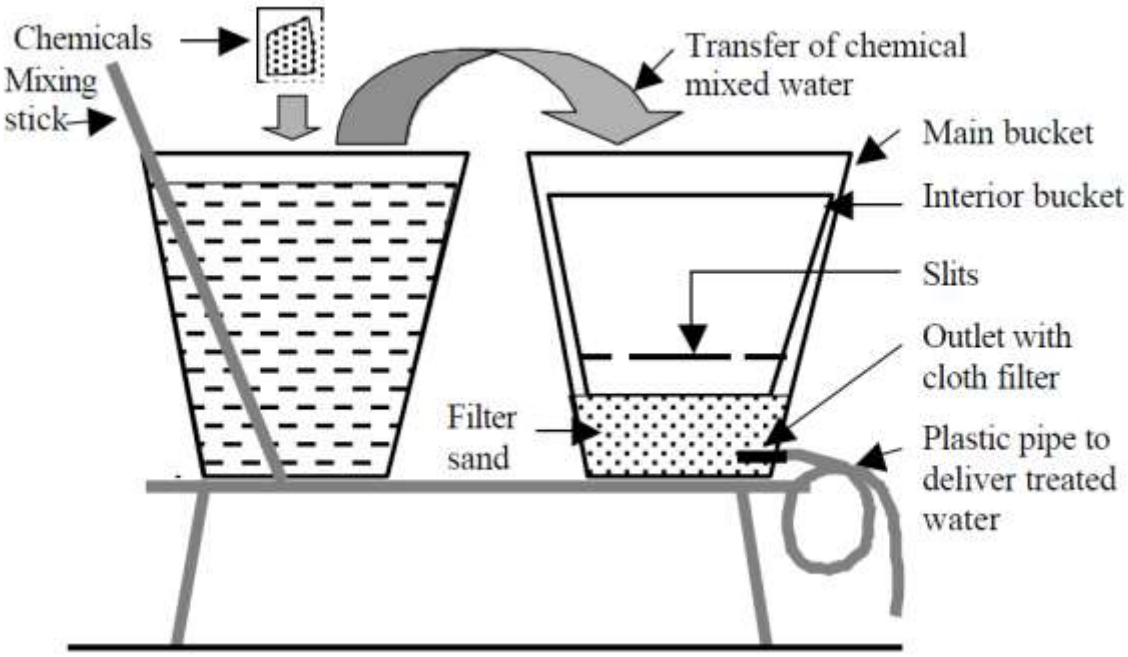


Figure 2.4: Steven Institute Technology for arsenic removal (Ahmed, 2001).

### 2.7.3 Three-pitcher method

This method is commonly applied for arsenic removal in Bangladesh and it was described by Khan et al., (2000). The system consists of three earthen pitchers (also called kolshis) placed over the other supported by the stand (Figure 2.5). The first and the second pitchers have a small opening that is covered with a polyester cloth at the bottom. Above the cloth in the top pitcher a bed of coarse sand and casting irons is placed to form a brickettes and in the middle pitcher. The brickettes are made of fine sand and charcoal that is placed above the cloth. Arsenic-rich water is poured into the top most pitcher and water passes through to the middle pitcher then to the bottom one, where arsenic free water is collected. This method uses locally available material and is therefore cost-effective and is used for arsenic removal at household level in rural areas of India and Bangladesh. The experiment reported by Khan et al., (2000) showed that arsenic concentrations can be lowered to < 10 µg/L for most of the treated samples even for samples having initial concentrations of 1100 µg/L.

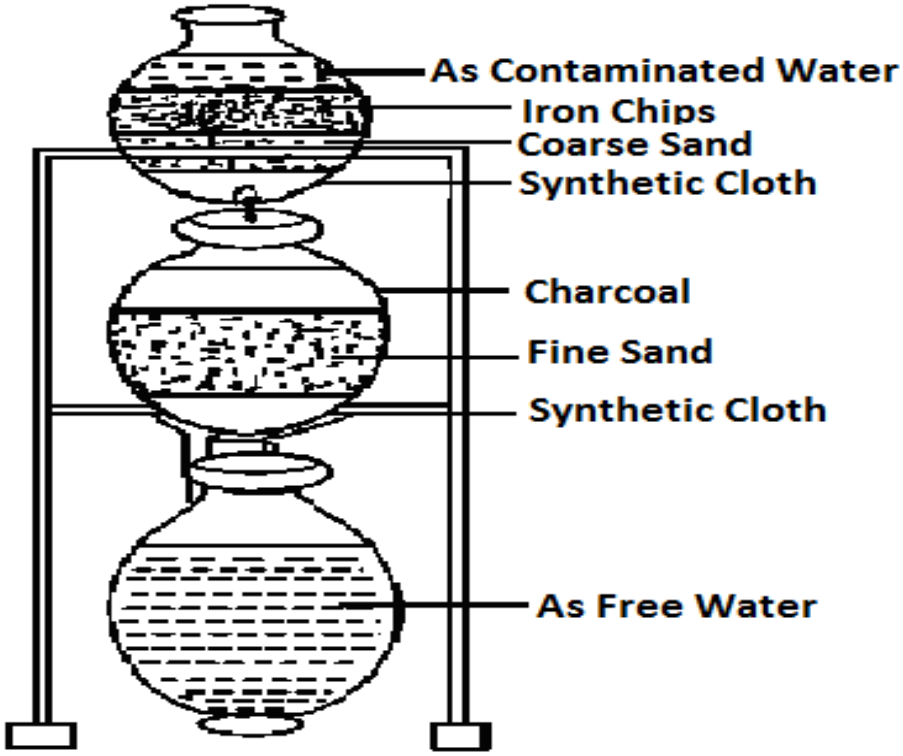


Figure 2.5: Schematic diagram for three pitcher method (Khan et al., 2000).

**2.8 Arsenic removal using clay soils**

Clay minerals are fine hydrous aluminosilicates with traces of iron, magnesium and other cations and anions. Clay soils possess firmly and structurally-arranged layered sheets of aluminosilicates in their crystalline structure. Each layer consists of two, three or four sheets of tetrahedral (T) $[SiO_4]^{4-}$ or octahedral (O) $[AlO_3(OH)_3]^{6-}$ units (Bhattachryya and Gupta, 2008). The interiors of these sheets are composed of smaller cations and their apices are occupied by oxygen from which some are bonded with protons such as -OH. This basic structural element is arranged to form a hexagonal network with each sheet (Mohan and Pittman, 2007; Hua, 2015). Recently clay soils have received great attention for use in water treatment due to their physicochemical properties such as high specific surface area, chemical and mechanical stability, high cation and anion exchange capacity and negative/positive character of surface and they have shown high adsorption capacity (Lee and Tiwari, 2012). Moreover, the adsorption capacity of clay can be improved by modification with polycation (such as, $Fe^{3+}$ $Al^{3+}$, $Mn^{2+}$) and cationic surfactant. The modification involves the replacement of exchangeable cations such as $Na^{+}$, $Ca^{2+}$, $K^{+}$ and $Mg^{2+}$ from the clay interlayers. Several studies on arsenate and arsenite removal using clay minerals and their oxides

from water have been reported. These include studies on surfactant modified bentonite clay (Su et al., 2011), aluminum pillared hexadecylammonium bromide (HDTMA) and alkyldimethylbenzylammonium Chloride (AMBA) modified sericite (Tiwari and Lee, 2012), ferric oxide modified diatomite (Knoerr et al., 2013), modified montmorillonite (Ren et al., 2014) bentonite based inorgano–organo-composites (Hua, 2015), kaolinite clay (Ding et al., 2015), hexadecylammonium bromide and aluminium modified bentonite and local clay soils (HDTMA-Al-bentonite and HDTMA-Al-local clay (LCAH)) materials (Lee et al., 2015), Moroccan clays (Bentahar et al., 2016), iron oxide and manganese oxide pillared clays (Mishra and Mahato et al., 2016).

### 2.9 Summary and the knowledge gaps

Arsenic is a trace element that has detrimental effects on human health after a long period of exposure. It is estimated that more than 200 million people worldwide are at risk of arsenic related diseases. The worst affected countries includes Bangladesh, India, China, Mexic, Thailand and Argentina. Little is known about the distribution of arsenic in African continent although higher concentration has been reported in some parts of Burkina Faso, South Africa, Ghana, Zimbabwe and Ethiopia. With little information available in Africa, the population which is at risk remain unknown. As such there is a need for studies that focuses on determination of arsenic in African waters particularly groundwater which is the main source of water for drinking purposes in majority of rural areas.

There are various techniques that are available for arsenic remediation. This includes adsorption, ion-exchange, membrane based techniques and precipitation and coagulation. Amongst these techniques, adsorption is often preferred for use in rural areas since it uses materials that are largely available in nature at little or no cost, easy to operate and has higher removal efficiency. Most of the proposed materials are effective at a narrow pH range and some cannot be regenerated effectively, while some are more effective towards As(V) which is known to be less toxic as compared to As(III). As such there is a need to develop a material that will be effective at wide range pH and have higher removal efficiency towards As(III) which is known to be more toxic. Furthermore, such adsorbent should be of low cost and be regeneratable to make it more sustainable for use in rural areas of African continent.

## References

Abdula, K. S. M. Jayasingheb, S. S. Chandanaa, E. P. S. Jayasumanac, C. P. & De Silva, M. C. S., 2015. Arsenic and human health effects: A review. *Environmental Toxicology and Pharmacology*, 40, pp. 828-846.

Abejón, A. Garea, A. & Irabien, A., 2015. Arsenic removal from drinking water by reverse osmosis: Minimization of costs and energy consumption. *Separation and Purification Technology*, 144, pp. 46-53.

Ahmad, S. A. & Khan, M. H., Ground Water Arsenic Contamination and Its Health Effects in Bangladesh. In S.J.S. Flora (Ed): Handbook of Arsenic Toxicology. 2015. Elsevier Inc.

Ahmed, M.A. (2001). 'An overview of arsenic removal technologies in Bangladesh and India'. In: Ahmed, M.F.; Ali, M.A. and Adeel, Z. (eds). Technologies for arsenic removal from drinking water: a compilation of papers presented at the International Workshop on Technologies for Arsenic Removal from Drinking Water. Dhaka, Bangladesh, Bangladesh University of Engineering and Technology and United Nations University. pp. 251-269.

Alarcón-Herrera, M. T., Bundschuh, J. Nath, B. Nicolli, H. B. Gutierrez, M. Reyes-Gomez, V. M. Nunez, D. Martín-Dominguez, I. R. Sracek, O., 2013. Co-occurrence of arsenic and fluoride in groundwater of semi-arid regions in Latin America: Genesis, mobility and remediation. *Journal of Hazardous Materials*, 262, pp. 960-969.

Ayotte, J. D. Belaval, M. Olson, S. A. Burow, K. R. Flanagana, S. M. Hinkle, S. R. & Lindsey, B. D. 2015. Factors affecting temporal variability of arsenic in groundwater used for drinking water supply in the United States. *Science of the Total Environment*, 505, pp.1370–1379.

Barringer, J. L. & Reilly, P. A., 2013. Arsenic in groundwater: A summary of sources and the biogeochemical and bydrogeologic factors affecting arsenic occurrence and mobility. U.S. Geological Survey, USA.

Bentahar, Y., Hurel, C., Draoui, K., Khairoun, S. & Marmier, N., 2016. Adsorptive properties of Moroccan clays for the removal of arsenic(V) from aqueous solution. *Applied Clay Science* 119, pp. 385–392.

Bhattacharya, P., Chatterjee, D. & Jacks, G., 1997. Occurrence of Arsenic-contaminated Groundwater in Alluvial Aquifers from Delta Plains, Eastern India: Options for Safe Drinking Water Supply. *International Journal of Water Resources Development*, 13(1), pp. 79-92.

Bhattachryya, K. G. & Gupta, S. S., 2008. Adsorption of few heavy metals on natural and modified kaolinite and montmorillonite: A review. *Advances in colloid and interface science*. 140, pp. 114-131.

Camacho, L. M. Ponnusamy, S. Campos, I. Davis, T. A. & Deng, S., Evaluation of Novel Modified Activated Alumina as Adsorbent for Arsenic Removal. In S.J.S. Flora (Ed): Handbook of Arsenic Toxicology. 2015. Elsevier Inc.

Chakraborti, D., Rahman, M. M., Mukherjee, A., Alauddin, M., Hassan, M., Dutta, R. N., Pati, S., Makherjee, S. C., Roy, S., Quamruzzman, Q., Rahman, M., Morshed, S., Islam, T., Sorif, S., Selim, M., Islam, R., Hossain, M., 2015. Groundwater arsenic contamination in Bangladesh—21 Years of research. *Journal of Trace Elements in Medicine and Biology*, 31, pp. 237–248.

Cheng, Z. Fu, F. Dionysiou, D. D. & Tang, B. 2016. Adsorption, oxidation, and reduction behaviour of arsenic in the removal of aqueous As(III) by mesoporous Fe/Al bimetallic particles. *Water Research*, 96, pp. 22-31.

Delowar, H. K. M. Uddin, I. El Hassan, W. H. A. Perveen, M. F. Irshad, M. Islam, A. F. M. S. & Yoshida, I., 2006. A comparative study of household groundwater arsenic removal technologies and their water quality parameters, *Journal of Applied Sciences*, 6(10), pp. 2193–2200.

Ding, W., Wang, Y, Yu, Y, Zhang, X., Li, J. & Wu, F., Photooxidation of arsenic(III) to arsenic(V) on the surface of kaolinite clay. *Journal of Environmental Sciences*, 23, pp. 29-37.

Fatoki, O. S. Akinsoji, O.S. Ximba, B.J. Olujimi, O. & Ayanda, O.S., 2013. Arsenic Contamination: Africa the Missing Gap. *Asian Journal of Chemistry*, 25(16), pp. 9263-9268.

Hassan, A. F. Abdel-Mohsen, A. M. & Elhadidy, H., 2014. Adsorption of arsenic by activated carbon, calcium alginate and their composite beads. *International Journal of Biological Macromolecules*, 68, pp. 125-130.

Hong, J., Zhu, Z., Lu, H. & Qiu Y. 2014. Synthesis and arsenic adsorption performances of ferric-based layered double hydroxide with alanine intercalation. *Chemical Engineering Journal*, 252, pp.267–274.

Hua, J., 2015. Synthesis and characterization of bentonite based inorgano–organo-composites and their performances for removing arsenic from water. *Applied Clay Science*, 114, pp. 239-246.

Kang, Y. Liu, G. Chou, C. Wong, M. H. Zheng, L. & Ding, R., 2011. Arsenic in Chinese coals: Distribution, modes of occurrence and environmental effects: Review. *Science of the Total Environment*, 412-413, pp. 1-13.

Khan, A. H. Rasul, S. B. Munir, A. K. M. Habibuddowla, M. Alauddin, M. Newaz, S. S. & Hussam, A., 2000. Appraisal of a simple arsenic removal method for groundwater of Bangladesh. *Journal of environmental science and health*, A35 (7), pp. 1021-1041.

Knoerr, R. Brendlé, J. Lebeau, B. & Demais, H., 2013. Preparation of ferric oxide modified diatomite and its application in the remediation of As(III) species from solution. *Microporous and Mesoporous Materials*, 169, pp.185-191.

Kowalski, K. P., 2014. Chapter 8: Advanced arsenic removal technologies review. Elsevier B.V.

Kumara, P. S. Floresa, R. Q. Sjöstedt, C. & Önnbya, L. 2016. Arsenic adsorption by iron–aluminium hydroxide coated onto macroporous supports: Insights from X-ray absorption spectroscopy and comparison with granular ferric hydroxides. *Journal of Hazardous Materials*, 302, pp. 66-174.

Langsch, J. E. Costa, M. Moore, L. Morais, P. Bellezza, A. & Falcão, S., 2012. New technology for arsenic removal from mining effluents. *Journal of Materials Research and Technology,* 1(3), pp.1 78-181.

Lata, S. & Samadder, S. R., 2016. Removal of arsenic from water using nano adsorbents and challenges: A review. *Journal of Environmental Management,* 166, pp. 387-406.

Lee, S. M. & Tiwari, D., 2012. Organo and inorgano-organo-modified clays in the remediation of aqueous solutions: An overview. *Applied Clay Science*, 59(60), pp. 84-102.

Lee, S. M., Lalhmunsiama, Thanhmingliana, &Tiwari, D., 2015. Porous hybrid materials in the remediation of water contaminated with As(III) and As(V). *Chemical Engineering Journal,* 270, pp.496-507.

Li, Y. Wang, J. Luan, Z. & Liang, Z., 2010. Arsenic removal from aqueous solution using ferrous based red mud sludge. *Journal of Hazardous Materials,* 177, pp. 131-137.

Litter, M. I., Alarcón-Herrera, M. T., Arenas, M. J., Armienta, M. A. & Avilés, M., et al., 2012. Small-scale and household methods to remove arsenic from water for drinking purposes in Latin America. *Science of the Total Environment*, 429, pp. 107–122.

Luqman, M. Javed, M. M. Yasar, M. Ahmad, J. & Khan, A., 2013. An overview of sustainable techniques used for arsenic removal from drinking water in rural areas of the Indo-Pak subcontinent. *Soil Environment*, 32(2), pp. 87-95.

Mandal, B. K., Suzuki, K. T., 2002. Arsenic round the world: a review. *Talanta,* 58 (1), pp.201-235.

McArthur, J. M. (1999). Arsenic poisoning in the Ganges delta. *Nature*, 401, pp. 545-547.

Mishra, T. & Mahato, D. K., 2016. A comparative study on enhanced arsenic(V) and arsenic(III) removal by iron oxide and manganese oxide pillared clays from ground water. *Journal of Environmental Chemical Engineering*, 4, pp. 1224–1230.

Mohana, D. & Pittman, C. U, 2007 Arsenic removal from water/wastewater using adsorbents: A critical review. *Journal of Hazardous Materials,* 142, pp.1–53.

Navoni, J. A. De Pietri, D. Olmos, V. Gimenez, C. Mitre, G. B, De Titto, E. & Lepori, E.C. V., 2014. Human health risk assessment with spatial analysis: Study of a population chronically exposed to arsenic through drinking water from Argentina. *Science of the Total Environment,* 499, pp. 66-174.

Pi, K. Wang. Y. Xie, X. Liu, Y. Ma, T. & Su, C., 2016. Multilevel hydrogeochemical monitoring of spatial distribution of arsenic: A case study at Datong Basin, northern China. *Journal of Geochemical Exploration,* 161, pp. 16–26.

Ren, X., Zhang, Z., Luo, H., Hu, B., Dang, Z., Yang, C., & Li, L., 2014. Adsorption of arsenic on modified montmorillonite. *Applied Clay Science,* 97–98, pp. 17–23.

Sami, K. & Druzynski A. L., 2003. Predicted Spatial Distribution of Naturally Occurring Arsenic, Selenium and Uranium in Groundwater in South Africa-Reconnaissance Survey. WRC Report No. 1236/1/03.

Sarkar, A. & Paul, B., 2016. The global menace of arsenic and its conventional remediation: A critical review. *Chemosphere,* 158, pp.37-49.

Shafiquzzaman, M. Azam, M.S. Nakajima, J. & Bari, Q.H., 2010. Arsenic leaching characteristics of the sludge's from iron based removal process. *Desalination,* 261, pp. 41-45.

Shankar, S. Shanker, U. & Shikha., 2014. Arsenic contamination of groundwater: A review of Sources, prevalence, health risks, and strategies for mitigation. *The Scientific World Journal*, pp. 1-18.

Shaoxian, S. & Marisol, G., 2014. Arsenic removal from water by the coagulation process. Elsevier B.V.

Sigdel, A., Park, J., Kwak, H. & Park, P., 2016. Arsenic removal from aqueous solutions by adsorption onto hydrous iron oxide-impregnated alginate beads. *Journal of Industrial and Engineering Chemistry*, 35, pp. 277–286.

Singh, R., Singh, S., Parihar, P., Singh, V. P. & Prasda, S. M. 2015. Arsenic contamination, consequences and remediation techniques: A review. *Ecotoxicology and Environmental Safety*, 112, pp. 247–270.

Smedley P. L & Kinniburgh, D. G., 2013. Arsenic in Groundwater and the Environment. British Geological Survey, Oxfordshire, UK.

Smedley, P. L, & Kinniburgh, D. G., 2002. A review of the source, behaviour and distribution of arsenic in natural waters. *Applied Geochemistry*, 17, pp. 517-568.

Smith, A. H. & Smith, M. M. H., 2004. Arsenic drinking water regulations in developing countries with extensive exposure. *Toxicology*, 198, pp. 39-44.

Sridharan, M. & Nathan, D. S., 2018. Chemometric tool to study the mechanism of arsenic contamination in groundwater of Puducherry region, South East coast of India. *Chemosphere*. 208, pp. 303-315.

Taheri, M., Gharaie, M. H. M., Mehrzad, J., Afshari, R. & Datta, S., 2017. Hydrogeochemical and isotopic evaluation of arsenic contaminated waters in an argillic alteration zone. *Journal of Geochemical Exploration,* 175, pp. 1–10.

Tiwari, D. & Lee, S. M., 2012. Novel hybrid materials in the remediation of ground waters contaminated with As(III) and As(V). *Chemical Engineering Journal,* 204-206, pp. 23-31.

Uddin, M.T. Mozumder, M.S.I. Figoli A. & Islam, M. A., 2007. Arsenic removal by conventional and membrane technology, *Indian Journal of Chemical Technology,* 14, pp. 451– 458.

Ungureanu, G., Santos, S., Boaventura, R. & Botelho, C., 2015. Arsenic and antimony in water and wastewater: Overview of removal techniques with special reference to latest advances in adsorption, *Journal of Environmental Management*, 151, pp. 326-342.

Walker, M. Seiler, R. L. & Meinert, M., 2008. Effectiveness of household reverse-osmosis systems in a Western U.S. region with high arsenic in groundwater. *Science of the total environment*, 389, pp. 245-252.

Wang, J. Wang, T. Burken, J. G. Chusuei, C. C. Ban, H. Ladwig, L. & Huang, C.P., 2008. Adsorption of arsenic (V) onto fly ash: A speciation-based approach. *Chemosphere*, 72, pp.381-388.

Wimalawansa, S. J., 2013. Purification of contaminated water with reverse osmosis: Effective solution of providing clean water for human needs in developing countries. *International Journal of Emerging Technology and Advanced Engineering*, 3(12), pp. 75-89.

World Health Organization (WHO) 2017 Guidelines for drinking-water quality: fourth edition incorporating the first addendum. Geneva: Switzerland. Licence: CC BY-NC-SA 3.0 IGO.

Xiea, L. Liu, P. Zheng, Z. Weng, S. & Huang, J., 2016. Morphology engineering of $V_2O_5/TiO_2$ nano-composites with enhanced visible light-driven photo functions for arsenic removal. *Applied Catalysis B: Environmental*, 184, pp. 347-354.

Zhang, L., Qin, X., Tang, J., Liu, W. & Yang, H. 2017. Review of arsenic geochemical characteristics and its significance on arsenic pollution studies in karst groundwater, Southwest China. *Applied Geochemistry*, 77, pp. 80-88.

# Chapter 3: Hydrogeochemical characteristics of arsenic contaminated water in Greater Giyani Municipality, Limpopo Province, South Africa

## 3 Abstract

This chapter evaluated the hydrogeochemical characteristics of groundwater in the Greater Giyani Municipality. Field parameters such as pH, EC and TDS were determined using Crison MM40 multimeter. The elemental composition of the water samples was determined using Ion Chromatography (IC) and inductively coupled mass spectrometry (ICP-MS). The results showed that the pH of the samples ranges from neutral to weakly alkaline. The abundance of major anions and cations are in the following order: $HCO_3^->Cl^->SO_4^{2-}>NO_3^-$ and $Na^+>Mg^{2+}>Ca^{2+}>K^+>Si^{4+}$, respectively. The piper diagram revealed that the hydrogeochemical facies identified in the study area include $CaHCO_3$ (90%) and mixed $CaNaHCO_3$ (10%) which shows the dominance of water-rock interaction. The water-rock interaction was further confirmed by the Gibbs diagram. The ionic ratio showed that the major ions originate from weathering of carbonate and silicate minerals. The concentration of arsenic was found to be ranging between 0.1 to 172.53 µg/L with the average of 32.21 µg/L. About 60% of the samples had an arsenic concentration above the WHO recommended limit of 10 µg/L. Since arsenic is toxic to human health, the present study recommend that further studies should be conducted to evaluate the degree of toxicity to human health and to develop arsenic remediation techniques that are flexible and sustainable for use in Greater Giyani Municipality. Furthermore, there should be a routine monitoring of borehole water quality in the area.

Keywords: Arsenic; Groundwater quality; Hydrogeochemical feacies; Water-rock interaction; Ionic ratio.

## 3.1 Introduction

Due to prevailing arid conditions in Limpopo Province, about 75% of the population depends solely on groundwater as a source of water supply for domestic use despite its quality and quantity (Odiyo and Makungo, 2012). The quality of groundwater is governed by various parameters such as the composition of recharging water, the mineralogy, reactivity of the geological formation of the aquifer and the impact of anthropogenic activities (Kouras et al., 2007). Furthermore, the chemical constituents and their mobility in groundwater are influenced by hydrogeochemical

processes such as dissolution, precipitation, ion-exchange, sorption, and desorption as well as the residence time during water-rock interaction (Sharif et al., 2008; Taheri et al., 2017).

The contamination of groundwater by arsenic is the main concern worldwide due to its implications on human health after a prolonged exposure. Exposure to arsenic has not only been linked to cancer but also to several health problems such as kidney diseases, diabetes, skin lesions, circulatory disorders and neurological complications (Mandal and Suzuki, 2002; Ayotte et al., 2015). The contamination of groundwater often results from weathering of arsenic-bearing minerals of sulphide, silicate and carbonate minerals (Smedley and Kinniburgh, 2002). Concentrations of arsenic beyond 10 µg/L in groundwater has been reported in several countries including Bangladesh, India, China, Burkina Faso, Zimbabwe and South Africa (Fatoki et al., 2013; Kempster et al., 2006; Sharif et al., 2008; Bretzler et al., 2017).

Greater Giyani Municipality is located within Giyani Greenstone belt in Limpopo province in the North Eastern part of South Africa. The area is well known for its gold mineralization which is closely associated with quartz vein, minor sulphides and carbonate veins (Carranza et al., 2015). Sulphides are mainly comprised of pyrite and arsenopyrite which may leach arsenic into groundwater depending on pH and redox potential. Few studies have been done concerning the characterization of groundwater in Greater Giyani Municipality with respect to arsenic. Samie et al. (2013) previously reported physicochemical properties of borehole water used in selected schools within Greater Giyani Municipality. Their results showed that groundwater from these boreholes is not suitable for drinking based on hardness and nitrate content. The concentrations of other trace elements such as arsenic was overlooked in the study. As such, there is still a need to evaluate the hydrogeochemical properties of groundwater in the Greater Giyani Municipality. The objective of this investigation is, therefore, to determine the chemical composition of groundwater in selected boreholes and ascertain its suitability for drinking purpose and lastly elucidate the relationship between arsenic and other chemical composition in groundwater.

## 3.2 Material and methods

### 3.2.1 Description of the study area

Figure 3.1 presents the location of Greater Giyani Municipality. It is one of the five (5) local municipalities falling within Mopani District Municipality in Limpopo Province. The municipality comprises of 91 villages and few towns of which Giyani is the largest and most densely populated

centre being the administrative capital with a population of 256,127 and area coverage of approximately 4,172 km². Giyani lies 470 km northeast of Johannesburg by road, 104 km from Tzaneen and 105 km from the Phalaborwa Gate of the Kruger National Park. Giyani is situated within the sub-tropical zone. The climate is characterized by hot summers and mild dry winters with average summer temperatures of 35 °C frequently exceeding 40 °C and winter average temperatures of 20 °C. Rainfalls generally between November and March with an average precipitation of 750 mm per year (Billay et al., 2014).

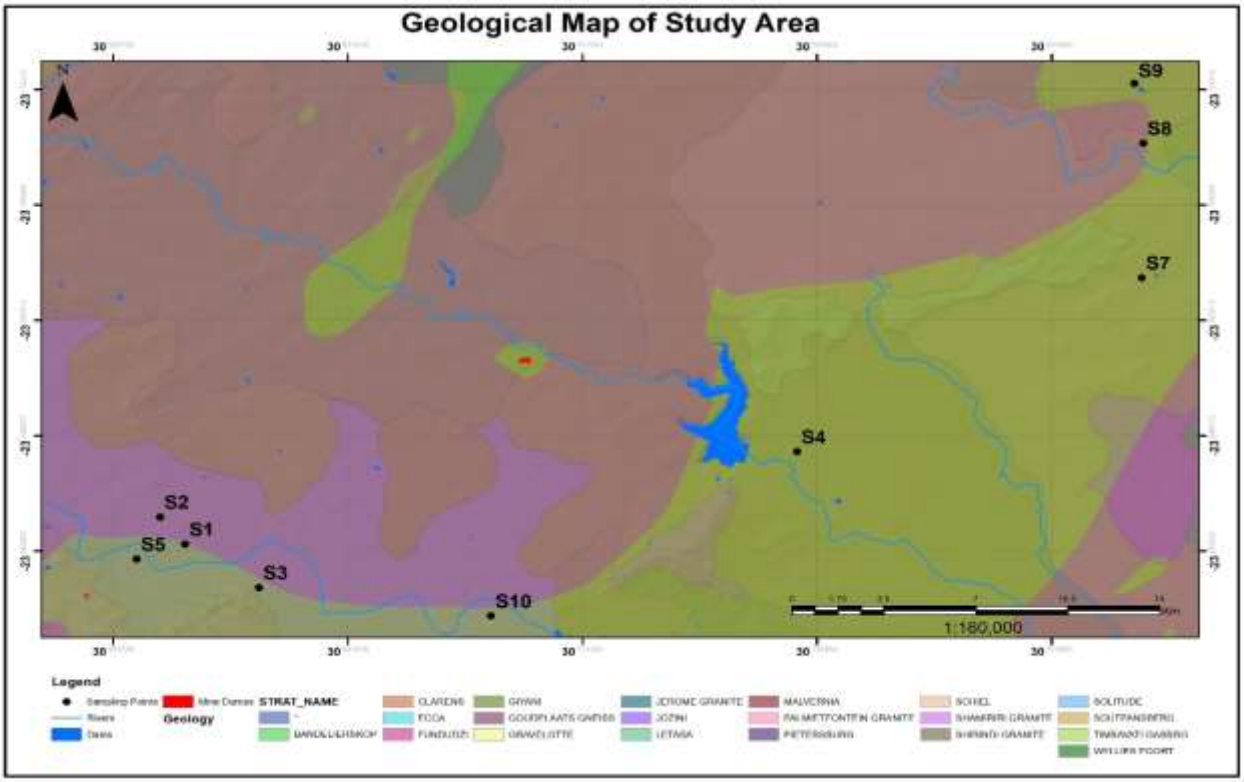


Figure 3.1: Location of the study area and sampling points.

### 3.2.2 Sampling Technique

A total of 10 groundwater samples were collected from spatially distributed boreholes in greater Giyani Municipality (Figure 3.1). The study area fall within arid to semi-arid climatic conditions and there are fewer functional boreholes and thus only ten groundwater samples could be collected. Samples were collected in duplicates using pre-cleaned 500 mL polyethene plastic bottles. The other set of samples was analyzed for anions and the other for cations. Samples for cations were acidified to pH < 2 using 3 M $HNO_3$ to prevent colloids formation. Prior to collection, water was allowed to flow freely until a stable pH, TDS and EC were recorded. The hydrochemical

parameters such as pH, TDS and EC were measured in the field using portable Crison MM40 multimeter. The instrument was calibrated prior to measurement. After collection, samples were then stored in a cooler box and transported to the laboratory where they were stored at a temperature < 4 $^{o}$C awaiting analysis.

### 3.2.3 Laboratory analysis

The anions such as $Cl^-$, $NO_3^-$ and $SO_4^{2-}$ were determined using Metrohm 850 Ion Chromatograph. The standard titrimetric method was employed to determine $HCO_3^-$ (Kouras et al., 2007). The concentration of $Na^+$, $Ca^{2+}$, $Mg^{2+}$, $K^+$, total arsenic and other metallic species were determined using Inductive Coupled Plasma Mass Spectrometry (ICP-MS) (Agilent 7900 ICP-MS, US) at the University of Stellenbosch. For quality assurance, all samples were analysed in duplicate and mean values were captured and blanks were set for control. All data were subjected to statistical evaluation employing Microsoft Office Excel 2010 while some of the graphical plots were carried out using Piper Trilinear diagram which was plotted with the aid of PAST Version 3.14.

## 3.4 Results and discussion

### 3.4.1 Major constituents of groundwater

The hydrochemical constituents of groundwater samples collected from Giyani Municipality are given in Table 3.1.

Table 3.1: Physicochemical parameters of groundwater samples collected from Greater Giyani Municipality. Except for elements marked (*) in µg/L all other elements are in mg/L.

| **Village Name** | **pH** | **TDS** | **EC (µS/cm)** | **$Cl^-$** | **$NO_3^-$** | **$SO_4^{2-}$** | **$HCO_3^-$** | **Ca** | **K** | **Mg** | **Na** | **Si** | **As*** | **Fe*** | **Mn*** | **Zn*** | **Ba*** | **B*** |
|---|---|---|---|---|---|---|---|---|---|---|---|---|---|---|---|---|---|---|
| Mapuve 1 | 6.03 | 475.30 | 791.30 | 19.20 | 2.90 | 9.58 | 54.90 | 38.60 | 23.50 | 21.60 | 56.80 | 0.02 | 0.10 | 0.60 | 11.42 | 1.12 | 0.22 | 23.20 |
| Mapuve 2 | 6.40 | 536.36 | 893.54 | 12.80 | 0.91 | 3.45 | 56.12 | 20.41 | 39.76 | 19.79 | 82.66 | 29.72 | 0.43 | 33.09 | 7.37 | 42.07 | 50.76 | 35.58 |
| Maswanganyi | 7.56 | 1862.32 | 3100.00 | 20.90 | 2.38 | 3.41 | 407.48 | 146.80 | 3.58 | 181.90 | 134.60 | 34.70 | 35.14 | 0.35 | 12.58 | 3.13 | 58.45 | 128.17 |
| Thomo | 8.01 | 1174.12 | 1958.26 | 19.24 | 1.30 | 6.16 | 627.08 | 85.86 | 11.42 | 97.21 | 173.20 | 26.00 | 0.26 | 1.30 | 1.32 | 4.80 | 270.29 | 344.77 |
| Klein Lethaba | 8.11 | 845.10 | 1409.04 | 26.20 | 0.14 | 8.91 | 902.80 | 53.11 | 4.68 | 99.83 | 85.05 | 31.86 | 172.53 | 1.53 | 0.64 | 1.82 | 117.56 | 486.76 |
| Mabangeni | 7.70 | 896.90 | 1493.01 | 16.93 | 0.10 | 21.18 | 380.64 | 106.10 | 1.10 | 86.08 | 74.12 | 33.36 | 56.65 | 0.37 | 0.92 | 3.41 | 20.84 | 71.32 |
| Muyexe | 7.82 | 1113.69 | 1865.20 | 21.70 | 2.56 | 9.22 | 256.20 | 96.41 | 2.82 | 123.60 | 78.23 | 43.22 | 12.30 | 3.95 | 6.08 | 38.31 | 34.46 | 71.39 |
| Jilongo | 7.77 | 572.23 | 952.98 | 19.05 | 3.25 | 5.81 | 222.04 | 50.79 | 4.10 | 143.10 | 93.94 | 44.15 | 21.68 | 1.14 | 0.88 | 11.72 | 28.28 | 146.51 |
| Mtititi | 8.07 | 1037.36 | 1728.00 | 20.70 | 0.14 | 8.61 | 802.76 | 43.67 | 2.65 | 49.05 | 49.85 | 18.49 | 22.34 | 0.89 | 0.14 | 1.26 | 94.15 | 51.59 |
| Xixaka | 7.51 | 161.40 | 269.68 | 26.40 | 1.90 | 12.20 | 102.48 | 16.22 | 4.57 | 8.43 | 15.91 | 4.72 | 0.72 | 11.71 | 0.33 | 2.17 | 91.83 | 33.84 |
| | | | | | | | | | | | | | | | | | | |
| Min | 6.03 | 161.40 | 269.68 | 12.80 | 0.10 | 3.41 | 54.90 | 16.22 | 1.10 | 8.43 | 15.91 | 0.02 | 0.10 | 0.35 | 0.14 | 1.12 | 0.22 | 23.20 |
| Max | 8.11 | 1862.32 | 3100.00 | 26.40 | 3.25 | 21.18 | 902.80 | 146.80 | 39.76 | 181.90 | 173.20 | 44.15 | 172.53 | 33.09 | 12.58 | 42.07 | 270.29 | 486.76 |
| Mean | 7.50 | 867.48 | 1446.10 | 20.31 | 1.56 | 8.85 | 381.25 | 65.80 | 9.82 | 83.06 | 84.44 | 26.62 | 32.21 | 5.49 | 4.17 | 10.98 | 76.68 | 139.31 |
| WHO (2017) | 6.5-8.5 | 1000 | 1500 | 250 | 50.00 | 500 | 500 | 200 | 200 | 200.00 | 200 | - | 10 | 300 | 400 | 3000 | 100 | 2400 |

N=2

The pH of the groundwater samples ranges between 6.03 and 8.11 with the average value of 7.5 indicating near neutral to weakly alkaline condition. The electrical conductivity (EC) and the total dissolved solids (TDS) were ranging between 296 and 3100 µS/cm and 161.4 and 1862.32 mg/L, respectively (Table 3.1). The WHO permissible values of pH, EC and TDS are 6.5-8.5, <1500 µS/cm and < 1000 mg/L (WHO, 2017). Out of the samples tested, 20 % were found to be having pH below the 6.5 whilst 40 % were having EC and TDS above the WHO permissible limit. No health implications associated with both pH, EC and TDS.

The concentration of $HCO_3^-$, $Cl^-$, $SO_4^{2-}$ and $NO_3^-$ as the major anions constituents in the groundwater were found to be ranging between 54.9 and 902.8, 12.8 and 26.40, 3.41 and 21.18 and 0.10 and 3.25 mg/L, respectively (Table 3.1). The average anionic dominance pattern follows the increasing order of $HCO_3^->Cl^->SO_4^{2-}>NO_3^-$. Higher concentration of $HCO_3^-$ could be attributed to the dissolution of carbonate mineral via biodegradation of organic matter (Choundhury et al., 2017). The concentration of $Cl^-$, $SO_4^{2-}$ and $NO_3^-$ were found to be within the WHO standards in all the boreholes. Out of the sampled boreholes, 30% had $HCO_3^-$ concentrations beyond the WHO guideline (500 mg/L).

The dominant cations are $Mg^{2+}$ (8-181.9 mg/L), $Na^+$ (15.91-173 mg/L) and $Ca^{2+}$ (16.22-146.80 mg/L) while K was the lowest ranging from 1.1 to 39.76 mg/L. On average the dominance of cations is in the order; $Na^+>Mg^{2+}>Ca^{2+}>K^+>Si^{4+}$. These cations are released from silicate and carbonate mineral weathering enhanced by respired $CO_2$ from oxic and anoxic organic matter degradation (Halim et al., 2009). The concentrations of Na, Mg, Ca, and K was within the WHO safe limits for drinking water. The piper diagram in Figure 3.2 was used to evaluate the hydrological facies and the water type in the study area (Piper, 1953). In the cation plot, it is observed that majority of the samples (90%) lies in the centre of the plot indicating the dominance of both $Ca^{2+}$, $Mg^{2+}$ and $Na^+$ ions while the anion plot showed the dominance of $HCO_3^-$ and $Cl^-$. The central diamond plot showed that groundwater samples in the study area are mainly Ca-$HCO_3$ water type (90%) and mixed CaNa-$HCO_3$ (10%). The principal water type depicts rock-water interaction involving the dissolution of rock-forming minerals by weathered zone above the underlying rocks.

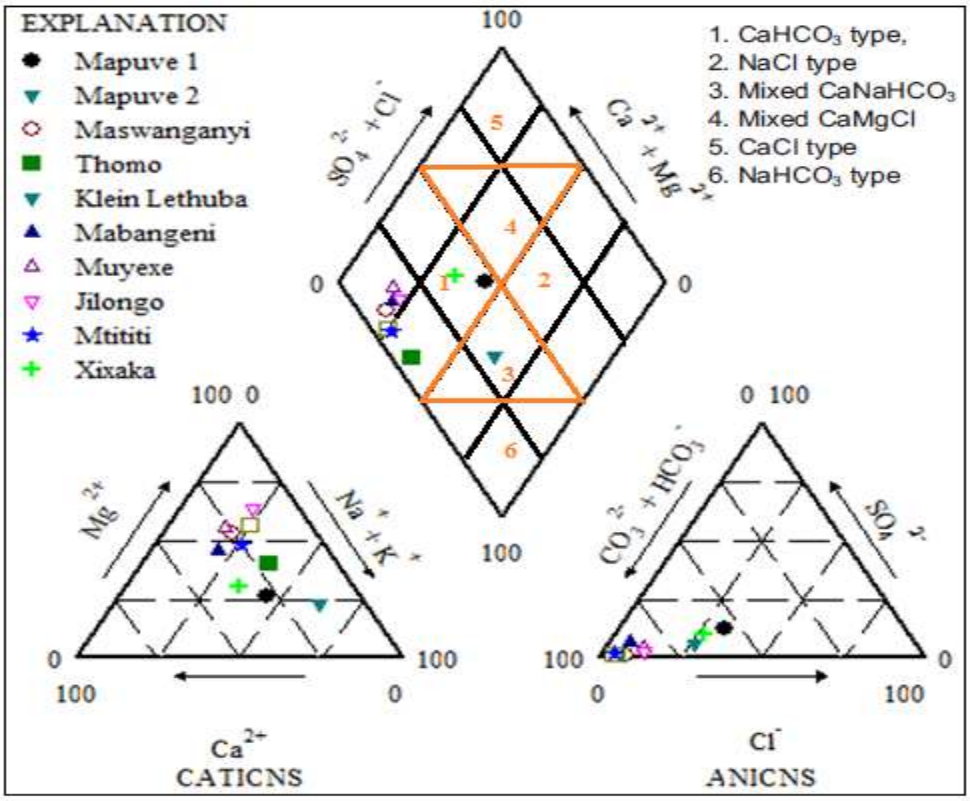


Figure 3.2: Piper diagram of the studied water samples.

The concentration of other trace elements such as As, Fe, Mn, Ba, B, and Zn was found to be ranging from 0.1-172, 0.35-33.9, 0.14-12.58, 0.22-270, 23.2-486.7 and 1.12-42.07 µg/L, respectively (Table 3.1). In relation to WHO limit for drinking water; the concentration of Fe, Mn, Ba, B and Zn were found to be within the recommended limit for human consumption. However, out of 10 tested boreholes, 60% contains As concentration beyond the permissible limit (10 µg/L). The maximum As concentration recorded is 172.53 µg/L which was recorded in the borehole at Klein Letaba. Prolonged exposure to even < 3 µg/L arsenic contaminated water may lead to server health problems including cancer to human (Smith and Smith, 2004; Taheri et al., 2017).

### 3.4.2 Mechanisms controlling groundwater chemistry

Gibbs diagrams are often used to give more insight on the mechanisms controlling the groundwater chemistry by plotting TDS vs. $Na^+/(Na^+ + Ca^{2+})$ and TDS vs. $Cl^-/Cl^- + HCO_3^-$ (Marandi and Shand, 2018). The Gibbs diagram for the studied water samples is depicted in Figure 3.3. Gibbs diagrams revealed that the chemical nature of the studied water samples is influenced by the water-rock interaction rather than evaporation, crystallization and precipitation.

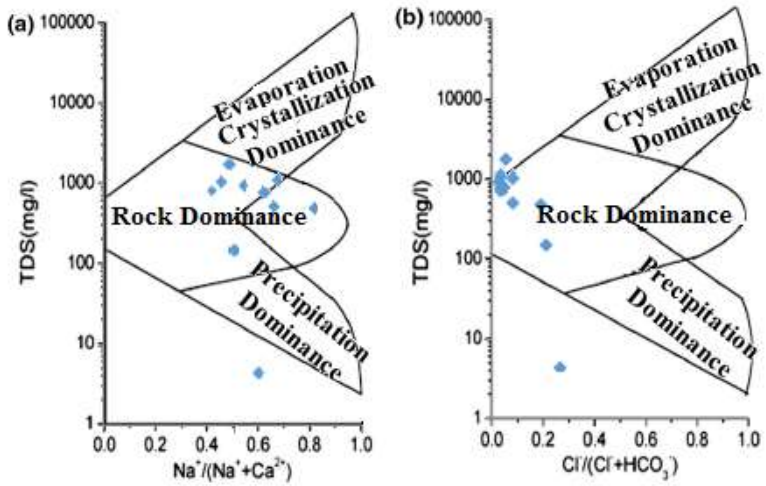


Figure 3.3: The Gibbs diagram for the studied water samples.

During water-rock interaction, chemical weathering and cation exchange processes within the aquifer control the concentration of cations in the water (Mushtaq et al., 2018). The ionic ratios, $HCO_3/\Sigma$anions, $Ca+Mg/HCO_3+ SO_4$, $Na/Cl+SO_4$, Ca/Mg and Na/Cl were examined to determine the probable source of major anions, cations and process affecting water chemistry (Berhe et al., 2017; Taheri et al., 2017). The ionic ratios of groundwater samples collected are shown in Table 3.2.

Table 3.2: Ionic ratio and possible source in Giyani water samples.

| Sample ID | Na/Cl | Ca/Mg | $HCO_3/\Sigma$anions | $Ca+Mg/HCO_3+SO_4$ | $Na/Cl+SO_4$ |
|---|---|---|---|---|---|
| Mapuve 1 | 2.96 | 1.79 | 0.63 | 0.93 | 1.97 |
| Mapuve 2 | 6.46 | 1.03 | 0.77 | 0.67 | 5.09 |
| Maswanganyi | 6.44 | 0.81 | 0.94 | 0.79 | 5.54 |
| Thomo | 9.00 | 0.88 | 0.96 | 0.2 | 6.82 |
| Klein Lethaba | 3.25 | 0.53 | 0.96 | 0.16 | 2.42 |
| Mabangeni | 4.38 | 1.23 | 0.91 | 0.47 | 1.94 |
| Muyexw | 3.61 | 0.78 | 0.88 | 0.82 | 2.53 |
| Jilongo | 4.93 | 0.35 | 0.89 | 0.85 | 3.78 |
| Mtititi | 2.41 | 0.89 | 0.96 | 0.11 | 1.70 |
| Xixaka | 0.60 | 1.92 | 0.72 | 0.24 | 0.41 |

The ratio between Na/Cl in the groundwater from Giyani was found to be ranging from 0.6 to 9 with the average value of 4.40 (Table 3.2). Majority of the samples (90%) has Na/Cl greater than 1 which indicate that groundwater has excess $Na^+$ ions. The surplus $Na^+$ may results from the weathering of silicate minerals and ion exchange processes (Berhe et al., 2017; Taheri et al., 2017). The $Na/Cl+SO_4$ ratios in 90% of the studies samples are > 1 implying that they are soda rich waters. The Ca/Mg ratio < 1 indicates dolomites dissolution whereas a ratio >1 is indicative of calcite contribution while >2 indicates the dissolution of silicate minerals (Redwan and Moneim, 2016). Amongst the tested samples, 60% have a Ca/Mg ratio below 1 revealing dissolution of dolomite while 40% has a Ca/Mg ratio between 1 and 2 suggesting calcite contribution. The ratio of $Ca+Mg/HCO_3+SO_4$ was < 1 with the average of 0.5 (Table 3.2). This suggests that weathering carbonates and silicates mineral is attributed to the abundance of ions in groundwater samples. The weathering of carbonates and silicate minerals is corroborated by the ratio of $HCO_3/\Sigma$anions which were found to be > 0.8 in 70% of the tested samples (Table 3.2) (Taheri et al., 2007; Tahoora et al., 2003). The decreasing $Ca+Mg/HCO_3+SO_4$ suggests the occurrence of ion exchange reactions (Redwan and Moneim, 2016).

### 3.4.3 Arsenic and other hydro-geochemical parameters

To investigate the relationship between arsenic and other hydro-geochemical parameters, scatter plots of pH, $HCO_3^-$, $SO_4^{2-}$, Fe, Mn against As were created and presented in Figures 3.4a-e. A weak to moderate correlation between arsenic and other hydrogeochemical parameters is observed. The plot between pH and As showed that samples with a higher concentration of As have pH between 7.5 and 8.11 (Figure 3.4a). Figure 3.4b showed the relationship between $HCO_3^-$ and As, it is observed that 60% of samples with higher As contains $HCO_3^-$ concentration >200 mg/L. Furthermore, samples with a higher concentration of As contains Fe concentration below 5 µg/L (Figure 3.4c). Very week correlation is observed between $SO_4^{2-}$, Mn and As (Figure 3.4 d-e).

The results from the scatter plots suggests that $HCO_3^-$ and pH are the main hydrogeochemical parameters that are influencing the concentration of arsenic in groundwater. The same observation has also been noted by several authors (Sako et al., 2016; Smedley et al., 2002). Higher concentration of $HCO_3^-$ is associated with increasing pH which promotes the desorption of As from the host mineral (Taheri et al., 2017). Furthermore, a higher concentration of $HCO_3^-$ inhibits

the adsorption of As by metal oxides. This phenomenon explains higher As concentration in samples with elevated $HCO_3^-$ concentration.

In summary, samples that contains arsenic concentration > 10 µg/L are accompanied by pH >7.5, higher $HCO_3^-$ and low Fe and Mn concentrations. These results suggest that the mechanism responsible for higher As concentration in groundwater from boreholes in Giyani Municipality is desorption of As from metal oxides such as Fe and Mn.

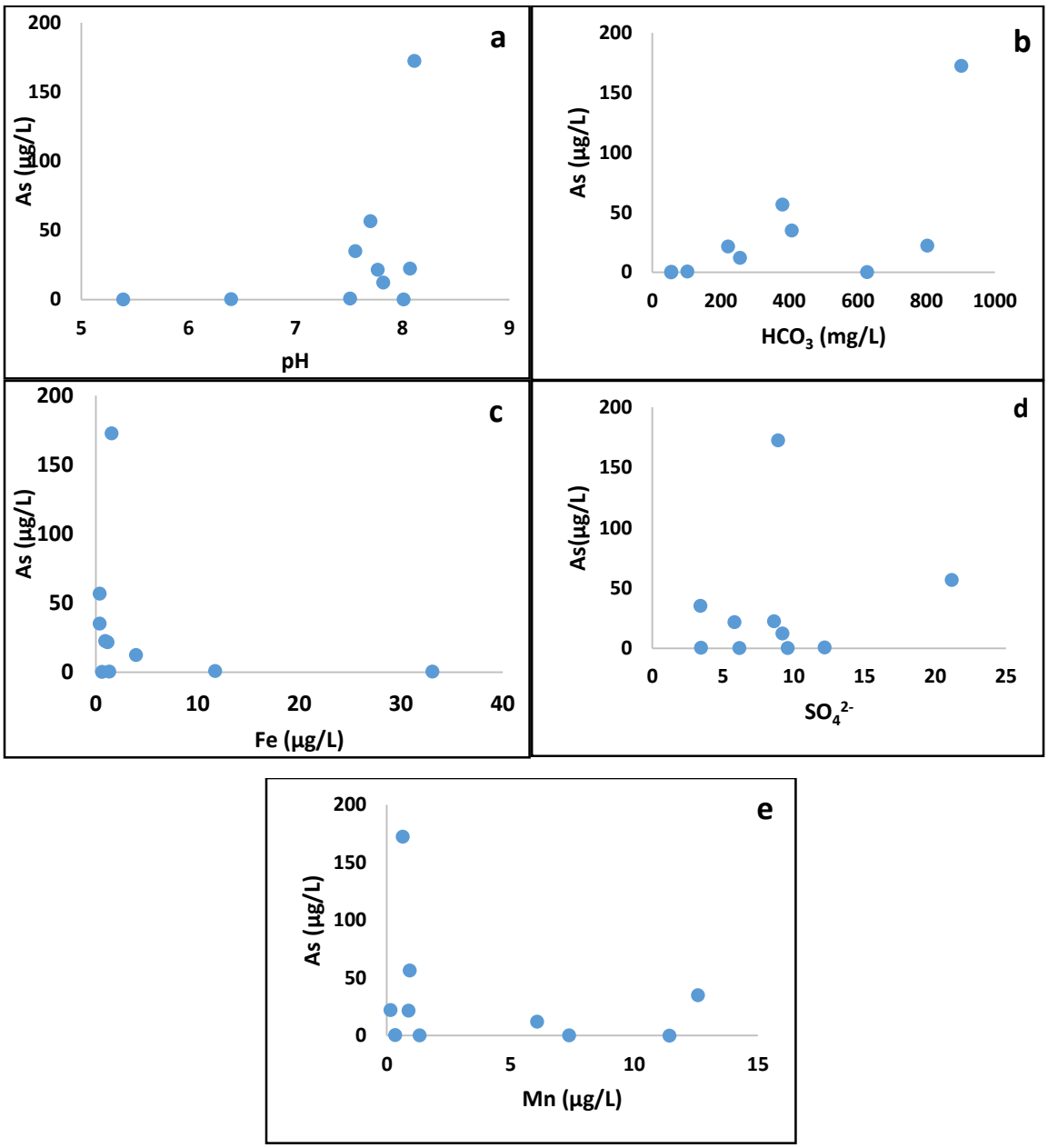


Figure 3.4: Relationship between arsenic concentration and (a) pH, (b) $HCO_3$, (c) Fe, (d), $SO_4$ and (e) Mn.

### 3.5 Conclusions

The hydro-geochemical characteristics of groundwater in Greater Giyani Municipality and their relationship to arsenic concentration were successfully evaluated. The pH of the groundwater samples ranges from neutral to weakly alkaline. The abundance of major anions and cations are in the following order: $HCO_3^->Cl^->SO_4^{2-}>NO_3^-$ and $Na^+ > Mg^{2+} > Ca^{2+} > K^+ > Si^{4+}$, respectively. The hydrogeochemical facies identified in the study area include $CaHCO_3$ (90%) and mixed $CaNaHCO_3$ (10%) which shows the dominance of water-rock interaction. The ionic ratio computed showed that the major ions originate from weathering of carbonate and silicate minerals. Amongst the tested samples, 60 % contains arsenic concentrations beyond the WHO permissible limit of 10 µg/L. The mean arsenic concentration was found to be 32.21 µg/L while the maximum concentration recorded was 172.53 µg/L. All samples with higher arsenic concentration were found to be having pH between 7.5 and 8.5 and $HCO_3$ > 200 mg/L. The following recommendations were made from this study:

(i) Routine monitoring of arsenic concentration in the Greater Giyani Municipality.

(ii) Epidemiological studies should be conducted to assess the correlation between arsenic and related diseases within the Giyani Municipality.

(iii) Studies focusing on arsenic developing arsenic remediation technique that is flexible and sustainable for use in Greater Giyani Municipality.

## References

Ayotte, J. D., Belaval, M., Olson, S. A., Burow, K. R., Flanagan, S. M., Hinkle, S. R., Lindsey, B, D., 2015 Factors affecting temporal variability of arsenic in groundwater used for drinking water supply in the United States. Science of Total Environment. 505, 1370-1379.

Berhe, B. A., Dokuz, U. E., Celik, M., 2017 Assessment of hydrogeochemistry and environmental isotopes of surface and groundwaters in the Kütahya Plain, Turkey. Journal of African Earth Sciences. 134, 230-240.

Billay, A., Sadeghi, M., Carranza, E. J. M., 2014 Predictive bedrock and mineral prospectively mapping in the Giyani Greenstone Belt, South Africa Mineral Resources Development Unit Meeting Points Mining Project. Report Number: 2014-0027.

Bretzler, A., Lalanne, F., Nikiema, J., Podgorski, J., Pfenninger, N., Berg, M., Schirmer, M., 2017 Groundwater arsenic contamination in Burkina Faso, West Africa: Predictiong and verifying regions at risk. Science of Total Environment. 584-585, 970-984.

Carranza, E. J. M., Sadeghi, M., Billay, A., 2015 Predictive mapping of prospectivity for orogenic gold, Giyani Greenstone belt (South Africa). Ore Geology Reviews. 71, 703-718.

Choundhury, R., Mahanta, C., Verma, S., Mukherjee, A., 2017 Arsenic distribution along the different hydrogeomorphic zones in parts of the Brahmaputra River Valley, Assam (India). Hydrogeology Journal. 25, 1153-1163.

Fatoki, O. S., Akinsoji, O. S., Ximba, B. J., Olujimi O., Ayanda, O. S., 2013 Arsenic Contamination: Africa the Missing Gap. Asian Journal of Chemistry. 25(16), 9263-9268.

Halim, M. A., Majumder, Nessa, S. A., Hiroshiro, Uddin, M. J., Shimada, J., Jinno, K., 2009 Hydrogeochemistry and arsenic contamination of groundwater in the Ganges Delta Plain, Bangladesh. Journal of Hazardous Materials. 164, 1335-1345.

Kempster P. L., Silberbauer, M., Akuhn A., 2006 Interpretation of drinking water quality guidelines-The case of arsenic. Water S.A. 33 (1), 95-100.

Kouras, A., Katsoyiannis, I., Voutsa, D., 2007 Distribution of arsenic in groundwater in area of Chalkidiki, Northern Greece. Journal of Hazardous Materials. 147, 890-899.

Mandal, B. K., Suzuki, K. T., 2002 Arsenic around the world: Review. Talanta. 58, 201-235.

Marandi, A., Shand, P., 2018 Groundwater chemistry and the Gibbs Diagram, Applied Geochemistry. Article in Press. doi: 10.1016/j.apgeochem.2018.07.009.

Mushtaq, N., Younas, A., Mashiatullah, A., Javed, T., Ahmad, A., Farooqi, A., 2018. Hydrogeochemical and isotopic evaluation of groundwater with elevated arsenic in alkaline aquifers in Eastern Punjab, Pakistan. Chemosphere. 200, 576-586.

Narany, T. S., Ramli, M. F., Aris, A. Z., Sulaiman, W. N. A., Juahir, H., Fakharian, K., 2014 Identification of the Hydrogeochemical Processes in Groundwater Using Classic Integrated Geochemical Methods and Geostatistical Techniques, in Amol-Babol Plain, Iran. The Scientific World Journal. 1-15.

Odiyo, J. O., Makungo, R., 2012 Fluoride concentrations in groundwater and impact on human health in Siloam Village, Limpopo Province, South Africa. Water SA. 38(5), 731-736.

Piper AM (1953) A graphic procedure in the geochemical interpretation of water analysis. USGS Groundwater Note, No. 12.

Redwan, M., Moneim, A. A. A., 2016 Factors controlling groundwater hydrogeochemistry in the area west of Tahta, Sohag, Upper Egypt. Journal of African Earth Sciences. 118, 328-338.

Sako, A., Bamba, O., Gordio, A., 2016 Hydrogeochemical processes controlling groundwater quality around Bomboré gold mineralized zone, Central Burkina Faso. Journal of Geochemical Exploration. 170, 58-71.

Samie, A., Makonto, O. T., Mojapelo, P., Bessong, P. O., Odiyo, J. O., Uaboi-Egbenni, P. O., 2013 Physico-chemical assessment of borehole water used by schools in Greater Giyani Municipality, Mopani district, South Africa. African Journal of Biotechnology. 12(30), 4858-4865.

Sharif, M. U., Davis, R. K., Steele, K. F., Kim, B., Kresse, T. M., Fazio, J. A., 2008 Inverse geochemical modeling of groundwater evolution with emphasis on arsenic in the Mississippi River Valley alluvial aquifer, Arkansas (USA). Journal of Hydrology. 350, 41-55.

Smedley, P. L., Kinniburgh, D. G., 2002 A review of the source, behavior and distribution of arsenic in natural waters. Applied Geochemistry. 17, 517-568.

Smedley, P. L., Nicolli, H. B., Macdonald, Barros, A. J., Tullio, J. O., 2002 Hydrogeochemistry of arsenic and other inorganic constituents in groundwaters from La Pampa, Argentina. Applied Geochemistry. 17, 259-284.

Smith, A. H., Smith, M. M. H., 2004 Arsenic drinking water regulations in developing countries with extensive exposure. Toxicology. 198-44.

Taheri, M., Gharaie, M. H. M., Mehrzad, J., Afshari, R., Datta, S., 2017 Hydrogeochemical and isotopic evaluation of arsenic contaminated water in an argillic alteration zone. Journal of Geochemical Exploration. 175, 1-10.

World Health Organization (WHO) 2017 Guidelines for drinking-water quality: fourth edition incorporating the first addendum. Geneva: Switzerland. Licence: CC BY-NC-SA 3.0 IGO.

# Chapter 4: Physicochemical characterization of smectite rich and kaolin clay: potential application in As(III) and As(V) removal from groundwater

## 4 Abstract

Chapter 3 revealed that 60% of boreholes in Greater Giyani Municipality contains arsenic concentration beyond World Health Organization recommended limit for drinking water of 10 µg/L. Due to toxicity of arsenic on human being, studies towards finding a feasible and sustainable material for arsenic removal were therefore recommended. Clay soils and clay minerals are known for their ability to uptake pollutants from the solution via adsorption and/or ion exchange processes. This chapter evaluates the physicochemical properties of locally available smectite rich clay soils and kaolin clay and their effectiveness towards As(III) and As(V) removal from groundwater. The clay soils were characterized by X-ray diffraction (XRD), x-ray fluorescence (XRF), Fourier Transform Infrared spectroscopy (FTIR), scanning electron microscopy (SEM) and Brunauer–Emmett–Teller (BET) techniques. Batch experiments were conducted to assess the efficiency of the two clay soils in arsenic removal under various operating conditions of contact time, adsorbent dosage, initial concentration and initial pH. The percentage As(V) removal by kaolin clay mineral was found to be 87.2% at pH 2. Conversely, the As(III) was greater than 60% at wide range of pH. The percentage of As(III) and As(V) removal by smectite rich clay soils was found to be optimum at pH between 6 and 8. The adsorption data for As(III) adsorption by smectite rich clay fitted better to pseudo second order while the data for As(V) fitted better to pseudo first order of reaction kinetics. On the other hand the adsorption data for both As(III) and As(V) adsorption by kaolin clay mineral fitted better to pseudo second order of reaction kinetics. The adsorption isotherm data for As(III) and As(V) removal by both clays fitted better to Freundlich isotherm. Adsorption of both species of arsenic onto the clay mineral occurred via electrostatic attraction and ion exchange mechanisms. The effects of co-existing anions towards the adsorption of As(III) and As(V) may be summarized in the following inhibition order; $CO_3^{2-}$>$SO_4^{2-}$>$F^-$≥ $Cl^-$. Both clay soils could be regenerated twice using $Na_2CO_3$ as a regenerant. The results obtained from this study proves that kaolin clay and smectite rich clay has a potential for use in adsorption of arsenic. However, surface modification by higher density cations is recommended to enhance the sorption capacity.

Keywords: *Adsorption; arsenic; batch experiment, characterization; kinetics and isotherms.*

## 4.1 Introduction

The presence of arsenic in groundwater has attained worldwide attention due to its negative implications on human health. Prolonged exposure to arsenic is linked to arsenicosis (Abdul et al., 2015). The disease is manifested by different types of cancer, kidney diseases, diabetes, skin lesions, circulatory disorders and neurological complications (Mandal and Suzuki, 2002; Duker et al., 2005; Ayotte et al., 2015; Cheng et al., 2017). These symptoms have been observed in more than 105 countries worldwide where groundwater contains arsenic concentration beyond World Health Organization permissible limit value of 0.01 mg/L (Chakraborti et al., 2016).

It is estimated that more than 200 million people worldwide are at health risk due to arsenic rich water (Sarkar and Paul, 2016). Countries that are worst affected includes India, Bangladesh, Mexico and China (Uddin et al., 2007; Mazumder and Dasgupta, 2011; Chakraborti et al., 2016). Details about the population at risk in Africa are sketchy. However, concentration exceeding 0.01 mg/L of arsenic in groundwater has been reported in countries like Burkina Faso, Ghana, Zimbabwe and South Africa (Kempster et al., 2006; Kortatsi et al., 2008; Mudyazhezha and Kanhukamwe, 2004; Bretzler et al., 2017). From chapter 3, it was noted that 60% of boreholes in greater Giyani Municipality contains arsenic concentration above 10 µg/L with maximum arsenic concentration of 172 µg/L recorded in one of the boreholes. Therefore there is a need to develop a flexible and sustainable method that can be used for arsenic removal from groundwater.

Arsenic removal techniques such as chemical precipitation, coagulation and floatation, ion-exchange, membrane, oxidation and adsorption have been reviewed (Mohan and Pittman, 2007; Ungureanu et al, 2015; Sarkar and Paul, 2016). Among the available techniques, adsorption remain the superior of them all due to its advantages such as, ease of operation, higher adsorption capacity, cost of operation and minimum risk (Ren et al., 2014; Chammui et al., 2014; Hua, 2015). Several adsorbents including hydrous ferric oxide (Wilker and Hering, 1999), coal fly ash (Wang et al., 2008), iron oxide coated cement (Kundu and Gupta, 2007), laterite soils (Maji et al., 2007), Kaolinite clay (Ding et al., 2015), Fe/Al bimetallic particles (Cheng et al., 2016) and iron oxide impregnated alginate beads (Sigdel et al., 2016) have been developed for arsenic removal.

The use of clay soils in arsenic removal has been extensively studied in different parts of the world and they have proved to be a promising adsorbent for arsenic from water (Mishra and Mahato, 2016; Bentahar et al., 2016). Their physicochemical properties such as larger specific surface area,

higher cation exchange capacity and chemical and mechanical stability makes them to be excellent adsorbent for pollutants (Bhattacharyya and Gupta, 2008). Furthermore, clay soils are naturally available in abundance at little or no cost. This study seek to evaluate the use of smectite rich clay soils and kaolin clay mineral collected from Mukondeni Village and Dzamba Village in Limpopo Province respectively for the removal of As(III) and As(V) from groundwater. The two villages are located in Vhembe District within Limpopo Province, South Africa. The physicochemical properties of Mukondeni smectite rich clay soils and its potential application in groundwater treatment has been reported previously by Mudzielwana et al., (2016). Moreover, Mukondeni clay soils has been used for a very long time to make ceramic water filters and have been found to be effective in improving water quality (Tyeryar et al., 2012). Physicochemical properties of Dzamba kaolin clay and its use in water treatment has never been evaluated. However, it has always been used by indigenous people for making clay pots. The objectives of this study are therefore: i) to evaluate and compare the physicochemical and mineralogical properties of the two locally available clay soils, ii) to evaluate their feasibility in arsenic (III) and (V) removal using batch experiments, iii) lastly to model the adsorption data and elucidate the arsenic adsorption mechanisms.

## 4.2 Material and Methods

### 4.2.1 Clay soil sampling and reagents

The smectite rich clay soils were collected from Mukondeni Village, Ha-Mashamba, Makhado Municipality while kaolin clay was collected from Dzamba Village, Thulamela Municipality, Limpopo Province, South Africa. All chemical reagents were purchased from Rochelle Chemicals & Lab Equipment CC, South Africa Ltd and were of analytical grade and they were used without further purification. Stock solutions containing 1000 mg/L As(III) and As(V) were prepared by dissolving 0.416 g $HAsNa_2O_4.7H_2O$ and 0.1733 g $AsNaO_2$ in 100 mL flask using Milli Q water (18.2 MΩ/cm). The solutions were preserved by adding few drops of 3 M $HNO_3$. Working solutions were prepared by appropriate dilutions.

### 4.2.2 Preparation of clay soils

Clay soils were washed with Milli-Q water (18.2 MΩ/cm) at a mass/volume ratio of 1:5 in a 1 L beaker. The mixture was stirred for 5 min, and the procedure was repeated twice. After stirring, mixtures were agitated for 15 min using a Stuart reciprocating shaker and then centrifuged for 10

min at 5000 rpm. Samples were then oven dried for 12 h at 105 °C and thereafter milled to pass through a 250 µm sieve.

### 4.2.3 Physicochemical characterization

Major and trace elemental constituents of the clay soils were characterized using S2 ranger X-ray fluorescence (Unrivalled XFlash detector resolution with 129 eV and 100 000 cps at Mn Kα). Mineralogical compositions was examined using D8 advance X-ray diffractometer (XRD) (Bruker, Germany) with Cu–Kα radiation as source. Functional groups were determined using ATR-Diamond FTIR (Bruker, Germany). Morphological analysis was carried out using scanning electron microscopy (SEM) (Leo1450 SEM, voltage 10 kV, working distance 14 mm). The pore size distribution, pore volume, and pore diameter were determined by Barrett Joyner Halenda (BJH) sorption model using a specific surface area analyzer (Autosorb-iQ & Quadrasorb SI, USA). Nitrogen adsorption-desorption isotherms were used to determine specific surface area of the adsorbent according to Brunauer Emmett Teller (BET) model. Point of Zero charge (pHpzc) was determined using titration method (Gitari et al., 2013).

### 4.2.4 Batch experiments

Batch adsorption experiments were conducted to evaluate the effect of contact time, adsorbent dosage, adsorbate concentration and pH in removal of As(III) and As(V) from groundwater using kaolin clay mineral and smectite rich clay soils. To evaluate the effect of contact time, 100 mL solution containing 5 mg/L of As(III) and As(V) was pipetted into 250 mL polyethylene bottles and mass of 0.15 g of kaolin clay mineral and smectite rich clay soils were added respectively to make up 0.15g/100 mL adsorbent dosage. Mixtures were then agitated for 10, 20, 30, 40, 50, 60, 90 and 120 min. After agitation, mixtures were filtered through 0.45 µm filter membranes. Samples were then refrigerated at 4 °C until analysis. To evaluate the effect of adsorbent dosage, 100 mL of 5 mg/L of As(III) and As(V) was pipetted into 250 mL polyethylene bottle. This was followed by addition of 0.1, 0.2, 0.3, 0.5, 0.7 and 1 g of kaolin clay mineral and smectite rich clay soils respectively into the plastic bottles. Mixtures were agitated for 60 min. To evaluate the adsorption isotherms, initial concentration of As(III) and As(V) varied from 1 to 15 mg/L and the adsorbent dosage of 0.7/100 mL adsorbent dosage of both clay soils was added. Mixtures were added and agitated for 60 min. To evaluate the effect of pH, the pH of the mixture was adjusted from 2-12 using 0.1 M NaOH and 0.1 M HCl. Adsorbent dosage of 0.7 g/100 mL of both clay soils was used

with the initial concentration of 5 mg/L was used. This was followed by agitation of the mixtures for 60 min. The adsorbents chemical stability was assessed by analyzing concentration of metal species in the filtrates obtained from effect of pH experiment using Inductively Coupled Plasma-Mass Spectrometer (Agilent 7900 ICP-MS, US). The influence of co-existing ions ($F^{-}$, $Cl^{-}$, $CO_3^{2-}$ and $SO_4^{2-}$) was evaluated at the initial concentration of As(III)/As(V) concentration of 5 mg/L, adsorbent dosage of 0.7 g/100 mL and 60 min contact time. The initial concentration of each co-existing ion was 5 mg/L. All experiments were conducted in triplicate and the mean values were reported.

### 4.2.5 Reuse and Regeneration of Adsorbent

To evaluate the reusability of the adsorbents, two repetitive adsorption cycles were conducted as follows: 100 mL of solution containing 5 mg/L of As(III) and As(V) was pipetted into 250 mL and 1 g of the clay soils was added to make adsorbent dosage of 1 g/100 mL. Mixtures were agitated for 60 min at 250 rpm. After agitation samples were filtered through 0.45 µm filter membranes. Residues were rinsed with Milli-Q water to remove free As(III) and As(V) ions and then oven dried at 105 $^{O}$C and reused for adsorption. For regeneration, residues were treated with 100 mL of 0.01 M $Na_2CO_3$ for 15 min to desorb the adsorbed ions thereafter samples were filtered to through 0.45 µm filter membrane and then washed gently with Milli-Q water. The regenerated adsorbent was then used for As(III) and As(V) removal. The same procedure was followed for both clay soil.

### 4.2.6 Analysis

Metrohm 850 professional ion chromatography (Switzerland) was used to analyze As(III) and As(V). Metrosep A Supp 5-150 column was used for separation and the guard column Metrosep A 4/5 was used. The eluent containing 15 mmol/L NaOH and 2.0 mmol/L $Na_2CO_3$ was used as the mobile phase for As(III) and As(V) analysis. For other co-existing anions NaHCO and $Na_2CO_3$ was used as mobile phase. The conductivity detector was used to estimate the concentration of different chemical species. For quality assurance of As(III) and As(V) analysis, samples were also analyzed using Inductively Coupled Plasma-Mass Spectrometer (Agilent 7900 ICP-MS, US). The As species distribution at various solution pH levels was determined using Visual MINTEQ Version 3.1. The MINTEQ geochemical program model aqueous solutions and the interactions of aqueous solutions with hypothesized assemblages of solid phases.

### 4.2.7 Calculating percentage of removal and adsorption capacity

Equation 4.1 and 4.2 were used to calculate the percentage removal and adsorption capacity respectively.

$$\%\, removal = \left(\frac{C_o - C_e}{C_o}\right) \times 100 \quad (4.1)$$

$$Q = \left(\frac{C_o - C_e}{m}\right) \times v \quad (4.2)$$

Where: $C_o$= initial concentration (mg/L), $C_e$ = concentrations at equilibrium (mg/L), $V$ = Volume of solution (L) and $m$ = Weight of the adsorbent (g).

## 4.3 Results and Discussion

### 4.3.1 Physicochemical Characterization

#### 4.3.1.2 Chemical Composition

Major and trace elemental compositions of kaolin clay and smectite rich clay soils are presented in Table 4.1. The results revealed that $SiO_2$ is the major oxide for smectite rich clay soils and kaolin clay mineral averaging 60.92% and 93.09%, respectively. High $SiO_2$ content could be ascribed to the presence of quartz as the major mineral. $Al_2O_3$ oxides were found to be 15.83% and 9.4% for both smectite rich clay soils and kaolin clay mineral, respectively. $Al_2O_3$ could be ascribed to the presence of feldspar mineral in the clay soils. $Fe_2O_3$ oxides were also identified amounting 5.96% in smectite rich clay soils and 2.77% in kaolin clay mineral. This could enhance the sorption of arsenic since iron oxides are known to be having stronger affinity towards arsenic (Mishra and Mahato, 2016).

Table 4.1: Major oxides and trace elemental composition of smectite rich clay soils and kaolin clay mineral.

| **Major oxides (% by weight)** | | | **Trace elements (mg/kg)** | | |
|---|---|---|---|---|---|
| **Chemical species** | **Smectite rich** | **Kaolin** | **Chemical species** | **Smectite rich** | **Kaolin** |
| $SiO_2$ | 60.92 | 93.1 | V | 132.7 | 154.7 |
| $Al_2O_3$ | 15.83 | 9.4 | Cr | 138.6 | 82.8 |
| $Fe_2O_3$ | 5.96 | 2.77 | Co | 13.6 | 6.5 |
| MgO | 3.85 | 0.41 | Zn | 85.2 | 53.1 |
| MnO | 0.1 | 0.02 | Ni | 602.6 | 134.6 |
| CaO | 1.63 | 0.44 | Cu | 56.1 | 153 |
| $Na_2O$ | 1.67 | 0.23 | As | 3.1 | 1.1 |
| $TiO_2$ | 0.63 | 0.7 | Cr | 368.6 | 28.8 |
| $K_2O$ | 1.3 | 0.1 | Zr | 164.23 | 194.7 |
| $P_2O_5$ | 0.03 | 0.02 | Ce | 68 | 40.7 |

#### 4.3.1.2 Mineralogical characterization

The XRD patterns of the two clays are presented in Figure 4.1a and b. The spectra of kaolin clay mineral (Fig 4.1a) showed a major diffraction peaks at 2θ degree = 24.58, 31.51, 42.38 and 61.0 which are attributed to quartz mineral. Kaolinite peaks were also observed at 2θ degree= 23.7 and 54.02. Amorphous phases were observed at 2θ degree <20. Due to the presence of kaolinite mineral the clay was then referred to as kaolin clay. The spectra of smectite rich clay (Fig 4.1b) showed major diffraction peaks at 2θ degree= 31.8, 37.02, 59.13 and 72.31 indicating the presence of quartz. The other peaks observed at 2θ degree= 7.64, 24.86 and 27.73 are attributed to smectite, microcline and albite, respectively.

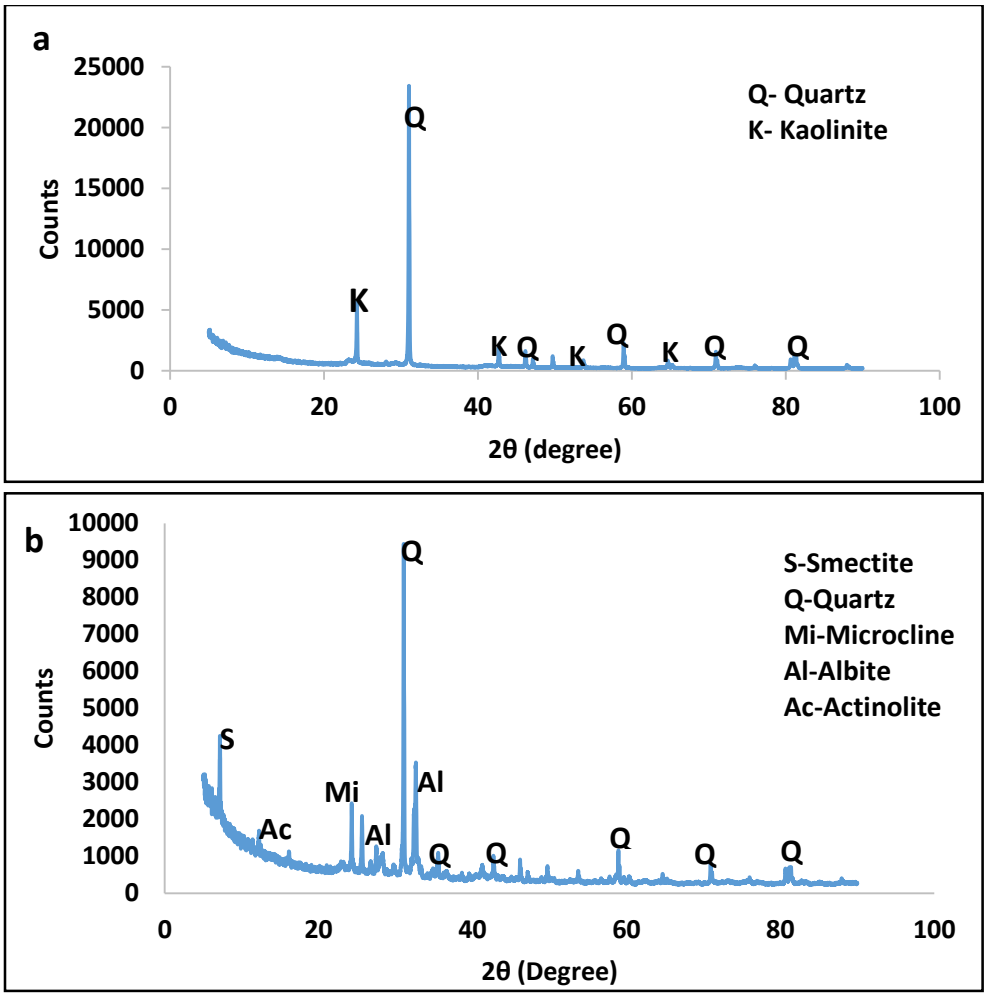


Figure 4.1: X-ray diffraction spectra of kaolin clay (a) and smectite rich clay (b).

**4.3.1.3 FTIR analysis**

Figure 4.2a and b present the infrared spectra of kaolin clay mineral and smectite rich clay soils before and after As adsorption. Strong bands for both clay soils were observed at the same wavelength regions. The bands observed at 3633 and 1601 $cm^{-1}$ could be attributed to vibration of hydroxyl groups in the clay due to physiosorbed water and the hydroxyl groups located between the octahedral and tetrahedral sheets of the clay. The band at 1020 $cm^{-1}$ could be associated with the vibration of Si-O. The bands at 918, 762.96, 665 and 532 $cm^{-1}$ could be ascribed to the vibration of Al-OH-Al, Al-O-Si, Al-O-Fe and Si-O-Fe bonds, respectively. These bonds confirms the presence of quartz and alumino-silicate minerals in both clay soils (Ayari et al., 2005; Fouodjouo et al., 2016; Favero et al., 2016). No new bands observed in the both clays after arsenic adsorption. However, an increase in the band transmittance intensity at both wavelength regions was observed. The increased intensity could be attributed to the formation of new bonds such as As-O-M (where;

M represent metals like Al, Si and Fe). Similar observation was observed in both clay soils. The adsorption of As could due to electrostatic attraction of As ions to positively charged ions in the clay surface and Van der Wall forces between the molecules in the clay surface and As atoms.

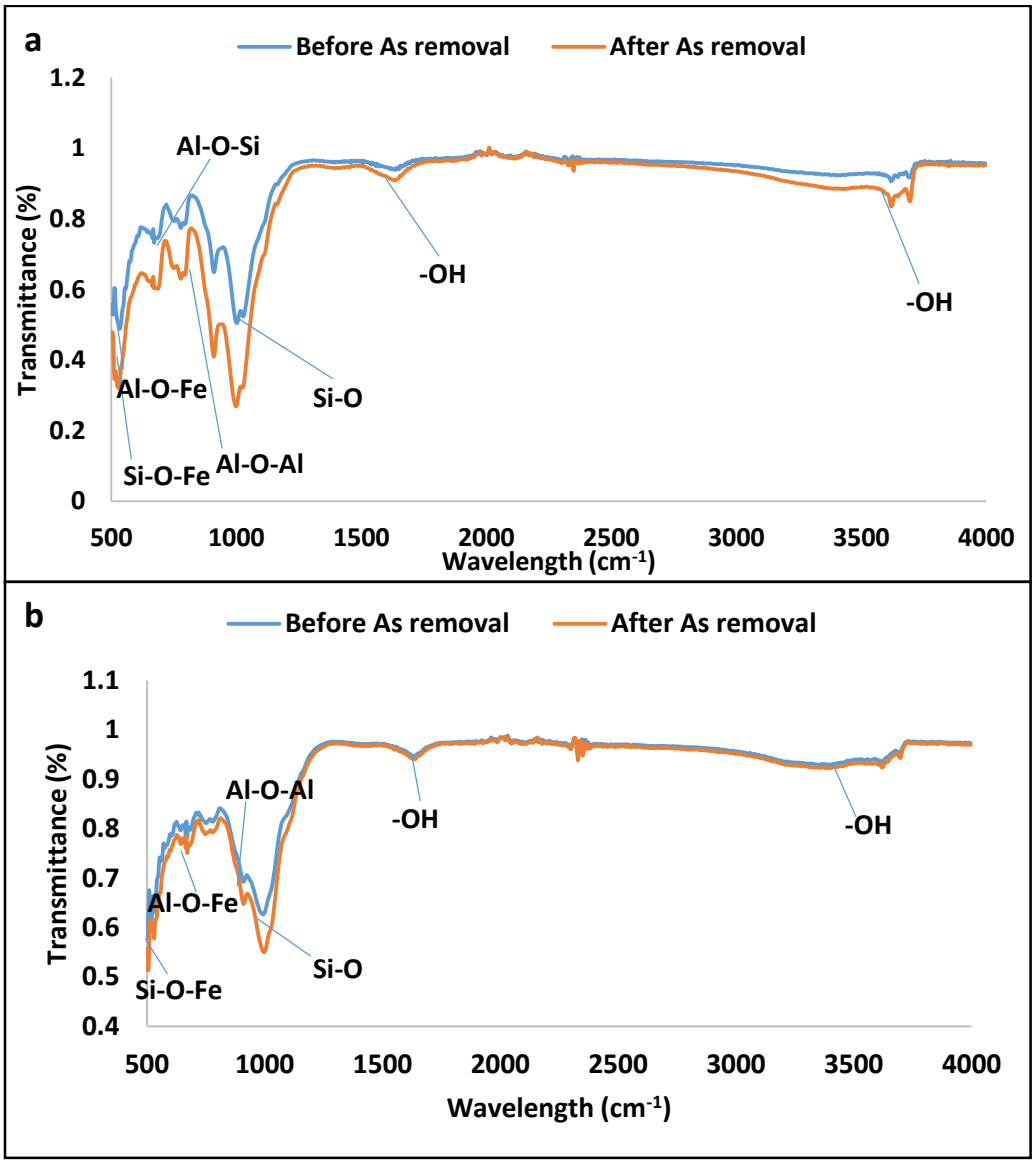


Figure 4.2: FTIR spectra of a) kaolin clay and b) smectite rich clay soils before and after As adsorption.

### 4.3.1.4 Morphological analysis

Figure 4.3a-d present the surface micrographs of kaolin clay and smectite rich clay soils before and after arsenic adsorption. The analysis revealed that the surface of kaolin cay is more porous and has some irregular shaped granules (Fig 4.3a). This surface could be favorable for molecular diffusion and could provide a larger surface area for the adsorption of contaminants. After arsenic

adsorption there was formation of larger granules in the surface of the clay which could be attributed to swelling during adsorption (Fig 4.3b). The morphology of smectite rich clay soils on the other hand is smooth with some flaky features (Fig 4.3c). After arsenic adsorption, the whole surface looking smooth and much saturated (Fig 4.3d).

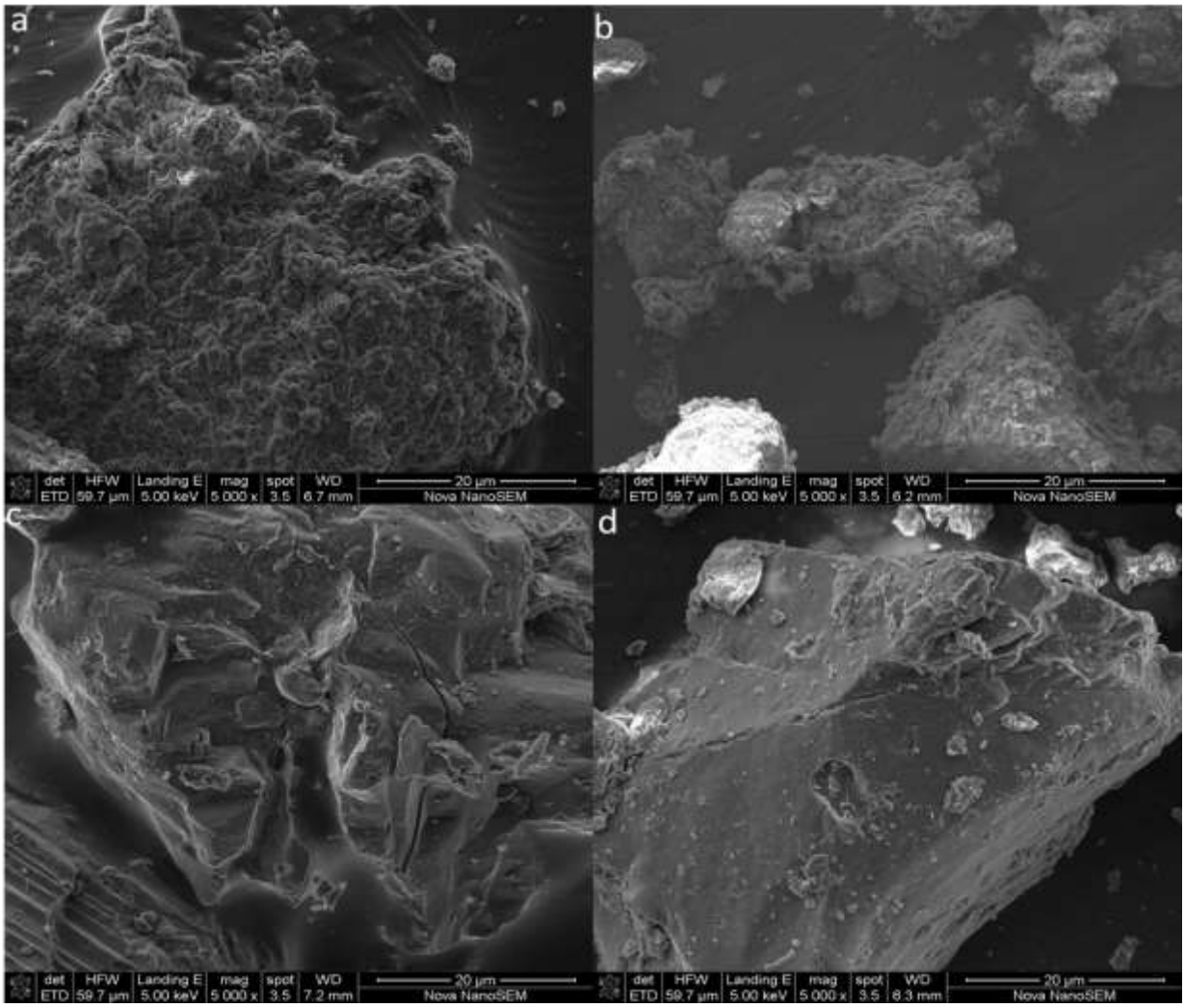


Figure 4.3: The micrographs of kaolin clay (a-b) and smectite rich clay soils (c-d) before and after arsenic adsorption.

### 4.3.1.5 Surface area and pore distribution analysis

Table 4.2 shows the total BET surface area, pore volume and the average pore diameter while Figure 4.4 presents the pore distribution of clay soils. It is evident that smectite rich clay soils has higher surface area compared to kaolin clay. Both clay soils displayed uniform pore distribution. A narrow mono-modal pores were observed at a range of 2.9 to 4.7 nm and majority of pores were

observed at a range beyond 5nm. The average pore diameter values for kaolin clay mineral and smectite rich clay soils were found to be 9.54 and 5.93 nm, respectively (Table 4.2). This indicates that both clay soils are mesoporous in nature.

Table 4.2: Surface area, pore volume and pore diameter of kaolin clay and smectite rich clay soils.

| | BET surface area ($m^2/g$) | Pore volume (cc/g) | Pore diameter (nm) |
|---|---|---|---|
| Kaolin clay | 19.02 | 0.04 | 9.54 |
| Smectite rich clay soils | 22.2 | 0.03 | 5.93 |

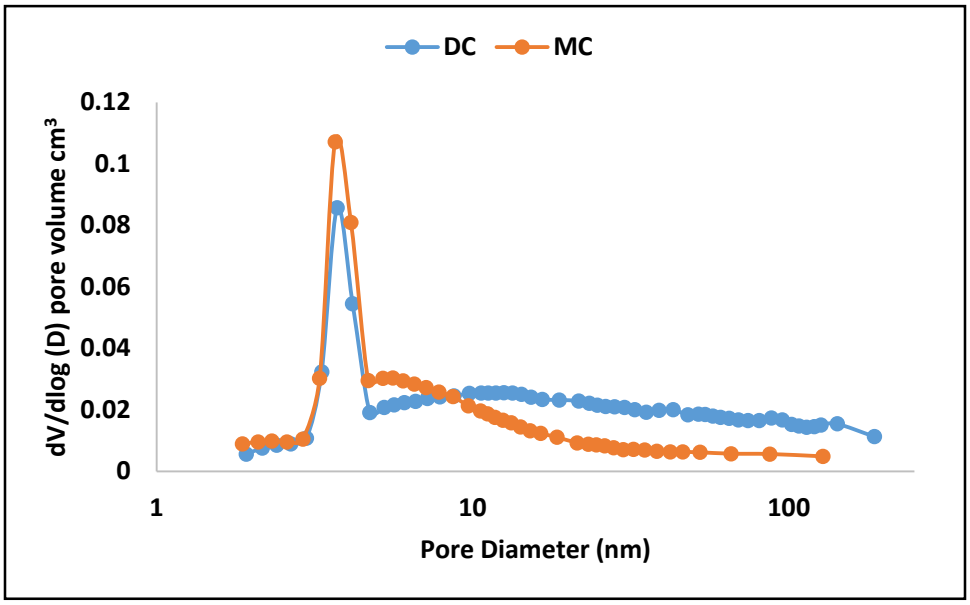


Figure 4.4: Pore distribution curve for kaolin clay and smectite rich clay soils.

### 4.3.2 Batch adsorption experiments

#### 4.3.2.1 Effect of contact time

The effect of contact time in the uptake of As(III) and As(V) by kaolin clay and smectite rich clay soils was conducted by varying the contact time from 10 to 120 min. The results are presented in Figure 4.5a and b respectively for kaolin clay and smectite rich clay soils. From the results it is observed that for both clay soils, percentage As(III) and As(V) removal increased with an increasing contact time. The sorption was fast within the first 60 min and there after it slowed down indicating that the equilibrium is reached. Therefore, for both clay soils 60 min was used as the optimum contact time for subsequent experiments.

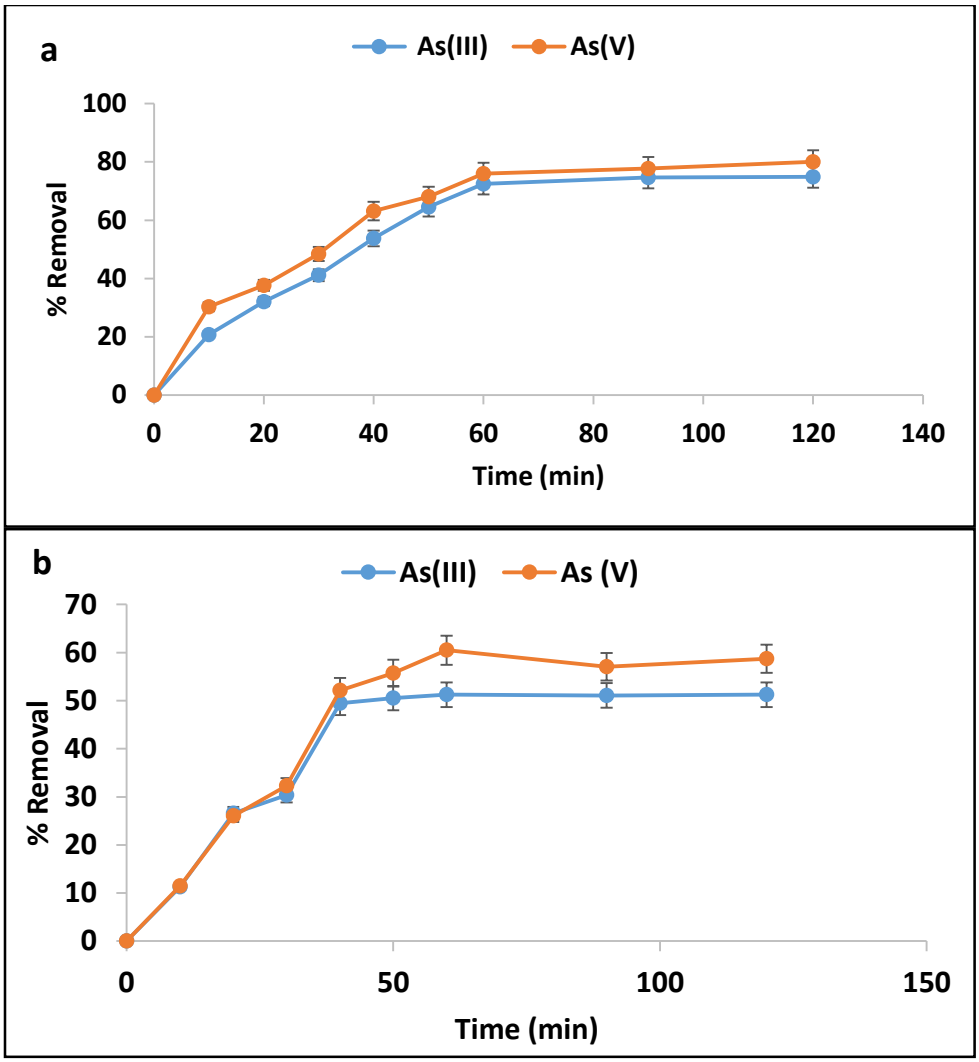


Figure 4.5: Adsorption of As(III) and As(V) onto kaolin clay (a) and smectite rich clay soils(b) (5 mg/L initial concentration, 0.15 g/100 mL adsorbent dosage, pH 6.53 and shaking speed of 250 rpm).

In order to explain the adsorption rate controlling factors and adsorption mechanisms, reaction kinetics models namely, pseudo first order (PFO) and pseudo second order (PSO) and the Weber Morris intra-particle diffusion models were used to fit the experimental data (Ho, 2004; Chen et al., 2011; Firdaous et al., 2017; Yoon et al., 2017). Pseudo first and second order models are expressed by the linear equation 4.3 and 4.4 respectively. Whereas, the Intra-particle diffusion is expressed by equation 4.5.

$$\log_{(qe-qt)} = \log q_e - \frac{K_{ad}t}{2.303} \quad (4.3)$$

$$\frac{t}{q_t} = \frac{1}{K_{2ads}q_e^2} + \frac{1}{q_e}t \quad (4.4)$$

$$q_t = K_i t^{0.5} + C_i \quad (4.5)$$

Where $q_e$ and $q_t$ (both in mg/g) are the amount adsorbed per unit mass at a time, t (in min). $K_{ad}$ ($min^{-1}$) and $K_{2ads}$ ($g.mg^{-1}/min$) are PFO and PSO rate constants, respectively. The value of $K_{ad}$ is determined from the slope and intercepts of log ($q_e$−qt) vs t and the value of $K_{2ads}$ is determined from the slope and intercepts of $t/q_t$ vs t. $K_i$ ($mg\ g^{-1}\ min^{-1}$) is the intra particle diffusion rate constant and is determined from the slope of $t^{0.5}$ vs $q_t$ and $C_i$ is the constant obtained from the intercept which reflects the thickness of the boundary layer, i.e. the larger the intercept, the greater the boundary layer effect. The positive value of $C_i$ indicates that intra-particle was the main mechanism for adsorption and external diffusion occurred to some degree. Figure 4.6a-f depicts the plots for pseudo first order, second order and intra-particle diffusion models respectively. The constant values of pseudo first order, pseudo second order and intra-particle diffusion are presented in Table 4.3 and 4.4, respectively.

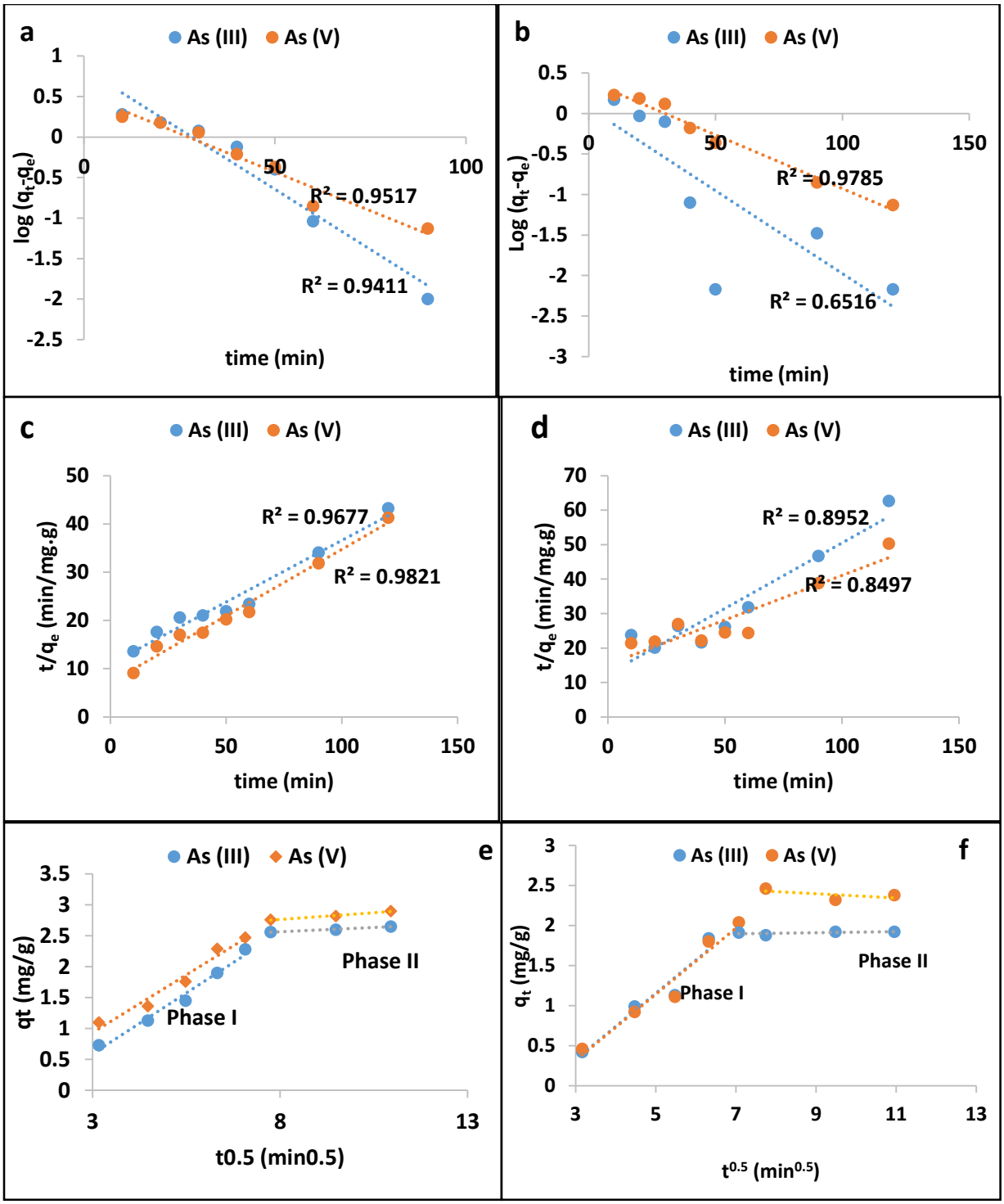


Figure 4.6: plot for pseudo first order (a-b), pseudo second order (c-d) and intra-particle diffusion (e-f) for kaolin clay (a, c and e) soils and smectite rich clay soils (b, d and f).

Table 4.3: Constant values for PFO and PSO reaction kinetics models for As(III) and As(V).

| | Smectite rich clay soils | | | Kaolin clay mineral | | |
|---|---|---|---|---|---|---|
| PFO | $Q_{e\ exp}$ (mg/g) | $K_{ad}$ ($min^{-1}$) | $R^2$ | $Q_e$ (mg/g) | $K_{ad}$ ($min^{-1}$) | $R^2$ |
| As(III) | 1.91 | 0.047 | 0.65 | 2.65 | 0.068 | 0.94 |
| As(V) | 2.46 | 0.030 | 0.97 | 2.9 | 0.043 | 0.95 |
| PSO | $Q_{e\ exp}$ (mg/g) | $K_{2ad}$ ($g.mg^{-1}.min^{-1}$) | $R^2$ | $Q_e$ (mg/g) | $K_{2ad}$ ($g.mg^{-1}.min^{-1}$) | $R^2$ |
| As(III) | 1.91 | 0.0115 | 0.89 | 2.65 | 0.0105 | 0.96 |
| As(V) | 2.46 | 0.0043 | 0.84 | 2.9 | 0.0059 | 0.98 |

Table 4.4: Constant values for intra-particle diffusion model for adsorption of As(III) and As(V).

| | As(III) | | | | | | As(V) | | | | | |
|---|---|---|---|---|---|---|---|---|---|---|---|---|
| | $K_{i1}$ ($mg/g.min^{0.5}$) | $C_1$ (mg/g) | $R^2$ | $K_{i2}$ ($mg/g.min^{0.5}$) | $C_2$ (mg/g) | $R^2$ | $K_{i1}$ ($mg/g.min^{0.5}$) | $C_{i1}$ (mg/g) | $R^2$ | $K_{i2}$ ($mg/g.min^{0.5}$) | $C_2$ (mg/g) | $R^2$ |
| Smectite | 0.41 | -0.91 | 0.92 | -0.02 | 2.63 | 0.37 | 0.41 | -0.91 | 0.95 | 0.006 | 1.84 | 0.36 |
| Kaolin | 0.39 | -0.59 | 0.98 | 0.027 | 2.34 | 0.98 | 0.37 | -0.18 | 0.96 | 0.043 | 2.41 | 0.98 |

Based on the correlation coefficient values obtained from the plots, the adsorption data of As(III) onto smectite rich clay soils was described by the pseudo second order of reaction kinetics while the data for As(V) adsorption was described by the pseudo first order (Table 4.3). Therefore, it can be concluded that the adsorption of As(III) and As(V) onto smectite rich clay soils occurred through chemisorption and physiosorption, respectively. The data for As(III) and As(V) onto kaolin clay fitted better to pseudo second order of reaction kinetics indicating that adsorption occurred through chemisorption (Table 4.3).

The intra-particle plot obtained from the adsorption data did not yield straight line indicating that intra-particle diffusion is not the only rate limiting step (Fig. 4.6e-f). The data exhibited two clearly defined two phases indicating that there are two main adsorption steps are taking place. This was observed in both clay soils. Phase I could be attributed to surface adsorption which completed within the first 60 min. Phase II at 60 min and beyond could be attributed to intra-particle diffusion adsorption at equilibrium. The rate constant values for adsorption of As(III) and As(V) by smectite and kaolin clay at phase I ($K_{i1}$) are higher than those obtained in phase II ($K_{i2}$) (Table 4.4). This indicates that adsorption at the boundary layer (phase I) was faster than the pore diffusion (phase II) and the diffusion resistance period is increased. The pore diffusion in phase II is confirmed by higher $C_i$ value.

### 4.3.2.2 Effect of adsorbent dosage

Figure 4.7a and b shows the effect of adsorbent dosage onto sorption of As(III) and As(V) by kaolin clay and smectite rich clay soils. It is evident that the percentage removal of both arsenic species increased with increasing adsorbent dosage. This could be attributed to increasing adsorption sites as the dosage increases. Furthermore, it is observed that the sorption of As(V) was higher compared to As(III). Adsorbent dosage 0.7 g/100 mL was then adopted as the optimum dosage for subsequent experiments.

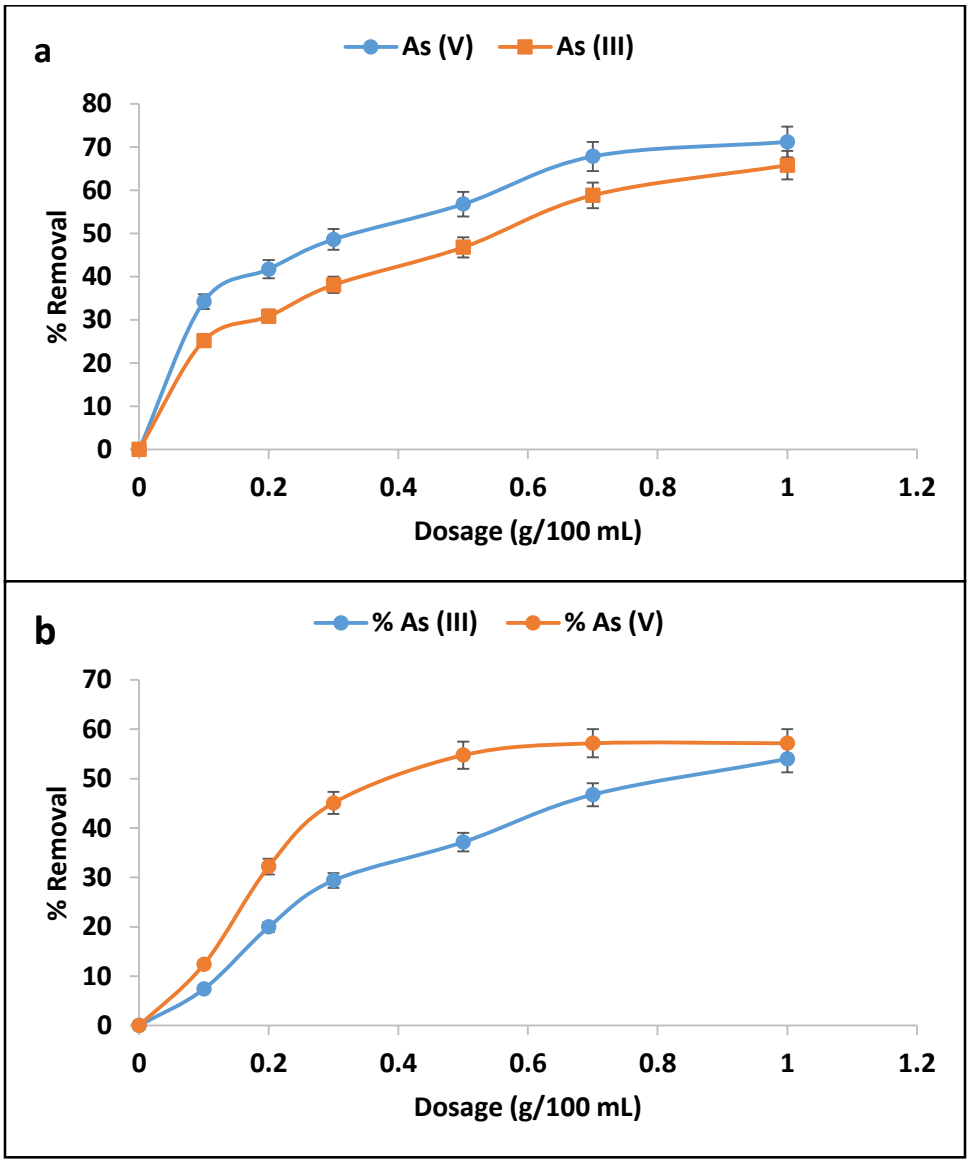


Figure 4.7: Adsorption of As(III) and As(V) onto a) kaolin clay and b) smectite rich clay soils as a function of adsorbent dosage (5 mg/L initial As(III) and As(V) concentration, 60 min contact time, pH 7.5±0.5).

### 4.3.2.3 Effect of adsorbate concentration

Figure 4.8a and b depicts the effect of adsorbate concentration onto As(III) and As(V) removal by kaolin clay and smectite rich clay soils, respectively. It is observed that the percentage removal of As(III) and As(V) decreased with increasing initial concentration. This was observed for both clay soils. The decrease in percentage removal could be attributed to availability of more As(III) and As(V) ions in the solution as the initial concentration increases. At lower initial concentration, the ratio of adsorbent's active sites to adsorbate concentration was high and as a results the interaction between the As(III) and As(V) with the adsorbent was efficient to for their removal.

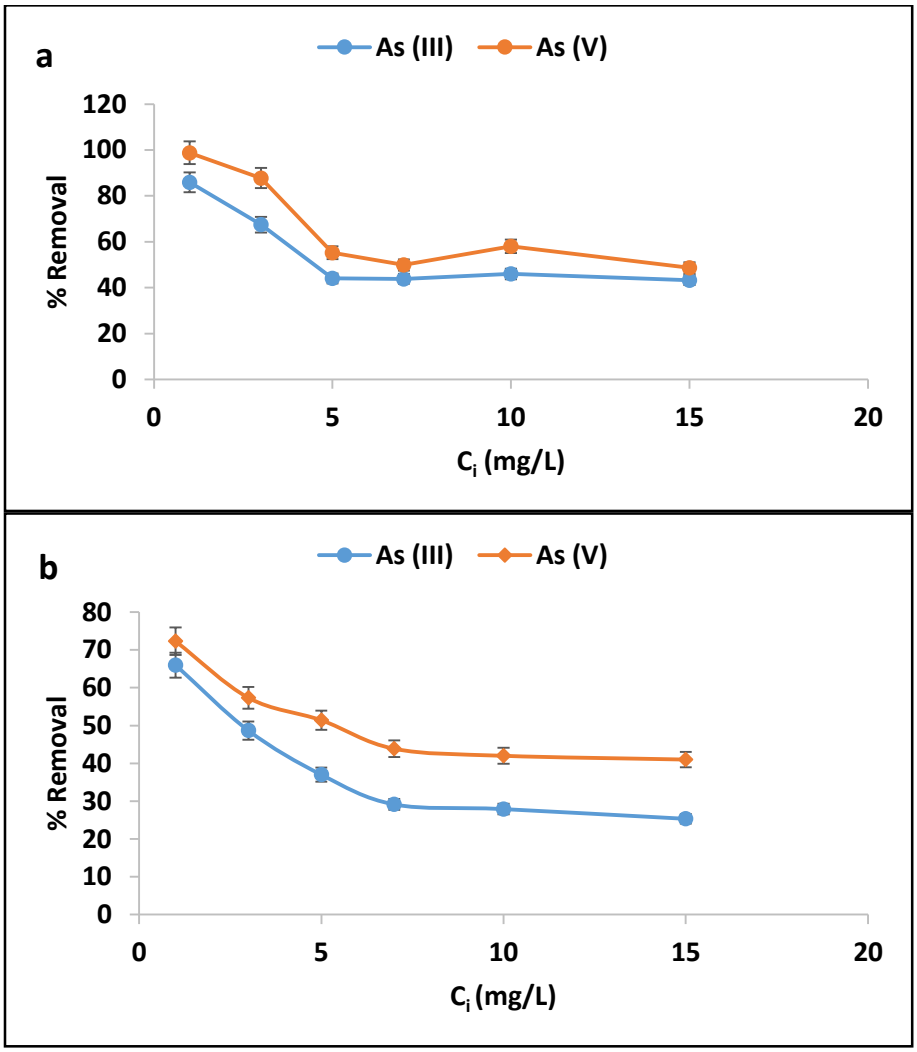


Figure 4.8: Adsorption of As(III) and As(V) onto a) kaolin clay and b) smectite rich clay soils as a function of initial concentration (0.7 g/100 mL adsorbent dosage, 60 min contact time, pH 7.5±0.5).

The adsorption data obtained at different initial concentration was fitted to Langmuir and Freundlich adsorption isotherm models in order to explain the relationship between the adsorbate molecules and the amount adsorbed on the adsorbent surface (Tran et al., 2017). Langmuir isotherm model assumes that adsorption takes place at specific homogeneous site of the adsorbent's surface (Chammui et al., 2014; Yoon et al., 2017). Furthermore, it assumes that there is no mutual interaction between the adsorbed molecules. This means once a molecule adheres on the surface, there is no further adsorption molecule that can be adsorbed at the same site. Conversely, Freundlich isotherm model assumes that the adsorbent surface is heterogeneous and there is mutual interaction between the adsorbate molecules leading to multilayer adsorption (Firdaous et al., 2017). Langmuir and Freundlich isotherm models can be expressed by equation 4.6 and 4.7 respectively.

$$\frac{C_e}{Q_e} = \frac{1}{Q_m b} + \frac{C_e}{Q_m} \tag{4.6}$$

$$\log Q_e = \log K_f + \frac{1}{n}\log Ce \tag{4.7}$$

Where: $C_e$ is the equilibrium concentration (mg/L); $Q_e$ is the adsorption capacity (mg/g); $Q_m$ is theoretical maximum adsorption capacity (mg/g) and $b$ is the Langmuir constant related to enthalpy of adsorption (L/mg). $Q_m$ and $b$ are determined from the slope and intercept of the plot of $\frac{C_e}{Q_e} Vs\ C_e$. $K_f$ is the Freundlich constant related to adsorption capacity and *1/n* is the adsorption intensity. When 0 < *1/n* < 1, the adsorption is favourable; when *1/n* = 1, the adsorption is irreversible; and when *1/n* > 1, the adsorption is unfavourable. The value of $K_f$ and *1/n* are obtained from the slope and intercepts of a linear plot of log $Q_e$ vs log $C_e$. Plots for Langmuir and Freundlich isotherms for As(III) and As(V) adsorption in kaolin clay mineral and smectite rich clay soils are presented in Figure 4.9a-d and the constant values are presented in Table 4.5.

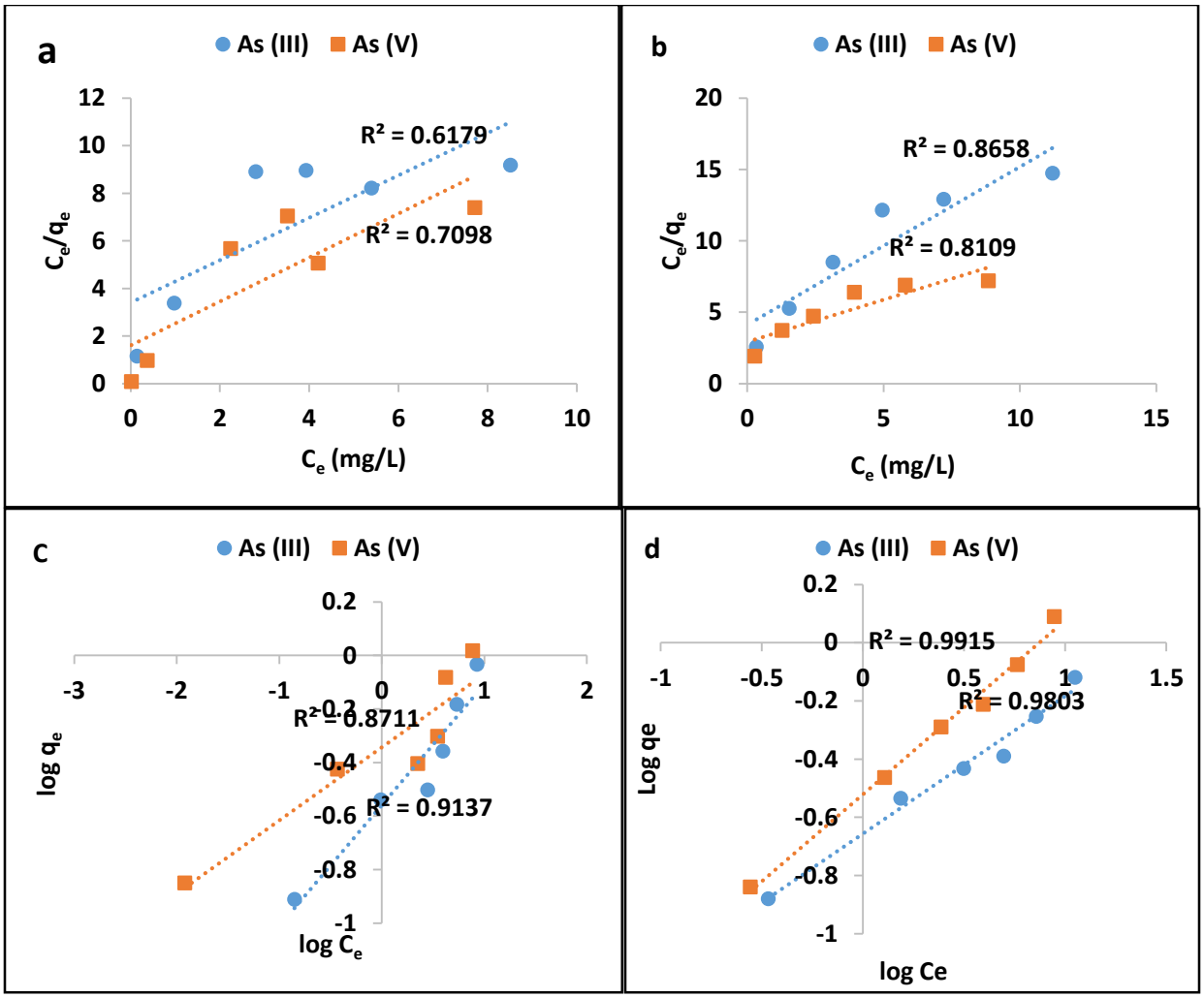


Figure 4.9: Langmuir (a-b) and Freundlich (c-d) isotherm plots for adsorption of As(III) and As(V) by kaolin clay mineral (a and c) and smectite rich (b and d).

Table 4.5: Constant values for Langmuir and Freundlich isotherms during the adsorption of As(III) and As(V).

| | Smectite rich clay soils | | | | Kaolin clay | | | |
|---|---|---|---|---|---|---|---|---|
| Langmuir Isotherm | $Q_e$ (mg/g) | $Q_m$ (mg/g) | B (L/mg) | $R^2$ | $Q_e$ (mg/g | $Q_m$ (mg/g) | B(L/mg) | $R^2$ |
| As(III) | 0.76 | 0.9 | 0.26 | 0.86 | 0.92 | 1.12 | 0.26 | 0.61 |
| As(V) | 1.23 | 1.69 | 0.2 | 0.81 | 1.04 | 1.08 | 0.55 | 0.70 |
| Freundlich isotherm | $Q_e$ (mg/g) | $K_f$ (mg/g) | 1/n | $R^2$ | $Q_e$ (mg/g) | $K_f$ (mg/g) | 1/n | $R^2$ |
| As(III) | 0.76 | 4.53 | 0.47 | 0.98 | 0.92 | 3.62 | 0.45 | 0.91 |
| As(V) | 1.23 | 3.32 | 0.59 | 0.99 | 1.04 | 2.2 | 0.27 | 0.87 |

Based on the correlation co-efficient values presented in Table 4.5, the adsorption data for both arsenic species fitted better to Freundlich adsorption isotherm as compared to Langmuir isotherm model. This was observed in both clay soils. Therefore, it can be concluded that the evaluated clay soils has heterogeneous surfaces in nature that enables multilayer adsorption. The value adsorption intensity (*1/n*) of As(III) and As(V) obtained for Freundlich isotherm also lies between 0 and 1 which further confirms that adsorption was favourable.

#### 4.3.2.5 Effect of initial pH

To evaluate the effect of pH, the initial pH of the solution was adjusted from 2 to 12 using 0.1 M NaOH and 0.1 M HCl. Figure 4.10 and b shows the relationship between As(V) and As(III) removal by kaolin clay and smectite rich clay soils as function of pH respectively. As(V) removal by kaolin clay was observed to be high at pH 2 and moderate between the 4 and 8. Further slight decrease was observed at pH >10 (Fig. 4.10a). Conversely, the removal of As(III) by kaolin clay mineral remained almost the same from initial pH of 2 to 10. Slight decrease was observed at pH>10 (Fig. 4.10a). The removal of As(III) and As(V) by smectite rich clay was observed to be higher at pH range 6-8 (Fig. 4.10b). Lower uptake for both arsenic species was observed in both acidic and alkaline pH range (Fig. 4.10b). The pHpzc of smectite rich clay soils and kaolin clay determined using solid titration were found to be 5.6 and 6.5, respectively. At the pH below the pHpzc the surface of the clay is positively charged while at pH beyond the pHpzc the surface negatively charged. It is expected that the sorption of negatively charged ions will be optimum at pH below the pHpzc and decrease at pH beyond the pHpzc.

The As(III) speciation demonstrates that at pH below 7.99, the dominant species is neutrally charged $H_3AsO_3$ while at pH beyond 7.99 it exist as $H_2AsO_3^-$ (Table 4.6). The sorption of As(III) could be due to ion exchange at pH below the pHpzc for both clay clays and Van der Waal attraction force when the pH of the solution is close to clay pHpzc. The As(V) speciation in Table 4.6 demonstrates that at pH around 2.5 it exist as neutrally charged $H_3AsO_4$ and at pH above 4.96 it exist as $H_2AsO_4^-$ and $HAsO_4^{2-}$ which can be adsorbed via ion exchange and electrostatic attraction at pH below the pHpzc (Chen et al., 2013). At pH beyond clay pHpzc the decrease in percentage As removal could be ascribed to two main factors namely; competition between the $OH^-$ in the solution and negatively charged As species and also to the electrostatic repulsion

between the surface of the clay soils. The adsorption mechanisms of As(III) and As(V) can be hypothesized by equation 4.8-4.12 (Li et al., 2011). Here M represent metals, Si, Al and Fe.

$$\equiv MOH + H_3As_3 \leftrightarrow \equiv MH_2As_3 + H_2O \quad (4.8)$$

$$\equiv MOH + H_2As_3^- \leftrightarrow \equiv MHAs_3^- + H_2O \quad (4.9)$$

$$\equiv MOH + H_3AsO_4 \leftrightarrow \equiv MH_2AsO_4 + H_2O \quad (4.10)$$

$$\equiv MOH + H_2AsO_4^- \leftrightarrow \equiv MHAsO_4^- + H_2O \quad (4.11)$$

$$\equiv MOH + HAs_4^{2-} \leftrightarrow \equiv MAs_4^{2-} + H_2O \quad (4.12)$$

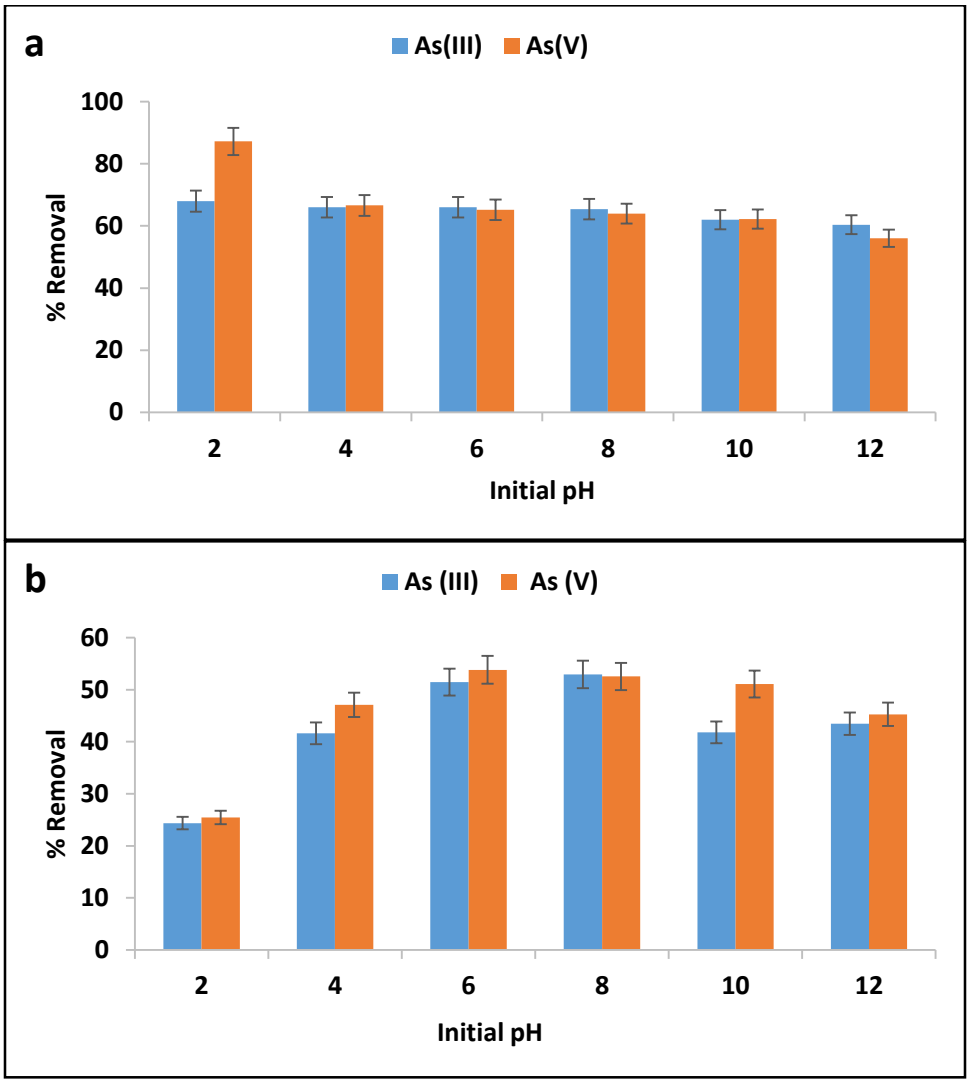


Figure 4.10: Adsorption of As(III) and As(V) onto kaolin clay (a) and smectite rich clay soils (b) as a function of solution pH (5 mg/L initial As(III) and As(V) concentration, 0.7 g/100 mL adsorbent dosage and 60 min contact time at 250 rpm).

Table 4.6: Arsenic species distribution at different equilibrium pH level.

| | As(V) | | | | As(III) | | |
|---|---|---|---|---|---|---|---|
| **Smectite rich clay soils** | | | | | | | |
| Eq. pH | $H_3AsO_4$ | $H_2AsO_4^-$ | $HAsO_4^{2-}$ | $AsO_4^{3-}$ | $H_3AsO_3$ | $H_2AsO_3^-$ | $HAsO_3^{2-}$ |
| 2.51 | 37.07 | 62.94 | - | - | 100.00 | - | - |
| 4.96 | 0.205 | 98.81 | 0.98 | - | 99.99 | - | - |
| 5.44 | 0.070 | 97.14 | 2.78 | - | 99.98 | 0.091 | - |
| 7.78 | - | 13.36 | 86.36 | - | 96.05 | 3.94 | - |
| 7.99 | - | 8.83 | 91.13 | 0.015 | 93.74 | 6.25 | - |
| 11.45 | - | - | 64.15 | 35.84 | 0.49 | 99.21 | 0.25 |
| **Kaolin clay** | | | | | | | |
| 03.62 | 4.50 | 95.44 | 0.042 | - | 100.00 | - | - |
| 6.41 | - | 78.92 | 21.07 | - | 99.82 | 0.174 | - |
| 6.96 | - | 51.25 | 48.78 | - | 99.38 | 0.61 | - |
| 7.02 | - | 47.78 | 52.21 | - | 99.29 | 0.76 | - |
| 9.46 | - | 0.32 | 99.17 | 0.47 | 33.67 | 66.31 | - |
| 11.53 | - | - | 59.38 | 40.61 | 0.41 | 99.27 | 0.30 |

### 4.3.3 Treatment of field water

The performance of the kaolin clay and smectite rich clay soils in arsenic removal from field groundwater samples was tested by treating borehole water collected from Siloam community borehole. Borehole water was spiked with As(III) and As(V) to get total arsenic concentration of 1.4 mg/L. Other parameters of groundwater are presented in Table 4.7. Field water was treated using adsorbent dosage of 0.7 g/100 mL and mixtures were agitated for 60 min at 250 rpm. The physicochemical parameters of the water after treatment are presented in Table 4.7. It is observed that smectite rich clay soils and kaolin clay were able to reduce As concentration to 0.45 and 0.36 mg/L, respectively. Both clay soils showed a potential for application in groundwater since they both showed the capacity to remove other co-existing ions. Amongst the two clay soils, kaolin clay mineral showed better removal efficiency compared to smectite rich clay soils.

Table 4.7: Physicochemical parameters of Siloam borehole water before and after treatment.

| **Chemical Parameters** | **Field water** | **Treaded with kaolin clay** | **Treated with smectite rich clay** | **SANS-241** |
|---|---|---|---|---|
| pH | 8.7 | 7.23 | 7.56 | 5.0-9.7 |
| As total | 1.45 | 0.36 | 0.45 | 0.01 |
| $F^-$ | 5.4 | 1.36 | 2.56 | 1.5 |
| $Cl^-$ | 31.59 | 26.45 | 23.68 | <300 |
| $SO_4^{2-}$ | 11.89 | 10.36 | 8.96 | <500 |
| $NO_3^-$ | 2.67 | N.D | 2.56 | <11 |
| $PO_4^{3-}$ | 1.3 | N.D | N.D | - |
| Al | 0.26 | 0.05 | 0.07 | 0.3 |
| Mn | 0.29 | 0.03 | 0.13 | 0.4 |
| Fe | 0.013 | 0.04 | 0.04 | 2 |
| Mg | 1.2 | 3.11 | 6.62 | - |
| Ca | 1.95 | 7.10 | 8.26 | - |
| K | 2.6 | 13.9 | 3.86 | - |
| Na | 70 | 89.8 | 32.4 | 200 |
| Zn | 0.08 | 0.011 | 0.019 | 5 |
| Cu | 2.45 | 0.013 | 0.01 | 2 |
| Si | 53.78 | 8.33 | 9.49 | - |

ND=Not Detected, All concentrations in mg/L.

### 4.3.4 Chemical stability assessment

The chemical stability of kaolin clay and smectite rich clay soils during arsenic adsorption was assessed by analyzing the metal concentration in filtrates obtained during the evaluation of pH. The results are presented in Figure 4.11. It is observed that at pH 6 all metal species were leached out from kaolin clay and smectite rich clay soils at trace concentrations which is within the SANS standards. This indicating that both clay soils are safe for use for arsenic removal. Metals such as Al and Si were leached at higher concentration at pH 2 and 12 by smectite and kaolin clays, respectively. This could be attributed to their dissolution. Higher concentration of Na could be attributed to NaOH used for adjusting pH.

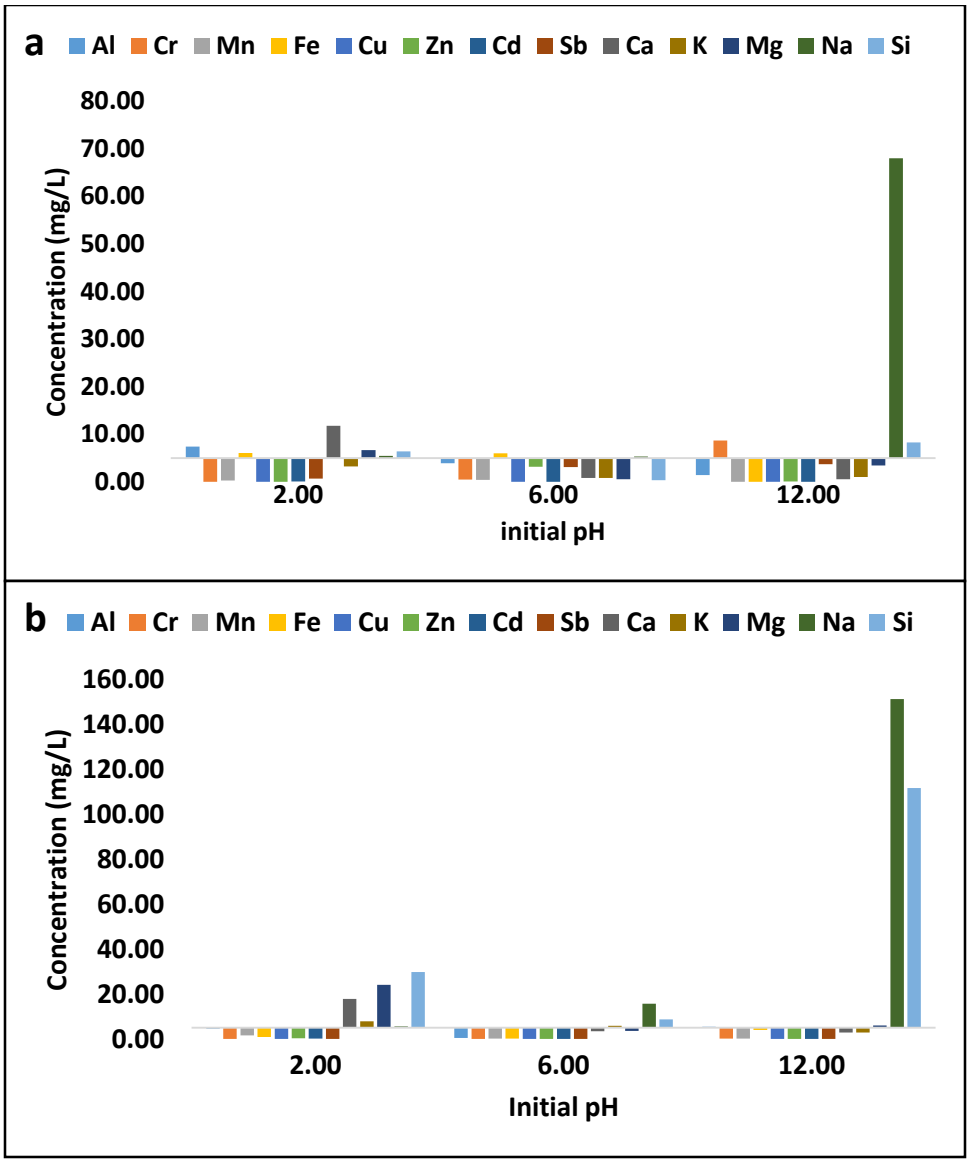


Figure 4.11: Concentration of leached metals from kaolin clay (a) and smectite rich clay soils (b) during As adsorption at different initial pH (5 mg/L initial As(III) and As(V) concentration, 0.7 g/100 mL adsorbent dosage and 60 min contact time at 250 rpm).

### 4.3.6 Effect of co-existing anions

The effect of co-existing anions in the adsorption of As(III) and As(V) by kaolin clay and smectite rich clay soil is presented in Figure 4.12a and b, respectively. It is observed that presence of $F^-$ and $Cl^-$ have slight effect on the adsorption of As(III) and As(V) as compared to the presence of $SO_4^{2-}$ and $CO_3^{2-}$. Decrease in As(III) and As(V) removal in the presence of $SO_4^{2-}$ and $CO_3^{2-}$ could be attributed to competition for adsorption sites from these anions. Carbonates increases the alkalinity of the solution which in turn increase the negative charges the adsorbent's surface leading to

decreased percentage of removal. The effects of co-existing anions towards the adsorption of As(III) and As(V) may be summarize in the following inhibition order: $CO_3^{2-}$>$SO_4^{2-}$>$F^-$≥ $Cl^-$. This observation was observed in both clay soils.

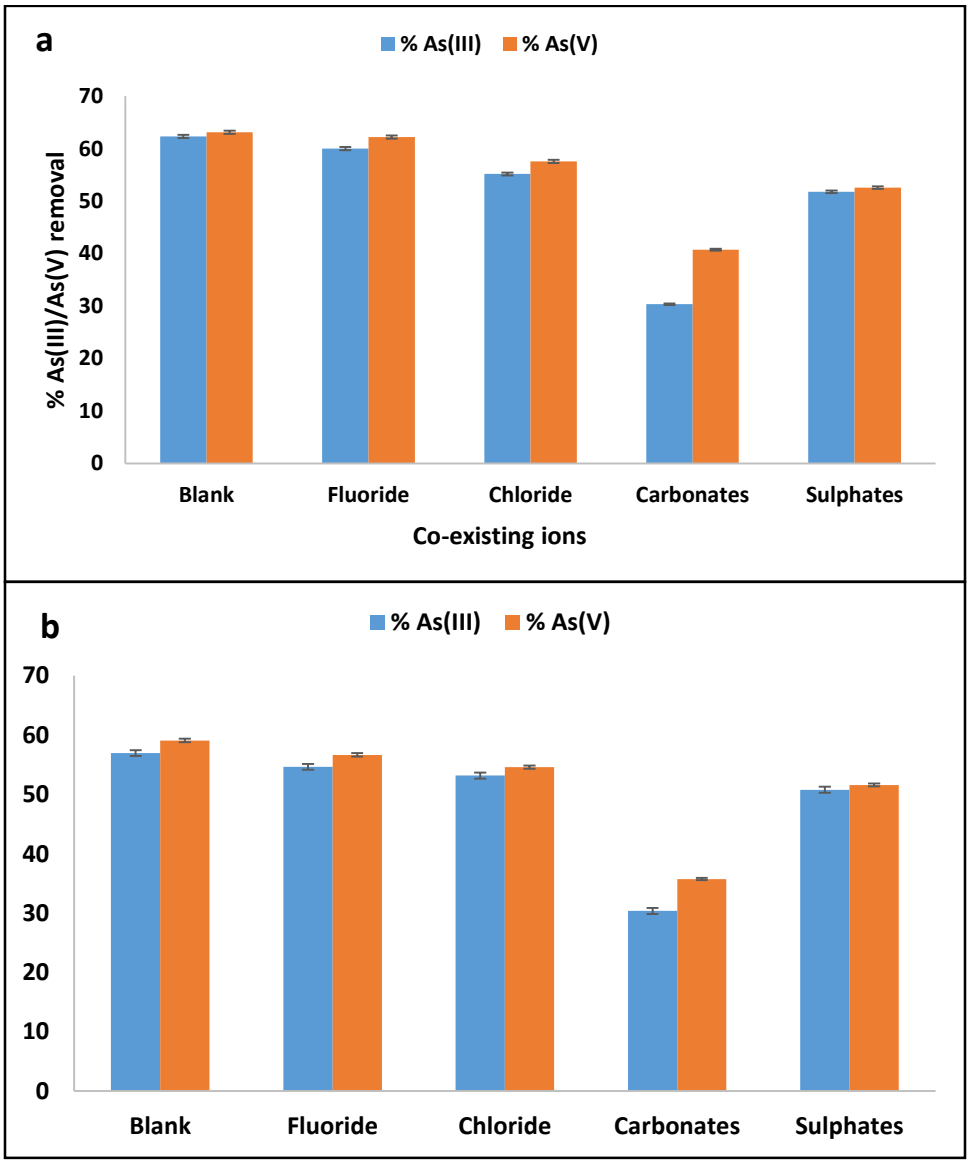


Figure 4.12: Effects of co-existing anions in the adsorption of As(III) and As(V) by kaolin clay (a) and smectite rich clay soils (b) clay soil (0.7 g/100mL adsorbent dosage, 5 mg/L initial concentration and 60 mins contact time).

### 4.3.7 Reuse and regeneration of the adsorbent

Reuse and regeneration potential experiment were conducted to evaluate the efficiency and sustainability of the clay soils for use in the field. Figure 4.13a and b depicts the percentage arsenic removal as a function of regeneration-reuse cycle. For kaolin clay, (Figure13a) the percentage of

As(III) removal decreased from 55.57 to 32.88% after reuse cycle and further decrease to 19.23% after the second cycle. Whereas, the percentage As(V) removal decreased from to 61.11 to 33.33% after first reuse cycle and further decreased to 26.11% after second regeneration. For smectite rich clay (Fig. 13b) the percentage As(III) and As(V) removal decreased from 37.30 to 13.46% and 45.18 to 27.77% respectively in the first cycle. After second regeneration cycle, the percentage As(III) removal decreased to 1.92% while for As(V) it decreased to 8.14%. The decrease in percentage removal after regeneration could be attributed to either destruction of clay structure as a results of treatment by $Na_2CO_3$ or inadequate reactivation of active sites. Amongst two clay soils kaolin clay showed better removal efficiency compared to smectite rich clay soils.

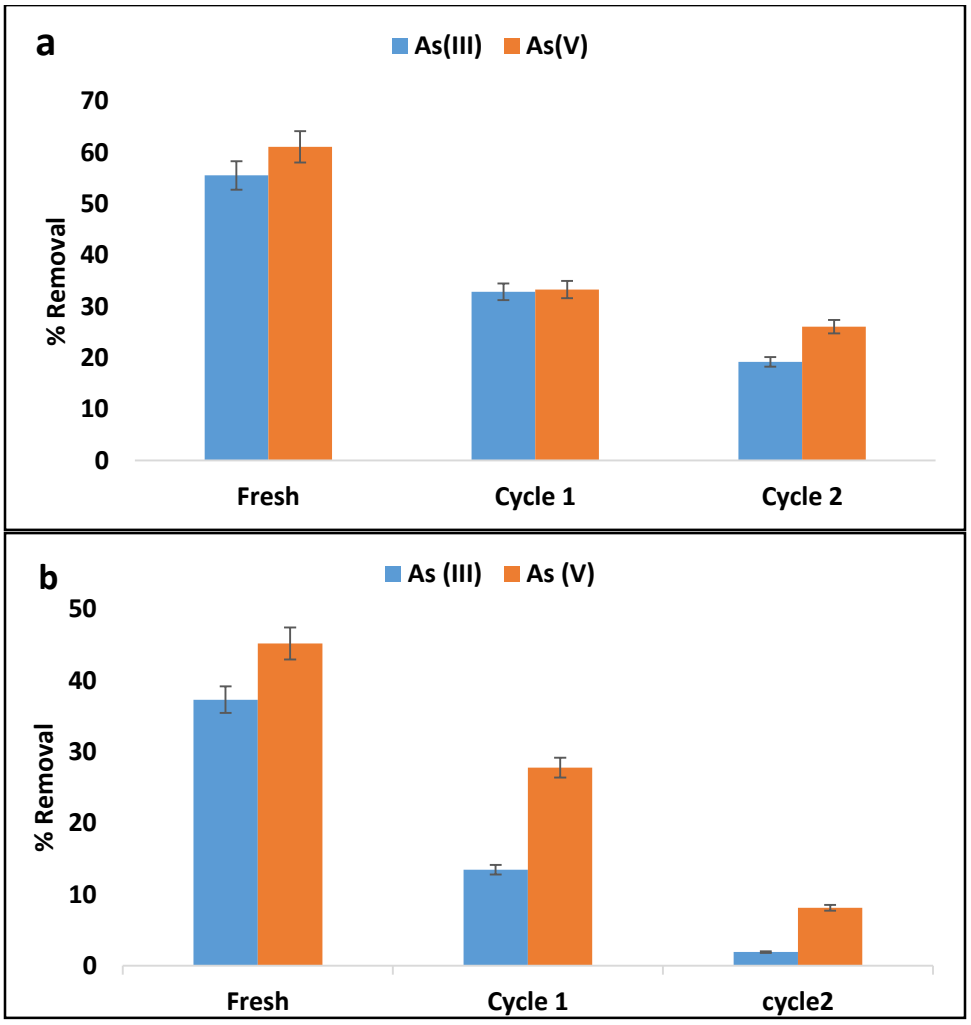


Figure 4.13: Adsorption-regeneration cycles for As(III) and As(V) removal by kaolin clay (a) and smectite rich clay soils (b) (1.0 g/100mL adsorbent dosage, 5 mg/L initial concentration and 60 min contact time).

## 4.4 Summary

The two clay soils were successfully characterized and evaluated for the removal of As(III) and As(V) from the groundwater. The results showed that both clay soils are rich in $SiO_2$ and $Al_2O_3$ oxides as such they belong to the group of alumino-silicate materials. The percentage As(V) removal by kaolin clay was found to be 87.2% at pH 2. Conversely, the As(III) was greater than 60% at wide range of pH. The percentage of As(III) and As(V) removal by smectite rich clay soils was found to be optimum at pH between 6 and 8. The adsorption kinetics data for the adsorption of As(III) by kaolin clay fitted better to pseudo second order of reaction kinetics while that of As(V) fitted betted better in pseudo first order of reaction kinetics. On the other hand, the data for adsorption of As(III) and As(V) by smectite rich clay soils fitted better to pseudo first order. The Weber-Morris model of intra-particle diffusion for the data obtained from both arsenic species showed two linear plot indicating that the adsorption of As(III) and As(V) by smectite rich clay and kaolin clay mineral involves both surface and intra-particle diffusion. Adsorption isotherm models revealed that the data fitted well to Freundlich adsorption isotherm indicating that the surface of the clay soils is heterogeneous in nature. The effects of co-existing anions towards the adsorption of As(III) and As(V) by both clay soils could be summarized in the following inhibition order: $CO_3^{2-}>SO_4^{2-}>F^-\geq Cl^-$. Regeneration study revealed that the percentage As(III) and As(V) removal by both clay decreases with continuous regeneration-reuse cycles. The results showed that both clay soils can be used for treatment of field water. However, further studies are recommended to improve their sorption capacity.

## References

Abdula, K. S. M. Jayasingheb, S. S. Chandanaa, E. P. S. Jayasumanac, C. P. & De Silva, M. C. S., 2015. Arsenic and human health effects: A review. *Environmental Toxicology and Pharmacology*, 40, pp.828-846.

Ayari, F., Srasra, E., Trabelsi-Ayadi, M., 2005. Characterization of bentonitic clays and their use as Adsorbent. *Desalination*, 185, 391‑397.

Ayotte, J. D. Belaval, M. Olson, S. A. Burow, K. R. Flanagana, S. M. Hinkle, S. R. & Lindsey, B. D. 2015. Factors affecting temporal variability of arsenic in groundwater used for drinking water supply in the United States. *Science of the Total Environment*, 505, pp.1370–1379.

Bentahar, Y., Hurel, C., Draoui, K., Khairoun, S. & Marmier, N., 2016. Adsorptive properties of Moroccan clays for the removal of arsenic(V) from aqueous solution. *Applied Clay Science* 119, pp.385–392.

Bhattachryya, K. G. & Gupta, S. S., 2008. Adsorption of few heavy metals on natural and modified kaolinite and montmorillonite: A review. *Advances in colloid and interface science*. 140, pp.114-131.

Bretzler, A., Lalanne, F., Nikiema, J., Podgorski, J., Pfenninger Numa, Berg, M., and Schirmer, M., 2017. Groundwater arsenic contamination in Burkina Faso, West Africa: Predicting and verifying regions at risk. Science of the Total Environment, 584-585, 984-970.

Chakraborti, D., Rahman, M. M., Ahamed, S., Dutta, N. R., Pati, S., Mukherjee, S. C., 2016. Arsenic groundwater contamination and its health effects in Patna district (capital of Bihar) in the middle Ganga plain, India. *Chemosphere*, 152, 520-529.

Chammui, Y., Sooksamiti, P., Naksata, W., Thiansem, S., Arqueropanyo, O., 2014. Removal of arsenic from aqueous solution by adsorption on Leonardite. *Chemical Engineering Journal*, 240 202-210.

Chen, B., Zhu, Z., Guo, Y., Qiu, Y., Zhao, J., 2013. Facile synthesis of mesoporous Ce–Fe bimetal oxide and its enhanced adsorption of arsenate from aqueous solutions. *Journal of Colloid and Interface Science*, 398, 142-151.

Chen, N., Zhang, Z., Feng, C., Li, M., Chen R., Sugiura, N., 2011. Investigations on the batch and fixed-bed column performance of fluoride adsorption by Kanuma mud. *Desalination*, 268, 76–82.

Cheng, Y. Y., Huang, N. C., Chang Y. T., Sung, J. M, Shen, K. H., Tsai, C. C., Guo, H. R., 2017. Associations between arsenic in drinking water and the progression of chronic kidney disease: A nationwide study in Taiwan. *Journal of Hazardous Materials*, 321, 432-439.

Cheng, Z. Fu, F. Dionysiou, D. D. & Tang, B. 2016. Adsorption, oxidation, and reduction behaviour of arsenic in the removal of aqueous As(III) by mesoporous Fe/Al bimetallic particles. *Water Research*, 96, pp.22-31.

Ding, W. Wang, Y. Yu, Y. Zhang, X. Li, Y. & Wu, F., 2015. Photooxidation of arsenic(III) to arsenic(V) on the surface of kaolinite clay. *Journal of Environmental Sciences*, 36, pp.29-37.

Duker, A. A, Carranza, E. J. M. & Hale, M. 2005. Arsenic geochemistry and health. *Environment International*, 31, pp.631– 641.

Favero, J.S., Peterle, J. P., Angeli, V. W., Brandalise, N. V., Gomes, L. B., Bergmann, L. B., Santos, V., 2016. Physical and chemical characterization and method for the decontamination of clays for application in cosmetics. *Applied Clay Science*, 124(125), 252-259.

Firdaous, L., Fertin, B., Khelissa, O. Dhainaut, M., Nedjar, N. Chataigné, G., Ouhoud, L., Lutin, F., Dhulster, P., 2017. Adsorptive removal of polyphenols from an alfalfa white proteins concentrate: Adsorbent screening, adsorption kinetics and equilibrium study. *Separation and Purification Technology*. 178, 29-39.

Fouodjouo, M., Nkaffo, H. F., Laminsi, S., Cassini, F. A., Brito-Benetoli., L. O. Debacher, N. A., 2016, Adsorption of copper (II) onto cameroonian clay modified by non-thermal plasma: Characterization, chemical equilibrium and thermodynamic studies. *Applied Clay Science*, 1-9.

Ho, S. H., 2004. Citation review of Lagergren kinetic rate equation on adsorption reactions. *Scientometrics*, 59(1), 171-177.

Hua, J., 2015. Synthesis and characterization of bentonite based inorgano–organo-composites and their performances for removing arsenic from water. *Applied Clay Science*, 114, pp.239-246.

James, J. A., Marshall, J. A., Hokanson, J. E., Meliker, J. R., Zerbe, G. O, Byers, T. E., 2013. A case-cohort study examining lifetime exposure to inorganic arsenic in drinking water and diabetes mellitus. *Environmental Research*, 123, 33–38.

Kempster, P. L., Silberbauer, M., Kuhn, A., 2006, Interpretation of drinking water quality guidelines – The case of arsenic. *Water SA*, 33 (1), 95-100.

Kortatsi, B. K., Asigbe, J., Dartey, G. A., Tay, C. Anornu, G. K. and Hayford, E., Reconnaissance Survey of Arsenic Concentration in Ground-water in South-eastern Ghana. *West African Journal of Applied Ecology*, 13, 16-26.

Kundu, S., Gupta, A. K., 2007. Adsorption characteristics of As(III) from aqueous solution on iron oxide coated cement (IOCC). *Journal of Hazardous Materials*, 142, 97–104.

Li, Z., Jeanc, J. S., Jiang, W. T., Chang, P. Chen, C. J., Liao, L., 2011. Removal of arsenic from water using Fe-exchanged natural zeolite. *Journal of Hazardous Materials*, 187, 318–323.

Maji, S. K., Pal A. & Pal, T., 2008 Arsenic removal from real-life groundwater by adsorption on laterite soil. *Journal of Hazardous Materials*, 151, pp.811–820.

Mandal, B. K. & Suzuki, K. T., 2002. Arsenic round the world: a review. *Talanta*, 58 (1), pp.201-235.

Mazumder, D. G., Dasgupta U. B., 2011. Chronic arsenic toxicity: Studies in West Bengal, India. *Kaohsiung Journal of Medical Sciences*, 27, 360-370.

Mishra, T. & Mahato, D. K., 2016. A comparative study on enhanced arsenic(V) and arsenic(III) removal by iron oxide and manganese oxide pillared clays from ground water. *Journal of Environmental Chemical Engineering*, 4, pp. 1224–1230.

Mohana, D. & Pittman, C. U, 2007 Arsenic removal from water/wastewater using adsorbents: A critical review. *Journal of Hazardous Materials,* 142, pp.1–53.

Mudyazhezha, S. and Kanhukamwe, R., 2004. Environmental monitoring of the effects of conventional and artisanal gold mining on water quality in Ngwabalozi River, Southern Zimbabwe. *International Journal of Engineering and Applied Sciences,* 4 (10), 13-18.

Mudzielwana, R., Gitari, W. M., Msagati, T. A. M., 2016. Characterisation of smectite-rich clay soil: Implication for groundwater defluoridation. South African Journal of Science, 112(11/12) 41-48.

Ren, X., Zhang, Z., Luo, H., Hu, B., Dang, Z., Yang, C., Li, L., 2014. Adsorption of arsenic on modified montmorillonite. *Applied Clay Sciences*. 97-98, pp.17-23.

Sarkar, A. & Paul, B., 2016. The global menace of arsenic and its conventional remediation: A critical review. *Chemosphere,* 158, pp.37-49.

Sigdel, A., Park, J., Kwak, H. & Park, P., 2016. Arsenic removal from aqueous solutions by adsorption onto hydrous iron oxide-impregnated alginate beads. *Journal of Industrial and Engineering Chemistry*, 35, pp.277–286.

Smith, A. H., Biggs, L. M., Moore, L., Haque, R., Steinmaus, C., Chung, Y., Hernandez, A. & Lopipero, P., 1999, Cancer risks for arsenic in drinking water: Implications for drinking water standards. Elsevier Science B.V.

Tyeryar, M., Hackett, C., Harsh D., Hackett, T., 2012. Establishing a ceramic water filter factory in Limpopo Province, South Africa. *Jefferson Public Citizens*, 3, 104–110.

Uddin, R., Saffoon, N., Alam, M. A., 2007. Arsenic, the poison and poisoned groundwater of Bangladesh: A review. *International Current Pharmaceutical Journal*, 1(1): 12-17.

Ungureanu, G., Santos, S., Boaventura, R. & Botelho, C., 2015. Arsenic and antimony in water and wastewater: Overview of removal techniques with special reference to latest advances in adsorption, *Journal of Environmental Management*, 151, pp. 326-342.

Wang, J., Wang, T., Burken, J. G., Chusuei, C. C., Ban, H., Ladwig, K., Huang, C. P., 2008. Adsorption of arsenic(V) onto fly ash: A speciation-based approach. *Chemosphere*, 72, 381-388.

Wilkie, J. A., Hering, J. G., 1999. Adsorption of arsenic onto hydrous ferric oxide: effects of adsorbate/adsorbent ratios and co-occurring solutes. *Colloids and Surfaces A: Physicochemical and Engineering Aspects*, 107, 97-110.

Yoon, Y., Zheng, M., Ahn, Y. T., Park, W. K., Yang, W. S., Kang, J. W., 2017. Synthesis of magnetite/non-oxidative graphene composites and their application for arsenic removal. *Separation and Purification Technology*, 178, 40-48.

# Chapter 5: Removal of arsenic from groundwater using Fe-Mn bimetallic oxide modified kaolin clay: Adsorption modelling and mechanistic aspect

## 5 Abstract

Chapter 4 reported the use of smectite rich clay soils and kaolin clay for use in arsenic removal from groundwater. Among the two clay minerals, kaolin clay showed higher adsorption efficiency towards arsenic. However, its applicability is limited due to poor regenerability and lower adsorption capacity as compared to other adsorbent in the literature. Further studies were therefore recommended to enhance its adsorption efficiency through modification. In this chapter, Fe-Mn bimetal oxide modified kaolin clay was successfully synthesized by precipitating $Fe^{3+}$ and $Mn^{2+}$ metal oxides onto the interlayer surface of kaolin clay. The physicochemical and mineralogical composition of the synthesized adsorbent were characterized using XRF, XRD, BET, SEM and FTIR. Modification of kaolin clay increased the surface area from 19.2 $m^2/g$ to 29.8 $m^2/g$ and further decreases the pore diameter of 9.54 to 8.5 nm. Furthermore, the percentage composition of $Fe_2O_3$ and MnO increased from 3.88 and 0.01% to 16.66 and 4.02% respectively after modification confirming that Fe and Mn oxides were successfully impregnated onto the clay interlayers. Batch experiments were used to evaluate the applicability of the adsorbent in As(III) and As(V) removal from the solution. A maximum As(III) and As(V) percentage removal of 82.75 and 81.64%, respectively were achieved at initial pH of 6 from initial concentration of 5 mg/L using adsorbent dosage of 0.4 g/100 mL and agitation time of 60 min at 250 rpm shaking speed. The adsorption data fitted to the pseudo second order of reaction kinetics indicating that adsorption of As(III) and As(V) occurred via chemisorption. Weber-Morris intra-particle diffusion model confirmed the occurrence of both surface and intra-particle diffusion adsorption processes. The adsorption isotherm data was described by Langmuir isotherm models showing a maximum As(III) and As(V) adsorption capacities of 2.16 and 1.56 mg/g, respectively at a temperature of 289 K. The presence of $SO_4^{2-}$ inhibits the adsorption of As(III) and As(V). The regeneration-reuse study showed that the synthesized adsorbent can be reused for a maximum of 6 adsorption-desorption cycles using $K_2SO_4$ as a regenerant. Column experiments were conducted to evaluate the applicability of the synthesized adsorbent in the field, a maximum breakthrough volume of ≈2 L was achieved at breakthrough point using a 5 g adsorbent dosage. The overall quality of the treated water was improved at the breakthrough point. Furthermore, the concentration of Fe and Mn were with the

WHO permissible limit. The results showed that Fe-Mn bimetal oxide modified kaolin clay evaluated in this study is a promising adsorbent for arsenic removal from groundwater.

*Keywords:* Adsorption; arsenic; kaolin clay; kinetics; isotherms, Fe-Mn bimetallic oxide.

## 5.1 Introduction

Contamination of groundwater by arsenic is now viewed as an environmental and public health issue globally with countries like India, Bangladesh, China, Mexico and Chile being the worst affected (Rahman et al., 2018; Bhowmick et al., 2018). It is estimated that more than 200 million people worldwide are at risk of arsenic poisoning from arsenic contaminated groundwater (Naujokas et al., 2013). Symptoms of arsenic poisoning includes various types of cancer, skin thickening and neurological disorder diseases after a long period of exposure (Mandal and Suzuki, 2002; Smith and Smith, 2004; Tiwari and Lee, 2012). The World Health Organization (WHO) reduced the standard for arsenic in drinking water from 50 µg/L to 10 µg/L in 1993 with the aim of reducing arsenic poisoning risk (WHO, 2011). Today, majority of community living in developing countries still depend on groundwater with arsenic concentration beyond 10 µg/L due to lack of alternative sources of arsenic free water.

In natural water, arsenic primarily occur in inorganic form as arsenite [As(III)] and arsenate [As(V)], depending on the redox conditions (Smedley and Kinnburgh, 2002). Arsenite is more mobile, highly toxic and difficult to remove as compared to arsenate. This is because it is neutrally charged at most pH ranges (Qi et al., 2015). Available arsenic removal techniques such as coagulation, ion-exchange, adsorption and precipitation have proven to be more effective for the removal of As(V) than As(III) which is highly toxic (Li et al., 2012). In conventional water treatment, pre-oxidation of As(III) to As(V) is necessary and recommended in order to achieve higher As(III) removal (Cui et al., 2014; Ding et al., 2015). This process is more complex and highly expensive. As such it is of high priority to develop alternative techniques that are sustainable and feasible and capable of effective and simultaneous removal of As(III) and As(V) from the solution (Qi et al., 2015).

In 2012 Zhang et al. successfully developed a novel binary sorbent from Fe-Mn oxides and achieved higher efficiency for both As(III) and As(V) removal from aqueous solution. The higher sorption efficiency of Fe-Mn binary sorbent emanate from the stronger binding capacity of iron oxides towards As(V) and the ability of manganese oxides to oxidize As(III) into As(V) (Zhang et

al., 2012; Cui et al., 2014; Ocinski et al., 2016). The arsenic removal mechanism by Fe-Mn binary oxide is coupled with oxidation and adsorption processes. Although Fe-Mn has higher efficiency towards both species of arsenic, its application on flow through systems is limited due to its weak mechanical strength and propensity to aggregate which results in extremely high pressure drop and poor hydraulic properties (Qi et al., 2015). Nonetheless, the use of Fe-Mn oxides adsorbents in arsenic removal is not economically viable because the production of Fe-Mn oxides sorbent is costly and may lead to leaching of Fe and Mn into the treated water (Lin et al., 2017). To overcome this, Qi et al. (2015) successfully developed Fe-Mn binary oxide impregnated chitosan beads which showed satisfactory hydraulic property and relatively good arsenic sorption performance. The chemical stability of the adsorbent was not reported.

Clay and clay minerals are largely found in nature at little or no cost. Furthermore, clays have shown higher adsorption efficiency towards the removal of inorganic contaminants from water. The higher sorption capacity of clay minerals originates from their physicochemical properties such as larger specific surface area, higher cation exchange capacity, and chemical and mechanical stability (Bhattacharyya and Gupta, 2008). Moreover, clays can be modified to enhance their adsorption capacity. Iron and manganese oxides have been used previously in modification of clay minerals for As(III) and As(V) removal. However, very little has been done on modification of clay minerals with Fe-Mn oxides bimetals for arsenic removal regardless of their advantage.

In this study, As(III) and As(V) adsorbent made of Fe-Mn binary oxides modified kaolin clay was prepared by impregnating Fe-Mn oxides onto the kaolin clay interlayers through co-precipitation. The adsorbent was characterized for its physicochemical and mineralogical composition using techniques such as BET, XRF, XRD, SEM and FTIR. Batch experiments were conducted to evaluate the effect of contact time, adsorbent dosage, adsorbate concentration, solution pH, common co-existing ions in As(III) and As(V) removal. The adsorption kinetics, adsorption isotherms and thermodynamics models were employed to evaluate the mechanism of As(III) and As(V) removal. Feasibility of regeneration and reuse together with the chemical stability of the synthesized adsorbent was also examined.

## 5.2 Material and Methods

### 5.2.1 Materials

Locally available kaolin clay soils containing quartz and kaolinite as main minerals was collected from Dzamba Village, Limpopo Province, South Africa. All chemical reagents including $FeCl_3$, $MnCl_2.4H_2O$, NaOH, $AsNaO_2$ and $HAsNa_2O_4$ were purchased from Rochelle Chemicals & Lab Equipment CC, South Africa Ltd and were of analytical grade and they were used without further purification. Stock solutions containing 1000 mg/L As(III) and As(V) were prepared by dissolving 0.1733 g $AsNaO_2$ and 0.476 g $HAsNa_2O_4$, respectively in a 100 mL flask using Milli-Q water (18.2 MΩ/cm). The solutions were preserved by adding few drops of 3 M $HNO_3$. Working solutions were prepared by appropriate dilutions.

### 5.2.2 Preparation of Fe-Mn oxide modified kaolin mineral

For modification of raw kaolin clay (RK) with Fe-Mn bimetal oxides, solutions containing 0.25 M $FeCl_3$, 0.25 M $MnCl_2.4H_2O$ and 2 M NaOH were prepared by dissolving appropriate amounts into 100 mL of Milli-Q water. Parameters optimized includes $Fe^{3+}$-$Mn^{2+}$ ratio, contact time, and aging time. The procedure is descried below.

#### 5.2.2.1 Effect of Fe-Mn ratio

Aliquots of 0.25 M $Fe^{3+}$ and 0.25 M $Mn^{2+}$ solutions were added together at different volume proportions in 250 mL plastic bottles to make up a final volume 10 mL. The volume ratio were 1:3; 1:1 and 3:1 (2.5:7.5; 5:5 and 7.5: 2.5 mL). A mass of 1 g of raw kaolin (RK) was weighed into each bottle and agitated for 10 min at 250 rpm to ensure proper soaking of kaolin clay mineral. Thereafter, pH of the solution was adjusted to 8.5 by adding 10 mL of 2 M NaOH drop wise into each of the bottles to precipitate $Fe^{3+}$ and $Mn^{2+}$ into their respective oxides. The mixtures were further agitated for 60 min at 250 rpm on a Stuart Reciprocator Table Shaker. After equilibration, samples were aged for 24 hours to ensure further oxidation of $Mn^{2+}$ into $Mn^{4+}$. Thereafter, mixtures were centrifuged at 3 000 rpm for 10 min. Solid residues were thereafter rinsed with Milli-Q water to a neutral pH. The rinsed FMK was then oven dried for 12 hours at 110 °C. The dry samples were milled to pass through 250 µm sieve and then stored in a zip sealed plastics. To find the optimum ratio, batch experiment were conducted as follows: 100 mL of a solutions containing 5 mg/L As(III)/As(V) was pipetted into 250 mL plastic bottle. A mass of 0.1 g of each FMK sample was then transferred into each plastic bottles. Mixtures were agitated for 60 min at 250 rpm in a

Table Shaker. Thereafter, mixtures were centrifuged at 2000 rpm and supernatants were analyzed for As(III) and As(V). Clay modified at a ratio of 3:1 yielded higher percentage As(III)/As(V) removal and was selected as the optimum.

#### 5.2.2.2 Effect of contact time in synthesis of Fe-Mn bimetal modified kaolin clay

To evaluate the effect of contact time in the synthesis of Fe-Mn modified kaolin clay (FMK), the optimum ratio of 3:1 of $Fe^{3+}$-$Mn^{2+}$ was maintained and the contact time was varied from 30 to 240 min at 250 rpm. After agitation the above procedure described in 2.2.1 for treating the residues and finding the optimum ratio was followed to find the optimum shaking time for FMK synthesis. The clay agitated for 60 min gave highest percentage As(III)/As(V) removal from the solution. Thereafter, 60 min was used as optimum contact time for synthesizing FMK.

#### 5.2.2.3 Effect of aging time

The effect of aging time was evaluated by varying the aging time from 24-62 hours. The procedure in 2.2.1 was followed to prepare FMK at ratio 3:1. However, prior to centrifuging, residues were aged for different times. After aging the clay was treated as described in 2.2.1. Residues aged for 48 hours gave highest As(III)/As(V) percentage removal from the solution and 62 hours was therefore chosen to be the optimum time.

#### 5.2.2.4 Synthesis of Fe-Mn bimetal oxide modified kaolin clay at optimized conditions

After optimizing the Fe: Mn ratio, contact time and aging time, the FMK was synthesized as follows: solutions containing 0.25 M $Fe^{3+}$ and 0.25 M $Mn^{2+}$, respectively were mixed together at a volume ratio of 7.5 mL: 2.5 mL (3: 1) in a 250 mL plastic bottle to make up a final volume of 10 mL. To this, 1 g of clay was added and the mixture was agitated for 10 min to ensure proper soaking. Thereafter, pH of the solution was adjusted to 8.5 by adding 10 mL of 2 M NaOH was added drop wise into each of the bottles to precipitate $Fe^{3+}$ and $Mn^{2+}$ into their respective oxides. The mixture was agitated on a Table shaker for further 60 min at 250 rpm and then aged for 62 hours. Thereafter, the mixture was centrifuged at 3000 rpm. Residues were washed with Milli-Q water to remove excess supernatants till the pH was close to neutral and then oven dried for 12 hours at 110 $^{O}$C. The modified clay was then milled to pass through 250 µm sieve and then stored in a zip lock plastic bag.

### 5.2.3 Physicochemical Characterization

The elemental composition of the modified clay were examined using S1 titan handheld XRF (Bruker, Germany). Mineralogical compositions was examined using D8 advance X-ray diffractometer (XRD) (Bruker, Germany) with Cu–Kα radiation as source. Functional groups were determined using ATR Diamond FTIR (Bruker, Germany). The morphological characteristics determined using scanning electron microscopy (SEM) (Leo1450 SEM, Voltage 10 kV, working distance 14 mm). The pore size distribution, pore volume, and pore diameter were determined by Barrett Joyner Halenda (BJH) sorption model using a specific surface area analyzer (Autosorb-iQ & Quadrasorb SI, USA). Nitrogen adsorption-desorption isotherms were used to determine specific surface area of the adsorbent according to Brunauer Emmett Teller (BET) model.

### 5.2.4 Batch Experiments

The efficiency of FMK in As(III) and As(V) removal was evaluated using batch experiments. Parameters such as contact time, adsorbent dosage, adsorbate concentration and initial solution pH were evaluated. To evaluate the effect of contact time, 100 mL solution contain 5 mg/L As(III)/As(V) was pipetted onto 250 mL plastic bottle and 0.1 g of the modified clay was added. Mixtures were agitated for various contact times ranging from 10 to 120 min on a Stuart Reciprocator Table Shaker. To evaluate the effect of adsorbent dosage, the clay mass was varied from 0.05 to 0.5 g. The effect of adsorbate concentration was evaluated at 298, 323 and 343 K by varying initial concentration from 1 to 30 mg/L. To evaluate the effect of pH, the initial solution pH was adjusted from 2 to 12 using 0.1 M NaOH and 0.1 M HCl. Filtrates obtained at different pH levels were analyzed for residual Fe and Mn concentration using ICP-MS technique in order to evaluate the adsorbent's stability. The effect of co-existing anions was carried out in the presence of 5 mg/L of $Cl^-$, $F^-$, $NO_3^-$, $CO_3^{2-}$, $SO_4^{2-}$. After agitation, samples were filtered using 0.45 µm pore filter membrane using a vacuum pump. The solution pH was measured using JENWAY 3510 pH meter. The residual As(III)/As(V) concentration was measured using ScTRACE Gold electrode attached to 884 professional VA Polarography (Metrohm, SA). A composite solution containing 1 mol/L sulfamic acid, 0.5 mol/L citric acid and 0.45 mol/L KCl was used as electrolyte. For total As concentration, $KMnO_4$ was added as an oxidizing agent. All experiments were carried out in triplicate and the mean values were reported. Equation 5.1 and 5.2 were used to compute the percentage removal and the adsorption capacity respectively.

$$\%\, removal = \left(\frac{C_i - C_e}{C_i}\right) \times 100 \quad (5.1)$$

$$q_e = \left(\frac{C_i - C_e}{m}\right) \times v \quad (5.2)$$

Where $C_i$ and $C_e$ represent the initial and equilibrium As(III) concentration (mg/L) respectively and m represent mass of the dry adsorbent (g). V is the volume ($L$) and $q_e$ is the adsorption capacity (mg/g).

### 5.2.5 Treatment of field water

The efficiency of FMK in arsenic removal from field groundwater was evaluated on a fixed-bed column. Fixed-bed column test was carried out using a plastic column with the internal diameter of 2.5 cm and a total length of 13.5 cm. A mass of 5 g of FMK was packed into the column to make up a bed depth of 1.2 cm. Groundwater collected from Siloam community borehole was spiked with arsenic to make up a total arsenic concentration of 0.5 mg/L and used as feed water. The feed water was passed through the column in an up-flow mode using a Gilson peristaltic pump at a flow rate of 1 mL/min. Figure 5.1 provides the experimental set up. The effluents were collected at a regular interval and analyzed for total arsenic concentration.

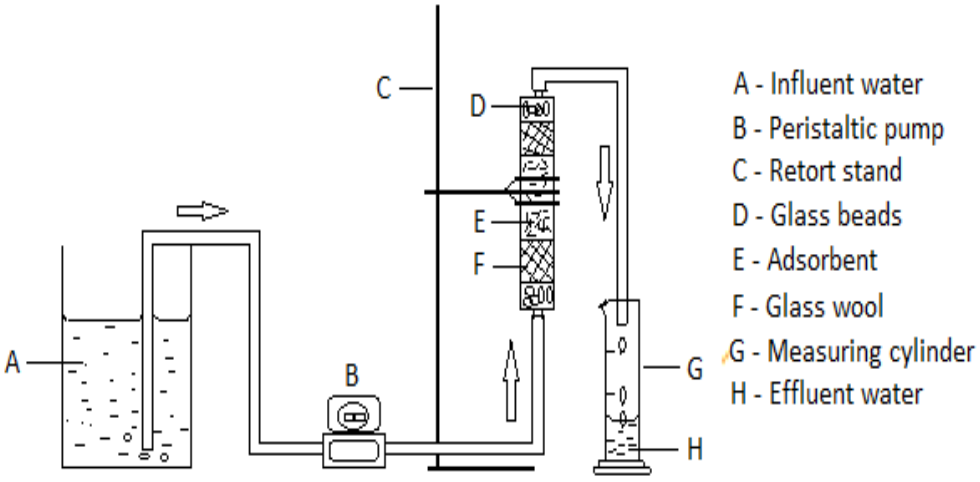


Figure 5.1: Experimental set-up for column experiments.

### 5.2.6 Adsorbent regeneration and reuse

In order to optimize the regeneration process, the efficiency of $Na_2CO_3$, $K_2SO_4$, KCl and $NaNO_3$ in desorption of As(III) and As(V) from the adsorbent was evaluated as follows: 1.0 g of

As(III)/As(V) loaded adsorbent was suspended onto 50 mL of solution containing 0.1 M of each of the solution mixtures were then agitated for 60 min. Thereafter, mixture were centrifuged and the residual As(III)/As(V) concentration was analysed. $K_2SO_4$ showed higher desorption efficiency therefore was used as the regenerant.

Total of 6 regeneration-reuse cycles were conducted as follows: 100 mL of solutions containing 0.5 mg/L of As(III)/As(V) were pipetted into 250 mL plastic bottle and 0.4 g of FMK was added to make adsorbent dosage of 0.4 g/100 mL. Mixtures were agitated for 60 min at 250 rpm. After agitation samples were filtered through 0.45 µm filter membranes. Residues were rinsed with Milli-Q water to remove free As(III) and As(V) ions and then oven dried at 105 $^{o}$C and treated with 100 mL of 0.1 M $K_2SO_4$ for 30 min to desorb the adsorbed ions thereafter samples were filtered to through 0.45 µm filter membrane and then washed gently with Milli-Q water. The regenerated adsorbent was then used for As(III)/As(V) adsorption. The procedure was repeated up to 6$^{th}$ adsorption cycles.

### 5.3 Results and Discussion

#### 5.3.1 Optimization of conditions for synthesizing FMK.

The optimization of Fe-Mn proportion ratio, contact time and aging time was conducted in order to find conditions that would yield higher As(III)/As(V) removal efficiency. The results for As(III) and As(V) removal efficiency obtained under different conditions are presented in Figure 5.2a-c. The results showed that the clay modified with higher volume of $Fe^{3+}$ (3:1) has higher efficiency for As(III) and As(V) removal as compared to the clay modified at $Fe^{3+}$: $Mn^{2+}$ ratio 1:1 and 1:3 (Figure 5.2a). This could be attributed to stronger affinity of Fe towards arsenic species. When varying the reaction time (Figure 5.2b) the clay prepared at 60 min contact time gave higher arsenic removal efficiency. When varying aging time (Figure 5.2c), the clay aged at 68 hours gave higher percentage arsenic removal as compared to clays aged for 24 and 48 hours. This could be attributed to complete precipitation of Fe and Mn to their respective oxides and enhanced surface area. The conditions for synthesizing FMK were established as follows: 3:1 Fe-Mn volume ratio, 60 min contact time and 62 hours aging time

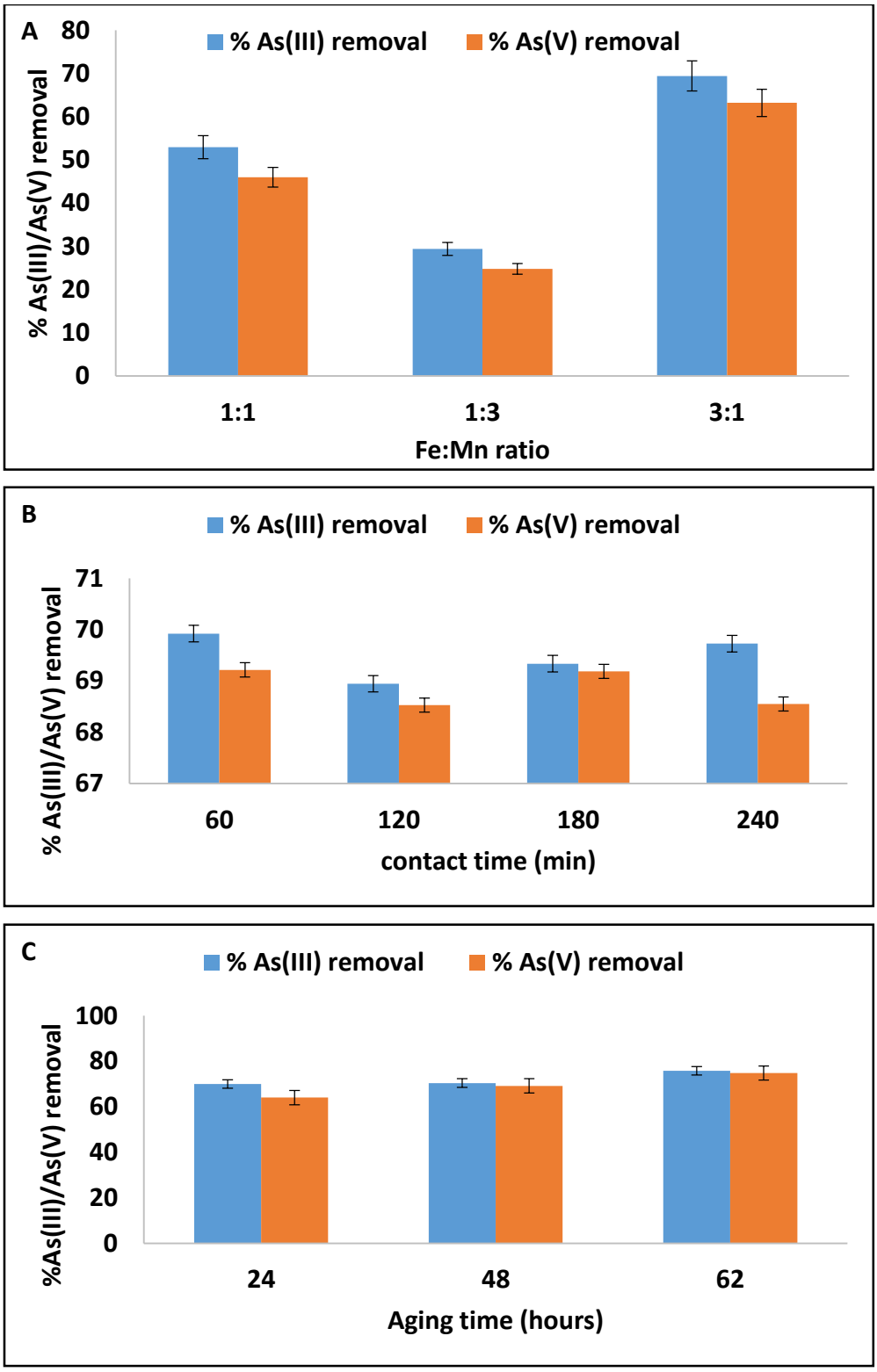


Figure 5.2: The effect on change of Fe: Mn ratio (a), contact time (b) and aging time (c) during synthesis of FMK onto As(III) and As(V) removal (5 mg/L initial As(III) and As(V) concentration, 30 min agitation time, 6.21 pH and 0.5 g/100 mL adsorbent dosage).

### 5.3.2 Physicochemical characterization

#### 5.3.2.1 Bulk chemical composition

The chemical compositions of raw kaolin (RK) and Fe-Mn modified kaolin mineral (FMK) are presented in Table 5.1.

Table 5.1: Chemical composition of RK and FMK.

| Oxides(%w/w) | $SiO_2$ | $Al_2O_3$ | $Fe_2O_3$ | MnO | MgO | CaO | $K_2O$ | $TiO_2$ |
|---|---|---|---|---|---|---|---|---|
| RK | 56.06 | 22.05 | 3.88 | 0.01 | 0.57 | 0.95 | 0.16 | 1.76 |
| FMK | 39.39 | 10.08 | 16.66 | 4.02 | LOD | 0.55 | 0.13 | 1.31 |

The analysis revealed that $SiO_2$ and $Al_2O_3$ are the major chemical oxides of RK averaging 56.06 and 22.05%, respectively. $Fe_2O_3$ was observed as one of the minor oxides averaging 3.88% while MnO was observed as a trace oxide (0.01%). After modification, the percentage composition of $SiO_2$ and $Al_2O_3$ decreased to 39.36 and 10.08%, respectively. Conversely, the percentage composition of $Fe_2O_3$ and MnO increased to 16.66 and 4.02%, respectively. The results suggest that the clay surface was successfully coated by Fe and Mn oxides. The percentage composition of MgO, CaO and $K_2O$ also decreased after modification.

#### 5.3.2.2 Mineralogical composition

The XRD spectrum of RK and FMK is presented in Figure 5.3.

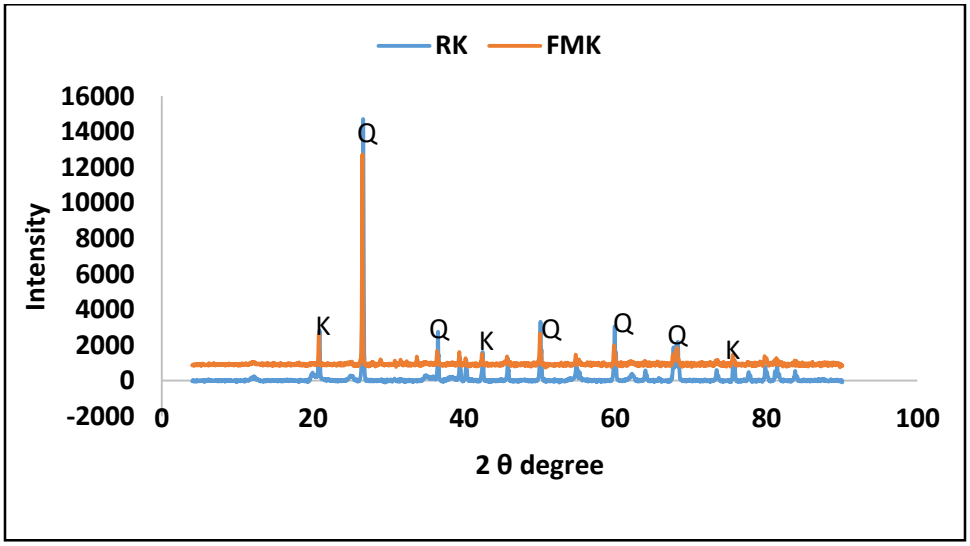


Figure 5.3: The XRD spectrum of RK and FMK.

The spectrum showed that the clay soils is mainly characterized by quartz and kaolin minerals (Fig. 5.3). No change is observed in the mineral phases after modification of the clay by Fe and Mn oxides. However, there was a reduction in the peak intensities which could be attributed to dilution and exchange of the chemical oxides during modification.

### 5.3.2.3 Morphological analysis

Figure 5.4A and B presents SEM micrographs of RK and FMK, respectively.

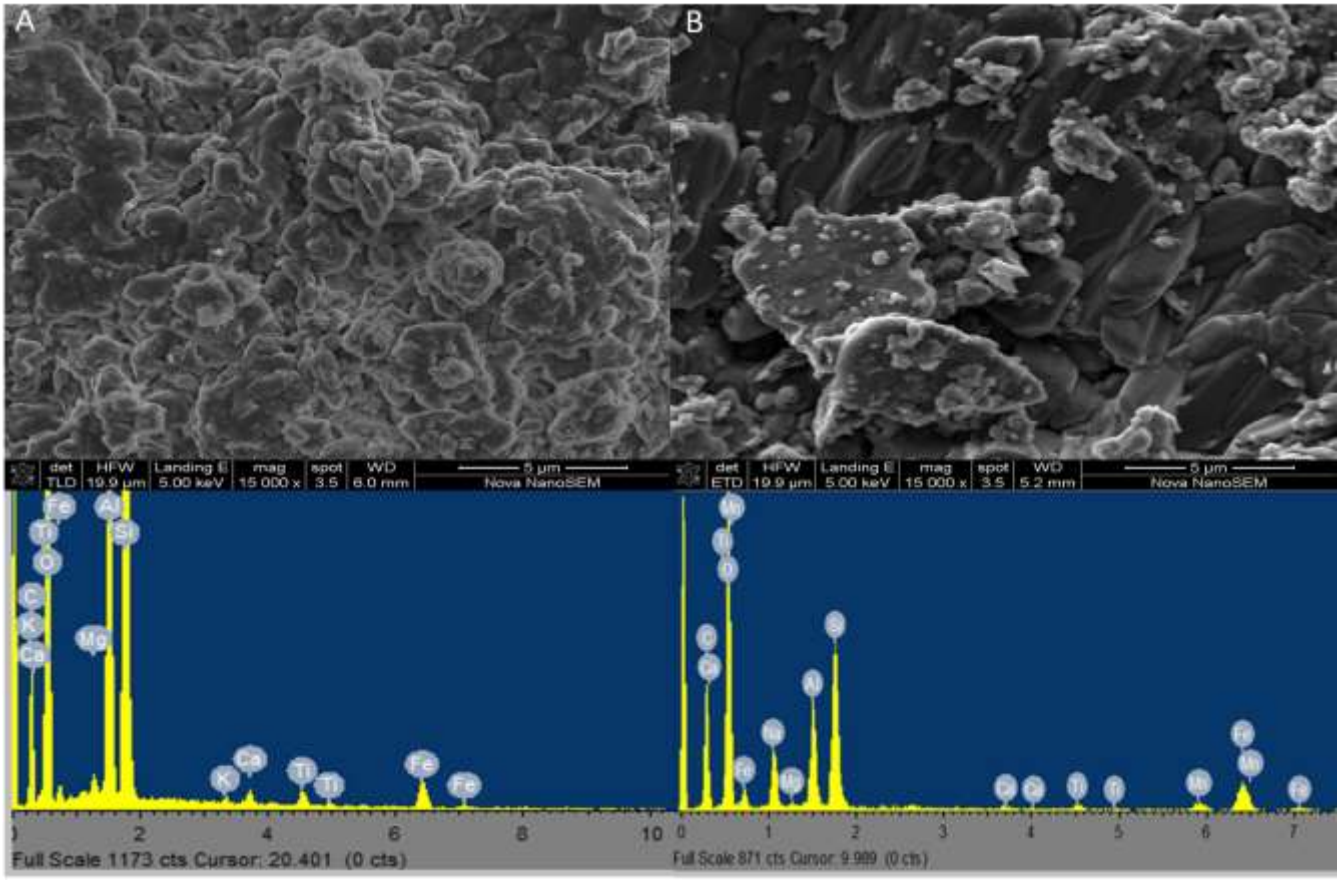


Figure 5.4: SEM Micrographs and EDS spectrums of RK (a) and FMK (b).

The morphology of the RK clay appears spongier with some irregular shaped agglomerates. After modification, the surface appears smoother with irregular shaped agglomerates on top. The EDS spectrum of FMK confirmed the presence of Mn and Fe on the surface of the clay, which shows that the surface of the clay has been modified successfully. Qualitative EDS showed an increase in Fe content from 3.7 to 9.4% and Mn which was not detected on raw clay was found to be 2.27% in the modified clay. This results proved that the clay surface was successfully coated.

### 5.3.2.4 Functional group analysis

Figure 5.5 present the FTIR spectrum of RK, FMK and arsenic loaded FMK.

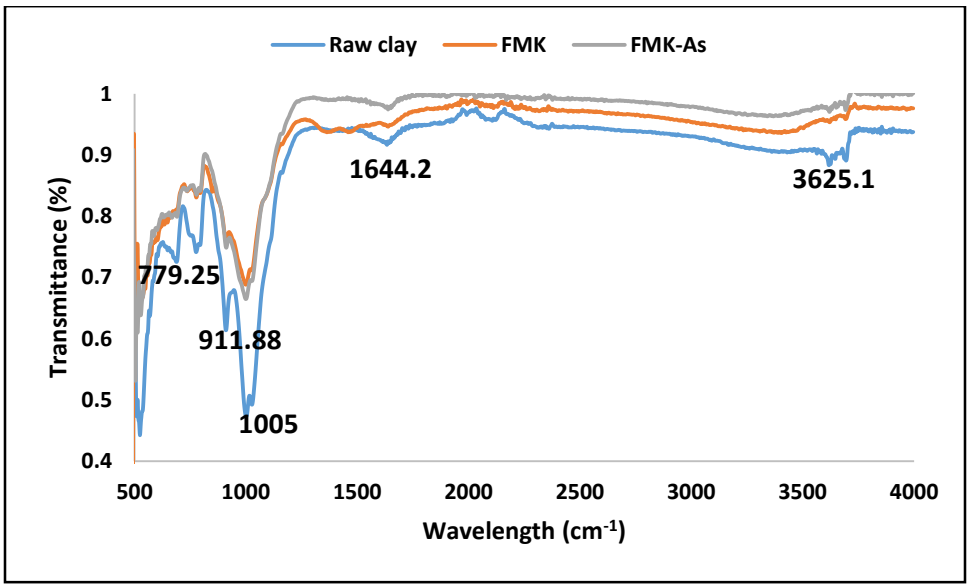


Figure 5.5: FTIR spectra for RK, FMK and FMK-As.

The band observed at 3625.11 $cm^{-1}$ in RK spectra can be ascribed to vibration of physiosorbed water molecules. The bands at 2077 and 1644.2 can also be ascribed to the hydroxyl groups located between the octahedral and tetrahedral sheets of the clay. The band at 1005 and at 911.88 $cm^{-1}$ could be attributed to the vibration and stretching of Si-O-Si and Al-OH-Al groups, respectively. The bands at 779.25 $cm^{-1}$ could be attributed to the vibration of Si-O groups. After modification, a decrease in the intensity of all the bands was observed. This could be attributed to dilution of $SiO_2$ and $Al_2O_3$ content during modification. A new band was observed at 1409.6 $cm^{-1}$ which could be attributed to Fe-OH and Mn-OH vibration. After arsenic adsorption a further decrease in bands intensity at 3625.11 $cm^{-1}$ 2077 and 1644.2 $cm^{-1}$ was observed. Which could be due to exchange of OH- groups for arsenic species. A slight increase was observed in the bands at 1005 and at 911.88 $cm^{-1}$ this could be ascribed to formation of arsenic containing mineral complexes. As such ion exchange and complexation are suggested as the main mechanisms for arsenic adsorption.

### 5.3.2.5 Surface area analysis

The BET surface area results are summarized in Table 5.2. It is observed that FMK has higher surface area and pore volume as compared to the RK. This could be attributed to propping up of the parent clay mineral interlayer structure during modification. Furthermore, the pore diameter

decreased from 9.54 nm to 8.5 nm after modification. The decrease in pore diameter could be an indication that the Fe and Mn oxides were diffused into the pores of RK during modification. Based on the average pore diameter range, the clay can be classified as a mesoporous material.

Table 5.2: BET surface area, pore volume and pore diameter of the RK and FMK.

| | BET Surface area ($m^2/g$) | Pore volume (cc/g) | Pore diameter (nm) |
|---|---|---|---|
| RK | 19.02 | 0.04 | 9.54 |
| FMK | 29.8 | 0.083 | 8.5 |

### 5.3.3.1 Batch experiments

### 5.3.3.2 Effect of contact time and adsorption kinetics

The effect of contact time on As(III) and As(V) adsorption capacity is presented in Figure 5.6. It is observed that the percentage As(III) and As(V) removal increased with increasing contact time. After 60 min, no significant change in the adsorption capacity for both arsenic species was observed. Therefore, 60 min was chosen as the optimum contact time for subsequent experiments.

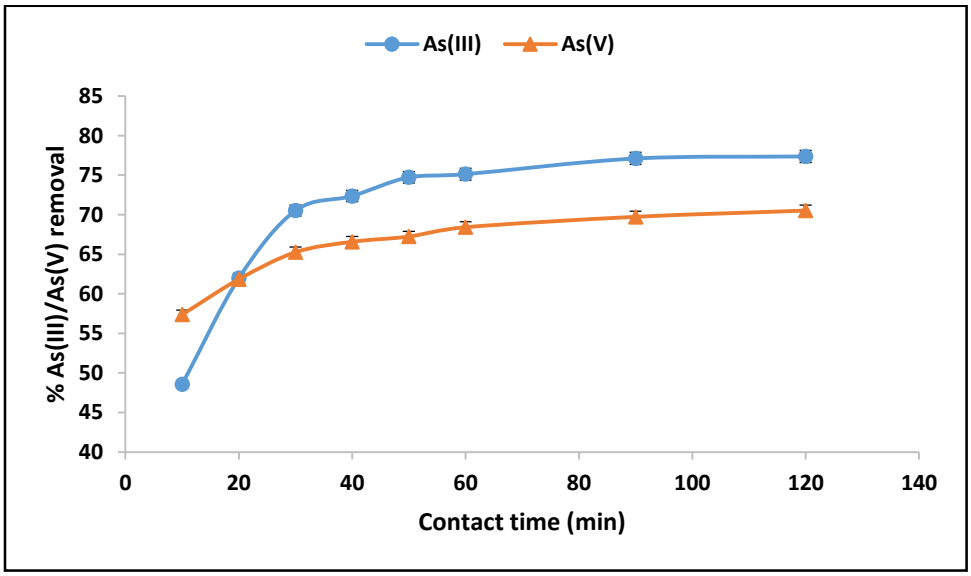


Figure 5.6: Adsorption kinetics and the effect of contact time in As(III) and As(V) adsorption by FMK (initial As(III)/As(V) concentration of 5 mg/L, adsorbent dosage of 0.1 g/100 mL, pH 6.2).

To further elucidate the As(III) and As(V) possible adsorption mechanism as well as the rate limiting factors such as mass transport and diffusion processes, the linear equations for pseudo first and second order reaction models together with the Weber Morris intra-particle diffusion

models were used (Tran et al., 2017, Ho, 2004,). The linear equations 5.3 and 5.4 represent the pseudo first and second order reaction kinetics models, respectively while equation 5 represent the intra-particle diffusion model.

$$\log(q_e - q_t) = -\frac{K_1 t}{2.303} + \log q_e \quad (5.3)$$

$$\frac{t}{q_t} = \left(\frac{1}{q_e}\right) t + \frac{1}{K_2 q_e^2} \quad (5.4)$$

$$q_t = K_{id} t^{1/2} + C_i \quad (5.5)$$

Where $q_e$ and $q_t$ (mg/g) are the adsorption capacities of As(III) and As(V) of the adsorbents at the equilibrium and at time t (min), $K_1$ ($min^{-1}$) and $K_2$ (mg/g. $min^{-1}$) are the rate constants of the pseudo first order equation and pseudo second order equation, respectively. The value of $K_1$ is determined from the slope of log $q_e$-$q_t$ vs time while the value of $K_2$ is determined from the slope of $t/q_t$ against time. $K_{id}$ (mg/g. $min^{1/2}$) is the intra-particle diffusion rate constant and $C_i$ is the intercept.

The plot for pseudo first order, second order and intra-particle diffusion are presented in Figure 5.7-5.9, respectively while the model constant values are presented in Table 5.3 and 5.4.

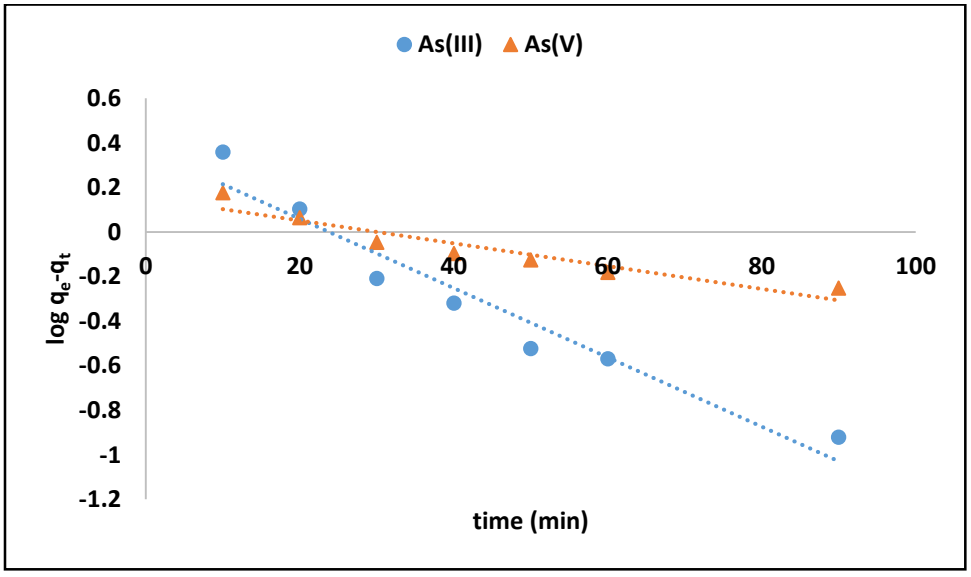


Figure 5.7: Pseudo first order plot for As(III) and As(V) sorption onto FMK.

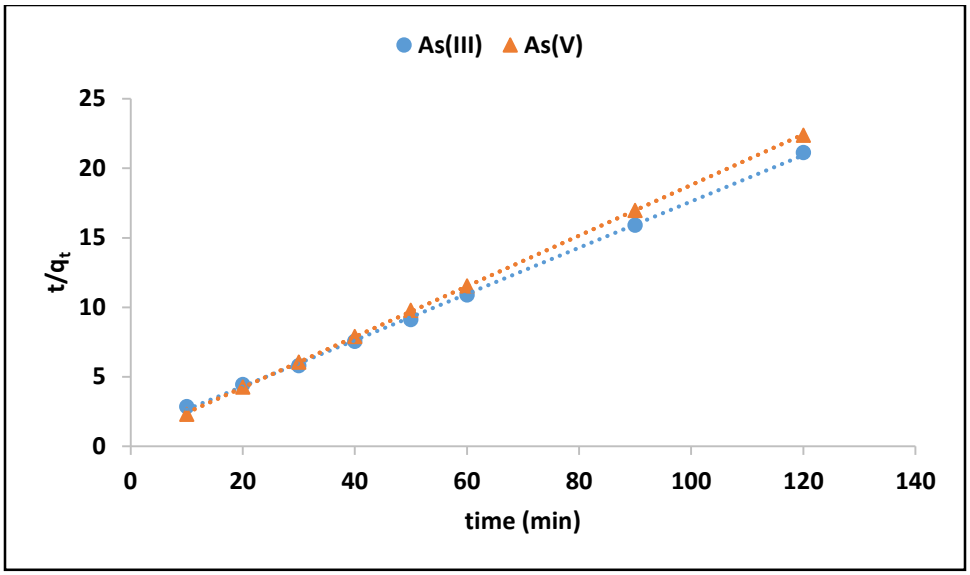


Figure 5.8: Pseudo second order plot for As(III) and As(V) sorption onto FMK.

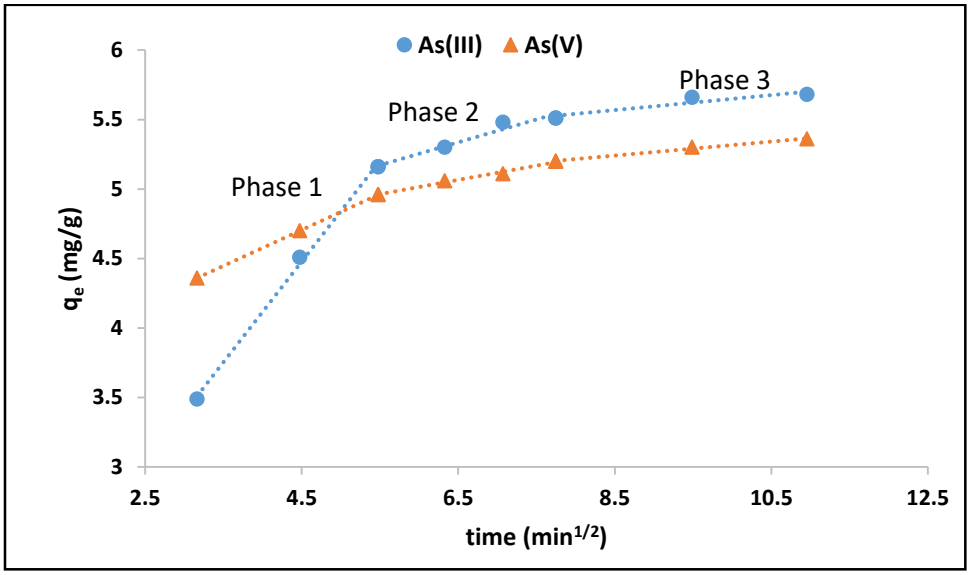


Figure 5.9: Intra-particle diffusion plot for As(III) and As(V) sorption onto FMK.

Table 5.3: Parameters for pseudo first and second order reaction kinetics model.

| | | Pseudo first order | | | Pseudo second order | | |
|---|---|---|---|---|---|---|---|
| | $q_{e\ exp}$ (mg/g) | $K_1$ ($min^{-1}$) | $q_{e\ cal}$ (mg/g) | $R^2$ | $K_2$ (mg/g. $min^{-1}$) | $q_{e\ cal}$ (mg/g) | $R^2$ |
| As(V) | 5.36 | 0.011 | 1.42 | 0.89 | 0.05 | 5.49 | 0.99 |
| As(III) | 5.63 | 0.034 | 2.34 | 0.94 | 0.02 | 6.0 | 0.99 |

Table 5.4: Parameters for intra-particle diffusion model.

| | $K_{id1}$ (mg/g. $min^{1/2}$) | $C_1$ | $K_{id2}$ (mg/g. $min^{1/2}$) | $C_2$ | $K_{id3}$ (mg/g. $min^{1/2}$) | $C_3$ |
|---|---|---|---|---|---|---|
| As(V) | 0.2 | 3.54 | 0.16 | 4.27 | 0.05 | 5.1 |
| As(III) | 0.72 | 1.2 | 0.1 | 4.40 | 0.05 | 4.81 |

The adsorption data was described better by the pseudo second order (Figure 5.7) as compared to the pseudo first order (Figure 5.8) of reaction kinetics. This is evident from the higher coefficient and the calculated adsorption capacities values (Table 5.3). The better fit to pseudo second order suggest that adsorption of both As(III) and As(V) was more of chemisorption than physiosorption. The intra-particle diffusion model plot (Figure 5.9) showed three clearly defined phases. This multi-linearity of the intra-particle diffusion plot suggests that adsorption of As(III) and As(V) onto FMK is a complex process. The first phase could be attributed to boundary layer adsorption where arsenic anions are being transferred from the bulk solution into the boundary layer of the adsorbents surface. The second phase indicate the intra-particle diffusion where arsenic anions are being diffused into the micro-pores and the mesopores of the adsorbent. The third phase could be attributed to the adsorption at equilibrium inside the adsorbents particles leading to chemisorption (Gupta and Bhattacharyya, 2011; Qi et al., 2015). The adsorption of rate constant ($K_{id}$) determined from the slope (Table 5.4) was higher at phase 1 indicating that adsorption at the boundary layer is occurred much faster as compared to intra-particle diffusion (phase 2) and equilibrium adsorption (phase 3). The value of C, the constant related to the boundary lay thickness, was found to be increasing from phase 1 to phase 3 (Table 5.4) indicating the increase in the boundary layer of the adsorbent particles.

#### 5.3.3.3 Effect of adsorbent dosage

The effect of adsorbent dosage in As(III) and As(V) removal and adsorption capacity is presented in Figure 5.10. The results showed that the percentage As(III) and As(V) removal increases with increasing adsorbent dosage. The trend is linked to increasing active adsorption sites for a limited As(III) and As(V) ions available in the solution as the adsorbent dosage increases. Therefore, 0.4 g/100 mL was chosen as the optimum adsorbent dosage for subsequent experiments.

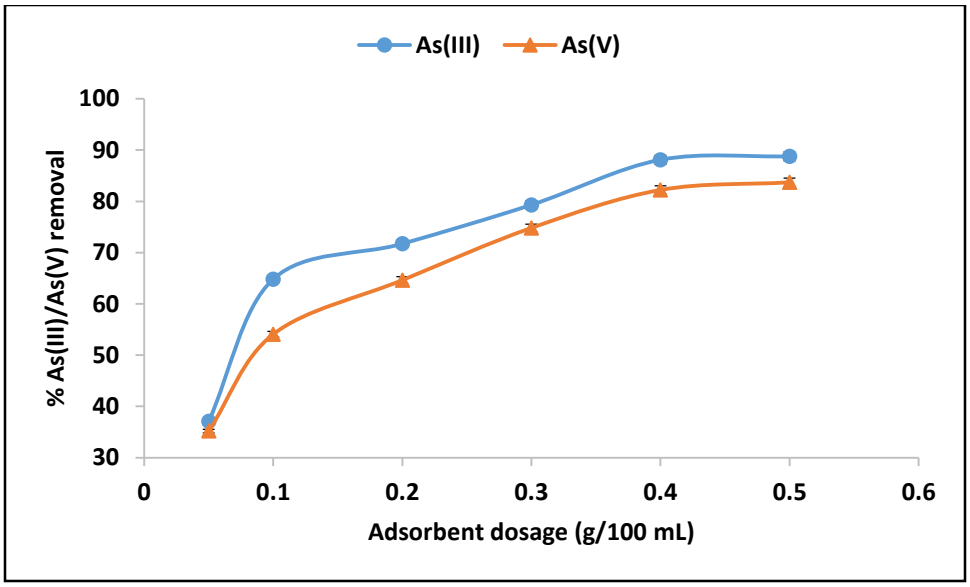


Figure 5.10: Effect of adsorbent dosage on As(III)/As(V) removal (Initial As(III)/As(V) concentration of 5 mg/L, 60 min contact time at 250 rpm shaking speed and initial pH 6.35).

### 5.3.3.4 Effect of adsorbate concentration and adsorption isotherms

The effect of initial adsorbate concentration in the adsorption of As(III) and As(V) was studied at a temperature of 298, 323 and 343 K. The results are presented in Figure 5.11a-b in terms of adsorption capacity against equilibrium concentration.

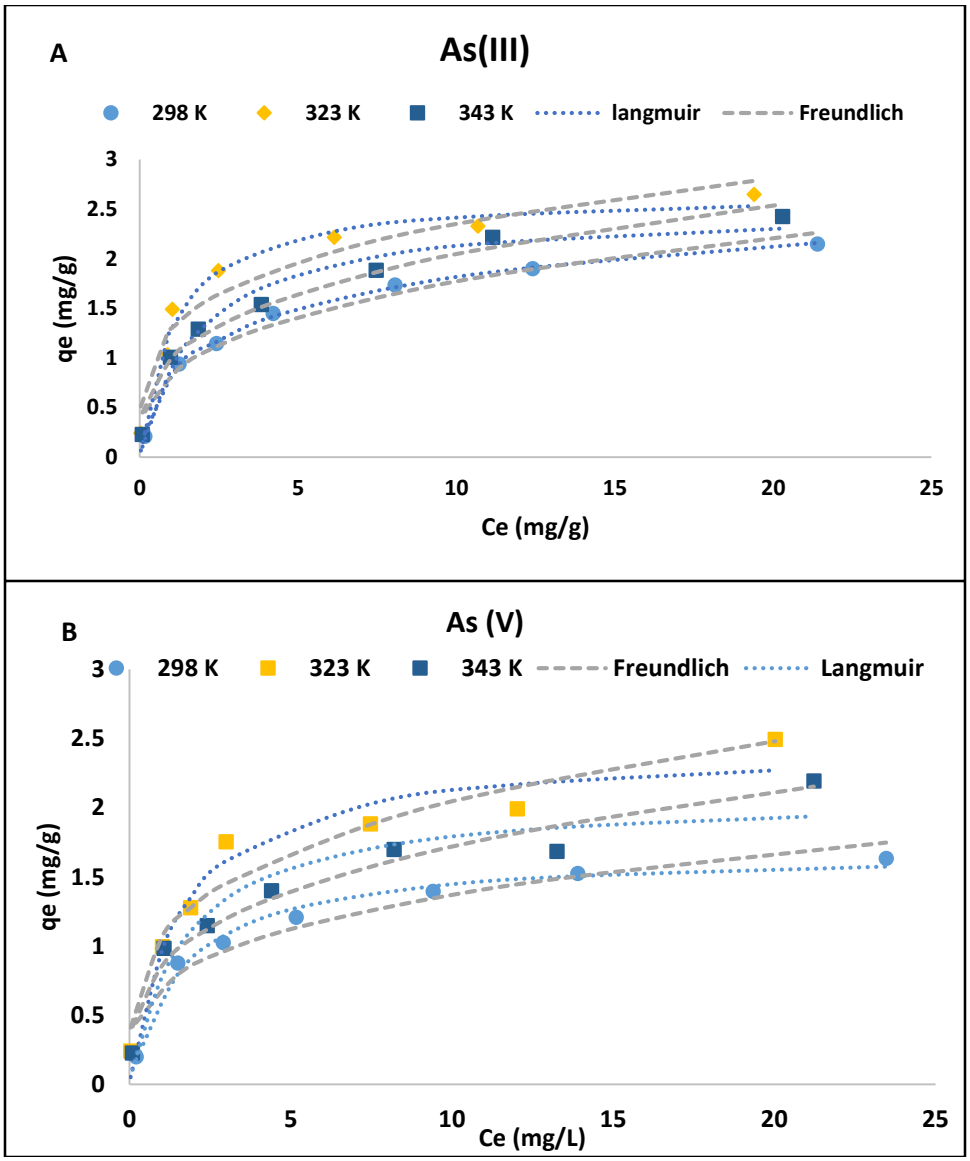


Figure 5.11: Effect of adsorbate concentration on As(III)/As(V) removal by FMK (0.4 g/100mL adsorbent dosage, 60 min contact time at 250 rpm and initial pH of 6.5).

Adsorption capacity increases with increasing equilibrium concentration. Increasing temperature from 298 to 323 K enhanced the adsorption capacity for both arsenic species while further increase to 343 K decreased the adsorption capacity. To further illustrate the relationship between the adsorbate concentration and the adsorbent the nonlinear equations for Langmuir (Equation 5.6) and Freundlich (Equation 5.7) isotherm model were used (Langmuir, 1918; Tran et al., 2017).

$$q_e = \frac{q_{max} b C_e}{1 + K_L C_e} \quad (5.6)$$

$$q_e = K_f C_e^{1/n} \quad (5.7)$$

Where $C_e$ (mg/L) is the As(III)/As(V) concentration at equilibrium, $q_e$ (mg/g) is the adsorption capacity at equilibrium, $Q_{max}$ (mg/g) is the maximum saturated monolayer adsorption capacity, $K_L$ (L/mg) is the constant related to the affinity between adsorbent and adsorbate, $K_F$ (mg/g) is the Freundlich constant related to adsorption capacity and $n$ is the Freundlich intensity parameter which indicate the magnitude of the adsorption driving force or the surface heterogeneity. The value of $Q_{max}$ and $K_L$ are determined from the slope and intercept of $C_e/q_e$ vs. $C_e$ while the value of $K_f$ and $n$ are determined from the slope and intercept of log $q_e$ vs. log $C_e$. The correlation co-efficient values competed from the nonlinear plots in Figure 5.11 and other constant parameters are presented in Table 5.5. The maximum adsorption capacities and $R^2$ values showed that the data for As(III) and As(V) fitted better to Langmuir model compared Freundlich adsorption isotherm model. This suggests that the surface of FMK is predominantly homogeneous and the adsorption of As(III) and As(V) occurred on a monolayered surface. For the data that is described by the Langmuir model, it is essential to calculate the dimensionless equilibrium parameter ($R_L$) at different temperatures using equation 8. Values of $R_L$ are presented in Table 5.5. It is noted that $R_L$ values for As(III) and As(V) are within the range of 0-1 which indicates that adsorption was favorable. This was further confirmed by the 1/n values for Freundluch constant related to adsorption intensity which also ranges between 0 and 1.

$$R_L = \frac{1}{1+K_L C} \quad (8)$$

Table 5.5: Constant parameters for Langmuir and Freundlich adsorption isotherm model.

| | | Langmuir | | | | Freundlich | | |
|---|---|---|---|---|---|---|---|---|
| | | $q_m$ | b | $R^2$ | $R_L$ | $K_f$ | 1/n | $R^2$ |
| As(III) | 298 K | 2.92 | 0.09 | 0.99 | 0.91-0.20 | 0.83 | 0.32 | 0.96 |
| | 323 K | 2.66 | 0.99 | 0.97 | 0.97-0.05 | 1.29 | 0.25 | 0.93 |
| | 343 K | 2.51 | 0.55 | 0.97 | 0.64-0.05 | 0.99 | 0.31 | 0.94 |
| As(V) | 298 K | 2.33 | 0.50 | 0.98 | 0.62-0.05 | 0.70 | 0.28 | 0.93 |
| | 323 K | 2.44 | 0.64 | 0.96 | 0.6-0.04 | 1.06 | 0.28 | 0.95 |
| | 343 K | 2.09 | 0.59 | 0.96 | 0.62-0.05 | 0.85 | 0.30 | 0.93 |

To further elucidate the adsorption mechanisms, the adsorption thermodynamics parameters such as Gibbs free energy change ($\Delta G^{o}$), enthalpy of change ($\Delta H^{o}$) and the entropy of change ($\Delta S^{o}$) were computed from equation 5.9-5.10.

$$\Delta G° = -RT \ln K_L \quad (5.9)$$

$$\ln K_L = -\frac{\Delta H°}{RT} + \frac{\Delta S°}{R} \quad (5.10)$$

Where $R$ is the molar gas constant, 8.314 J $mol^{-1}K^{-1}$, T is the absolute temperature in Kelvin, $\Delta G^{O}$ (KJ/mol) is the Gibbs free energy change. $\Delta H^{O}$ (J/mol) is enthalpy change, $\Delta S^{O}$ (J/mol) is the change in entropy and $K_L$ (L/mg) is the constant derived from Langmuir isotherm model. Values $\Delta H$ and $\Delta S$ of are determined from the slope and intercept of a plot of $\ln K_L$ against 1/T (Figure 5.12). Thermodynamic parameters are presented in Table 5.6. It is observed that values for $\Delta G^{O}$ for both arsenic species were found to be negative. This was observed at both temperatures studied. Negative $\Delta G^{O}$ implies that adsorption of As(III) and As(V) onto FMK was spontaneous and favorable. $\Delta H^{O}$ value for As(III) was found to be negative while it was positive for As(V). This indicates that adsorption of As(III) was exothermic while adsorption of As(V) was endothermic. Exothermic reaction involves both physiosorption and chemisorption whereas endothermic is attributed to chemisorption (Tran et al., 2016). The value of $\Delta S^{o}$ for both arsenic species was found to be positive, indicating arsenic species were randomly distributed on the surface of the adsorbent.

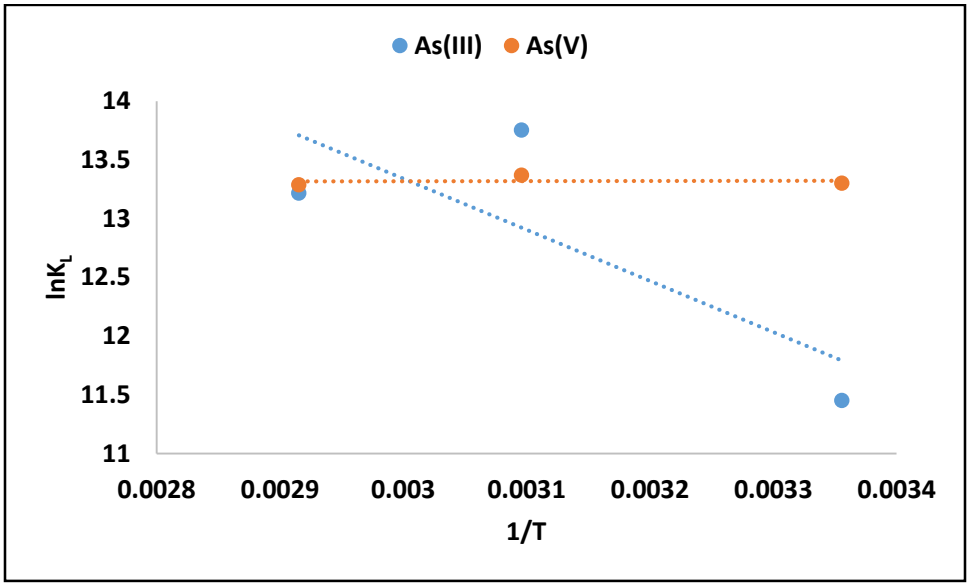


Figure 5.12 $\ln K_L$ as a function of reciprocal of adsorption temperature.

Table 5.6: Thermodynamics parameters for As(III) and As(V) adsorption onto FMK.

| | $\Delta G^O$ (KJ/mol) | $\Delta H^O$ (J/mol) | $\Delta S^O$ (J/mol) |
|---|---|---|---|
| As(III) | 298 K= -28.37<br>323 K= -36.93<br>343 K= -37.69 | -36184.27 | 219.47 |
| As(V) | 298 K= -32.95<br>323 K= -35.9<br>343 K= -37.83 | 84.44 | 110.48 |

### 5.3.3.5 Effect of Initial pH

The effect of pH onto As(III) and As(V) removal is presented in Figure 5.13.

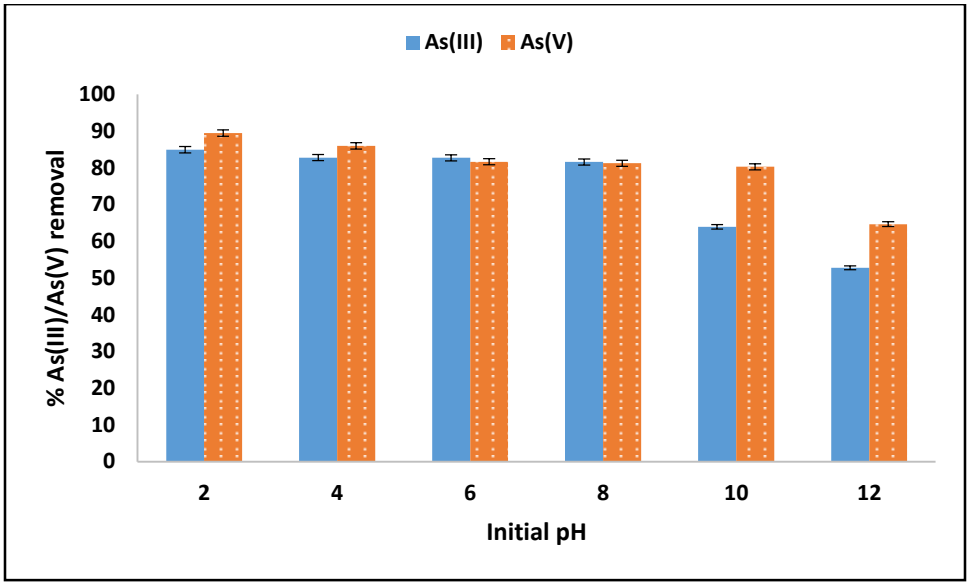


Figure 5.13: The effect of initial pH on As(III)/As(V) removal onto FMK (Initial As(III)/As(V) concentration 5 mg/L, 0.4 g/100 mL adsorbent dosage, 60 min contact time at 250 rpm shaking speed).

The percentage As(III) removal remained almost constant at pH levels between 2 and 8 and decreased at pH >10. At pH below 9, As(III) exist as neutrally charged $H_3AsO_3$ while negatively $H_2AsO_3^-$ and $HAsO_3^{2-}$ dominates at pH above 9. Therefore, the decrease in As(III) removal could be attributed to electrostatic repulsion at the surface since the material surface is also negatively charged at alkaline pH levels.

The percentage As(V) removal on the other hand, was optimum at acidic pH and then remained constant at pH range 6-10. Further increase in pH to 12 decreased the percentage As(V) removal.

The As(V) species largely exist as negatively charged $H_2AsO_4^-$, $HAsO_4^{2-}$ and $AsO_4^{3-}$ at both acidic and alkaline pH values. At acidic pH values, the adsorbents surface is positively charged and this will enhance As(V) removal through electrostatic attraction. At alkaline pH values, the adsorbent surface is largely negatively charged, this enhances electrostatic repulsion between As(V) species and adsorbent charges hence the decrease in percentage of removal.

### 5.3.3.6 Effect of Co-existing Anions

Groundwater generally contain other co-existing anions such as $F^-$, $Cl^-$, $SO_4^{2-}$, $CO_3^{2-}$ and $NO_3^-$ that could hinder the adsorption of arsenic. Figure 5.14 present the effects of these co-existing anions on As(III) and As(V) removal. It is observed that the presence of $SO_4^{2-}$ decreased the percentage As(III) and As(V) removal from 95.47 and 95% to 92 and 91%, respectively. However, the percentage of removal for both species was still beyond 90% The presence of other co-existing anions did not show any significant effects on both As(III) and As(V) removal. This results implies that FMK synthesized in this study is selective towards arsenic species and it can therefore be used for treatment of groundwater containing other co-existing anions.

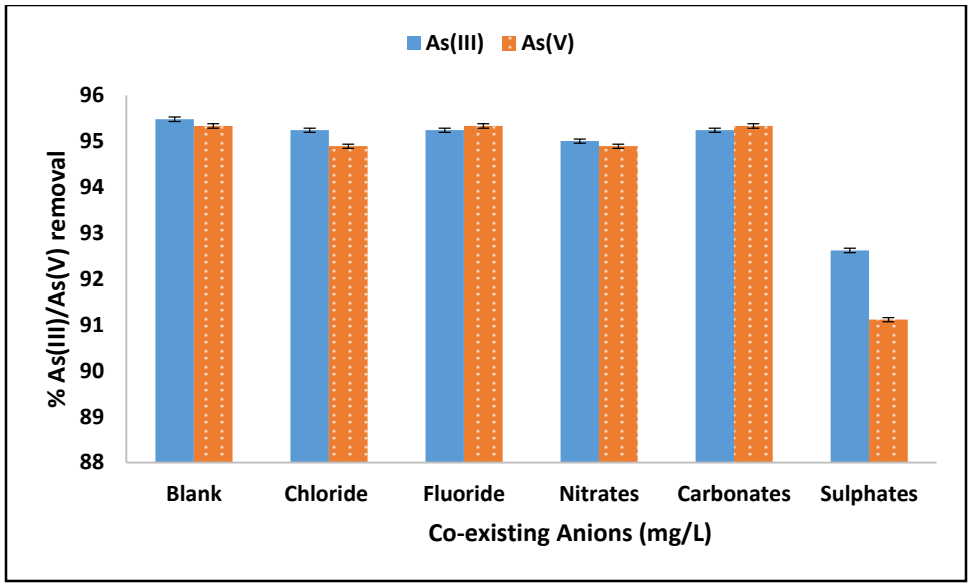


Figure 5.14: The variation of As(III)/As(V) removal in the presence of other co-existing anions (0.4 g/100 mL adsorbent dosage, 4.1 mg/L initial As(III)/As(V) concentration, 60 min contact time at 250 rpm).

### 5.3.3.7 Desorption and Reusability of the Adsorbent

Figure 5.15 depicts the effectiveness of $Na_2CO_3$, $K_2SO_4$, KCl and $NaNO_3$ in desorption of As(III) and As(V) from the used adsorbent. It is observed that $K_2SO_4$ has a greater potential to desorb

arsenic from the adsorbent. The desorption of As(III) and As(V) could be attributed to ion-exchange mechanism between arsenic species and the guest anions. Therefore, $K_2SO_4$ was selected for use as a regenerant.

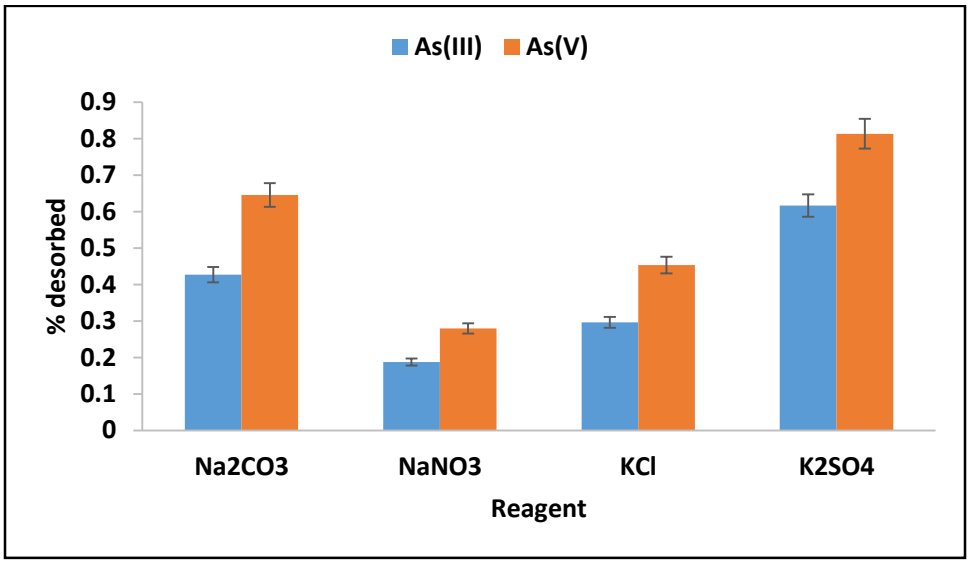


Figure 5.15: Desorption of As(III) and As(V) from the spent sorbent using various reagents.

After regeneration by $K_2SO_4$, the adsorbent was used for arsenic adsorption. Figure 5.16 presents the adsorption cycles using regenerated FMK. It is observed that the percentage As(III) and As(V) removal decreased with increasing adsorption-desorption cycles. However, it is interesting to note that adsorption remained beyond 85% even at $6^{th}$ cycle. The decrease in percentage removal could be due to inadequate reactivation of the adsorption sites. These results indicates that FMK is a sustainable adsorbent for use in arsenic removal since it can be regenerated easily.

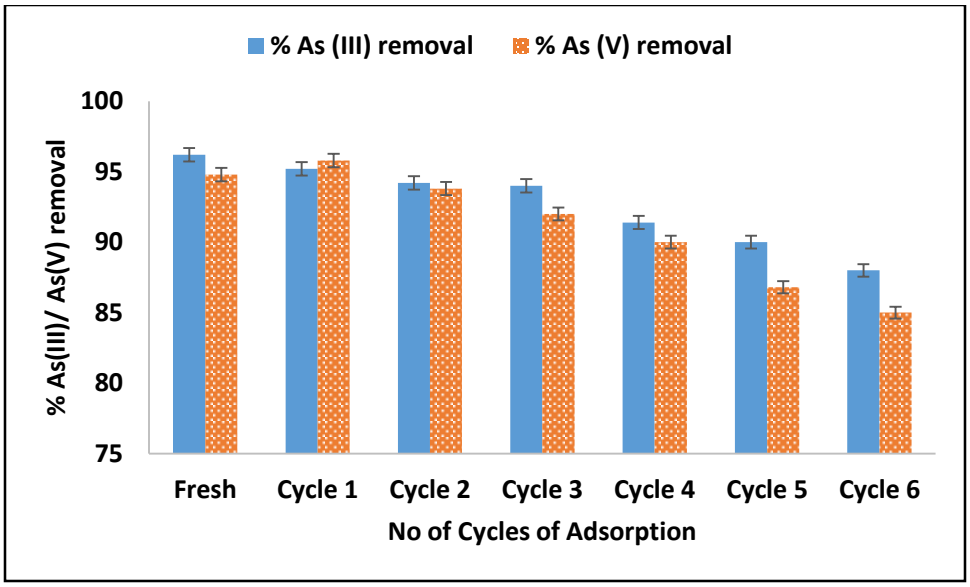


Figure 5.16: The variation of As(III)/As(V) removal by FMK as a function of regeneration cycles.

### 5.3.3.8 Chemical stability of the adsorbent

The chemical stability of the adsorbent was assessed by evaluating the leaching of Fe and Mn from the adsorbent at various pH levels. The results are presented in Figure 5.17. At extreme pH levels, the concentration of Fe in the treated water was found to be greater than WHO guideline value (0.3 mg/L). There is no health based guideline value proposed for iron, however, concentrations above 0.3 mg/L Fe may change the turbidity of the water (WHO, 2017). The concentration of Mn at all the pH levels was found to be below the WHO guideline value (0.4 mg/L). The results showed that developed FMK is suitable for use in arsenic remediation from groundwater.

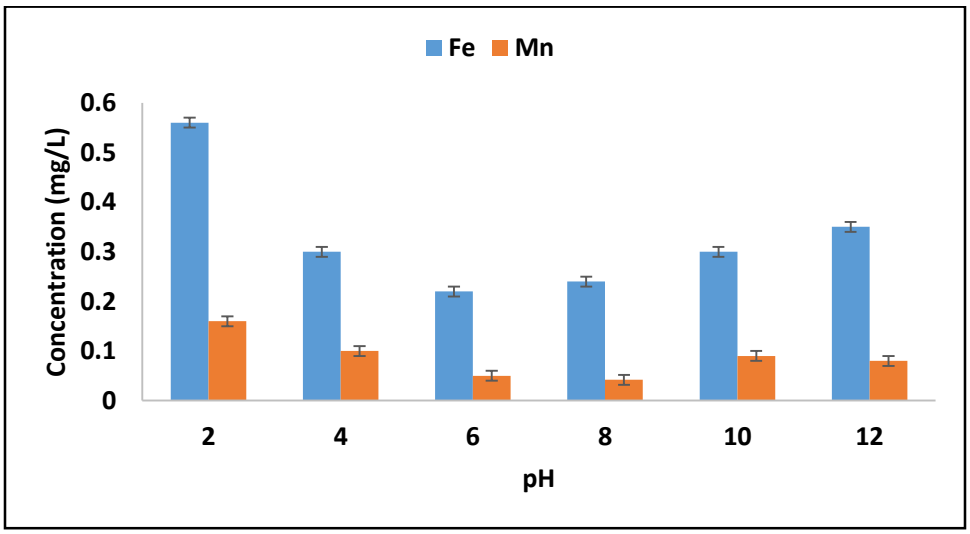


Figure 5.17: Residual concentration of Fe and Mn at various pH levels.

### 5.3.4 Column breakthrough experiment

The field application of FMK in arsenic removal from groundwater was tested in a fixed bed column. The physicochemical parameters of the field water before treatment and at breakthrough point are presented in Table 5.7 and the column breakthrough curve is presented in Figure 5.18. The point when the effluent concentration is equivalent to WHO limit of arsenic in drinking water 0.01 mg/L was taken as the breakthrough point. The results indicates that the breakthrough point was reached after treatment of ≈2 L of groundwater from the initial spiked arsenic concentration of 0.5 mg/L using 5 g mass of the adsorbent. The adsorbent was exhausted after treatment of ≈3.5 L volume of solution. Therefore, it can be assumed that for a household that consumes 20 L of water a day, FMK amount of 50 g will be required daily to treat arsenic contaminated water with initial arsenic concentration of 0.5 mg/L. Thus, in order to treat 20 L daily for a period of 6 month about 9.1 kg will be required. Other physicochemical parameters where found to be within the WHO standard at breakthrough point (Table 5.7).The results obtained proved that FMK synthesized in this study is suitable for use in groundwater defluoridation.

Table 5.7: Physicochemical parameters of field water before treatment and at breakthrough point.

| **Parameter** | **Before treatment** | **Breakthrough point** | **WHO guideline (2017)** |
|---|---|---|---|
| pH | 8.7 | 7.98 | 5.0-9.7 |
| As Total | 0.5 | 0.01 | 0.01 |
| $F^-$ | 5.4 | 0.57 | 1.5 |
| $Cl^-$ | 31.59 | 49.21 | <300 |
| $SO_4^{2-}$ | 11.89 | 3.42 | <500 |
| $NO_3^-$ | 2.67 | ND | 50 |
| $PO_4^{3-}$ | 1.3 | ND | - |
| Al | <0.001 | 0.04 | 0.3 |
| Mn | 0.02 | 0.12 | 0.4 |
| Fe | 0.013 | 0.30 | 0.3 |
| Mg | 8.98 | 6.85 | 200 |
| Na | 70.36 | 68.4 | 200 |
| Ca | 10.87 | 7.21 | 200 |

Note: ND= Not detected, All concentration in mg/L.

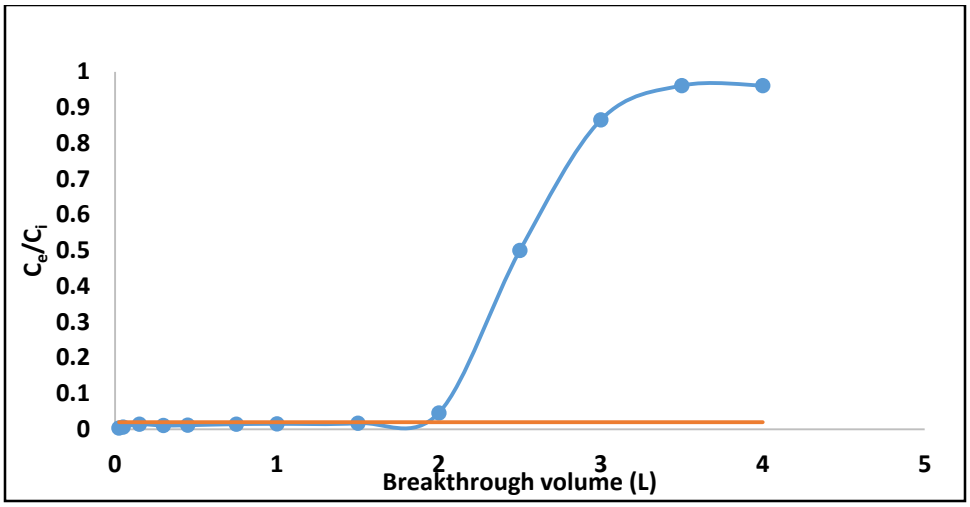


Figure 5.18: The breakthrough curve for As removal from groundwater (initial As concentration of 4.45 mg/L, 2.5 g adsorbent mass, 1.2 mL/min flow rate, 7.2 initial pH).

### 5.4 Adsorption mechanism

The adsorption data was described better by pseudo second order of reaction kinetics indicating that the adsorption of both As(III) and As(V) was more of chemical processes. Furthermore, the data did not fit onto intra-particle diffusion model suggesting that possibility of boundary layer and intra-particle diffusion sorption. Depending on the solution pH and the arsenic species, adsorption of As(III) and As(V) can be ascribed to various mechanisms such as ion exchange and electrostatic attraction and complexation. Arsenate [As(V)] exist as $H_2AsO_4^-$, $HAsO_4^{2-}$ and $AsO_4^{3-}$ respectively at both acidic and alkaline pH values. At acidic pH, the surface of FMK is positively charged and therefore, As(V) will be electrostatically attracted to the adsorbent's surface which is then followed by a strong inner sphere complexation at equilibrium (Lee at al., 2015). As the pH increases the surface of the adsorbent becomes negatively charged, this will results in electrostatic repulsion. Therefore, As(V) adsorption will be through ion exchange. Equation 5.11-5.13 hypothesize the adsorption of As(V) onto FMK.

$$\equiv MOH + H_3AsO_4 \leftrightarrow \equiv MH_2AsO_4 + H_2O \quad (5.11)$$

$$\equiv MOH + H_2AsO_4^- \leftrightarrow \equiv MHAsO_4^- + H_2O \quad (5.12)$$

$$\equiv MOH + HAs_4^{2-} \leftrightarrow \equiv MAs_4^{2-} + H_2O \quad (5.13)$$

Arsenite [As(III)] occurs as neutrally charged $H_3AsO_3$ at pH < 9 and as negatively charged $H_2AsO_3^-$ and $HAsO_3^{2-}$ at pH above 9 (Ren et al., 2014). Therefore, its adsorption could be due to

ion exchange at both pH levels (Equation 5.14-5.15). Its higher sorption capacity can be ascribed to its oxidation into As(V) by the manganese oxides used to synthesize the adsorbent (Equation 5.16) (Li et al., 2012). In summary, the removal of As(III) is coupled with oxidation and adsorption.

$$\equiv MOH + H_3As_3 \leftrightarrow\equiv MH_2As_3 + H_2O \quad (5.14)$$

$$\equiv MOH + H_2As_3^- \leftrightarrow\equiv MHAs_3^- + H_2O \quad (5.15)$$

$$MnO_2 + H_3AsO_3 + 2H^+ \rightarrow Mn^{2+} + H_3AsO_3 + H_2O \quad (5.16)$$

### 5.5 Comparison to other adsorbent

Table 5.8 compares the Langmuir's maximum adsorption capacity of FMK synthesized in this study with other reported adsorbents. It is noted that adsorption capacity of the presently reported adsorbent is lower than that of the other adsorbent. However, it should not be ignored that adsorption capacity depends on the factors such as adsorbate concentration and adsorbent used during the experiment. The adsorbate concentration range used in the present study and the adsorbent dosage used are low compared to those used in other study and hence lower adsorption capacity is recorded. With this in mind FMK is also a promising adsorbent for arsenic remediation.

Table 5.8: Comparison of Langmuir maximum adsorption capacity for different adsorbent.

| **Adsorbent** | **Experimental conditions** | **As(III) adsorption capacity** | **As(V) adsorption capacity** | **References** |
|---|---|---|---|---|
| FMCB | 5-60 mg/L; 1 g/L; pH 7, 298 K | 54.2 | 39.1 | Qi et al., 2015 |
| Fe-Mn binary oxide activated carbon | 1-600 mg/L; 0.1g/30 mL; pH 4, 298 K | 18.4 | 16.0 | Ryu et al., 2017 |
| Fe-Mn binary oxides loaded zeolite | 2-300 mg/L; 0.5 g/L; pH 7; 298 K | 49.73 | 46.98 | Kong et al., 2014 |
| Mg-Fe-Ala-LDH | 1-15 mg/L; 0.2 g/100 mL; pH 6; 298 K | 49.8 | 23.6 | Hong et al., 2014 |
| Fe-Mn bimetal kaolin clay | 1-30 mg/L; 0.4 g/100 mL; pH 6.5; 298 K | 2.92 | 2.30 | Present study |

## 5.6 Summary

Fe-Mn bimetal oxide modified kaolin clay mineral was successfully prepared and used for As(III) and As(V) remediation from groundwater. A maximum As(III) and As(V) percentage removal of 82.75 and 81.64%, respectively were achieved at initial pH of 6 from initial concentration of 5 mg/L using adsorbent dosage of 0.4 g/100 mL and agitation time of 60 min at 250 rpm. Column experiments were conducted to evaluate the applicability of the synthesized adsorbent in the field, a maximum breakthrough volume of ≈2 L was achieved at breakthrough point using a 5 g adsorbent dosage. The adsorption kinetics data fitted better to pseudo second order of reaction kinetics while the adsorption isotherm data was described by Langmuir isotherm model. Adsorption thermodynamics study showed that adsorption of As(III) is exothermic in nature while adsorption of As(III) is endothermic. The FMK developed can be effectively regenerated and reused for up to 6 adsorption cycles using $K_2SO_4$ as regenerant. The adsorption of As(III) and As(V) was found to be limited in the presence of $SO_4^{2-}$. The results showed that FMK developed in this study is a promising adsorbent for arsenic removal from groundwater.

## References

Bhattachryya, G. K. & Gupta, S.S., 2008. Adsorption of a few heavy metals on natural and modified kaolinite and montmorillonite: A review. *Advances in Colloid and Interface Science,* 140, pp. 114–131.

Bhowmick, S., Pramanik, S., Singh, P., Mondal, P., Chatterjee, D. & Nriagu, J., 2018. Arsenic in groundwater ofWest Bengal, India: A review of human health risks and assessment of possible intervention options. *Science of the Total Environment,* 612, pp. 148–169.

Cui, H.J. Cai, J.K. Zhao, H. Yuan, B. A., C.L. & Fu, M.L., 2014. Fabrication of magnetic porous Fe–Mn binary oxide nanowires with superior capability for removal of As(III) from water. *Journal of Hazardous Materials,* 279, pp. 26–31.

Ding, W., Wang. Y., Yu. Y., Zhang, X., Li, J. & Wu, F., 2015. Photooxidation of arsenic(III) to arsenic(V) on the surface of kaolinite clay. *Journal of Environmental Sciences,* 36, pp. 29-37.

Ho, Y.S., 2004. Citation review of Lagergren kinetic rate equation on adsorption reactions. *Scientometrics,* 59(1), pp. 171-177.

Hong, J., Zhu, Z., Lu, H. & Qui, Y., 2014. Synthesis and arsenic adsorption performances of ferric-based layered double hydroxide with a-alanine intercalation. *Chemical Engineering Journal*. 252, pp. 267–274.

Kong, S., Wang, Y., Hu, Q. & Olusegun, A. K., 2014. Magnetic nanoscale Fe–Mn binary oxides loaded zeolite for arsenicremoval from synthetic groundwater. *Colloids and Surfaces A: Physicochemical and Engineering Aspects.* 457, pp. 220-227.

Langmuir, I., 1918. The adsorption of gases on plane surfaces of glass, mica and platinum. *Journal of the American Chemical Society,* 40 (9), pp. 1361-1403.

Lee, S.M., Lalhmunsiama, Thanhamingliana, & Tiwari, D., 2015. Porous hybrid materials in the remediation of water contaminated with As(III) and As(V*). Chemical Engineering Journal,* 270, pp. 496–507.

Li, X. He, K. Pan, B. Zhang, S. Lu, L. & Zhang, W., 2012. Efficient As(III) removal by macroporous anion exchanger-supported Fe–Mn binary oxide: Behavior and mechanism. *Chemical Engineering Journal,* 193(194); 131–138.

Mandal, B. K. & Suzuki, K. T., 2002. Arsenic round the world: a review. Talanta, 58, pp. 201–235.

Naujokas, M. F. Anderson, B. Ahsan, H. Aposhian H. V. Graziano, J. H. & Thompson, C. W.A., 2013. The Broad Scope of Health Effects from Chronic Arsenic Exposure: Update on a Worldwide Public Health Problem. *Environmental Health Perspectives,* 121(3), pp. 295-302.

Ocinski, D., Sobala, I. J., Mazur, P., Raczyk, J. & Balawejder, E. K., 2016. Water treatment residuals containing iron and manganese oxides for arsenic removal from water – Characterization

of physicochemical properties and adsorption studies. *Chemical Engineering Journal*, 294, pp. 210–221.

Qi, J. Zhang, G. & Li, H., 2015. Efficient removal of arsenic from water using a granular adsorbent: Fe–Mn binary oxide impregnated chitosan bead. *Bioresource Technology*, 193, pp. 243–249.

Rahman, M. A. Rahman, A. Khan, M. Z. K. & Renzaho, A. M. N., 2018. Human health risks and socio-economic perspectives of arsenic exposure in Bangladesh: A scoping review. *Ecotoxicology and Environmental Safety*, 150, pp. 335–343.

Ren, H. Zhang, Z. Luo, H. Hu, B. Dang, Z. Yang, C. & Li, L, 2014. Adsorption of arsenic on modified montmorillonite. *Applied Clay Science*, 97–98, pp. 17–23.

Ryu, S, R., Jeon, E, K., Yang, J. S. & Baek, K., 2017. Adsorption of As(III) and As(V) in groundwater by Fe–Mn binary oxide-impregnated granular activated carbon (IMIGAC). *Journal of the Taiwan Institute of Chemical Engineers.* 72, pp. 62–69.

Smedley, P.L, & Kinniburgh, D. G., 2002. A review of the source, behavior and distribution of arsenic in natural waters. *Applied Geochemistry*, 17, pp. 517-568.

Smith, A.H. & Smith M.M.H., 2004. Arsenic drinking water regulations in developing countries with extensive exposure. *Toxicology*, 198, pp. 39–44.

Tiwari, D. & Lee, S.M., 2012. Novel hybrid materials in the remediation of ground waters contaminated with As(III) and As(V). *Chemical Engineering Journal*, 204–206, pp. 23–31.

Tran, H. N. You, S. J. Bandegharaei, A. H. & Chao, H. P. 2017. Mistakes and inconsistencies regarding adsorption of contaminants from aqueous solutions: A critical review. *Water Research*, 120, pp. 88-116.

Weber, W. J. Morris, J. C., 1963. Kinetics of adsorption on carbon from solution. *Journal of the Sanitary Engineering Division*, 89(2), pp. 31-60.

World Health Organization (WHO) 2017 Guidelines for drinking-water quality: fourth edition incorporating the first addendum. Geneva: Switzerland. Licence: CC BY-NC-SA 3.0 IGO.

Zhang, G., Liu, H., Qu, J. & Jefferson, W., 2012. Arsenate uptake and arsenite simultaneous sorption and oxidation by Fe–Mn binary oxides: Influence of Mn/Fe ratio, pH, $Ca^{2+}$, and humic acid. *Journal of Colloid and Interface Science*, 366, pp. 141–146.

Zhang, G. S., Qu, J. H., Liu, H. J., Liu, R. P. & Li, G. T., 2007. Removal Mechanism of As(III) by a Novel Fe-Mn Binary Oxide Adsorbent: Oxidation and Sorption. *Environmental Science and Technology*, 41(13), pp. 4613-4619.

# Chapter 6: Preparation of surfactant modified kaolin clay mineral for As(III) and As(V) removal: Adsorption kinetics, isotherms and thermodynamics

## 6 Abstract

Apart from the modification of clay with inorganic polycations, cationic surfactants can also be used to enhance the adsorption capacity of the clay minerals. The modification of clay minerals with cationic surfactant involves ion exchange reaction between the exchangeable cations in the clay interlayers such as $Na^{+}$, $Ca^{2+}$, $Mg^{2+}$, $H^{+}$ and $Mg^{2+}$ and the quaternary ammonium cations in the surfactant. The cationic surfactant may also be retained primarily on the outer surface of the clay forming a bilayer. This result in the reversal of charges on the external surface of the clay providing sites were anions can be retained while neutral species can partition into the hydrophobic core introduced. This chapter present the modification of kaolin clay mineral by hexadecyltrimethylamonium bromide (HDTMA-Br) cationic surfactant and its application in arsenic remediation from groundwater. The X-ray diffraction (XRD) and X-ray fluorescence (XRF) were used to determine mineralogical and elemental composition of the adsorbent. The surface chemistry was determined using Fourier Transform Infra-red spectrum (FTIR) technique while surface morphology and surface area were determined using scanning electron microscopy (SEM) and BET techniques, respectively. Effectiveness of the adsorbent in arsenic removal was tested using batch experiments. The results revealed that adsorption of As(III) and As(V) is optimum at pH range 4-8. The maximum As(III) and As(V) adsorption capacities were found 2.33 and 2.88 mg/g, respectively after 60 min contact time. Pseudo first order model of reaction kinetics described the adsorption data for As(V) better while pseudo second order model described As(III) adsorption data. The adsorption isotherm data for As(III) and As(V) fitted well to Langmuir model indicating that adsorption of both species occurred on a mono-layered surface. Adsorption thermodynamics model revealed that adsorption of As(III) and As(V) was spontaneous and exothermic. The As(III)/As(V) adsorption mechanism was ascribed to electrostatic attraction between the positive charge in the adsorbent surface arsenic oxyanions and also ion exchange between the hydroxyl group and arsenic species. The presence of $Mg^{2+}$ and $Ca^{2+}$ increased As(III) and As(V) adsorption efficiency. The regeneration study showed that synthesized adsorbent can be used for up to 5 times. Surfactant modified kaolin clay mineral showed higher adsorption capacity towards As(III) and As(V) as compared to unmodified kaolin clay mineral and competitive with other adsorbent in the literature. The results obtained from this study revealed

that surfactant modified kaolin mineral is a candidate material for arsenic remediation from groundwater.

Keywords: Adsorption; kaolin clay mineral; kinetics; isotherms; thermodynamics; surfactant.

## 6.1 Introduction

Groundwater is the common source of water in majority of rural areas particularly in arid and semi-arid regions where surface water resources and rainfall are scarce. However, groundwater often contain toxic elements such as arsenic. In groundwater, arsenic exist as oxyanions of trivalent arsenite [As(III)] under oxidizing conditions and pentavalent arsenate [As(V)] under reducing conditions (Smedley and Kinniburgh, 2002; Duker et al., 2005; Choong et al., 2007). The prolonged exposure to groundwater containing higher concentrations of inorganic arsenic is linked to different types of cancer, neurological diseases and cardiovascular diseases (Smith et al., 1999; Smith and Smith, 2004; Bardach et al., 2015; Sarkar and Paul, 2016).

The World Health Organization (WHO) has estimated that at least 200 million people in more than 50 counties worldwide relies on water containing arsenic concentrations above the permissible limits of 10 µg/L (WHO, 2017). The worst affected countries includes Bangladesh, India, Argentina, Mexico, and China. In Africa, the estimate of people exposed to higher concentration of arsenic is unknown. However, higher concentrations of arsenic has been reported in countries like South Africa, Burkina Faso, Ghana and Zimbabwe (Kempster et al., 2007; Fatoki et al., 2013; Bretzler et al., 2017). Owing to toxicity of arsenic efforts towards monitoring and removal of arsenic from groundwater to a permissible levels for drinking purposes are being encouraged.

So far, several techniques including oxidation (McCann et al., 2018), coagulation and precipitation (Cui et al., 2015), adsorption (Ren et al., 2014), ion exchange (Pakzadeh and Batista, 2011) and membrane techniques (Kang et al., 2000) have been developed and tested for their efficiency in arsenic removal. However, most of these techniques are more expensive, generates toxic sludge and requires skilled labor for operation (Sarkar and Paul, 2016). Adsorption technique appears to be the suitable method that can be applied for arsenic removal particularly in rural areas because it uses materials that are found at little or no costs such as clay minerals (Bentahar, 2016), activated carbon (Arcibar-Orozco, 2014), activated alumina, bone char (Saikia et al., 2017) and coal fly ash (Wang et al., 2008). Furthermore, adsorption technique is simple in design.

Synthesis of organically modified clay minerals for arsenic removal has recently received great attention from researchers. Organoclays are prepared through intercalation of cationic surfactant onto the interlayers of the clay minerals. This is achieved through ionic exchange between $Na^{+}$, $Ca^{2+}$, $K^{+}$ and $Mg^{2+}$ in the clay interlayers and the cationic surfactant where the net surface charges of the clay are reversed from negative to positive (Su et al., 2010). This modification enhances the sorption of anions via ion exchange (Reeve and Fallowfield, 2018). Su et al. (2011) prepared a surfactant modified bentonite clay for As(V) and As(III) removal from aqueous solution and reported maximum adsorption capacity of 0.288 and 0.102 mg/g for As(V) and As(III), respectively. The achieved results were higher than those achieved from unmodified bentonite under the same experimental conditions. Chutia et al. (2009) also reported an improved sorption capacity of hexadecyltrimethylamonium bromide (HDTMA) modified mordenite and clinoptilolite clay minerals for As(V) as compared to unmodified ones. Although the reported adsorbents have shown greater potential for use in arsenic remediation, several features regarding their practical application in groundwater treatment has not been addressed. This includes their regeneration and reuse potential, leaching and chemical stability of the adsorbent and the thermodynamics of As(III)/As(V) adsorption onto organo-clay.

Nevertheless, little has been done on the modification of kaolin clay mineral using cationic surfactant for As(III)/As(V) removal. This study aims at preparing a surfactant modified kaolin clay mineral for simultaneous As(III) and As(V) removal from groundwater. Batch experiments were used to evaluate the effects of contact time and adsorption isotherm, effect of adsorbate concentration and adsorption isotherms and thermodynamics, effect of pH and co-existing ions. Furthermore, the regeneration and reuse of adsorbent were evaluated.

## 6.2 Material and Methods

### 6.2.1 Materials

Natural kaolin clay mineral was collected from Dzamba Village in Limpopo Province, South Africa. Hexadecyltriammonium bromide (HDTMA-Br) was purchased from Merk chemicals, South Africa. Other analytical grade reagents including $HAsNa_2O_4.7H_2O$ and $AsNaO_2$ were purchased from Rochelle Chemicals, South Africa.

### 6.2.2 Synthesis of surfactant modified kaolin clay (SMK)

Prior to modification the clay was cleaned using Milli-Q water at a mass/volume ratio of 1:5 to remove suspended organic matter. Clay sample was then oven dried at 105 $^{O}$C for 12 hours. Dried clay was then pulverized using a mortar and pestle to pass through 250µm sieve. To find the optimum concentration to prepare surfactant modified kaolin clay mineral, solutions containing 0.5, 1, 2, 3 and 5 mM were prepared by dissolving appropriate amounts of HDTMA in 100 mL of Milli-Q water at 35$^{o}$C. This was followed by adding 1 g of raw kaolin clay (RK) into respective solutions. Mixtures were agitated at 250 rpm for 60 min contact time, and filtered through 0.45 µm membrane filters. Residues were washed with Milli-Q water several times to remove excess surfactant. Obtained residues were then oven dried at 60 $^{O}$C for 12 hours and then pulverized using mortar and pestle to pass through 250 µm sieve. Batch experiments for arsenic were then conducted to find the optimum concentration using initial arsenic concentration of 5 mg/L and adsorbent dosage of 0.1 g/100 mL. The clay prepared using 5 mM HDTMA concentration yielded higher arsenic removal and was chosen for further experiments and characterization.

### 6.2.3 Characterization of the material

The raw kaolin (RK) and the surfactant modified kaolin clay (SMK) were characterized using the following techniques: X-ray diffraction (XRD) and X-ray fluorescence (XRF) for mineralogical and elemental composition. Infra-red spectrum of the material were obtained using Fourier Transform Infra-red spectrum equipped with ATR-Diamond (Bruker, Germany). Morphological characteristics were determined using scanning electron microscopy (SEM) (Leo1450 SEM, voltage 10 kV, working distance 14 mm). The pore size distribution, pore volume, and pore diameter were determined by Barrett Joyner Halenda (BJH) sorption model using a specific surface area analyzer (Autosorb-iQ & Quadrasorb SI, USA). Nitrogen adsorption-desorption isotherms were used to determine specific surface area of the adsorbent according to Brunauer Emmett Teller (BET) model. The pHpzc of the clay was determined using titration method as described by Gitari et al. (2013).

### 6.2.4 Batch adsorption

Stock solutions containing 1000 mg/L As(III) and As(V) were prepared by dissolving an appropriate amount of salt in Milli-Q water (18.2 MΩ/cm). The working solutions were prepared through appropriate dilutions from the stock solution. To evaluate the optimum contact time and

the adsorption kinetics, the contact time was varied from 10 to 120 min. adsorbate dosage of 0.15 g/100 mL and adsorbate concentration of 5 mg/L was maintained. After agitation the residual As(III)/As(V) concentration were determined using gold wire electrode attached 884 professional VA (Metrohom, SA). The optimum adsorbent dosage was evaluated by varying adsorbent dosage from 0.05-0.5 g/100 mL. Contact time of 60 min and adsorbate concentration of 5 mg/L were maintained. To evaluate the adsorbate concentration and adsorption isotherms, the initial concentration of As(III)/As(V) was varied from 1 to 30 mg/L and the adsorbent dosage of 0.4 g/100 mL, contact time of 60 min were maintained. The experiment was conducted at a temperature of 298, 323 and 343 K. The obtained data was used to evaluate the adsorption thermodynamics. The effect of initial pH was evaluated at initial adsorbate concentration of 5 mg/L, contact time of 60 min and adsorbent dosage of 0.4 g/100 mL. The initial pH was adjusted from 2-12 using 0.01 M NaOH and 0.01 M HCl. The influence of co-existing ions ($F^-$, $Cl^-$, $NO_3^-$, $CO_3^{2-}$, $SO_4^{2-}$, $Mg^{2+}$ and $Ca^{2+}$) was evaluated at the initial concentration As(III)/As(V) concentration of 3 mg/L, adsorbent dosage of 0.4 g/100 mL, 60 min contact time. The initial concentration of each co-existing ion was 5 mg/L. All experiments were conducted in triplicate and the mean values were reported. Unless otherwise stated, experiments were conducted at room temperature and initial pH of 6±0.5.

### 6.2.5 Desorption and adsorbent regeneration

The efficiency of $Na_2CO_3$, $K_2SO_4$, KCl and $NaNO_3$ to desorb As(III)/As(V) from the SMK was evaluated by suspending 0.1 g of arsenic loaded sorbent onto 50 mL solution containing 0.1 M of each of the regenerant and the mixtures were agitated for 60 min. After agitation, samples were filtered through 0.45 µm pore filter membrane. The effect of $Na_2CO_3$ concentration in desorption of As(III)/As(V) was evaluated by varying the concentration from 0.01 to 1 M.

To evaluate the regeneration and reuse potential of the adsorbent: As(III)/As(V) removal experiment was conducted by treating solution containing 5 mg/L As(III)/As(V) with 1.0 g of SMK at initial pH of 6 for 60 min. After agitation, mixtures were filtered through 0.45 µm filter membranes. Residues were washed with Milli-Q water and oven dried for 12 hours at 60 $^oC$. The obtained residues were pulverized with a mortar and pestle to pass through 250 µm sieve, weighed and then reused for As(III)/As(V) removal. After the experiment, residues were regenerated using 100 mL of 0.01 M $Na_2CO_3$ by agitating the mixture for 60 min. After regeneration the

As(III)/As(V) experiment was conducted as in other experiments. The regeneration-reuse cycle were continued up to 5$^{th}$ cycle.

### 6.2.6 Column experiments

Column tests were carried using a plastic column with the internal diameter of 2.5 cm and a total length of 13.5 cm. 5 g of the modified clay was packed in the column to make a bed height of 1.2 cm. Groundwater collected from Siloam community borehole was used as feed water. It was spiked with arsenic solution to get desired total arsenic concentration of 0.5 and 1.5 mg/L. The feed water was passed through the column in an up-flow mode using a Gilson peristaltic pump at a flow rate of 1.5 mL/min. The effluents were collected at a regular interval and analyzed for total arsenic concentration. Figure 6.1 present the set-up for column experiment.

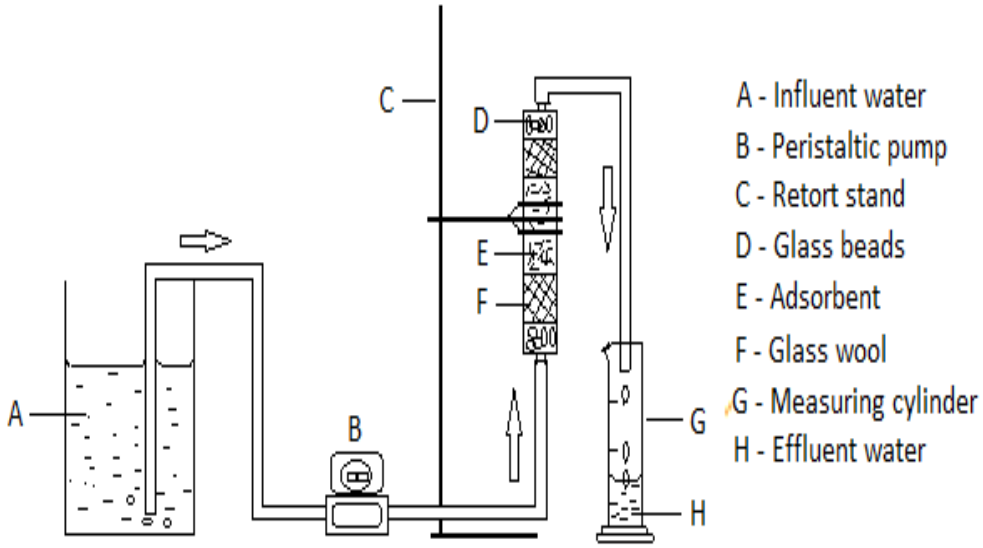


Figure 6.1: Experimental set-up for column experiments.

### 6.2.7 Analysis of residual arsenic

The residual As(III)/As(V) concentration was measured using ScTRACE Gold electrode attached to 884 professional VA Polarography (Metrohm, SA). A composite solution containing 1 mol/L sulfamic acid, 0.5 mol/L citric acid and 0.45 mol/L KCl was used an electrolyte. For total As concentration, $KMnO_4$ was added as an oxidizing agent. For quality control, samples were also analyzed using metrohm 850 professional ion chromatography (Switzerland) for As(III) and As(V) concentration. Metrosep A Supp 5-150 column was used for separation and the guard column Metrosep A 4/5 was used. The eluent containing 15 mmol/L NaOH and 2.0 mmol/L $Na_2CO_3$ was

used as the mobile phase. The concentration of As(III) was determined without suppression. The conductivity detector was used to estimate the concentration of different chemical species. Some samples were further analyzed using ICP-MS.

### 6.3 Results and Discussion

#### 6.3.1 XRD analysis

Figure 6.2 presents the XRD pattern of raw kaolin (RK) and surfactant modified kaolin (SMK) clay minerals. There is no change observed in the XRD pattern of the kaolin clay mineral after modification with HDTMA. This could be indicating that sorption of HDTMA onto the surface of kaolin clay mineral did not affect the clay interlayers. The same observation was reported by Sun et al. (2017) during modification of illite clay using CTAB. The analysis further revealed that the clay soils contains kaolinite and quartz as the mineral phases.

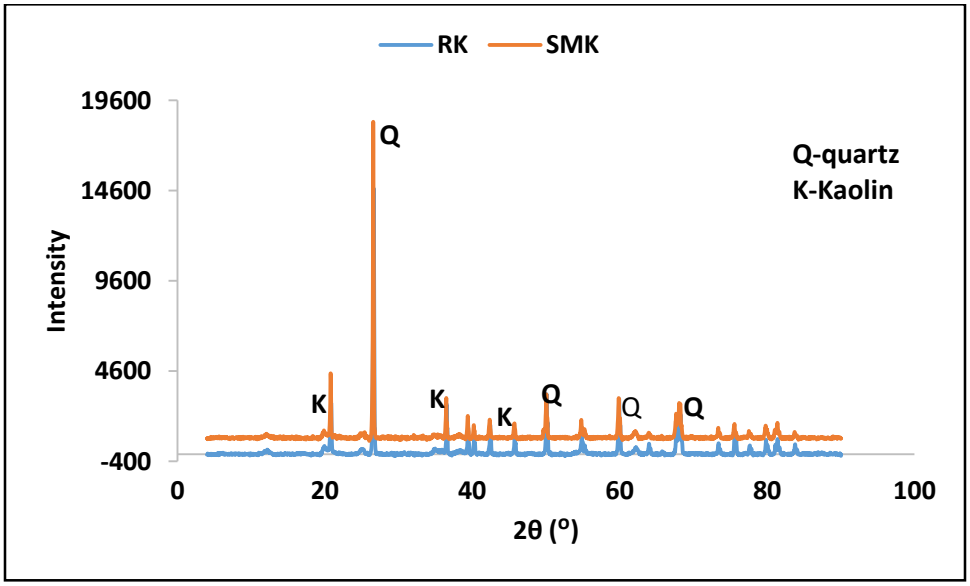


Figure 6.2: X-ray diffraction patterns of RK and SMK.

#### 6.3.2 Elemental composition

Table 6.1 presents the elemental composition of raw and modified kaolin mineral determined using XRF. The results showed that $SiO_2$ and $Al_2O_3$ are the main constituents of the clay mineral averaging 57.1 and 22.05%, respectively followed by $Fe_2O_3$ averaging 3.88%. These results confirms that this clay is an alumino-silicate material. After modification the content of $SiO_2$, $Al_2O_3$ and $Fe_2O_3$ decreased to 51.97, 18.79 and 2.85 %, respectively. This could be attributed to their dilution during intercalation of cationic surfactant interlayers. The content of exchangeable

oxides such as MgO, CaO and $K_2O$ decreased after modification (Table 6.1). This suggest that the modification involves ion exchange reaction between $Mg^{2+}$, $K^+$ and $Ca^{2+}$ and the surfactant.

Table 6.1: Elemental composition of RK and SMK.

| **Oxides** | **RK (%w/w)** | **SMK (%w/w)** |
|---|---|---|
| $SiO_2$ | 57.1 | 51.67 |
| $Al_2O_3$ | 22.05 | 18.79 |
| $Fe_2O_3$ | 3.88 | 2.85 |
| MgO | 0.57 | <LOD |
| MnO | 0.02 | 0.02 |
| CaO | 0.95 | 0.39 |
| $K_2O$ | 0.16 | 0.01 |
| $TiO_2$ | 1.76 | 1.0 |
| $P_2O_5$ | 0.02 | 0.041 |

*LOD: Limit of Detection

### 6.3.3 FTIR analysis

The FTIR spectrums of RK, HDTMA, SMK before and after arsenic removal are presented in Figure 6.3. For the raw kaolin clay mineral, the absorption bands at 3698.54 and 1695.25 $cm^{-1}$ is ascribed to –OH stretching vibration in physiosorbed water. Bands at 1003.68 and 964.92 $cm^{-1}$ are attributed to the vibration of Si-OH and Al-OH bonds, respectively. The bands at lower wavelength are ascribed to the vibration of Al-O-Si and Si-O-Si networks. The HDTMA spectrum showed a stronger absorption bands at the region of 2849.72 and 2917.03 $cm^{-1}$ which could be assigned to the C-H stretching bond of the methyl ($-CH_3$) and methylene ($-CH_2$) groups. The band at 1462.59 $cm^{-1}$ could be attributed to the vibration of C-C-C flexural vibration associated with methylene groups. The bands at 911.82 $cm^{-1}$ and 966.9 $cm^{-1}$ are associated with the vibration and stretching of C-N bonds. The successful modification of the kaolin mineral is confirmed by the bands at 2858.13 and 2923.41 $cm^{-1}$ which are ascribed to the vibration of C-H bonds. Furthermore, there is an increase in transmittance intensity of the band at 911.82 $cm^{-1}$ and 966.9 $cm^{-1}$, respectively for the modified kaolin mineral. After arsenic removal, no change was observed in the spectrum of the modified clay. This indicates that there was no substantial change had taken in the integrity of

the original sorbent. This could suggest that adsorption of arsenic could be through surface complexation.

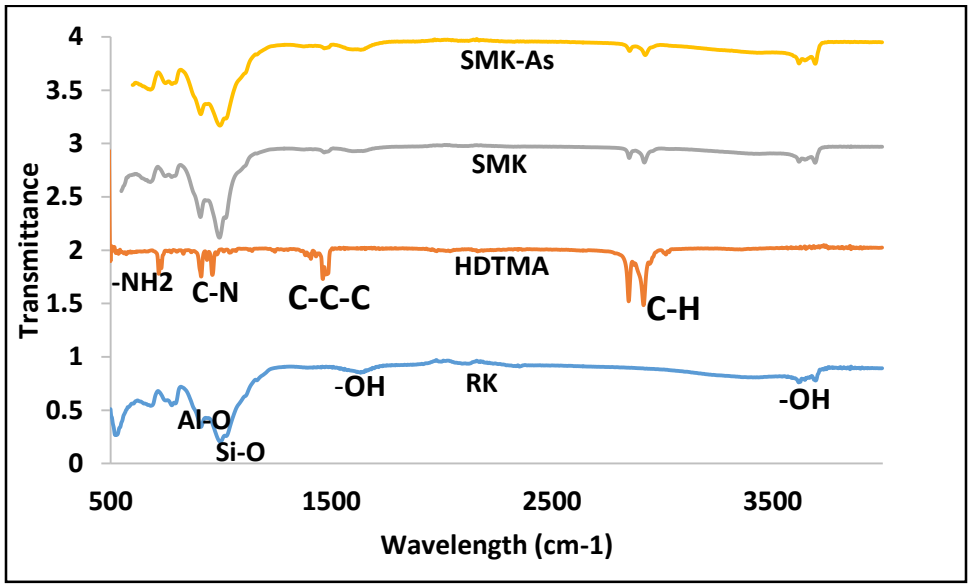


Figure 6.3: FTIR spectrum of RK, HDTMA and SMK before and after As removal.

### 6.2.4 Surface morphology

The SEM micrographs of RK and SMK together with their respective EDX spectrum are presented in Figure 6.4A-D. The analysis revealed that RK has a spongy like morphology with different sized agglomerates of fine particles (Fig. 6.4A). No significant change can be observed on the surface of the clay after modification (Fig. 6.4B). However, the surface seemed covered with small particles, suggesting a better adhesion of small particles onto the larger ones. This could be attributed to change in the surface hydrophobicity and thus free adhesion (Sun et al., 2017). The SEM-EDX spectrum confirmed the presence of exchangeable cations such as $K^{+}$, $Mg^{2+}$ and $Ca^{2+}$ in RK (Fig. 6.4C) clay and the absence of these cations in the SMK spectrum (Fig. 6.4D). This results are complimented by the XRF results (Table 6.1) which showed the decrease in percentage weight of MgO, CaO and $K_2O$ oxides.

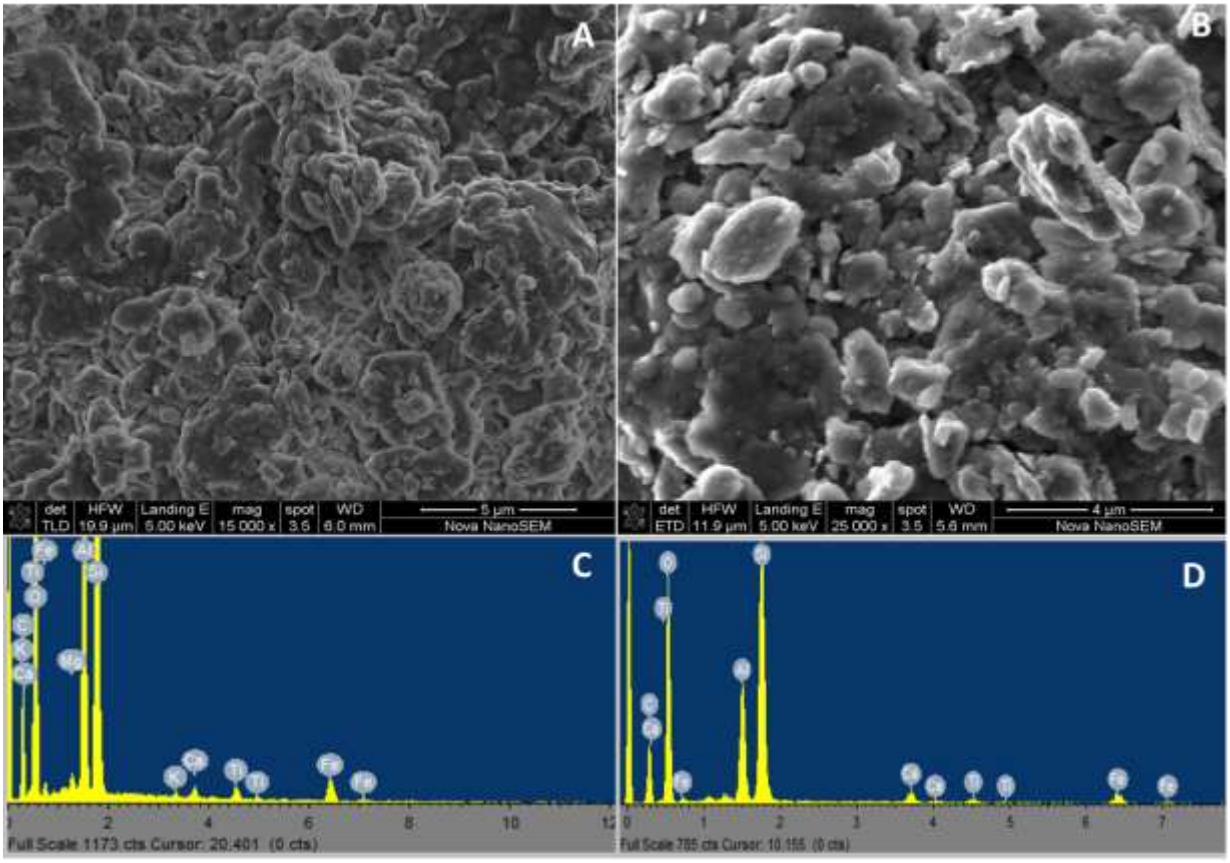


Figure 6.4: SEM micrographs and EDX spectrums of RK (A and C) and SMK (B and D).

### 6.3.5 Surface area analysis

Table 6.2 present the BET surface area, pore volume and pore diameter determined using nitrogen adsorption and desorption. The analysis revealed that the total surface area of kaolin clay decreased drastically from 18.61 to 3.39 $m^2/g$ after modification with the cationic surfactant. Conversely, the pore volume and the pore diameter increased from 0.04 to 0.07 cc/g and 9.53 to 20.41 nm, respectively. This results are similar to the ones reported by Zhu and Zhu (2007) and Lee et al. (2015) for surfactant modified clays. The decrease in surface area and the increase in pore volume and pore diameter is attributed to the fact that intercalated surfactant filled up most of the gallery space in the clay surface resulting in propping up of the interlayer leading to increased pore volume and pore diameter. Based on the average pore diameter it is concluded that the synthesized material is mesoporous.

Table 6.2: Surface area, pore volume and pore diameter of RK and SMK.

| | BET surface area ($m^2/g$) | Pore volume (cc/g) | Pore diameter (nm) |
|---|---|---|---|
| RK | 19.02 | 0.04 | 9.53 |
| SMK | 3.39 | 0.07 | 20.41 |

### 6.3.6 pH point of zero charge (pHpzc)

Figure 6.5 presents the $pH_{pzc}$ of the RK and SMK. The results showed that modification of kaolin clay mineral increased the pHpzc of the clay from 6.5 to 7.5. The pHpzc represent the pH at which the net surface charge of the clay will be zero. At pH above the pHpzc the clay will be negatively charged while at pH below the pHpzc the clay will be positively charged (Gitari et al., 2013). The increase in pHpzc after modification indicates that modification of the clay by HDTMA enhanced the net positive charges of the clay mineral. This could enhance the pH range at which the adsorption of arsenic oxyanions will be optimum.

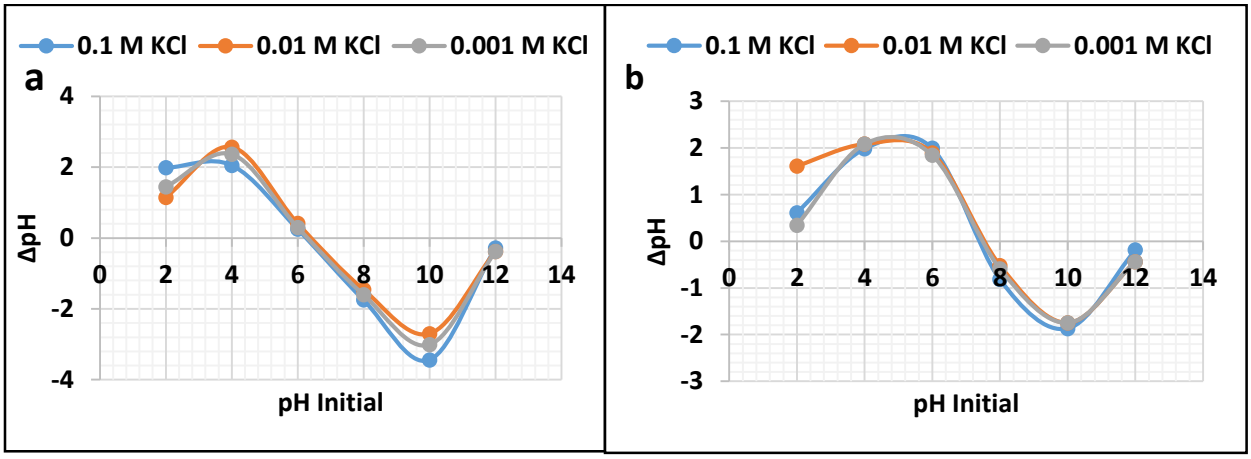


Figure 6.5: pHpzc of RK (a) and SMK (b).

### 6.3.7 Effect of contact time and adsorption kinetics

Figure 6.6 shows the effect of contact time on percentage As(III) and As(V) removal by SMK. It is observed that the percentage of removal for As(III) and As(V) was rapid within the first 60 min of contact time and relatively slower at contact time beyond 60 min which indicate that the adsorbent surface is saturated and the system has reached equilibrium. The rapid adsorption at contact time below 60 min could be attributed to large number of available active sorption sites

for As(III) and As(V) on the surface of the adsorbent. Therefore, 60 min was chosen to be the optimum contact time for further experiments.

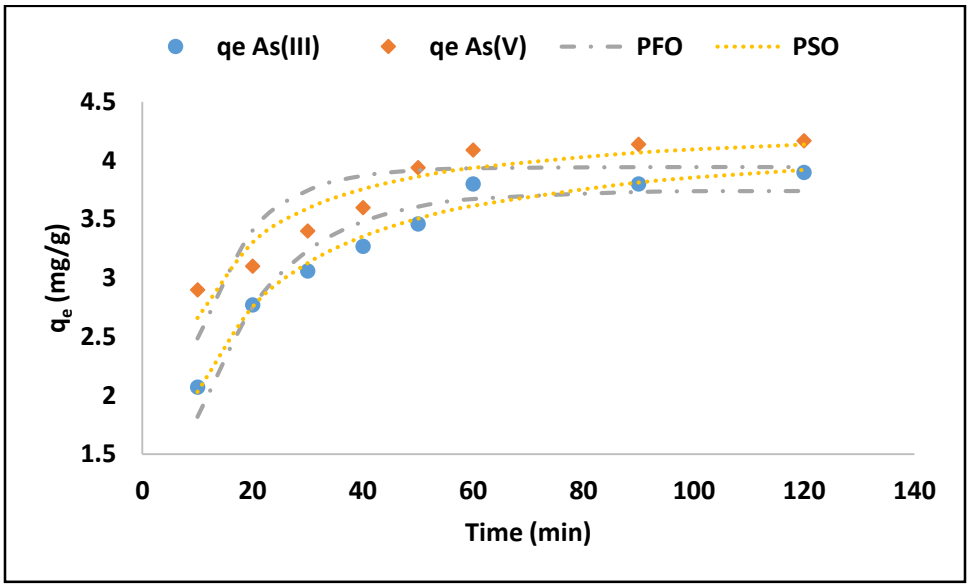


Figure 6.6: Adsorption kinetics for As(III) and As(V) onto SMK (initial concentration of 5 mg/L, adsorbent dosage of 0.1 g/100 mL, pH 6).

In order to determine the efficiency of the adsorption processes and to provide the insight of the As(III) and As(V) adsorption mechanism as well as the rate limiting steps, the commonly used pseudo-first-order (PFO) and pseudo-second-order (PSO) reaction kinetics models together with the intra-particle diffusion model of Weber-Morris were applied to fit the experimental data (Gupta et al., 2011, Tran et al., 2017). Pseudo-first-order and pseudo-second-order reaction models are expressed by equation 6.3 and 6.4 while equation 6.5 expresses the intra-particle diffusion model (Ho et al., 1996; Ho et al., 2004; Weber and Morris, 1963).

$$q_t = q_e(1 - e^{-k_1 t}) \quad (6.3)$$

$$q_t = \frac{q_e^2 k_2 t}{1 + k_2 q_e t} \quad (6.4)$$

$$q_t = k_i t^{0.5} + C \quad (6.5)$$

Where $q_e$ (mg/g) and $q_t$ (mg/g) represent the adsorption capacity at equilibrium and at time t (min), respectively; $k_1$ ($min^{-1}$), $k_2$ (g/mg.min), $k_i$ ($mg/g.min^{-0.5}$) are rate constants for PFO, PSO and intra-particle diffusion model, respectively and C, intercept is the constant associated to the thickness

of the boundary layer. Higher value of C correspond to the greater effect on the limiting boundary layer.

The nonlinear plots for PFO and PSO kinetics models for As(III) and As(V) adsorption are presented in Figure 6.6. The PFO and PSO parameters estimated by nonlinear regression are presented in Table 6.3.

Table 6.3: Constant parameters for pseudo-first-order and pseudo-second-order models of reaction kinetics.

| | PFO | | | PSO | | |
|---|---|---|---|---|---|---|
| | $q_e$ (mg/g) | $K_1$ ($min^{-1}$) | $R^2$ | $q_e$ (mg/g) | $K_2$ (g/mg.min) | $R^2$ |
| As(III) | 3.7 | 0.1 | 0.92 | 2.1 | 0.27 | 0.88 |
| As(V) | 3.99 | 0.09 | 0.66 | 4.35 | 0.03 | 0.98 |

Based on the correlation coefficient ($R^2$) and the model adsorption capacity values, the adsorption of As(III) was described better by PFO while the data for As(V) was described better by PSO. This indicate that adsorption of As(III) onto SMK occurred via physiosorption whereas the adsorption of As(V) occurred through chemisorption. The intra-particle plot presented in Figure 6.7 exhibited two clearly defined phases which indicates the possibility of external surface adsorption on the macro-pores (phase 1) and intra-particle diffusion into micro-pores and mesopores of the adsorbent (phase 2). At phase 1 arsenic molecules are attracted physically to the surface while at phase 2 arsenic molecules are adsorbed through ion exchanges between the hydroxyl ions and arsenic ions within the particles. The model constant are as presented in Table 6.4 shows that the $K_{i1}$ values are higher than the $k_{i2}$ values indicating that the external surface adsorption was much faster than the intra-particle diffusion. The intra-particle diffusion in phase 2 was confirmed by higher $C_2$ value which is an indication of thicker boundary (Table 6.4).

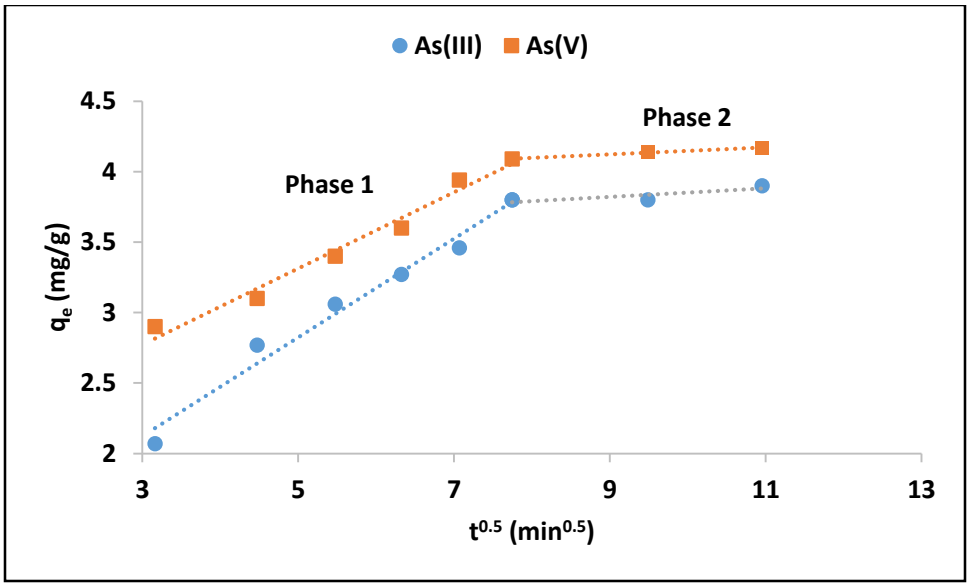


Figure 6.7: Intra-particle diffusion model for As(III) and As(V) adsorption onto SMK.

Table 6.4: Constant parameters for intra-particle diffusion model.

| | $K_{i1}$ (mg/g.$min^{-0.5}$) | $C_1$ | $K_{i2}$ (mg/g.$min^{-0.5}$) | $C_2$ |
|---|---|---|---|---|
| As(III) | 0.35 | 1.07 | 0.03 | 3.54 |
| As(V) | 0.27 | 1.96 | 0.02 | 3.89 |

### 6.3.8 Effect of adsorbent dosage

Figure 6.8 depicts the effect of adsorbent dosage onto As(III) and As(V) adsorption by SMK. It is observed that the removal of efficiency of As(III) and As(V) increased with increasing adsorbent dosage from 0.05 g/100 mL to 0.2 g/100 mL where it reached the plateau. The adsorption efficiency remained almost constant at dosage beyond 0.2 g/100 mL indicating that the adsorbent has reached its maximum sorption capacity. The increase in removal efficiency with adsorbent dosage could be attributed to increasing number of active sites available for As(III) and As(V) sorption. For subsequent experiments, 0.4 g/100 mL adsorbent dosage was used in order to ensure optimum uptake of As(III) and As(V) species.

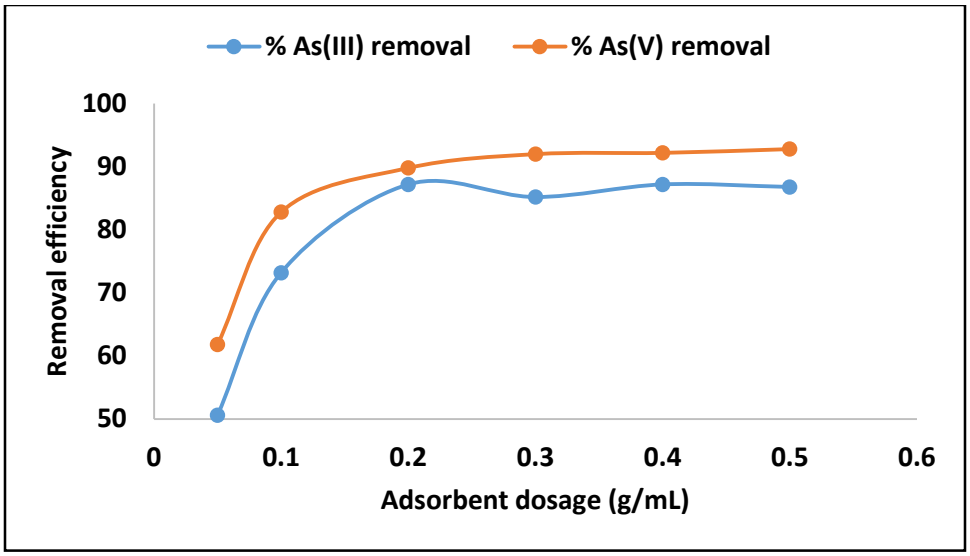


Figure 6.8: Effect of adsorbent dosage on As(III) and As(V) removal (Adsorbate concentration: 5 mg/L; contact time: 60 min; shaking speed: 250 rpm; pH 6±0.5).

### 6.3.9 Adsorption isotherms

To evaluate As(III) and As(V) adsorption isotherms, the initial concentration was varied from 1 to 30 mg/L and the experiment was repeated at a temperature of 298, 323 and 343 K. The results are presented in Figure 6.9. It is observed that As(III) and As(V) adsorption capacities increase with increasing equilibrium concentration. The same trend was observed at both temperatures. In order to describe the relationship between the adsorbate concentration and adsorbent, the non-linear equations of Langmuir (Eq. 6.6) and Freundlich (Eq. 6.7) adsorption isotherm models were used to describe the data (Firdaous et al., 2017).

$$q_e = \frac{q_{max} b C_e}{1 + b C_e} \quad (6)$$

$$q_e = K_f C_e^{1/n} \quad (7)$$

Where $q_e$ (mg/g) is the adsorption capacity, $C_e$ (mg/L) is the As(III) and As(V) concentration at equilibrium, b (L/mg) is the equilibrium adsorption constant related to the affinity of the binding sites, $q_{max}$ (mg/g) is the maximum monolayer adsorption capacity of the adsorbent. The higher the b and $q_{max}$ values the better the adsorbent (Tran et al., 2017). $K_f$ (mg/g) is the Freundlich constant related to adsorption capacity and 1/n is the dimensionless parameter for Freundlich adsorption isotherm model related to adsorption intensity which indicates the magnitude of the adsorption driving force or surface heterogeneity. Adsorption is favorable when 1/n < 1, unfavorable when

1/n >1, linear when 1/n = 1 and irreversible when 1/n = 0. Langmuir and Freundlich adsorption isotherm nonlinear fitting curves for As(III) and As(V) adsorption by SMK are presented in Figure 6.9 and the models constant values are presented in Table 6.5.

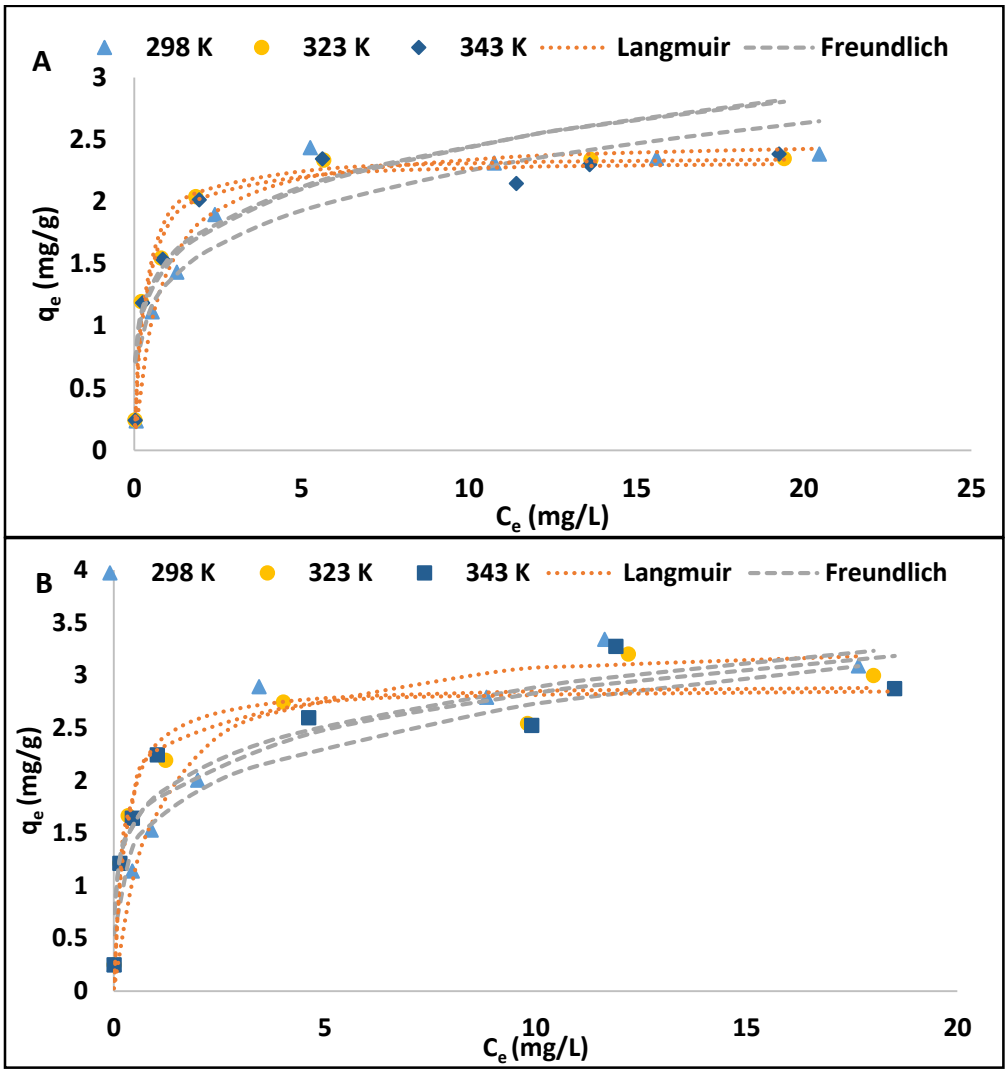


Figure 6.9: Adsorption isotherms for As(III) (a) and As(V) (b) adsorption onto SMK (adsorbent dosage: 0.4 g/100 mL, pH: 6±0.5, contact time: 60 min and shaking speed: 250 rpm).

Table 6.5: Adsorption isotherm parameters for As(III) and As(V) adsorption onto SMK.

| | | Langmuir | | | Freundlich | | |
|---|---|---|---|---|---|---|---|
| | | $q_m$ (mg/g) | B (L/mg) | $R^2$ | $K_f$ (mg/g) | 1/n | $R^2$ |
| As(III) | 298 K | 2.51 | 1.32 | 0.97 | 1.34 | 0.22 | 0.85 |
| | 323 K | 2.37 | 3.71 | 0.97 | 1.54 | 0.2 | 0.88 |
| | 343 K | 2.33 | 3.27 | 0.97 | 1.48 | 0.21 | 0.88 |
| As(V) | 298 K | 3.36 | 1 | 0.96 | 1.62 | 0.22 | 0.86 |
| | 323 K | 2.9 | 3.98 | 0.95 | 1.84 | 0.19 | 0.90 |
| | 343 K | 2.88 | 3.72 | 0.94 | 1.82 | 0.19 | 0.88 |

Based on the regression co-efficient value, the adsorption data fitted better to Langmuir adsorption isotherm model. This suggests that adsorption of As(III) and As(V) occurred on a mono-layered surface of SMK. Once the adsorbate molecule occupies a site, no further adsorption can take place on that site (Hong et al., 2014). The maximum adsorption capacity for Langmuir adsorption isotherm model ($q_{max}$) was observed to be decreasing with increasing temperature. The results showed that SMK has a stronger affinity towards As(V) as compared to As(III). The essential characteristics of the Langmuir isotherm model can be expressed by the dimensionless constant which is also called a separation factor or equilibrium parameter, $R_L$ which is expressed by Equation 8 (Tran et al., 2017).

$$R_L = \frac{1}{1+bC_0} \quad (8)$$

Where $R_L$ is the dimensionless separation factor, $C_0$ is the initial As(III) and As(V) concentration and b (L/mg). Adsorption is favorable when $R_L$ <1, unfavorable when $R_L$>1, linear when $R_L$=0 and when $R_L$ = 1 adsorption is irreversible. The calculated $R_L$ values for adsorption of As(III) and As(V) are presented in Figure 6.10 and b. It is observed that $R_L$ values for both arsenic species lies between 0 and l indicating that was favorable. This findings are in good agreement with the 1/n value obtained from Freundlich adsorption isotherm (Table 6.5) which also suggested that adsorption was favorable.

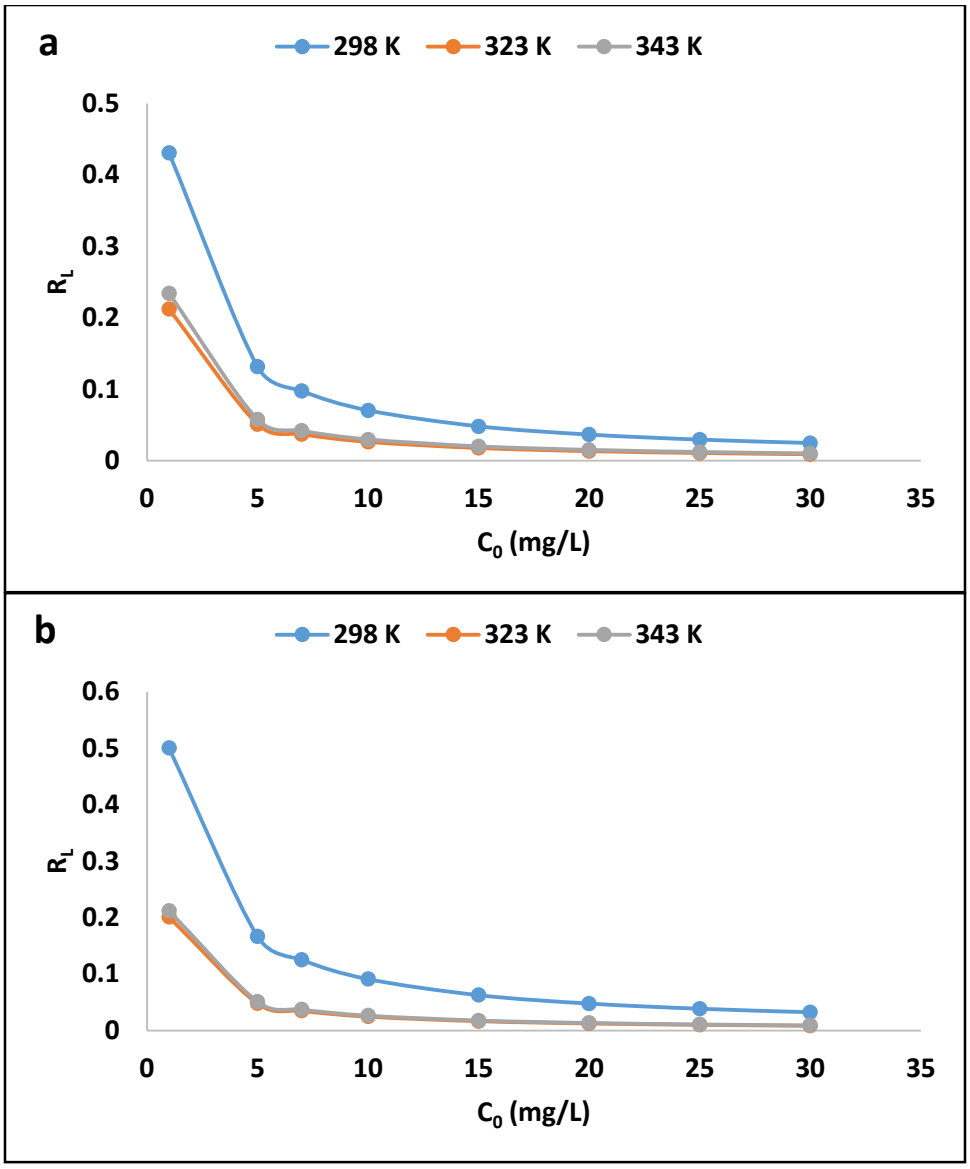


Figure 6.10: Values for separation factor, $R_L$ for the adsorption of As(III) (a) As(V) (b).

### 6.3.10 Adsorption thermodynamics

In order to confirm the As(III)/As(V) adsorption mechanism, the adsorption thermodynamic parameters ($\Delta G^o$, $\Delta H^o$ and $\Delta S^o$) determined from the Gibbs free energy equation (Eq. 6.9) (Tran et al., 2016).

$$\Delta G° = \Delta H° - T\Delta S° \quad (6.9)$$

Where $\Delta G^o$ is the Gibbs free energy change constant, $\Delta H^o$ is the standard enthalpy change while $\Delta S^o$ is the standard entropy change. For every spontaneous sorption process, $\Delta G^O$ value must be negative (Lonappan et al., 2018).

In sorption equilibria, the equilibrium constant, $K_L$ which is the Langmuir constant is related to Gibbs free energy change by the equation 6.10 (Gitari et al., 2017):

$$\Delta G^\circ = -RT \ln K_L \quad (6.10)$$

Where $R$ is the molar gas constant, 8.314 J mol$^{-1}$K$^{-1}$, T is the absolute temperature in Kelvin.

Equation 11 is obtained by substituting equation 6.9 into 6.10.

$$\ln K_L = -\frac{\Delta H^\circ}{RT} + \frac{\Delta S^\circ}{R} \quad (6.11)$$

The Gibbs free energy change ($\Delta G^O$) is directly calculated from equation 6.9, while the change in enthalpy ($\Delta H^o$) and the change in entropy ($\Delta S^o$) are determined from the slope and intercept of a plot of ln$K_L$ against 1/T (Figure 6.11). Thermodynamic parameter are presented in Table 6.6 below. The negative value of $\Delta G^O$ suggest that the adsorption of As(III) and As(V) was spontaneous. The positive value of $\Delta S^O$ suggests that As(III)/As(V) ions were randomly distributed on the surface of the adsorbent during adsorption process (Lin et al., 2017). The negative $\Delta H^O$ value indicates that the adsorption of As(III) and As(V) was exothermic reaction. This means the reaction for adsorption of As(III) and As(V) releases heat energy to its surroundings (Tran et al., 2016). Exothermic reactions involves both physiosoprtion and chemisorption adsorption processes. This indicates strong interaction between As(III)/As(V) and the adsorbent sites.

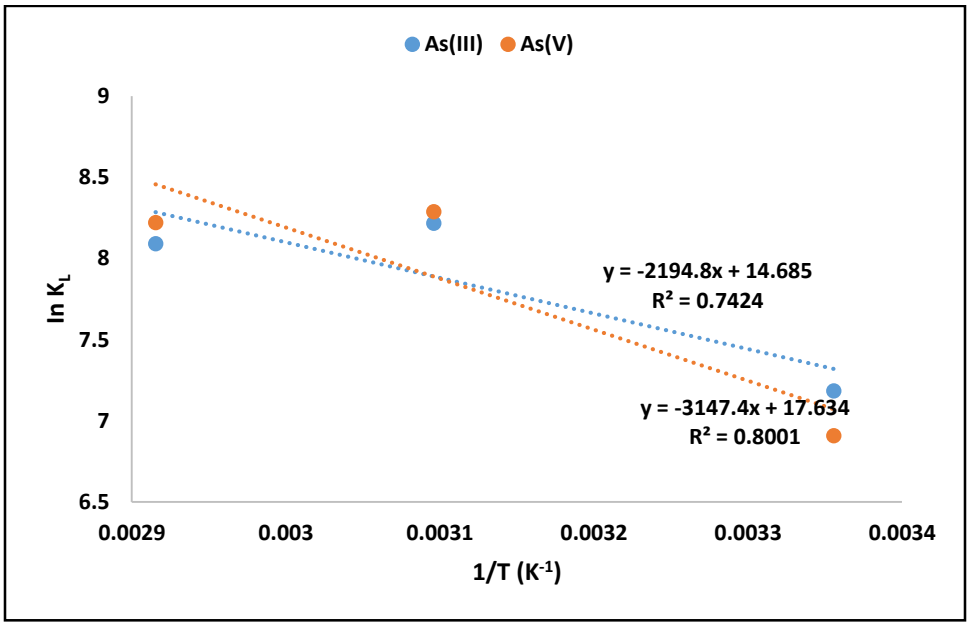


Figure 6.11: Values of ln $K_L$ as a function of reciprocal of adsorption temperature.

Table 6.6: Thermodynamic parameters

| | $\Delta G^O$ (KJ/mol) | $\Delta H^O$ (KJ/mol) | $\Delta S^O$ (kJ/mol×K) |
|---|---|---|---|
| As(III) | 298 K= -27.75<br>323 K= -32.85<br>343 K= -34.53 | -18.24 | 18.7 |
| As(V) | 298 K= -27.06<br>323 K= -33.04<br>343 K= -34.89 | -26.17 | 21.65 |

### 6.3.11 Effect of initial pH

The effect of pH on As(III) and As(V) adsorption is presented in Figure 6.12. It is observed that the removal of As(III) and As(V) was optimum at moderate pH range (pH= 4-8). However, the removal was negligible at extreme acidic and alkaline conditions. The behavior of As(III) and As(V) at various pH levels can be explained based on the arsenic speciation and also the overall surface charges of the adsorbent. The pH point of zero charge (pHpzc) of the SMK evaluated using titration was found to be ≈7.5. Therefore, below this pH the adsorbent is positively charged and above this pH the adsorbent is negatively charged. The speciation of As(III) carried out using Visual MINTEQ 3.1 version has revealed that at pH below 8, As(III) exist as neutrally charged $H_3AsO_3$ and beyond this pH the negatively charged species $H_2AsO_3^-$, $HAsO_3^{2-}$ and $AsO_3^{3-}$ dominate the solution. This findings corroborated with the observations reported by Lee et al. (2015). Low uptake of As(III) at lower pH where $H^+$ dominate the surface of the adsorbent could be attributed to suppressed deprotonating of neutrally charged $H_3AsO_3$ (Bhowmick et al., 2014). At moderate pH there is low charge density on the surface of the adsorbent which facilitate the Van der Waal attractive forces resulting in optimum uptake of As(III). Furthermore, at extreme alkaline pH levels both the surface and As(III) possess negative charges resulting in strong repulsive forces and consequently low As(III) uptake (Lee et al., 2015).

On the other hand, As(V) speciation revealed that at pH< 2, the neutral species $H_3AsO_4$ dominate the solution. Low uptake could be due to restricted interaction between the neutrally charged As(V) species and the positively charged adsorbent surface. As the solution pH increases the negatively charged species such as $H_2AsO_4^-$, $HAsO_4^{2-}$ and $AsO_4^{3-}$. The dominance of this species at pH below the pHpzc enhances the adsorption of As(V) through attraction to positively charged surface followed by ion exchange and also through inner sphere complexation (Tiwari et al., 2012). At pH

beyond the pHpzc, a decrease in As(V) could be attributed to repulsive forces between the abundant $OH^-$ on the surface and negatively charged As(V) species.

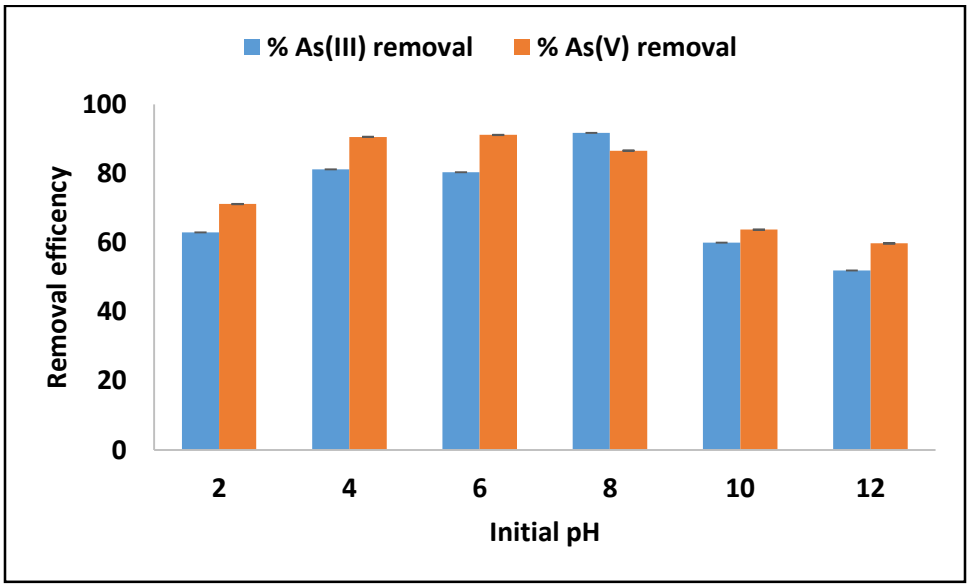


Figure 6.12: effect of pH onto As(III)/As(V) removal by SMK.

### 6.3.12 Effect of co-existing ions

Groundwater naturally contains co-existing ions that could affect the adsorption of As(III) and As(V). To evaluate the effect of co-existing ions, As(III) and As(V) adsorption experiment was conducted in the presence of 10 mg/L of $F^-$, $Cl^-$. $NO_3^-$, $CO_3^{2-}$, $SO_4^{2-}$, $Mg^{2+}$ and $Ca^{2+}$. The results are presented in Figure 6.13. It is evident that the presence of $F^-$, $Cl^-$, $NO_3^-$, $CO_3^{2-}$ and $SO_4^{2-}$ inhabits the percentage As(III) and As(V) removal. This suggests that these anions compete with arsenic species leading to its reduced percentage of removal. Conversely, the presence of $Mg^{2+}$ and $Ca^{2+}$ increased the percentage of As(III) and As(V) removal. The percentage As(III) removal increased from 81.2% to 98% and 93.8% while that of As(V) increased from 86.6% to 98.2% and94.8% respectively in the presence of $Mg^{2+}$ and $Ca^{2+}$. Similar results were reported by Qi et al. (2015) during the adsorption of As(III) and As(V) onto Fe-Mn binary oxide impregnated chitosan beads who cited that $Mg^{2+}$ and $Ca^{2+}$ enhances the positive charges and create more active sites on the surface of the adsorbent leading to higher sorption of As(III) and As(V) via attraction.

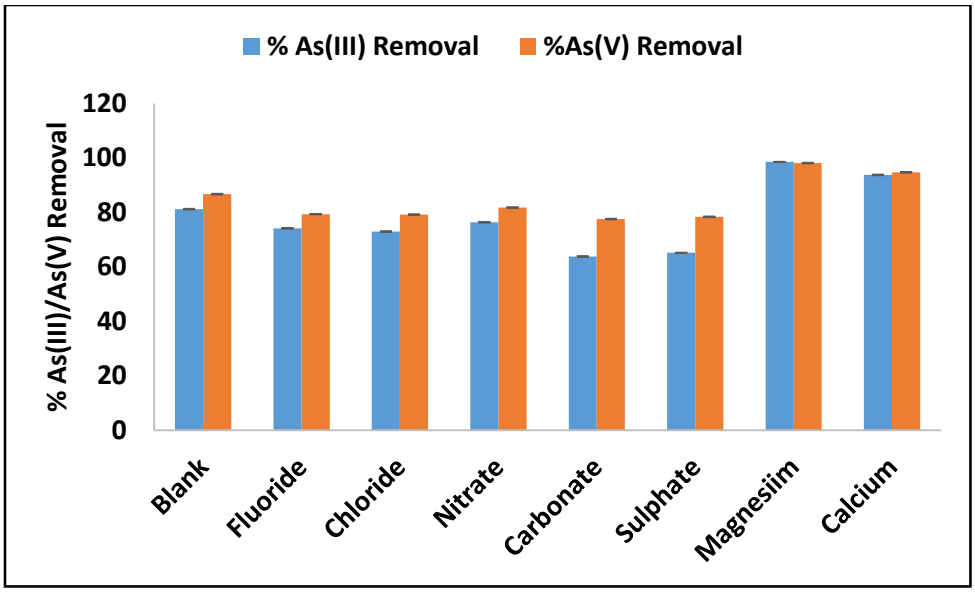


Figure 6.13: Effect of co-existing ions during the adsorption of As(III) and As(V) by SMK.

**6.4 Desorption As-loaded surfactant modified kaolin clay**

Desorption experiments were conducted to evaluate the stability of As(III)/As(V) loaded onto the SMK. $Na_2CO_3$, $NaNO_3$, KCl, $K_2SO_4$ were used as desorbing reagents and the results are presented in Figure 6.14a. It is observed that $Na_2CO_3$ desorbed higher percent of As(III) and As(V) as compared to other desorbing agent. This results implies that $Na_2CO_3$ is the best candidate for regenerating the spent sorbent since it has higher potential to leach out adsorbed arsenic oxyanions from the adsorbent. In order to see the effect of concentration in desorption of As(III)/As(V), solutions containing 0.01 M, 0.1 M and 1.0 M of $Na_2CO_3$ were prepared and used as desorbing agent. The results are presented in Figure 14b. It is observed that increasing concentration from 0.01 M to 1 M increases the percentage desorption of As(III)/As(V) from the adsorbent. This could be due to increasing concentration of $CO_3^{2-}$ which interact more with positively charged surface of the adsorbent leading to desorption of adsorbed arsenic oxyanions. Slight difference is observed when 0.1 M and 1 M $Na_2CO_3$ were used. Therefore, 0.1 M $Na_2CO_3$ was used for sorbent regeneration.

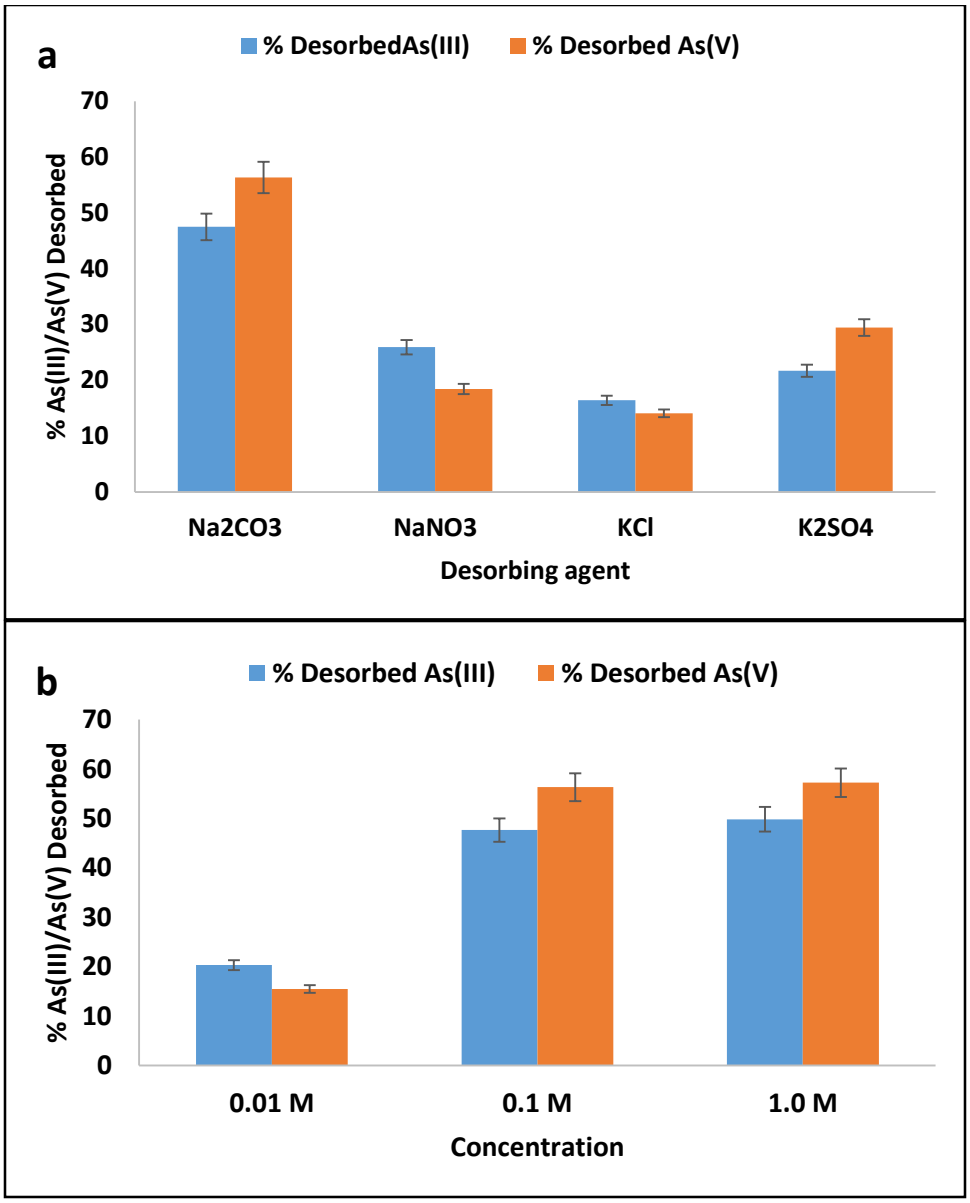


Figure 6.14: Desorption of As(III) and As(V) using different reagents (a) and Effect of $Na_2CO_3$ in desorption of As(III) and As(V) (b).

### 6.5 Regeneration and reuse of adsorbent

A sustainable and cost effective adsorbent for As(III)/As(V) removal from groundwater should be regenerated. To evaluate the regeneration potential of arsenic loaded SMK, five consecutive adsorption-desorption cycles were conducted using 0.1 M $Na_2CO_3$ as a regenerating agent. In Figure 15 it is observed that the As(III)/As(V) removal efficiency decreased with continuous regeneration from 95.8 and 97.6%, respectively achieved from the fresh sorbent to 54.1 and 62.3%, respectively at $5^{th}$ cycle of reuse. Sahu et al. (2016) observed the same trend for arsenic removal

using Ce-Fe bimetal metal oxides. The decrease in adsorption efficiency could be due to inadequate regeneration of the adsorbent's active sites. According to United States Environmental Protection Agency (U.S EPA) solids waste that leaches out arsenic concentration above 5 mg/L are considered to be hazardous (U. S EPA, 1992). In the present investigation, the total concentration leached from SMK after every cycle of regeneration was found to be below 0.5 mg/L. This suggest that disposing exhausted SMK into the environment may not lead to any environmental hazards.

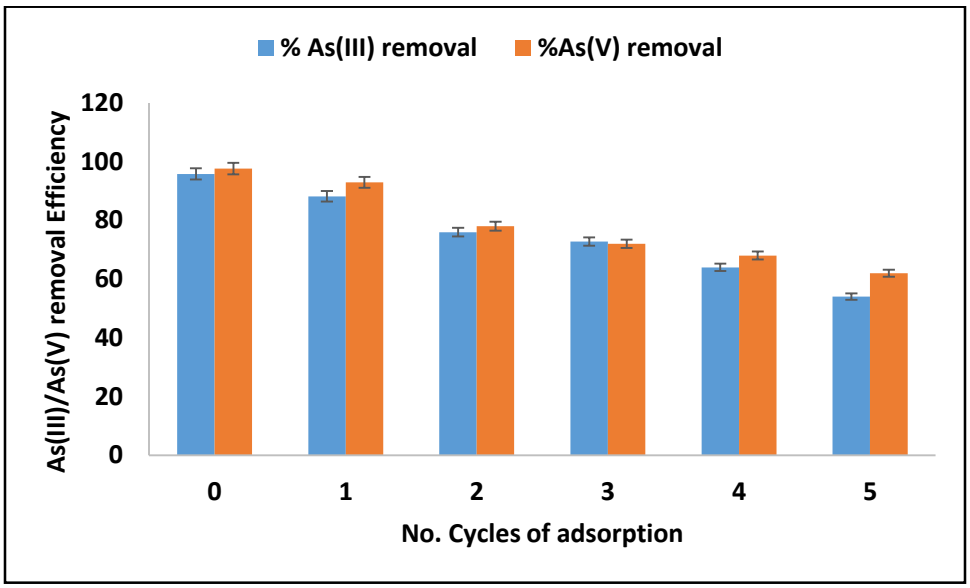


Figure 6.15: As(III) and As(V) percentage of removal by SMK as a function of regeneration cycle.

**6.6 Column experiment**

Column test were conducted to evaluate the practical applicability of SMK in the arsenic removal from groundwater. Groundwater with physicochemical properties in Table 6.7 was spiked with groundwater to get a total arsenic concentration of 0.5 and 1.5 mg/L. Figure 6.16 presents the breakthrough curves obtained at different initial concentration. It is observed that increasing concentration of feed water decreases the breakthrough point (i.e. the point at which the As concentration in the effluent is equivalent to 0.01 mg/L (WHO guideline value)). This could be attributed to increasing driving force as the concentration increases leading to faster saturation of the adsorbent sites. At initial concentration of 0.5 mg/L, the throughput volume was 875 mL when the breakthrough point was reached ($C_e/C_o$= 0.02). Conversely, at initial concentration of 1.5 mg/L the breakthrough point ($C_e/C_o$= 0.06) was reached when the throughput volume (200 mL). It is interesting to note that at breakthrough point the physicochemical properties of the field water was

improved (Table 6.7). The adsorbent exhaustion rate (AER) determined using equation 6.12 were found to be 5 g/L and 25 g/L for 0.5 mg/L and 1.5 mg/L, respectively.

$$AER = \frac{mass\ of\ the\ adsorbent\ (g)}{Breakthrough\ volume\ (L)} \quad (6.12)$$

The obtained results suggest that SMK produced in this study is a suitable adsorbent for arsenic removal from groundwater. In order to treat 20 L water containing arsenic concentration below 0.5 mg/L for a period of 6 month on a daily basis an estimate of 20.8 kg of SMK will be required. Based on the results presented here, SMK synthesized in this study can be used for treatment of arsenic contaminated water.

Table 6.7: Physicochemical composition of groundwater at breakthrough point

| **Parameter** | **Before treatment** | **Breakthrough point** | **WHO guideline (2017)** |
|---|---|---|---|
| pH | 8.7 | 6.98 | 5.0-9.7 |
| As Total | 0.5 | 0.01 | 0.01 |
| $F^-$ | 5.4 | 0.98 | 1.5 |
| $Cl^-$ | 31.59 | 22.1 | <300 |
| $SO_4^{2-}$ | 11.89 | 4.89 | <500 |
| $NO_3^-$ | 2.67 | ND | 50 |
| $PO_4^{3-}$ | 1.3 | ND | - |
| Mg | 8.98 | 8.12 | 200 |
| Na | 70.36 | 69.12 | 200 |
| Ca | 10.87 | 8.12 | 200 |

*ND=Not detected

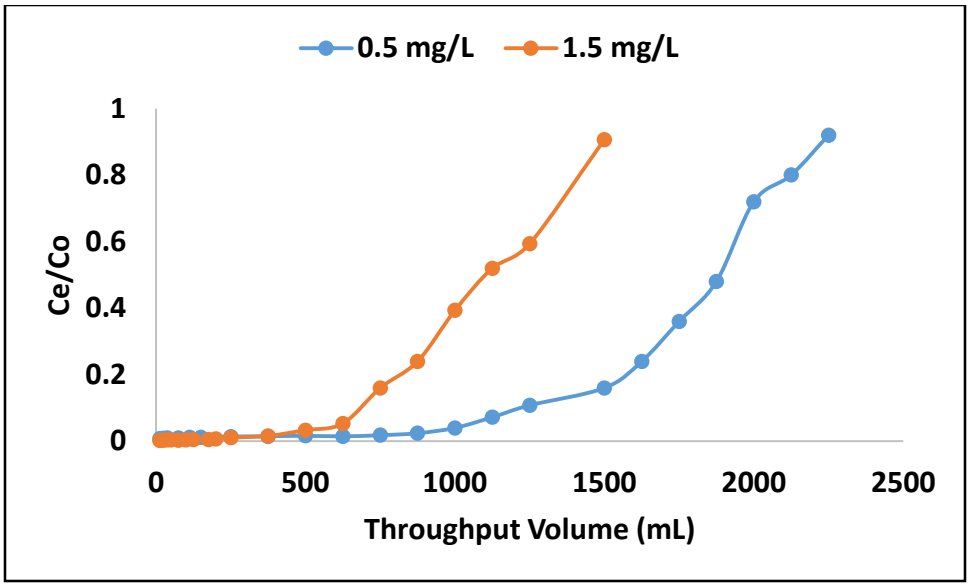


Figure 6.16: Breakthrough curves for arsenic removal from spiked groundwater by SMK.

### 6.7 Comparison with other adsorbents

In order to evaluate the competitiveness of SMK prepared in this study we compared the As(III) and As(V) adsorption capacity achieved in this study with the capacities reported in the literature. Table 6.8 shows the comparison with other adsorbent. From the table it is noticeable that SMK produced in this study is competitive over other adsorbent that have been reported in the literature and has a greater potential for use in arsenic removal.

Table 6.8: Comparison with other adsorbents.

| **Adsorbent** | **Experimental conditions** | **As(III) adsorption capacity (mg/g)** | **As(V) Adsorption capacity (mg/g)** | **Reference** |
|---|---|---|---|---|
| Al-HDTMA sericite | Concentration=1-20 mg/L, pH =4.5, adsorbent dosage = 0.2 5/100 mL | 0.33 | 0.85 | Tiwari et al., 2012 |
| Al-AMBA-sericite | Concentration=1-20 mg/L, pH =4.5, adsorbent dosage = 0.2 5/100 mL | 0.43 | 0.51 | Tiwari et al., 2012 |
| Surfactant modified bentonite | Concentration =0.2-60 mg/L; pH = 8.63 ; Adsorbent dosage, 1 g/100 mL | 0.102 | 0.288 | Su et al., 2011 |
| Activated carbon-alumina composite | Concentration = 10-300 mg/L; pH = 3, adsorbent dosage= 2 g/L | 14.28 | 23.80 | Karmacharya et al., 2016 |
| Tire rubber alumna composite | Concentration = 10-300 mg/L; pH = 3; adsorbent dosage = 2 g/L | 13.51 | 19.60 | Karmacharya et al., 2016 |
| HDTMA-Al-bentonite | Concentration= 2-18 mg/L; pH= 4.5; adsorbent dosage; 0.1 g/50 mL | 2.47 | 8.93 | Lee et al., 2015 |
| HDTMA-Local-clay | Concentration= 2-18 mg/L; pH= 4.5; adsorbent dosage; 0.1 g/50 mL | 2.18 | 4.1 | Lee et al., 2015 |
| HDTMA modified kaolin (SMK) | Concentration= 1-30 mg/L; pH =6±0.5; adsorbent dosage = 0.4 g/100 mL | 2.3 | 2.88 | Present study |

## 6.8 Summary

In the present study, natural kaolin clay mineral was successfully modified through intercalation of HDTMA-Br surfactant onto the interlayers. The results from BET surface area showed that the modification of clay by HDTMA-Br reduced the total surface area from 18.61 to 3.39 $m^2/g$ and

the pore diameter increased from 9.53 to 20.41 nm. The synthesized adsorbent showed a maximum As(III) and As(V) adsorption capacities of 2.3 and 2.88 mg/g, respectively. The adsorption kinetics data for As(III) was described through PSO model while the data for As(V) was described by PFO model indicating that adsorption of As(III) was through chemisorption while the adsorption of As(V) was through physiosorption. Furthermore, the isotherm data for both As(III) and As(V) was best described by the Langmuir adsorption model indicating that adsorption occurred on a monolayered surface. Adsorption thermodynamics models revealed that during adsorption process As(III) and As(V) ions were distributed randomly and adsorption process was spontaneous and exothermic. The presence of anions such as $F^-$, $Cl^-$, $NO_3^-$, $SO_4^{2-}$ and $CO_3^{2-}$ decreased the adsorption efficiency while the presence of $Ca^{2+}$ and $Mg^{2+}$ increased the adsorption efficiency. The regeneration study revealed that SMK synthesized in this study can be used for up to 5 adsorption-desorption cycles. The results obtained from this present investigation showed that SMK is promising adsorbent for arsenic removal from groundwater.

## References

Arcibar-Orozco, J. A., Jouse, D. B., Rios-Hurtado, J. C. & Rangel-Mandez, J. R., 2014. Influence of iron content, surface area and charge distribution in the arsenic removal by activated carbons. *Chemical Engineering Journal,* 249, pp. 201-209.

Bardach, A. E., Ciapponi, A., Soto, N., Chaparro, M. R., Calderon, M., Briatore, A., Cadoppi, N., Tassara, R. & Litter, M. I., 2015. Epidemiology of chronic disease related to arsenic in Argentina: A systematic review. *Science of Total Environment,* 538, pp. 802-816.

Bentahar, Y., Hurel, C., Draoui, K., Khairoun, S. & Marmier, N., 2016. Adsorptive properties of Moroccan clays for the removal of arsenic(V) from aqueous solution. *Applied Clay Science,* 119, pp. 385-392.

Bhowmick, S., Chakraborty, S., Mondal, P., Renterghm, M.V., Berghe, S.V., Roman-Ross, G., Chatterjee, D. & Iglesias, M., 2014. Montmorillonite-supported nanoscale zero-valent iron for removal of arsenic from aqueous solution: Kinetics and mechanism. *Chemical Engineering Journal*, 243, pp. 14-23.

Bretzler, A., Lalanne, F., Nikiema, J., Podgorski, J., Pfenninger, N., Berg, M. & Schirmerm, M., 2017. Groundwater arsenic contamination in Burkina Faso, West Africa: Predicting and verifying regions at risk. *Science of Total Environment,* 584-585, pp. 958-970.

Choong, T.S.Y., Chuah, T.G., Robiah, T., Koay, F.L.G. & Azni, I., 2007. Arsenic toxicity, health hazards and removal techniques from water: an overview. *Desalination,* 217, pp. 193-166.

Chutia, P., Kato, S., Kojima, T., Satokawa, S., (2009) Adsorption of As(V) on surfactant-modified natural zeolites. *Journal of Hazardous Materials,* 162, pp. 204-211.

Cui, J., Jing, C., Che, D., Zhang, J. & Duan, S., 2015. Groundwater arsenic removal by coagulation using ferric(III) sulfate and polyferric sulfate: A comparative and mechanistic study. *Journal of Environmental Sciences,* 32, pp. 42-53.

Duker, A. A., Carranza, E. J. M. & Hale, M., 2005. Arsenic geochemistry and health. *Environment International,* 31, pp. 631-641.

Fatoki, O. S, Akinsoji, O. S., Ximba, B. J., Olujimi, O., Ayanda, O. S., 2013. Arsenic contamination: Africa the missing gap. *Asian Journal of Chemistry,* 52(16), pp. 9263-9268.

Firdaous, L., Fertin, B., Khelissa, O., Dhainaut, M., Nedjar, N., Chataigne, G., Ouhoud, L., Lutin, F., Dhulster, P., 2017. Adsorptive removal of polyphenols from an alfalfa white proteins concentrate: Adsorbent screening, adsorption kinetics and equilibrium study. *Separation and Purification Technology,* 178, pp. 29-39.

Gitari, W. M., Izuagie, A. A. & Gumbo, J. R., 2017. Synthesis, characterization and batch assessment of groundwater fluoride removal capacity of trimetal Mg/Ce/Mn oxide-modified diatomaceous earth. *Arabian Journal of Chemistry*. In press.

Gupta, S. S., Bhattachryya, K. G., 2011. Kinetics of adsorption of metal ions on inorganic materials: A review. *Advanced in Colloid and Interface Science,* 162, pp. 39-58.

Ho, Y. S., 2004. Citation review of Lagergren kinetic rate equation on adsorption reactions. *Scientometrics,* 59(1), pp. 171-177.

Ho, Y. S., Wase, D. A. J. & Forster, C. F., 1996. Kinetic studies of competitive heavy metal adsorption by sphagnum moss peat. *Environmental Technology,* 17 (1), pp. 71-77.

Kang, M., Kawasaki, M., Tamada, S., Kamei, T., Magara, Y., 2000. Effects of pH on the removal of arsenic and antimony using reverse osmosis membranes. *Desalination,* 131, pp. 293-298.

Karmacharya, M. S., Gupta, V. K., Tyagi, I., Agarwal, S., Jha, V. K., 2016. Removal of As(III) and As(V) using rubber tire derived activated carbon modified with alumina composite. *Journal of Molecular Liquids,* 216, pp. 836-844.

Kempster, P. L., Silberbauer, M., Kuhn, A., 2007. Interpretation of drinking water quality guidelines- The case of arsenic. *Water SA,* 33(1), pp. 95-100.

Lee, S. M., Lalmunsama, Thanhimngliana, Tiwari, D., 2015. Porous hybrid materials in the remediation of water contaminated with As(III) and As(V). *Chemical Engineering Journal,* 270, pp. 496-507.

Lin, L., Qiu, W., Wang, D., Huang, Q., Song, Z. & Chau, H. W., 2017. Arsenic removal in aqueous solution by a novel Fe-Mn modified biochar composite: Characterization and mechanism. *Ecotoxicology and Environmental Safety,* 144, pp. 514-521.

Lonappan, L., Rouissi, T., Brar, S. K., Verma, M., Suramphalli, R. Y., 2018. An insight into the adsorption of diclofenac on different biochars: Mechanisms, surface chemistry, and thermodynamics. *Bioresource Technology,* 249, pp. 386-394.

Pakzadeh, B. & Batista, J. R., 2011. Surface complexation modeling of the removal of arsenic from ion-exchange waste brines with ferric chloride. *Journal of Hazardous Material,* 188, pp. 399-407.

Qi, J., Zhang, G., Li, H., 2015. Efficient removal of arsenic from water using a granular adsorbent: Fe–Mn binary oxide impregnated chitosan bead. *Bioresource Technology,* 193, pp. 243-249.

Reeve, P.J., Fallowfield, H.J., 2018. Natural and surfactant modified zeolites: A review of their applications for water remediation with a focus on surfactant desorption and toxicity towards microorganisms. *Journal of Environmental Management,* 205, pp. 253-261.

Ren, X., Zhang, Z., Lou, H., Hu, B., Dang, Z., Yang, C., Li, L., 2014. Adsorption of arsenic on modified montmorillonite. *Applied Clay Science,* 97-98, pp. 17-23.

Sahu, U. K., Sahu, M. K., Mohapatra, S. S., Patel, R. K., 2016. Removal of As(V) from aqueous solution by Ce-Fe bimetal mixed oxide. *Journal of Environmental Chemical Engineering,* 4, pp. 2892-2899.

Saikia, R., Goswami, R., Bordoloi, N., Senapati, K. K., Pant, K. K., Kumar, M., Kataki, R., 2017. Removal of arsenic and fluoride from aqueous solution by biomass based activated biochar: Optimization through response surface methodology. *Journal of Environmental Chemical Engineering,* 5, pp. 5528-5539.

Sarkar, A. & Paul, B., 2016. The global menace of arsenic and its conventional remediation – A critical review. *Chemosphere,* 158, pp. 37-49.

Smedley, P.L. & Kinniburgh, D.G., (2002) A review of the source, behaviour and distribution of arsenic in natural waters. *Applied Geochemisty*, 17, pp. 517-568.

Smith, A. H., Biggs, M. L., Moore, L., Haque, R., Steinmaus, C., Chung, J., Hernandez, A. & Lopipero P., 1999. Cancer risks from arsenic in drinking water: Implications for drinking water standards. In W.R. Chappell, C.O. Abernathy and Calderno (eds) Arsenic exposure and human effects. Elsevier Science, pp. 191-199.

Smith, A. H. & Smith M. M. H., (2004) Arsenic drinking water regulations in developing countries with extensive exposure. *Toxicology,* 198, pp. 39-44.

Su, J., Huang, H. G., Jin, X. Y., Lu, X. Q., Chen, Z. L., 2011. Synthesis, characterization and kinetic of a surfactant-modified bentonite used to remove As(III) and As(V) from aqueous solution. *Journal of Hazardous Materials,* 185, pp. 63-70.

Sun, K., Shi, Y., Chen, H., Wang, X. & Li, Z., 2017. Extending surfactant-modified 2:1 clay minerals for the uptake and removal of diclofenac from water. *Journal of Hazardous Materials*, 323A, pp. 567-574.

Tiwari, D., Lee, S. M., 2012. Novel hybrid materials in the remediation of ground waters contaminated with As(III) and As(V). *Chemical Engineering Journal,* 204-206, pp. 23-31.

Tran, H. N., You, S. J., Chao, H. P., 2016. Thermodynamic parameters of cadmium adsorption onto orange peel calculated from various methods: A comparison study. *Journal of Environmental Chemical Engineering,* 4, pp. 2671-2682.

Tran, H. N., You, S. J., Hosseini-Bandegharaei, A., Chao, H. P., 2017. Mistakes and inconsistencies regarding adsorption of contaminants from aqueous solutions: A critical review. *Water Research,* 120, pp. 88-116.

US Environmental Protection Agency. 1992. Tittle: 40 Codes of Regulations, , Washington, DC, (Part 261, 31).

Wang, J., Wang, T., Burken, J. G., Chusuei, C. C., Ban, H., Ladwig, K., Huang, C. P., (2008) Adsorption of arsenic (V) onto fly ash: A speciation-based approach. *Chemosphere*, 72, pp. 381-388.

Weber, W. J., Morris, J. C., 1963. Kinetics of adsorption on carbon from solution. *Journal of Sanitary Engineering Division*, 89 (2), pp. 31-60.

World Health Organization, 2017. Guidelines for Drinking-water Quality, 4th eds. Geneva: Switzerland.

Zhu, L., Zhu, R., 2007. Simultaneous sorption of organic compounds and phosphate to inorganic–organic bentonite from water. *Separation and Purification Technology,* 54, pp. 71-76.

# Chapter 7: Adsorption of As(III) and As(V) using inorgano-organo modified kaolin clay mineral: Batch and column studies


## 7 Abstract

In this chapter, inorgano-organo modified kaolin clay mineral was successfully synthesized through intercalation of $Fe^{3+}$ and $Mn^{2+}$ oxides and HDTMA-Br surfactant onto the interlayers of the clay mineral. The applicability of the clay in arsenic removal was assessed using batch and column experiments. The batch experiments showed that As(III) removal was optimum at the pH range of 4-6, while the As(V) removal was optimum at pH range 4-8. The adsorption data for both species of arsenic fitted better to pseudo second order of reaction kinetics which suggest that the dominant mechanism of adsorption was chemisorption. The intra-particle diffusion model showed bilinear plot which suggest that the adsorption of As(III) and As(V) is a complex process involving film diffusion and intra-particle diffusion. The isotherm studies showed that the data fitted better to Langmuir isotherm model indicating that adsorption of both As(III) and As(V) occurred on a monolayered surface. The maximum adsorption of As(III) and As(V) capacities at room temperature as determined by Langmuir model were found to be 7.99 mg/g and 7.32 mg/g, respectively. The thermodynamic studies for sorption of As(III) and As(V) showed that values of $\Delta G^O$ and $\Delta H^O$ were negative indicating that adsorption process occurred spontaneously and is exothermic in nature. The effect of co-existing ions showed that the adsorption of As(III) and As(V) is enhanced by the presence of $Mg^{2+}$ and $Ca^{2+}$ and is inhibited by the presence of $F^-$, $Cl^-$, $NO_3^-$, $CO_3^{2-}$ and $SO_4^{2-}$. The regeneration study showed that the inorgano-organo modified kaolin clay mineral can be reused for up 7 adsorption-regeneration cycles using 0.01 M HCl as a regenerant. The column data showed that the breakthrough point occurs after treating 1380 mL and 1500 mL volumes of water containing both As(III) and As(V), respectively. This was achieved after treating water containing 0.5 mg/L As(III) and As(V) concentration using the bed mass of 5 g and flow rate of 1.5 mL/min. Thomas kinetic model and Yoon-Nelson model showed that the rate of adsorption increases with increasing flow rate and initial concentration and decreases with increasing the bed mass. In comparison with other adsorbents, inorgano-organo modified kaolin clay mineral proved to be superior over other clay based adsorbents in the literature.


Keywords: Adsorption kinetics; arsenic; batch experiments; column experiments; kaolin clay mineral; inorgano-organo modified clay.

## 7.1 Introduction

Clays and their minerals are known for their important role in the environment of acting as natural scavenger of pollutants through ion exchange and adsorption processes. Their physicochemical properties such as larger specific surface area, higher cation exchange capacity, chemical and mechanical stability and layered structure have made them to be excellent adsorbent material (Bhattacharyya and Gupta, 2008). Furthermore, clay can be modified using inorganic polycations with higher charge density and cationic surfactants to enhance their adsorption capacity (Tiwari and Lee, 2012). In chapter 5 and 6, locally available kaolin mineral was successfully modified using Fe-Mn bimetal oxide and HDTMA-Br cationic surfactant and applied in As(III) and As(V) removal from groundwater. The modified kaolin clay mineral showed an improved adsorption capacity as compared to the raw kaolin clay mineral reported in Chapter 4. To be precise: the raw kaolin clay mineral showed a maximum As(III) and As(V) adsorption capacities of 1.12 and 1.08 mg/g, respectively, Fe-Mn bimetal modified kaolin clay mineral showed maximum As(III) and As(V) adsorption capacities of 2.16 and 1.56 mg/g, respectively and HDTMA modified kaolin mineral showed maximum As(III) and As(V) adsorption capacities of 2.3 and 2.88 mg/g, respectively.

Based on Chapter 5 and 6 findings, modification of clay mineral with inorganic poly-cations enhances the sorption of As(III) while surfactant modification enhances As(V) sorption. In the recent years, synthesis of inorgano-organo clay mineral has received greater attention from researchers due to their important features such as, possession of two sorption sites which in turn enhances the sorption capacity and also good settling property (Tiwari and Lee, 2012). Furthermore, inorgano-organo modified clay minerals have shown higher sorption capacity for both As(III) and As(V) species (Ren et al., 2014 and Hua, 2015). Therefore, this chapter aims at fabricating a composite adsorbent which is consist of inorgano-organo modified kaolin clay mineral and to further evaluate its adsorption capacity towards simultaneous removal of As(III) and As(V). Characterization techniques such as BET, SEM, XRF, XRD and FTIR were employed to evaluate the physicochemical and mineralogical composition of the inorgano-organo adsorbent fabricated. The As(III) and As(V) removal efficiency of the adsorbent was tested using batch and column experiments. Lastly, the adsorption kinetics, isotherms and thermodynamics models were applied to elucidate the adsorption mechanisms.

## 7.2 Material and Methods

### 7.2.1 Materials

Raw kaolin clay (RK) was collected from Dzamba Village in Limpopo Province, South Africa. $FeCl_3$, $MnCl_2.4H_2O$, NaOH, $AsNaO_2$ and $HAsNa_2O_4$ were purchased from Rochelle Chemicals & Lab Equipment CC, South Africa Ltd. Hexadecyltriammonium bromide (HDTMA-Br) was purchased from Merck chemicals, South Africa. All chemicals were of analytical grade and they were used without further purification.

### 7.2.2 Synthesis of inorgano-organo clay

Inorgano-organo modified kaolin clay (IOK) was synthesized as follows: 0.25 M $Fe^{3+}$ and 0.25 M $Mn^{2+}$ were prepared by dissolving a known amounts of $FeCl_3$ and $MnCl_2.4H_2O$ into 250 mL volumetric flasks. Extracts of 0.25 M $Fe^{3+}$ and 0.25 M $Mn^{2+}$ were mixed at a volume ratio of 3:1 in a 250 mL plastic bottle and 1 g of kaolin clay mineral was added and soaked for 10 min. Thereafter, pH of the solution was adjusted to 8.5 by adding 10 mL of 2 M NaOH drop wise into each of the bottles to precipitate $Fe^{3+}$ and $Mn^{2+}$ into their respective oxides. Thereafter, 100 mL of 5 mM HDTMA-Br was added to the mixture and agitated for 60 min at 250 rpm and then aged for 62 hours. The mixture was then centrifuged at 3000 rpm. Residues were washed with Milli-Q water to remove excess supernatants and then oven dried for 12 hours at 60 $^{O}$C. The modified clay was then milled to pass through 250 µm sieve and then stored in a zip lock plastic bag.

### 7.2.3 Characterization of the material

X-ray diffraction (XRD) and X-ray fluorescence (XRF) techniques were employed to examine the mineralogical and elemental composition of the clay, respectively. Infra-red spectrum of the material were obtained using Fourier Transform Infra-red spectrum equipped with ATR-Diamond (Bruker, Germany). Morphological characteristics were determined using scanning electron microscopy (SEM) (Leo1450 SEM, voltage 10 kV, working distance 14 mm). The pore size distribution, pore volume, and pore diameter were determined by Barrett Joyner Halenda (BJH) sorption model using a specific surface area analyzer (Autosorb-iQ & Quadrasorb SI, USA). Nitrogen adsorption-desorption isotherms were used to determine specific surface area of the adsorbent according to Brunauer Emmett Teller (BET) model.

### 7.2.4 Batch experiments

Stock solution containing 1 000 mg/L As(III) and As(V) was prepared by dissolving an appropriate amounts of $AsNaO_2$ and $HAsNa_2O_4$ in Milli-Q water (18.2 MΩ/cm). The working solutions were prepared through appropriate dilutions from the stock solution. To evaluate the optimum contact time and the adsorption kinetics, the contact time was varied from 10 to 120 min. Adsorbent dosage of 0.1 g/100 mL and adsorbate concentration of 0.5 mg/L were maintained. After agitation the residual As(III)/As(V) concentration were determined using gold wire electrode attached 884 professional VA (Metrohom, SA). To evaluate the adsorbate concentration and adsorption isotherms, the initial concentration of As(III)/As(V) was varied from 0.5 to 30 mg/L and the adsorbent dosage of 0.1 g/100 mL, contact time of 60 min were maintained. The experiment was conducted at a temperature of 298, 323 and 343 K. The obtained data was used to evaluate the adsorption thermodynamics. The effect of initial pH was evaluated at initial adsorbate concentration of 0.5 mg/L, contact time of 60 min and adsorbent dosage of 0.1 g/100 mL. The initial pH was adjusted from 2-12 using 0.01 M NaOH and 0.01 M HCl. The influence of co-existing ions ($F^-$, $Cl^-$, $NO_3^-$, $CO_3^{2-}$, $SO_4^{2-}$, $Mg^{2+}$ and $Ca^{2+}$) was evaluated at the initial concentration As(III)/As(V) concentration of 0.5 mg/L, adsorbent dosage of 0.1 g/100 mL and 60 min contact time. The initial concentration of each co-existing ion was 5 mg/L. All experiments were conducted in triplicate and the mean values were reported. Unless otherwise stated, experiments were conducted at room temperature and initial pH of 6 ± 0.5.

### 7.3.5 Column experiments

The laboratory scale fixed bed column experiments were carried out to evaluate the performance of inorganic-organo modified kaolin clay mineral towards the removal of As(III) and As(V) from the solution. A plastic column with the internal diameter of 2.5 cm and a total length of 13.5 cm was used for column adsorption experiments. The adsorbent in the column bed was fused within the glass wool supported by the glass beads as shown in Figure 7.1. The influent solution containing a known concentration of As(III) and As(V) was pumped in an upward mode using a Gilson peristaltic pump to avoid channeling inside the column. The parameters evaluated includes effect of flow rate, adsorbent bed mass and initial concentration. To evaluate the effect of flow rate, influent solution containing 1 mg/L of As(III) and As(V) and the bed mass of 5 g were used. The flow rates of 1.5 and 2 mL/min were used. For the effect of bed mass, known concentration of 1 mg/L of both As(III) and As(V) was used and the flow rate of 1.5 mL/min was maintained

while the bed masses of 2 g and 5 g were used. To evaluate the effect of influent concentration, the bed mass of 5 g and flow rate of 1.5 mL/min were maintained while the initial concentrations of 0.5 and 1 mg/L were used. The performance of the fixed bed column was expressed through the theory of breakthrough curves which gives of clear indication of breakthrough point (the point at which the As(III)/As(V) concentration is exceed 10 µg/L).

q

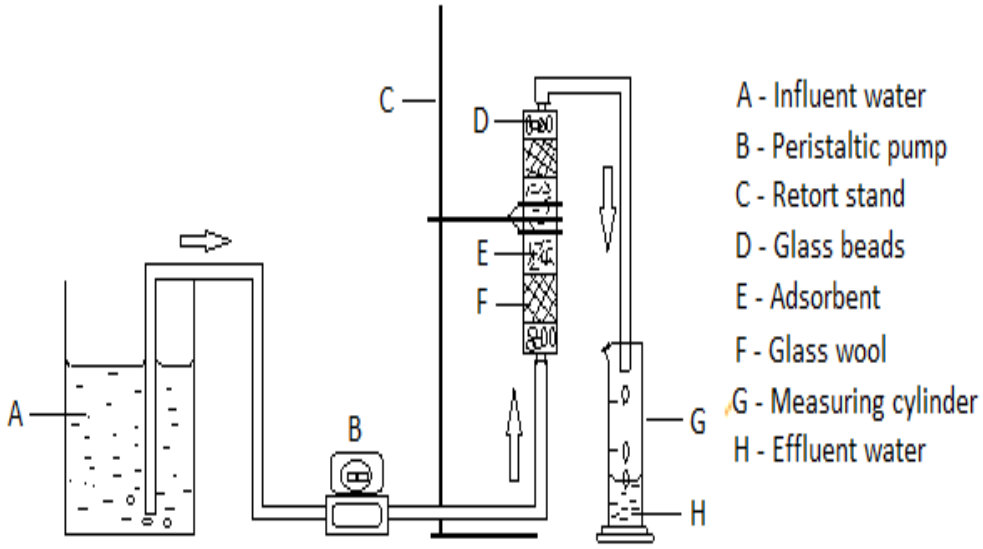


Figure 7.1: Experimental set-up for column experiments.

### 7.2.6 Adsorbent regeneration-reuse cycles

To evaluate the regeneration and reuse potential of the adsorbent: As(III)/As(V) removal experiment was conducted by treating solution containing 0.5 mg/L As(III)/As(V) with 1.0 g of IOK at initial pH of 6 for 60 min. After agitation, mixtures were filtered through 0.45 µm filter membranes and the residuals of As(III) and As(V) were analysed. Residues were washed with Milli-Q water and oven dried for 12 hours at 60 $^{O}$C and then residues were regenerated using 100 mL of 0.01 M HCl by agitating the mixture for 60 min. The obtained residues were rinsed with excess of Milli-Q water and then oven dried for 12 hours at 60 $^{O}$C and then pulverized with a mortar and pestle to pass through 250 µm sieve. After regeneration the As(III)/As(V) experiment was conducted as in other experiments. The regeneration-reuse cycle were continued up to 7$^{th}$ cycle.

### 7.2.7 Analysis of residual arsenic

The residual As(III)/As(V) concentration was measured using ScTRACE Gold electrode attached to 884 professional VA Polarography (Metrohm, SA). A composite solution containing 1 mol/L sulfamic acid, 0.5 mol/L citric acid and 0.45 mol/L KCl was used an electrolyte. For total As concentration, $KMnO_4$ was added as an oxidizing agent. For quality control, samples were also analyzed using metrohm 850 professional ion chromatography (Switzerland) for As(III) and As(V) concentration. Metrosep A Supp 5-150 column was used for separation and the guard column Metrosep A 4/5 was used. The eluent containing 15 mmol/L NaOH and 2.0 mmol/L $Na_2CO_3$ was used as the mobile phase. The concentration of As(III) was determined without suppression. The conductivity detector was used to estimate the concentration of different chemical species. Some samples were further analyzed using ICP-MS.

## 7.3 Results and Discussion

### 7.3.1 Physicochemical Characterization

#### 7.3.1.1 Elemental composition

Table 7.1 present a comparison of the elemental composition between the RK and IOK. It is observed that $SiO_2$, $Al_2O_3$ are the major oxides the kaolin clay mineral. After modification the contents of $SiO_2$ and $Al_2O_3$ decreased from 57.1 and 22.05% to 32.29 and 8.75%, respectively. Conversely, $Fe_2O_3$ and MnO increased from 3.88 and 0.02 to 9.31 and 1.23, respectively.

Table 7.1: Elemental composition of RK and IOK.

| **Oxides** | **RK (%w/w)** | **IOK (%w/w)** |
|---|---|---|
| $SiO_2$ | 57.1 | 32.29 |
| $Al_2O_3$ | 22.05 | 8.74 |
| $Fe_2O_3$ | 3.88 | 9.31 |
| MgO | 0.57 | 0.74 |
| MnO | 0.02 | 1.23 |
| CaO | 0.95 | 0.21 |
| $K_2O$ | 0.16 | 0.08 |
| $TiO_2$ | 1.76 | 0.82 |
| $P_2O_5$ | 0.02 | 0.012 |

### 7.3.1.2 Mineralogical composition

Figure 7.2 shows the XRD spectra of RK and IOK. Both spectrums showed the presence of kaolin and quartz as the dominant minerals in the clay. The intensity of the peaks increased after introduction of $Fe^{3+}$ and $Mn^{2+}$ oxides and HDTMA-Br cationic surfactant into the clay interlayers. This indicates that these ions were successfully intercalated onto the clay interlayers.

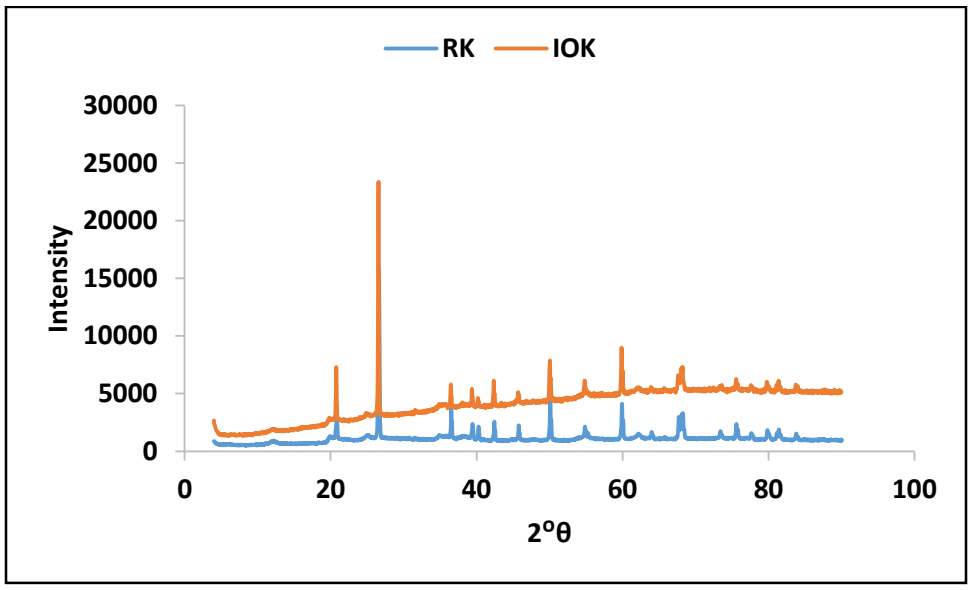


Figure 7.2: XRD pattern of RK and IOK.

### 7.3.1.3 FTIR analysis

Figure 7.3 presents the FTIR spectrum of RK, IOK and IOK after arsenic removal. The bands at 3453 and 1645 $cm^{-1}$ are ascribed to the vibration and stretching of hydroxyl groups and water molecules within the clay interlayers. The prominent IR peaks at wavelength region of 1030 $cm^{-1}$ could be due to the vibration of Si-O bonds. The bands at 906, 790 and 540 cm-1 could be due to the vibration of Al-O, Mn-O and Fe-O, respectively. After modification by new bands were observed at 2930 and 2846 cm-1 indicating the presence of $–CH_2$ bonds which confirm the introduction of HDTMA within the clay interlayers (Thanhumingliana and Tiwari et al., 2015). Furthermore, the intensity of bands at 1030, 906, 790 and 540 $cm^{-1}$ increased. This could be attributed to increased concentration of $Fe_2O_3$ and MnO contents as confirmed by XRF analysis. After arsenic removal a new band was observed at 778 $cm^{-1}$ which could be ascribed to As-O bond. The intensity of bands at other wavelength ranges decreased after arsenic removal. This confirms the ion exchange between the hydroxyl groups in the clay interlayers and arsenic species and

surface complexation between arsenic and Fe, Mn, Al and other metals in the surface of the clay minerals.

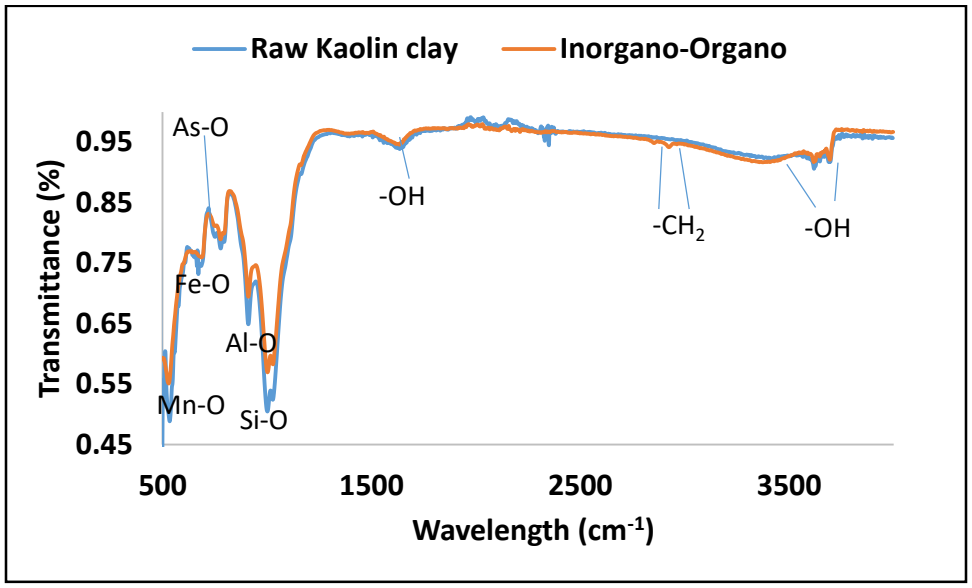


Figure 7.3: FTIR spectrum of raw kaolin (RK), inorgano-organo modified kaolin clay mineral (IOK) before and after arsenic adsorption.

### 7.3.1.4 Morphological analysis

Figure 7.4 presents the SEM micrographs of RK and IOK. No significant difference observed in the raw and modified kaolin clay mineral. The raw kaolin clay mineral has spongy like rough and porous surface with some irregular shapes. After modification, micrographs shows larger pores. This could be attributed to swelling and expansion of the clay interlayers during modification. The SEM-EDS spectrums of RK shows the presence of Fe, Al, Si, Mg, Ti, K Ca and C. The spectrum of IOK showed a new peak showing Mn was observed.

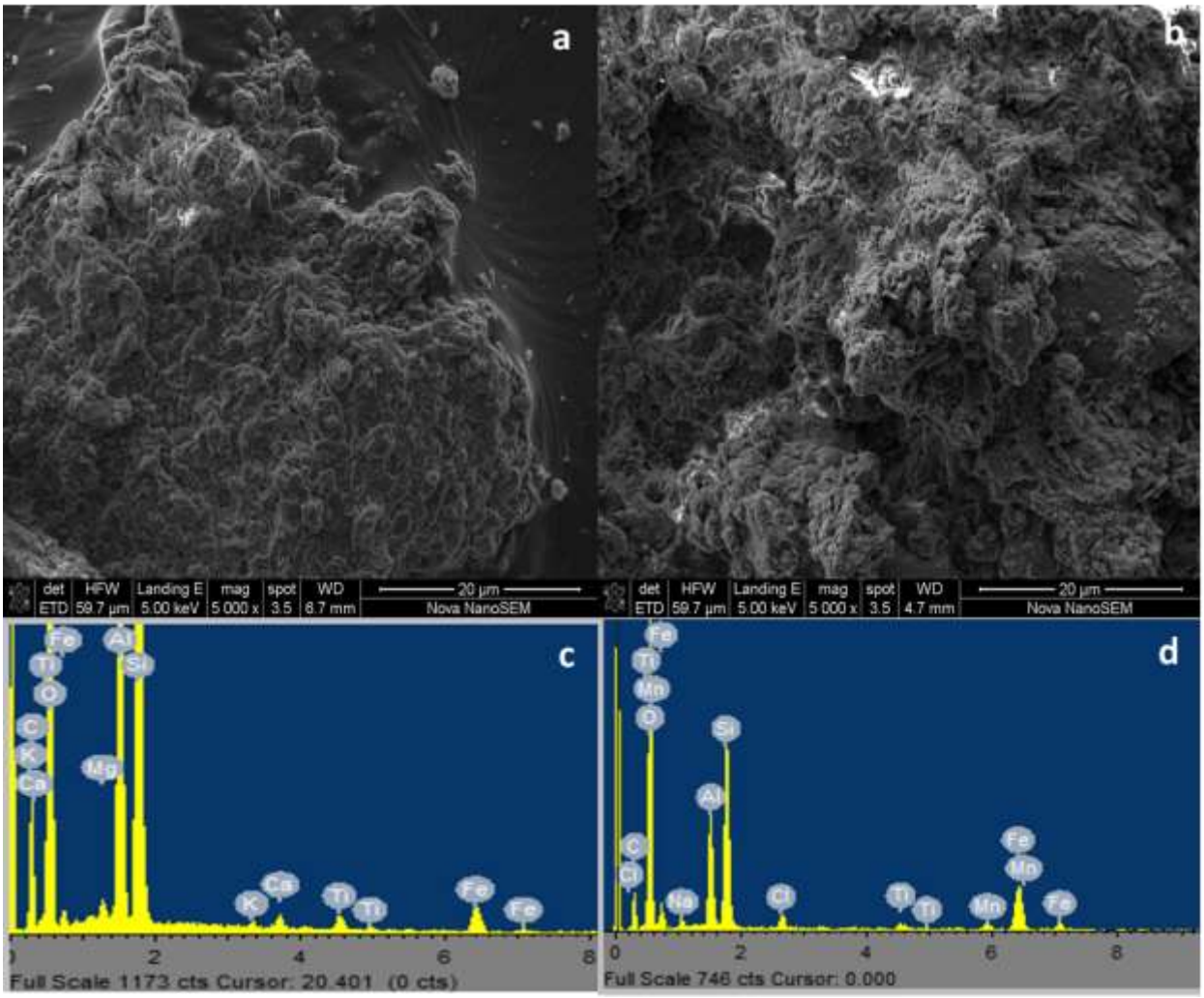


Figure 7.4: SEM micrographs and SEM-EDS spectrum of RK (a, c) and IOK (b, d)

### 7.3.1.5 Surface area analysis

The surface area and pore analysis are summarized in Table 7.2. It is noted that the total BET surface area of the kaolin clay mineral increased from 19.02 $m^2/g$ to 87.51 $m^2/g$ after modification with $Fe^{3+}$ and $Mn^{2+}$ polycations and HDTMA surfactant. Furthermore, the pore volume increased from 0.04 to 0.09 $cm^3/g$ after modification. The increase in surface area and pore volume could provide more active sites for sorption of ions leading to higher sorption capacity. The average pore size decreased from 9.54 to 4.68 nm after modification. The pore diameter within 2 and 50 nm indicates mesopore nature of the material.

Table 7.2: Surface area and pore analysis.

| | Surface area ($m^2/g$) | Pore volume ($cm^3/g$) | Pore diameter (nm) |
|---|---|---|---|
| RK | 19.02 | 0.04 | 9.54 |
| IOK | 87.51 | 0.09 | 4.68 |

### 7.3.2 Batch experiments

#### 7.3.2.1 Effect of pH

The effect of pH in As(III) and As(V) removal is presented in Figure 7.5. The percentage As(V) removal was found to be optimum at pH between 4 and 8 and inhibited as the solution pH becomes acidic and strong alkaline. The adsorption of As(III) on the other hand was found to be optimum at pH between 4 and 6. The decrease in percentage arsenic removal at strong alkaline pH could be attributed to electrostatic repulsion since both As(III) and As(V) exist as negatively charged species such as $HAsO_4^{2-}$, $AsO_4^{3-}$, $H_2AsO_3^-$ and $HAsO_3^{2-}$ (Smedley and Kinnburg, 2002). The decrease in percentage As(III) and As(V) removal as the pH goes to 2 could be attributed to the fact that these species exist as neutrally charged $H_3AsO_4$ and $H_3AsO_3$ making it difficult to remove via electrostatic attraction to positively charged surface (Lee et al., 2015).

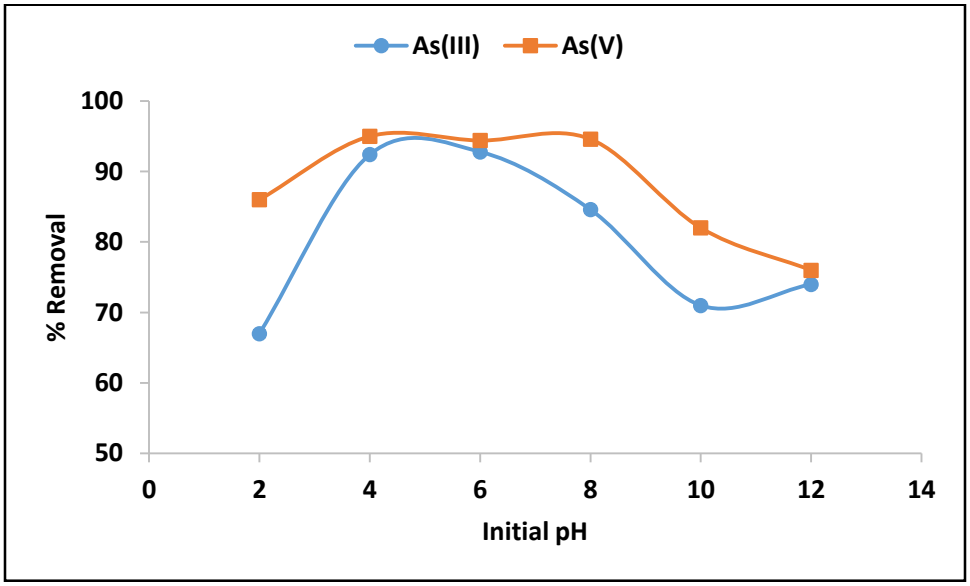


Figure 7.5: Variation of As(III) and As(V) percentage removal with initial pH.

### 7.3.2.2 Adsorption kinetics

Adsorption kinetics studies were performed in order to predict the rate of adsorption and to give insight in the rate limiting factor and the adsorption mechanism. Figure 7.6a and b presents the variation of As(III) and As(V) adsorption capacity with time. It is seen that the adsorption capacity increased with increasing contact time. The adsorption capacity increased rapidly within the first 40 min and then proceed at slow rate up to 120 min suggesting that the system has reached equilibrium. The same trend was observed for arsenic species.

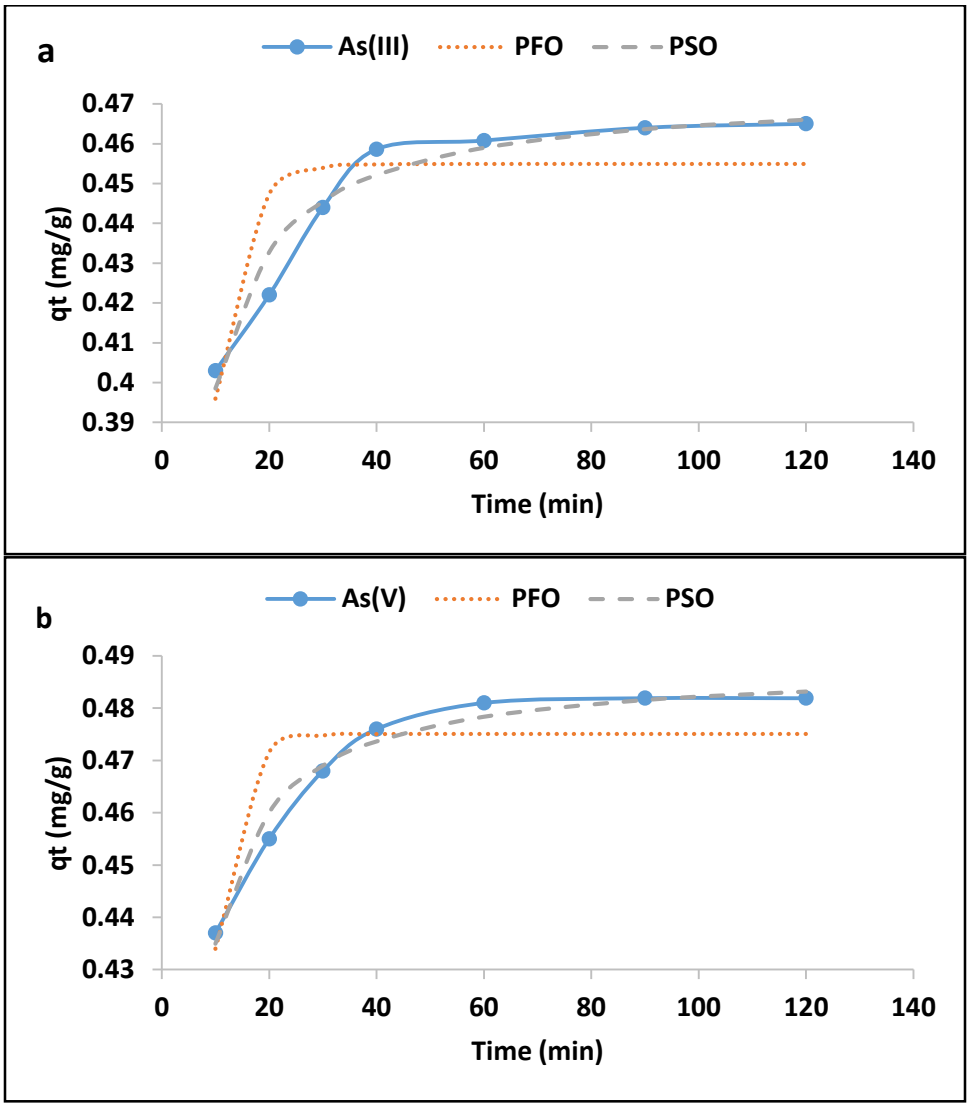


Figure 7.6: Variation of adsorption capacity of As(III)(a) and As(V)(b) by IOK (0.1 g/100 mL adsorption dosage, 0.5 mg/L adsorbate concentration, pH 6.5±0.2).

The pseudo first and second order of reaction kinetics models were used to predict the rate and the mechanism of As(III) and As(V) adsorption onto IOK. The mathematical representation of the

models are depicted in equation 7.1 and 7.2, respectively (Qi et al., 2015; Munagapati and Kim, 2017).

$$q_t = q_e(1 - e^{-k_1 t}) \quad (7.1)$$

$$q_t = \frac{q_e^2 k_2 t}{1 + k_2 q_e t} \quad (7.2)$$

Where $q_e$ and $q_t$ are the equilibrium capacities (mg/g) of the sorbent at equilibrium and at any given time, t (min), respectively; $k_1$ (min-1) and $k_2$ (g/mg.min) are the pseudo first order and second order rate constants for adsorption processes, respectively. The nonlinear plots are presented in Figure 7.6 while the constants are presented in Table 7.3.

Table 7.3: Parameters for pseudo first and second order reactions.

| | **Pseudo first order** | | | **Pseudo second order** | | |
|---|---|---|---|---|---|---|
| | $q_e$ (mg/g) | $K_1$ ($min^{-1}$) | $R^2$ | $q_e$ (mg/g) | $K_2$ (g/mg.min) | $R^2$ |
| As(III) | 0.45 | 0.20 | 0.70 | 0.47 | 1.12 | 0.94 |
| As(V) | 0.47 | 0.24 | 0.80 | 0.48 | 1.67 | 0.98 |

The $R^2$ values obtained from pseudo second order for As(III) and As(V) were found to be 0.94 and 0.98 higher than those pseudo first order (0.70 and 0.80). Furthermore, the theoretical adsorption capacity and reaction rate for pseudo second order were found to be higher compared to those from pseudo first order (Table 7.3). These values indicate that the adsorption data fitted better to pseudo first order of reaction kinetics. It can therefore be concluded that adsorption of both As(III) and As(V) occurred via chemisorption, which involves the ion exchange reaction between the hydroxyl ions in the surface of the adsorbent and the As(III) and As(V) species (Tran et al., 2017).

To further elucidate the rate limiting steps, the adsorption kinetics data was fitted to intra-particle diffusion model of Weber Morris (Weber and Morris, 1963). Equation 3 presents the linearized form of intra-particle diffusion model.

$$q_t = k_i t^{0.5} + C \quad (7.3)$$

Where $q_t$ (mg/g) is the adsorption capacity at a given time, t (min); $K_i$ ($mg/g.min^{0.5}$) is the rate of intra-particle diffusion model, C (mg/g) is the constant associated with the thickness of the

boundary layer, where the higher value of C corresponds to a greater effects of the limitation boundary layer. Generally, adsorption of ions onto solids surface involves the transfer of adsorbate from the bulk solution to the external surface (film diffusion) of the adsorbent, surface diffusion and pore diffusion or both surface and pore diffusion of adsorbate onto the particles leading to chemisorption (Gupta et al., 2011; Tran et al., 2017). If the plot of qt against $t^{0.5}$ is linear or passes through origin, the adsorption is solely governed by intra-particle diffusion. However, if the plot yields two or more linear plots, then adsorption is governed by both surface and intra-particle diffusion. The intra-particle plot and the constant parameters for adsorption of As(III) and As(V) is presented in Figure 7.7 and Table 7.4, respectively.

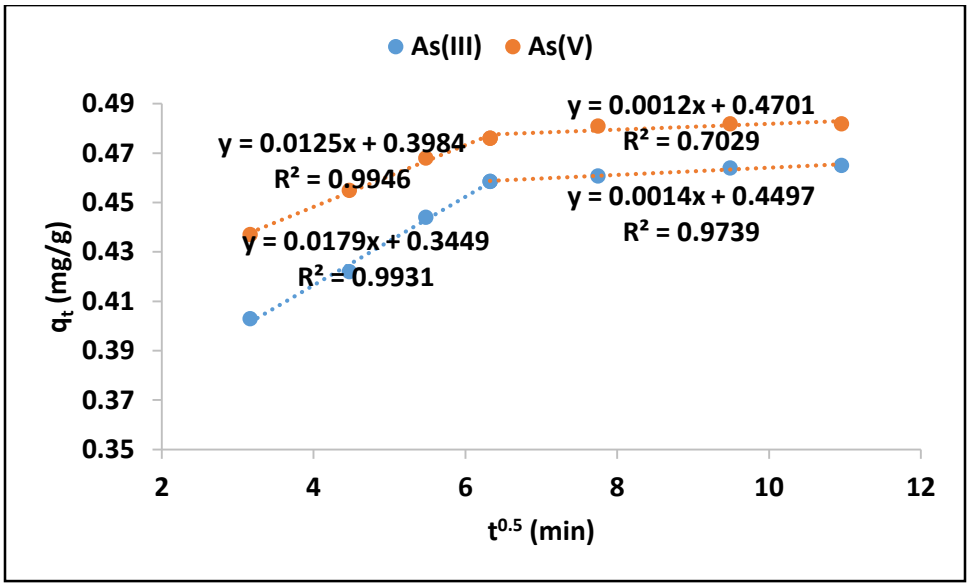


Figure 7.7: Weber-Morris intra-particle plot for As(III) and As(V) adsorption onto Inorgano-organo modified kaolin clay mineral.

Table 7.4: Constant parameters for Weber-Morris intra-particle model.

| | $K_1$ (mg/g.$min^{0.5}$) | $C_1$ (mg/g) | $K_2$ (mg/g.$min^{0.5}$) | $C_2$ (mg/g) |
|---|---|---|---|---|
| As(III) | 0.013 | 0.39 | 0.0012 | 0.47 |
| As(V) | 0.017 | 0.34 | 0.0014 | 0.44 |

The plot for both species (Fig. 7.7) yielded bilinear plots indicating the presence of both surface film diffusion (phase 1) and intra-particle diffusion (phase 2). Ryu et al. (2017) observed the same trend during adsorption of As(III) and As(V) onto Fe-Mn modified activated carbon. Phase 1 indicates the film diffusion which could be attributed to attraction of As(III) and As(V) onto the

film or boundary layer of the adsorbent. Phase 2 reflects the intra-particle diffusion where in As(III) and As(V) ions diffuse into the pores of the adsorbent. This phase involves ion exchange between the hydroxyl ions and arsenic species and weak hydrogen bonding. The rate constant for surface adsorption at phase 1 was found to be higher than the adsorption rate at phase 2. This suggest that intra-particle diffusion is a slower process compared to surface adsorption. This results suggest that adsorption of As(III) and As(V) is a complex process involving both surface and intra-particle diffusion.

#### 7.3.2.3 Adsorption isotherms

The adsorption isotherms were evaluated by varying the initial adsorbate concentration from 0.5 to 30 mg/L. The experiment was conducted at 298, 323 and 343 K. The results are presented in Figure 7.8a and b in terms of equilibrium concentrations against adsorption capacity. As expected, the adsorption capacity increases with increasing equilibrium As(III) and As(V) concentration. Furthermore, the adsorption capacity increased with increasing temperature. Equation 7.4 and 7.5 of Langmuir and Freundlich adsorption isotherms, respectively were used to explain the relationship between the adsorbent and the adsorbate (Tran et al., 2016).

$$q_e = \frac{q_{max} b C_e}{1 + b C_e} \tag{7.4}$$

$$q_e = K_f C_e^{1/n} \tag{7.5}$$

Where $q_e$ (mg/g) is the adsorption capacity, $C_e$ (mg/L) is the As(III) and As(V) concentration at equilibrium, b (L/mg) is the equilibrium adsorption constant related to the affinity of the binding sites, $q_{max}$ (mg/g) is the maximum monolayer adsorption capacity of the adsorbent. $K_f$ (mg/g) is the Freundlich constant related to adsorption capacity and 1/n is the dimensionless parameter for Freundlich adsorption isotherm model related to adsorption intensity which indicates the magnitude of the adsorption driving force or surface heterogeneity. The nonlinear plots of Langmuir and Freundlich isotherms are presented in Figure 7.8a and b for As(III) and As(V), respectively while the models constant parameters are presented in Table 7.5.

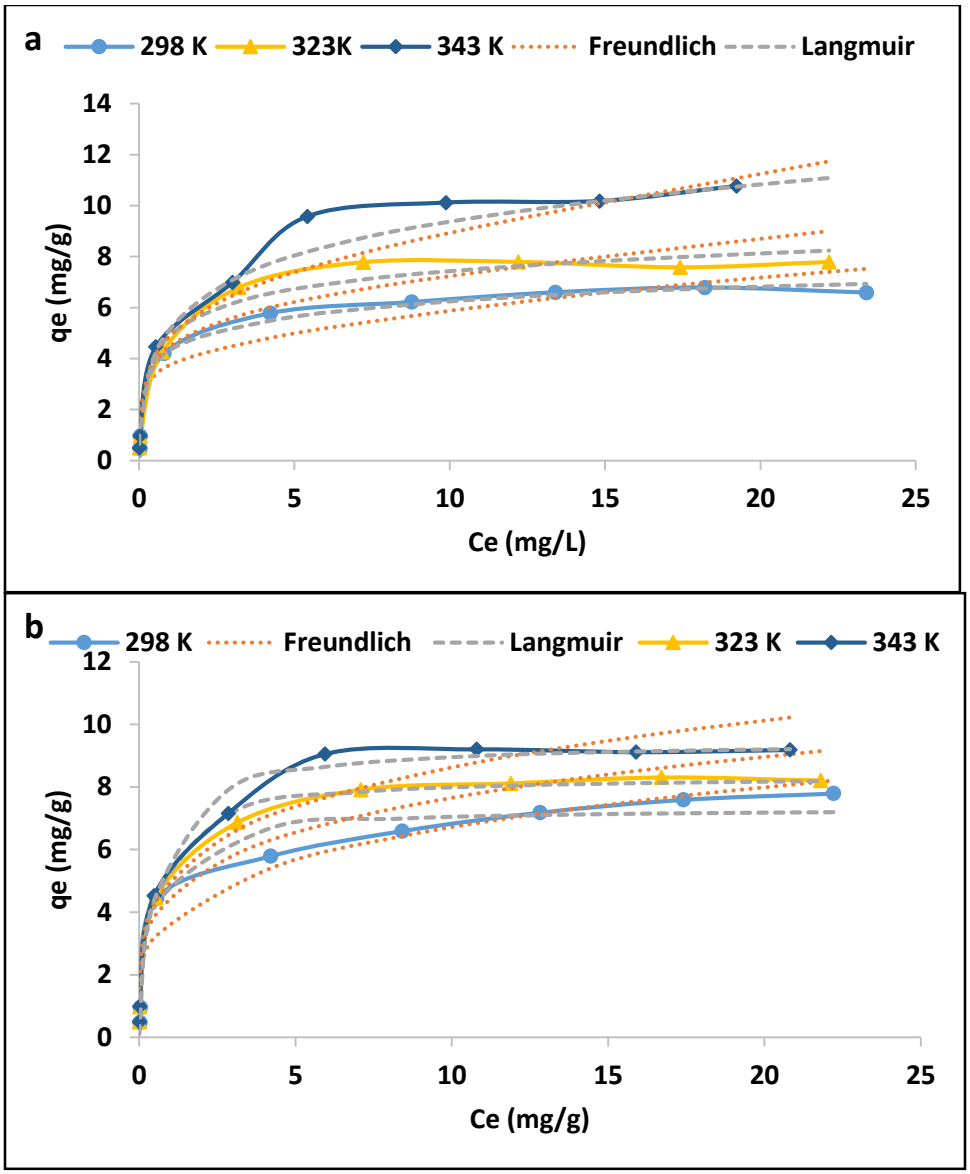


Figure 7.8: Adsorption isotherms for (a)As(III) and (b)As(V) (0.1 g/100 mL adsorbent dosage, 0.5-30 mg/L initial concentration, 60 min contact time, pH 6.5±0.2).

Table 5: Langmuir and Freundlich adsorption isotherm parameters.

| | | Langmuir | | | Freundlich | | |
|---|---|---|---|---|---|---|---|
| | | $q_m$ (mg/g) | B (L/mg) | $R^2$ | $K_f$ (mg/g) | 1/n | $R^2$ |
| As(III) | 298 K | 7.99 | 0.21 | 0.98 | 1.88 | 0.4 | 0.90 |
| | 323 K | 9.8 | 0.17 | 0.97 | 2.15 | 0.42 | 0.89 |
| | 343 K | 15.15 | 0.09 | 0.99 | 1.96 | 0.52 | 0.95 |
| As(V) | 298 K | 7.32 | 2.48 | 0.96 | 3.76 | 0.25 | 0.93 |
| | 323 K | 8.36 | 2.10 | 0.99 | 4.52 | 0.22 | 0.93 |
| | 343 K | 9.45 | 1.78 | 0.98 | 5.07 | 0.23 | 0.93 |

The adsorption isotherm data for As(III) and As(V) adsorption onto inorgano-organo kaolin clay mineral was described by Langmuir isotherm model rather than Freundlich isotherm model. This suggest that the adsorption of As(III) and As(V) occurred on a monolayered surface. The maximum adsorption capacities for As(III) were found to be 7.99, 9.88 and 15.15 mg/g at 298, 323 and 343 K, respectively while for As(V) adsorption capacities were found to be 7.32, 8.36 mg/g at these temperature ranges (Table 7.5).

### 7.3.2.4 Adsorption thermodynamics

To further elucidate the adsorption mechanisms, thermodynamics parameters such as Gibbs energy change ($\Delta G^O$), the enthalpy change ($\Delta H^O$), and the entropy ($\Delta S^O$) were determined from Equation 7.6 and 7.7 (Singh et al., 2016).

$$\Delta G° = -RT \ln K_L \quad (7.6)$$

$$\ln K_L = -\frac{\Delta H°}{RT} + \frac{\Delta S°}{R} \quad (7.7)$$

Where $R$ is the molar gas constant, 8.314 J $mol^{-1}K^{-1}$, T is the absolute temperature in Kelvin, $\Delta G^O$ (KJ/mol) is the Gibbs free energy change. $\Delta H^O$ (J/mol) is enthalpy change, $\Delta S^O$ (J/mol) is the change in entropy and $K_L$ (L/mg) is the constant derived from Langmuir isotherm model. Values $\Delta H$ and $\Delta S$ of are determined from the slope and intercept of a plot of $\ln K_L$ against 1/T (Figure 7.9). The thermodynamic parameters are shown in Table 7.6.

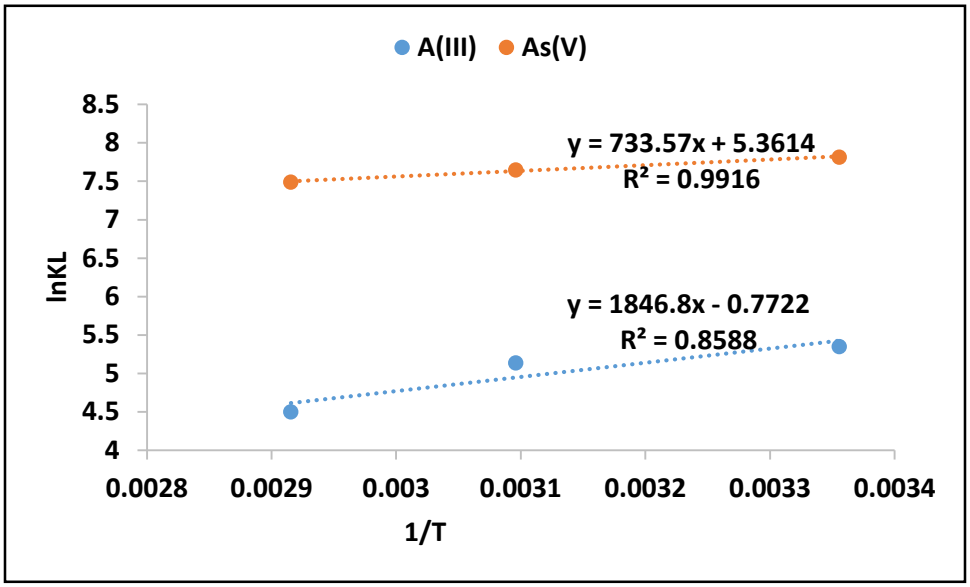


Figure 7.9: $\ln K_L$ as a function of reciprocal of adsorption temperature.

Table 7.6: Thermodynamics parameters for As(III) and As(V) adsorption by Inorgano-organo modified clay.

| | $\Delta G^O$ (KJ/mol) | $\Delta H^O$ (KJ/mol) | $\Delta S^O$ (J/mol) |
|---|---|---|---|
| As(III) | 298 K= -13.27<br>323 K= -13.79<br>343 K= -12.83 | -15.35 | 6.4 |
| As(V) | 298 K= -19.36<br>323 K= -20.54<br>343 K= -21.35 | -6.09 | 44.57 |

The value of enthalpy of change ($\Delta G^O$) for the adsorption of As(III) and As(V) onto Inorgano-organo modified kaolin clay mineral was found to be negative at both initial temperatures. This suggest that adsorption of As(III) and As(V) occurred spontaneously. The $\Delta H^O$ value was found to be negative which indicating exothermic nature of the adsorption process. Exothermic reactions involves both physiosorption and chemisorption processes (Tran et al., 2016). The positive value of $\Delta S^O$ suggest that As(III) and As(V) were randomly distributed on the surface of the adsorbent.

### 7.3.2.5 Effect of co-existing ions

Figure 7.10 depicts the influence co-existing anions in adsorption of As(III) and As(V) by IOK. It is observed that the presence of $Ca^{2+}$ and $Mg^{2+}$ slightly increases the adsorption As(III) and As(V). This could be an indication that the presence of $Ca^{2+}$ and $Mg^{2+}$ makes the surface of the adsorbent to be more positively charged which consequently facilitate the attraction of As(III) and As(V)

onto the created sorption sites (Qi et al., 2015). The presence of co-existing anions inhabited the sorption As(III) and As(V). The adsorption of As(III) decreased significantly in the presence of carbonates while the adsorption of As(V) decreased significantly in the presence of sulphate. The decrease in percentage removal in the presence of anions could be attributed to competition for adsorption sites between the co-existing anions and arsenic species.

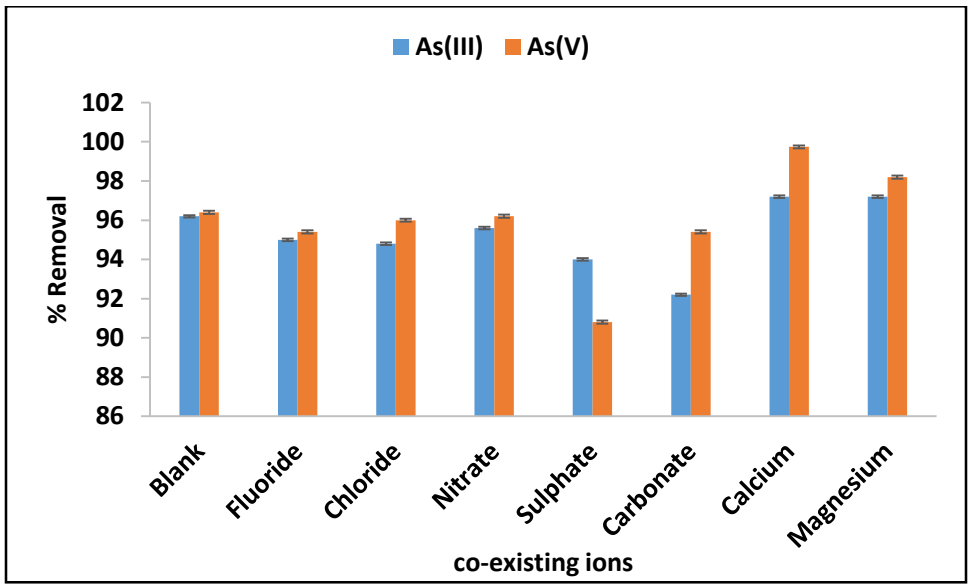


Figure 7.10: Effect of co-existing ions in the adsorption of As(III) and As(V) from the solution.

**7.3.2.6 Regeneration study**

The regeneration and reuse of adsorbent was studied using 0.01 M HCl as a regenerating agent and the results for 7 successive cycles are presented in Figure 7.11. The percentage As(III) and As(V) removal achieved from the regeneration cycle 1 to cycle 5 was found to be greater than 95% which is relatively equal to the percentage removal achieved from the virgin material. This could be an indication that treatment of the adsorbent with HCl increases the positive sites on the surface of the material. Slight decrease as the reuse-regeneration cycles continues to $7^{th}$ cycle. The decrease could be due to inadequate regeneration of the sorption sites. This results suggests that IOK is a good material for use in arsenic removal from groundwater as it can be regenerated.

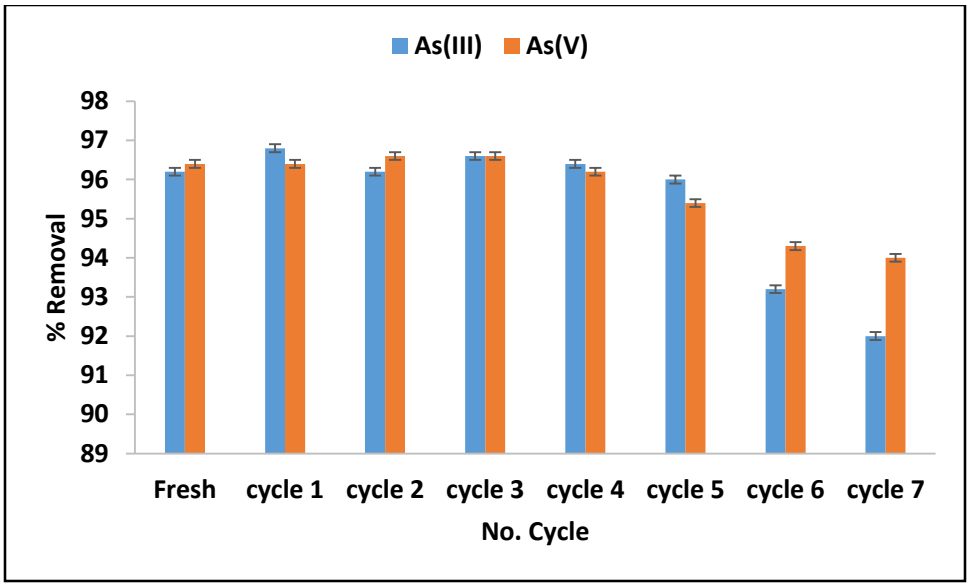


Figure 7.11: Variation of As(III) and As(V) removal as a function of regeneration-reuse cycles (1 g/100 mL adsorbent dosage, 0.5 mg/L As(III) and As(V) concentration, pH 6±0.5).

### 7.3.3 Column breakthrough curves

The experimental data obtained at various parameters such as the flow rate, adsorbent mass and initial As(III) and As(V) concentration is presented in Figure 7.12-7.14 by plotting $C_f/C_i$ against the breakthrough volume (mL) as the breakthrough curves. The breakthrough parameters are depicted in Table 7.7.

Figure 7.12a-b shows the effect of flow rate on breakthrough performance for As(III) and As(V) removal, respectively. It is observed that the breakthrough point (point at which effluent concentration is 0.01 mg/L) decreases with increasing flow rate. The trend was the same both As(III) and As(V). For As(III) the volume treated at breakthrough point decreased from 700 mL at 1.5 mL/min to 320 mL at 2.5 mL/min (Figure 7.12a). Conversely, for As(V) volume at breakthrough point decreased from 950 mL to 550 mL at 1.5 mL/min and 2 mL/min, respectively (Figure 7.12b). The decrease in the volume treated at breakthrough point with increasing flow rate could be attributed to the fact that increasing flow rate reduces the contact time between As(III)/As(V) ions and the adsorbent bed and therefore limiting the possibility of intra-particle diffusion (Setshedi et al., 2014).

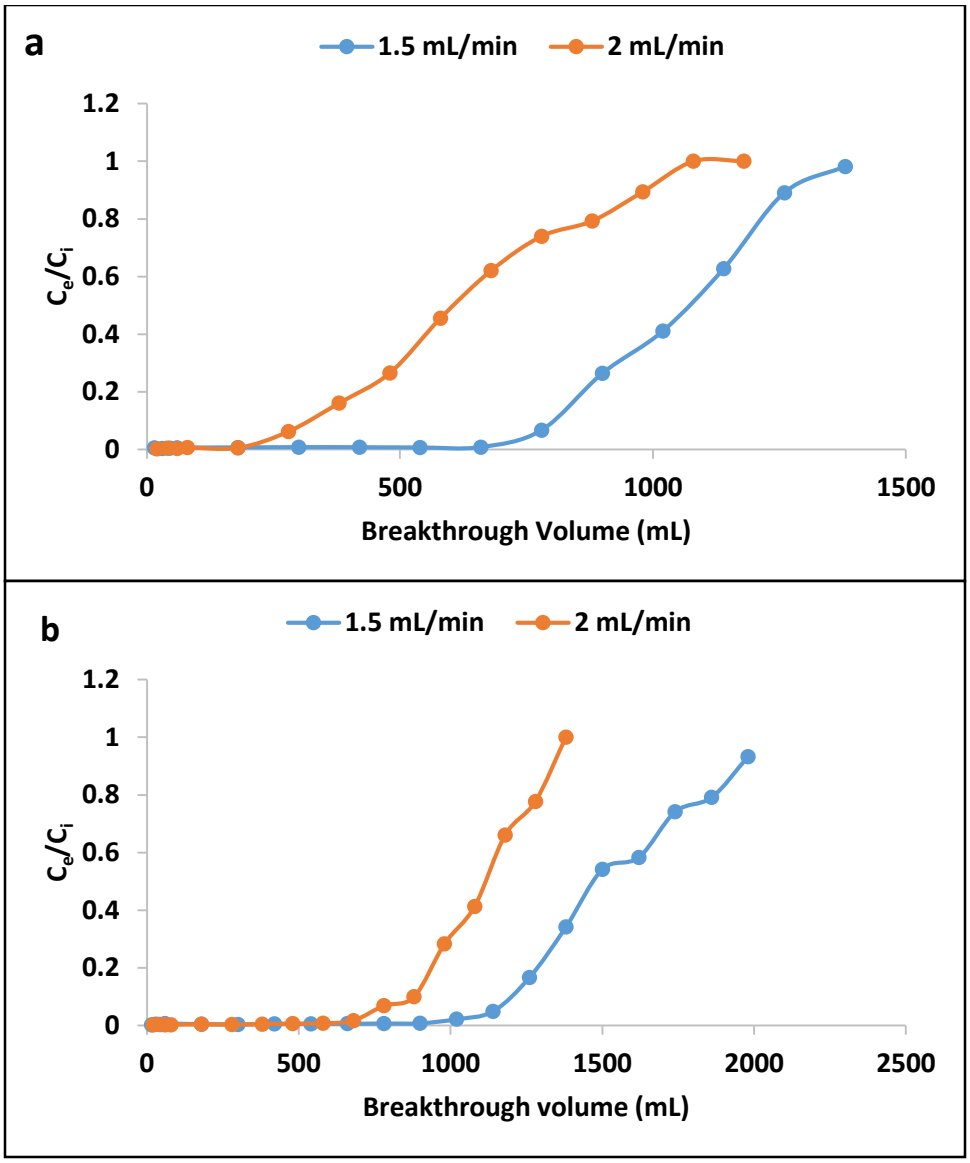


Figure 7.12: The variation of breakthrough volumes for a) As(III) and b)As(V) at various flow rates (bed mass of 5 g, initial concentration 1 mg/L of As(III) and As(V) and flow rate varied from 1.5 mL/min to 2 mL/min).

The effect of adsorbent bed mass on breakthrough point is presented in Figure 7.13. It is observed that the breakthrough point increased with increasing adsorbent mass. This could be due to the fact that increasing bed mass enhances the active sites for As(III)/As(V) sorption leading to late breakthrough time and more water treated at breakthrough point. Quantitatively, the volumes of the water treated at the breakthrough point were 180 mL and 700 mL at 2 g and 5 g, respectively for As(III) (Figure 7.13a) and 300 mL and 950 mL at 2 g and 5 g, respectively for As(V) (Figure 7.13b).

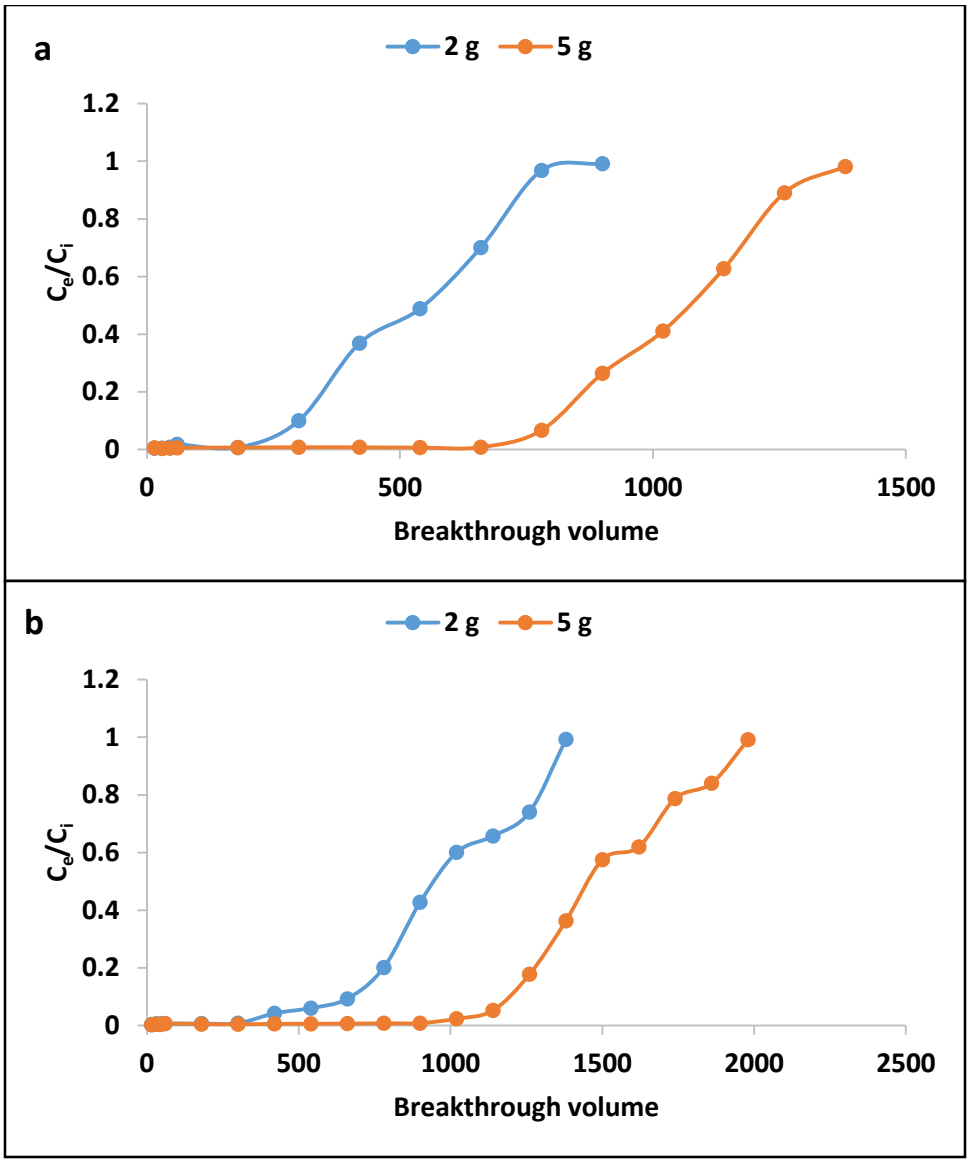


Figure 7.13: Variation of breakthrough volumes for a) As(III) and b) As(V) at various bed masses (bed mass varied from 2 to 5 g, initial concentration 1 mg/L of As(III) and As(V) and flow rate of 1.5 mL/min).

The relationship between the adsorbate concentration and the breakthrough volume is depicted in Figure 7.14. It is noted that the breakthrough volumes decreases with increasing adsorbate concentration. This could be attributed to increasing driving force for mass transfer as the initial concentration increases leading to faster saturation of the adsorbent and hence low volume treated at the breakthrough point (Podder and Majumder, 2016). The volumes treated at the breakthrough point were 1380 mL at 0.5 mg/L and 700 mL at 1 mg/L for As(III) (Figure 7.14a). For As(V) the

volumes treated at breakthrough point were 1500 and 950 mL at 0.5 and 1 mg/L, respectively (Figure 7.14b).

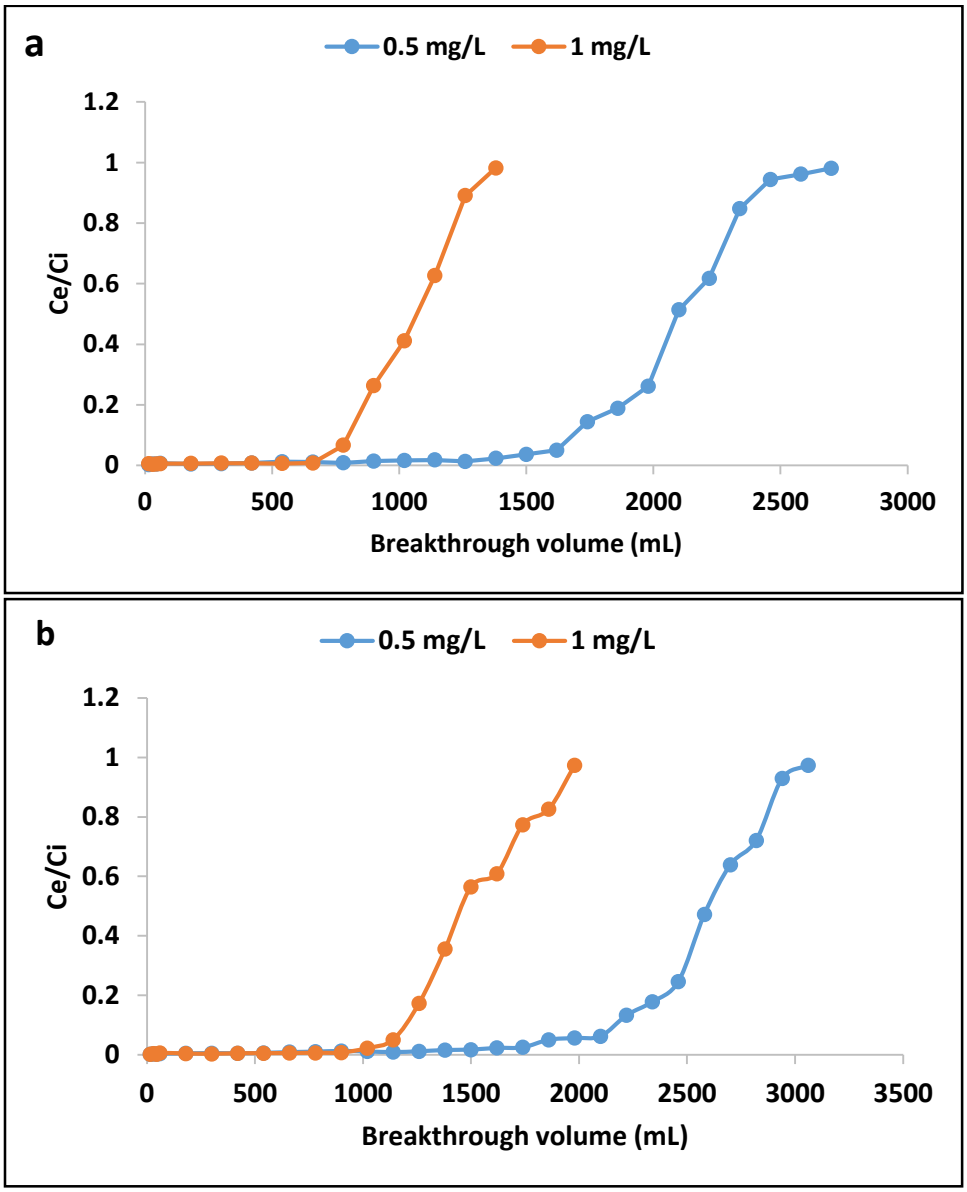


Figure 7.14: The variation of breakthrough volumes for a) As(III) and b) As(V)with adsorbate concentration (bed mass of 5 g, initial concentration varied from 0.5 to 1 mg/L of As(III) and As(V) and flow rate of 1.5 mL/min).

### 7.3.4 Column performance indicator

Column performance indicator was assessed by calculating the number of bed volumes (BVs) treated and the adsorbent exhaustion rate (AER) using equation 7.8 and 7.9, respectively (Setshedi et al., 2014).

$$BV = \frac{volume\ at\ breakthrough\ point\ (L)}{volume\ of\ adsorbent\ bed\ (L)} \quad (7.8)$$

$$AER = \frac{Adsorbent\ mass\ (g)}{Volume\ of\ water\ treated\ (L)} \quad (7.9)$$

For a fixed bed column, there is direct relationship between the column performance and the number of bed volumes treated. The higher the number of bed volumes treated, the better the column performance. On the other hand, the lower the adsorbent saturation rate the better the column performance. The values of BV's and AER determined from the column data is presented in Table 7.8. It is noted that the fixed bed column developed in the present investigation performed better at flow rate of 1.5 mL/min, initial concentration of 0.5 mg/L and bed mass of 5 g where the total number of BV's were 276 and 300 for As(III) and As(V), respectively. Under these experimental conditions the adsorbent saturation rate was 0.0018 and 0.0016 g/L for As(III) and As(V), respectively.

In order to treat 50 L under the optimum conditions for As(III) removal (0.5 mg/L initial concentration, 5 g adsorbent mass and 1.5 mL/min flow rate) it will require almost 55.55 hours with an adsorbent dosage of 181 g thus for a period of 6 month an estimate of 66 kg will be required. The proposed adsorbent may be limited by the flow rate as such effort need to be directed towards enhancing the permeability of the adsorbent to shorten the time required to treat water.

Table 7.8: Summary of fixed bed performance indicators.

| | **Flow rate (mL/min)** | **Bed Mass (g)** | **Concentration (mg/L)** | **$V_b$ (mL)** | **$V_e$ (mL)** | **BV** | **AER (g/L)** |
|---|---|---|---|---|---|---|---|
| As(III) | 1.5 | 5 | 1 | 700 | 1300 | 140 | 0.003 |
| | 2 | 5 | 1 | 320 | 900 | 64 | 0.005 |
| | 1.5 | 2 | 1 | 180 | 780 | 90 | 0.002 |
| | 1.5 | 5 | 1 | 700 | 1380 | 140 | 0.004 |
| | 1.5 | 5 | 1 | 700 | 1380 | 140 | 0.004 |
| | 1.5 | 5 | 0.5 | 1380 | 2700 | 276 | 0.002 |
| As(V) | 1.5 | 5 | 1 | 950 | 1980 | 190 | 0.002 |
| | 2 | 5 | 1 | 550 | 1280 | 110 | 0.004 |
| | 1.5 | 2 | 1 | 300 | 1380 | 150 | 0.001 |

| | | | | | | | |
|---|---|---|---|---|---|---|---|
| | 1.5 | 5 | 1 | 950 | 1980 | 190 | 0.002 |
| | 1.5 | 5 | 1 | 950 | 1980 | 190 | 0.002 |
| | 1.5 | 5 | 0.5 | 1500 | 3060 | 300 | 0.001 |

*$V_b$= volume at breakthrough point; $V_e$= Volume at exhaustion point; BV= Bed Volumes; AER= Adsorbent saturation rate.

### 7.4 Column data modelling

In order to ensure a successful design of a fixed bed column, there is a need to understand and describe the behavior of adsorbate solute in a fixed bed. Several mathematical models have been proposed and applied to predict the dynamic behavior of the fixed bed column performance (Paudyal et al., 2013; Ghosh et al., 2014. Yang et al., 2015). In the present study, Thomas and Yoon-Nelson models were employed to describe the data.

#### 7.4.1 Thomas Model

Thomas model was proposed based on the assumption that mass transport resistance is proportional to the axial dispersion and the thickness of the liquid film on the particle surface (Ghosh et al., 2014). Furthermore, the model suggests that adsorption follows Langmuir adsorption-desorption kinetics and the adsorption rate is dependent on the surface interaction between the adsorbate and the vacant sites of the adsorbent (Chatterjee et al., 2017). Equation 7.10 depicts the linear equation of Thomas model.

$$\ln\left(\frac{C_o}{C_t}-1\right)=\frac{K_{TH}q_oM}{Q}-K_{TH}C_ot \qquad (7.10)$$

Where $K_{TH}$ (mL/min/mg) is the rate constant, $C_o$ and $C_t$ (mg/L) represent the influent and the effluent concentrations respectively, $q_o$ (mg/g) is the total adsorption capacity, m (g) is the mass of the adsorbent, Q (mL/min) is the flow rate and t (min) is time. Values of $q_o$ and $K_{TH}$ are determined from the slope an intercept of $\ln(C_o/C_t-1)$ vs. time. The constant parameters obtained from the plots of $\ln(C_o/C_t-1)$ vs time are presented in Table 7.9. It is noted that the rate constant decreases with increasing the bed mass and increasing feed concentration. Conversely, the adsorption rate increases with increasing flow rate (Table 7.9). Decreasing $K_{th}$ value could favor the diffusion mass transfer of As(III) and As(V) ions. The value of $q_o$ increased with increasing inlet concentration and further decreased with increasing flow rate and bed mass. The increase in $q_o$ with increase in influent concentration could be attributed to increasing concentration gradient which creates higher driving force and thereby increases adsorption capacity. The trends were

observed for both species of arsenic. The correlation coefficient values were found to be >85 for at both experimental conditions.

Table 7.9: Theoretical breakthrough parameters as determined from Thomas breakthrough model.

| | **Flow rate (mL/min)** | **Bed Mass (g)** | **Concentration (mg/L)** | **$K_{TH}$ (mL/min/mg)** | **$q_o$ (mg/g)** | **$R^2$** |
|---|---|---|---|---|---|---|
| As(III) | 1.5 | 5 | 1 | 0.0078 | 0.244 | 0.85 |
| | 2 | 5 | 1 | 0.014 | 0.168 | 0.96 |
| | 1.5 | 2 | 1 | 0.012 | 0.329 | 0.96 |
| | 1.5 | 5 | 1 | 0.0062 | 0.308 | 0.87 |
| | 1.5 | 5 | 0.5 | 0.0094 | 0.208 | 0.87 |
| | 1.5 | 5 | 1 | 0.0083 | 0.23 | 0.87 |
| As(V) | 1.5 | 5 | 1 | 0.0062 | 0.326 | 0.89 |
| | 2 | 5 | 1 | 0.015 | 0.23 | 0.91 |
| | 1.5 | 2 | 1 | 0.0074 | 0.64 | 0.94 |
| | 1.5 | 5 | 1 | 0.0064 | 0.123 | 0.89 |
| | 1.5 | 5 | 0.5 | 0.0057 | 0.349 | 0.86 |
| | 1.5 | 5 | 1 | 0.0046 | 0.423 | 0.86 |

### 7.4.2 Yoon-Nelson Model

Yoon-Nelson model was developed to analyze the breakthrough curve behavior by providing more information about the breakthrough rate in a fixed bed column and the time entailed to achieve 50% breakthrough (Yoon and Nelson; 1984). It assumes that the decreasing rate of the probability for each molecule adsorption is favorably related to the probability of adsorbate and breakthrough within the bed (Ahmed and Hameed, 2018). The linear form of Yoon-Nelson is expressed by equation 7.11 (Vardhan and Srimurali, 2018).

$$\ln \frac{C_t}{C_{o-}\, C_t} = K_{YN} t - \tau K_{YN} \qquad (7.11)$$

Where $\tau$ (min) is the time required for 50% breakthrough of the adsorbate and $K_{YN}$ ($min^{-1}$) is the rate constant. Values of $\tau$ and $K_{YN}$ are determined from the slope and intercept of $\ln(C_t/C_o\text{-}C_t)$ vs.

time. Table 7.10 presents the theoretical parameters determined from Yoon-Nelson model. It is noted that increasing the flow rate increases the rate of adsorption and further reduces the time it takes to achieve 50% of the breakthrough curve. In addition, the time required to achieve 50% of the breakthrough decreases with increasing initial concentration and increases with increasing bed mass. The correlation coefficient values obtained from Yoon-Nelson model were found to be >0.85 corresponding to the values obtained from Thomas breakthrough model. The modeling results suggests that the breakthrough column for the adsorption of As(III) and As(V) performs better at lower flow rate and inlet concentration and higher bed mass.

Table 7.10: Yoon-Nelson model constant parameters.

| | **Flow rate (mL/min)** | **Bed Mass (g)** | **Concentration (mg/L)** | **$K_{YN}$ ($min^{-1}$)** | **$\tau$ (min)** | **$R^2$** |
|---|---|---|---|---|---|---|
| As(III) | 1.5 | 5 | 1 | 0.017 | 708.54 | 0.85 |
| | 2 | 5 | 1 | 0.091 | 331.34 | 0.96 |
| | 1.5 | 2 | 1 | 0.0161 | 329.81 | 0.96 |
| | 1.5 | 5 | 1 | 0.0091 | 708.54 | 0.85 |
| | 1.5 | 5 | 0.5 | 0.0047 | 1392.05 | 0.87 |
| | 1.5 | 5 | 1 | 0.0083 | 767.180 | 0.87 |
| As(V) | 1.5 | 5 | 1 | 0.0062 | 1088.72 | 0.89 |
| | 2 | 5 | 1 | 0.0113 | 629.73 | 0.93 |
| | 1.5 | 2 | 1 | 0.0095 | 627.4 | 0.94 |
| | 1.5 | 5 | 1 | 0.0062 | 1125.18 | 0.89 |
| | 1.5 | 5 | 0.5 | 0.0035 | 1854.08 | 0.86 |
| | 1.5 | 5 | 1 | 0.0062 | 1088.77 | 0.89 |

### 7.5 Comparison with other adsorbents

Table 7.11 present the comparison for As(III) and As(V) adsorption capacities of different adsorbent reported in the literature with the maximum adsorption capacity obtained from the present study. From the table it can be noted that the maximum adsorption capacity obtained from the present study is quite higher as compared to those reported in the literature.

Table 7.11: Comparison of adsorption capacities.

| **Adsorbent** | **Experimental conditions** | **$q_e$ As(III) (mg/g)** | **$q_e$ As(V) (mg/g)** | **Ref** |
|---|---|---|---|---|
| HDTMA-Al-bentonite | Initial concentration: 2-18 mg/; Adsorbent dosage: 2 g/L; pH: 4.5 | 2.24 | 8.93 | Lee et al., 2015 |
| Iron impregnated charred GAP | Initial concentration: 0.05-200 mg/L; Adsorbent dosage: 0.5g/100 mL; pH:7 | 3.25 | 5.09 | Yin et al., 2017 |
| Aluminum pillared HDTMA sericite | Initial concentration: 1 to 20 mg/L; adsorbent dosage: 0.2g/100 mL; pH 4.5. | 0.40 | 0.46 | Tiwari and Lee, 2012 |
| CTMAB-Fe-Montmorillonite | Initial concentration: 1-60 mg/L; adsorbent dosage: 0.1 g/25 mL; pH 6.5 | 11.36 | 8.85 | Ren et al., 2014 |
| Fe/Mn-HDTMA kaolin mineral | Initial concentration: 0.5-30 mg/L; adsorbent dosage; 0.1 g/100 mL; pH:6.5±0.5, Temp: 298 K | 7.99 | 7.32 | Present study |

## 7.6 Summary

In this chapter, IOK for As(III) and As(V) remediation from groundwater was successfully fabricated. The surface area analysis revealed that the modification of clay with inorganic and organic solutions increased the surface area and pore volumes of the clay from 19.02 to 87.51 $m^2/g$ and 0.04 to 0.09 $cm^3/g$, respectively. Furthermore, average pore size decreased from 9.54 to 4.68 nm after modification. The batch experiments showed that As(III) removal was optimum at the pH range of 4-6 while the As(V) removal was optimum at pH range 4-8. The adsorption data for both species of arsenic fitted better to pseudo second order of reaction kinetics which suggest that the dominant adsorption mechanism was chemisorption. The intra-particle diffusion model showed bilinear plot indicating that the adsorption of As(III) and As(V) is a complex process involving film diffusion and intra-particle diffusion. The isotherm studies showed that the data fitted better to Langmuir isotherm model as compared to Freundlich model indicating that adsorption of both As(III) and As(V) occurred on a monolayered surface. The maximum adsorption As(III) and As(V) capacity at room temperature as determined by Langmuir model

were found to be 7.99 mg/g and 7.32 mg/g, respectively. The thermodynamic studies for sorption of As(III) and As(V) showed that values of $\Delta G^O$ and $\Delta H^O$ were negative indicating that adsorption process occurred spontaneously and is exothermic in nature. Furthermore, $\Delta S^O$ value was found to be positive which suggest that As(III) and As(V) were randomly distributed on the surface of the adsorbent. The effect of co-existing ions showed that the adsorption of As(III) and As(V) is enhanced by the presence of $Mg^{2+}$ and $Ca^{2+}$ and is inhabited by the presence of $F^-$, $Cl^-$, $NO_3^-$, $CO_3^{2-}$ and $SO_4^{2-}$. The regeneration study showed that the inorgano-organo modified kaolin clay mineral can be reused for up 7 adsorption-regeneration cycles using 0.01 M HCl as a regenerant. The column data showed that a the breakthrough point occurs after treating 1380 mL and 1500 mL volumes of water containing for As(III) and As(V), respectively. This was achieved after treating water containing 0.5 mg/L As(III) and As(V) concentration using the bed mass of 5 g and flow rate of 1.5 mL/min. The column data was successfully modelled using Thomas kinetic model and Yoon-Nelson model. Both models showed that the rate of adsorption increases with increasing flow rate and initial concentration and decreases with increasing the bed mass. In comparison with other adsorbents, inorgano-organo modified kaolin clay mineral proved to be superior over other clay based adsorbents in the literature. This findings showed that inorgano-organo modified kaolin clay developed in this study is suitable for use in removal of arsenic from groundwater. However, further studies are recommended to enhance the permeability of the material so to reduce the amount of time required to treat water.

## References

Ahmed M. J., Hameed, B. H., 2018. Removal of emerging pharmaceutical contaminants by adsorption in a fixed bed column: A review. *Ecotoxicology and Environmental Safety*. 149, pp. 257–266.

Bhattacharyya, K. G., Gupta, S. S., 2008. Adsorption of a few heavy metals on natural and modified kaolinite and montmorillonite: A review. *Advances in Colloid and Interface Science*. 140, pp. 114–131.

Chatterjee, S., Sivareddy, I., De, S., 2017. Adsorptive removal of potentially toxic metals (cadmium, copper, nickel and zinc) by chemically treated laterite: Single and multicomponent batch and column study. *Journal of Environmental Chemical Engineering*. 5, pp. 3273–3289.

Ghosh, A., Chakrabarti, S., Ghosh, U. C., Fixed-bed column performance of Mn-incorporated iron(III) oxide nanoparticle agglomerates on As(III) removal from the spiked groundwater in lab bench scale. *Chemical Engineering Journal.* 248, pp. 18–26.

Gupta, S.S., Bhattachryya, K.G., 2011. Kinetics of adsorption of metal ions on inorganic materials: A review. *Advanced in Colloid and Interface Science.* 162, pp. 39-58.

Hua, J., 2015. Synthesis and characterization of bentonite based inorgano–organo-composites and their performances for removing arsenic from water. *Applied Clay Science.* 114, pp. 239–246.

Lee, S. M., Lalhmunsiama, Thanhmingliana, Tiwari, D., 2015. Porous hybrid materials in the remediation of water contaminated with As(III) and As(V). *Chemical Engineering Journal*. 270, pp. 496–507

Lee, S. M., Tiwari, D., 2012. Organo and inorgano-organo-modified clays in the remediation of aqueous solutions: An overview. *Applied Clay Science*. 59-60, pp. 84–102.

Munagapati, V. S., Kim, D. S., 2017. Equilibrium isotherms, kinetics, and thermodynamics studies for congo red adsorption using calcium alginate beads impregnated with nano-goethite. *Ecotoxicology and Environmental Safety.* 141, pp. 226–234.

Paudyal, H., Pangeni, B., Inoue, K., Kawakita, H., Ohto, K., Alam, S., 2013. Adsorptive removal of fluoride from aqueous medium using a fixed bed column packed with Zr(IV) loaded dried orange juice residue. *Bioresource Technology.* 146, pp. 713–720.

Podder, M. S., Majumder, C. B., 2016. Fixed-bed column study for As(III) and As(V) removal and recovery by bacterial cells immobilized on Sawdust/MnFe2O4 composite. *Biochemical Engineering Journal*. 105, pp. 114-135.

Qi, J., Zhang, G., Li, H., 2015. Efficient removal of arsenic from water using a granular adsorbent: Fe–Mn binary oxide impregnated chitosan bead. Bioresource Technology, 193, pp. 243–249.

Ren, X., Zhang, Z., Luo, H., Hu, B., Dang, Z., Yang, C., Li, L., 2014. Adsorption of arsenic on modified montmorillonite. *Applied Clay Sciences*. 97-98, pp.17-23.

Ryu, S. R., Jeom, E. K., Yang, J. S., Baek, K., 2017. Adsorption of As(III) and As(V) in groundwater by Fe–Mn binary oxide-impregnated granular activated carbon (IMIGAC). *Journal of the Taiwan Institute of Chemical Engineers.* 72, pp. 62–69.

Setshedi, K. Z., Bhaukim, M., Onyango, M. S., Maity, A., 2014. Breakthrough studies for Cr(VI) sorption from aqueous solution using exfoliated polypyrrole-organically modified montmorillonite clay nanocomposite. *Journal of Industrial and Engineering Chemistry*. 20, pp. 2208–2216.

Singh, M., Dosanjhm H. S., Singh, H., 2016. Surface modified spinel cobalt ferrite nanoparticles for cationic dye removal: Kinetics and thermodynamics studies. *Journal of Water Process Engineering*. 11 (2016) 152–161.

Smedley, P. L., Kinniburgh, D. G., 2002. A review of the source, behaviour and distribution of arsenic in natural waters. *Applied Geochemistry*. 17, pp. 517–568.

Thanhmingliana, Tiwari D., 2015. Efficient use of hybrid materials in the remediation of aquatic environment contaminated with micro-pollutant diclofenac sodium. *Chemical Engineering Journal*. 263, pp. 364–373.

Tiwari, D., Lee, S. M., 2012. Novel hybrid materials in the remediation of ground waters contaminated with As(III) and As(V). *Chemical Engineering Journal*. 204–206, pp. 23–31.

Tran, H. N., You, S. J., Chao, H. P., 2016. Thermodynamic parameters of cadmium adsorption onto orange peel calculated from various methods: A comparison study. *Journal of Environmental Chemical Engineering.* 4, 2671–2682.

Tran, H.N., You, S.J., Hosseini-Bandegharaei, A., Chao, H.P., 2017. Mistakes and inconsistencies regarding adsorption of contaminants from aqueous solutions: A critical review. *Water Research.* 120, pp. 88-116.

Vardhan, C. N. V., Srimurali, M., 2018. Preparation of Lanthanum Impregnated Pumice for defluoridation of water: Batch and column experiments. J*ournal of Environmental Chemical Engineering.* 6, pp. 858–865.

Weber, W.J., Morris, J.C., 1963 Kinetics of adsorption on carbon from solution. *Journal of Sanitary Engineering Division.* 89 (2), pp. 31-60.

Yang, Q., Zhong, Y., Li, X., Li, X., Lou, K., Wu, X., Chen, H., Liu, Y., Zeng, G., 2015. Adsorption-coupled reduction of bromate by Fe(II)–Al(III) layered double hydroxide in fixed-bed column: Experimental and breakthrough curves analysis. *Journal of Industrial and Engineering Chemistry*. 28, pp. 54–59.

Yin, H., Kong, M., Gu, X., Chen, H., 2017. Removal of arsenic from water by porous charred granulated attapulgite-supported hydrated iron oxide in bath and column modes. *Journal of Cleaner Production.* 166, pp. 88-97.

Yoon, Y. H., Nelson, J. H., 1984. Application of gas adsorption kinetics. I. A theoretical model for respirator cartridge service life. *American Industrial Hygiene Association Journal.* 45(8), pp. 509-516.

# Chapter 8: Conclusions and Recommendations

## 8.1 Conclusions and Recommendations

This work was designed with the main objective of synthesizing $Fe^{3+}/Mn^{2+}$ bimetal oxide and hexadecyltrimethylammonium bromide modified locally available clay soil for arsenic removal. The specific objectives were:

- To evaluate the arsenic concentration in selected boreholes in Greater Giyani Municipality, Limpopo Province.
- To evaluate the physicochemical properties of the locally available smectite rich clay soils and kaolin clay mineral and compare their effectiveness towards arsenic removal from groundwater
- To evaluate the optimum conditions for synthesizing $Fe^{3+}/Mn^{2+}$ bimetal oxide and hexadecyltrimethylammonium bromide (HDTMA-Br) modified clay mineral for As(III) and As (V) removal from groundwater.
- To evaluate the regeneration potential of the synthesized adsorbent

All the above objectives were successfully achieved and the following conclusions were made from each specific objective:

When evaluating the arsenic concentration and hydrochemistry water samples collected from Greater Giyani Municipality it was found that the pH of the groundwater samples ranges from neutral to weakly alkaline. Furthermore, the abundance of major anions and cations were in the following order: $HCO_3^->Cl^->SO_4^{2-}>NO_3^-$ and $Na^+ > Mg^{2+} > Ca^{2+} > K^+ > Si^{4+}$, respectively. The hydrogeochemical facies identified in the study area include $CaHCO_3$ (90%) and mixed $CaNaHCO_3$ (10%) which shows the dominance of water-rock interaction. Amongst the tested samples, 60 % contains arsenic concentrations beyond the WHO permissible limit of 10 µg/L. The mean arsenic concentration was found to be 32.21 µg/L while the maximum concentration recorded was 172.53 µg/L. All samples with higher arsenic concentration were found to be having pH between 7.5 and 8.5 and $HCO_3^-$ > 200 mg/L. The following recommendations were made from this objective:

(i) Routine monitoring of arsenic concentration in the Greater Giyani Municipality.

(ii) Epidemiological studies should be conducted to assess the correlation between arsenic and related diseases within the Giyani Municipality.

(iii) Studies focusing on arsenic developing arsenic remediation technique that is flexible and sustainable for use in Greater Giyani Municipality.

The second objective focused on evaluating the physicochemical characteristics of the two locally available clays and to further evaluate their effectiveness towards arsenic removal. It was found that both clays are alumino-silicate silicate materials and are mesoporous in nature. The clay from Dzamba is rich in kaolin mineral while the clay from Mukondeni is rich in smectite mineral. Kaolin clay showed higher efficiency towards As(III) and As(V) from water as compared to smectite rich clay soils. Furthermore, both clays showed poor regeneration potential. From this objective, the modification of kaolin clay was recommended in order to enhance its sorption capacity and regeneration potential.

The third objective was achieved by modifying the kaolin clay mineral with $Fe^{3+}$ and $Mn^{2+}$ bimetal oxide and HDTMA-Br cationic surfactant, respectively and lastly, $Fe^{3+}$ and $Mn^{2+}$ bimetal oxides were combined with HDTMA-Br cationic surfactant to obtain inorgano-organo modified kaolin clay. From this objective it was noted that modification of kaolin clay do not alter the mineralogical composition of the clay. However, the modification changes the chemical composition and the surface properties such as surface area, pore volume and pore diameter. Modified clays showed improved adsorption capacity and the regeneration potential as compared to the raw kaolin clay. Amongst three modified adsorbents, inorgano-organo modified clay showed higher adsorption capacity towards As(III) and As(V) from groundwater. The regeneration study showed that both clays can be successfully regenerated making them suitable for use in arsenic removal in developing countries. The synthesized adsorbents were considered not hazardous since the concentration below 5 mg/L was recorded during desorption studies. From objective, the major recommendation was that further studies should be conducted to enhance the permeability of both modified clays in order to enhance the volume of water that can be treated on a daily basis without affecting the adsorption capacity.

### 8.2 Future work

Based on the conclusions and recommendations from the present investigation studies should be conducted to evaluate the following:

- The link between arsenic exposure and arsenic related diseases.
- Seasonal variation of arsenic concentration in borehole water in greater Giyani Municipality.
- Increasing the permeability of the clays without altering the adsorption capacity.
- Better ways to handle the adsorbent developed in this study for use at household level.
- Other materials for arsenic removal from low cost materials.
- Cytotoxicity study of HDTMA after the use in adsorption of As.